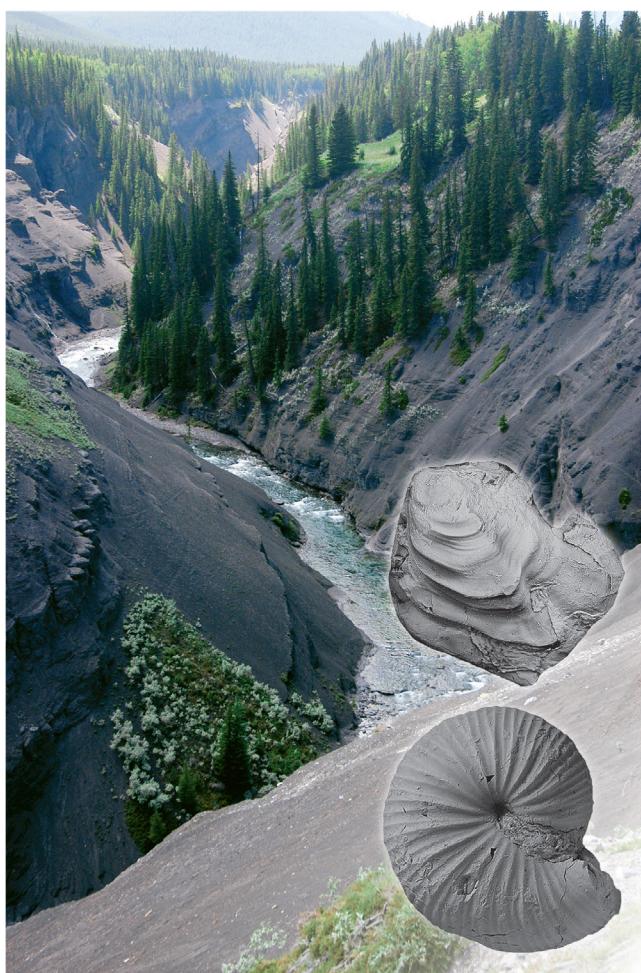

ALLOSTRATIGRAPHY AND BIOSTRATIGRAPHY
OF THE UPPER CRETACEOUS
(CONIACIAN-SANTONIAN)
WESTERN CANADA FORELAND BASIN

NEIL H. LANDMAN, A. GUY PLINT, AND
IREK WALASZCZYK (EDITORS)



BULLETIN OF THE AMERICAN MUSEUM OF NATURAL HISTORY

ALLOSTRATIGRAPHY AND BIOSTRATIGRAPHY OF
THE UPPER CRETACEOUS
(CONIACIAN-SANTONIAN)
WESTERN CANADA FORELAND BASIN

Edited by

NEIL H. LANDMAN

*Division of Paleontology,
American Museum of Natural History*

A. GUY PLINT

*Department of Earth Sciences,
University of Western Ontario, London, Ontario*

IREK WALASZCZYK

*Faculty of Geology,
University of Warsaw, Warszawa, Poland*

BULLETIN OF THE AMERICAN MUSEUM OF NATURAL HISTORY

Number 414, 172 pp., 76 figures (including 11 foldouts), 11 tables

Issued June 26, 2017

CONTENTS

Preface.....	4
References.....	6
Acknowledgments.....	7
Chapter 1.....	9
Abstract.....	9
Introduction.....	10
Tectonic and Paleogeographic Overview of the Basin.....	11
Previous Stratigraphic Studies.....	11
Lithostratigraphy.....	11
Biostratigraphic Studies.....	13
Allostratigraphic Studies.....	15
Previous Work.....	15
Data and Methods.....	15
Allostratigraphic Terminology.....	16
Carbon-Isotope Analysis.....	16
Establishing Regional Allostratigraphic Correlations.....	17
The Character and Significance of Flooding Surfaces.....	17
Use of Distinctive Flooding Surfaces to Establish Correlation to Outcrop.....	20
Continuity of Bounding Surfaces.....	24
Sedimentology.....	25
Principal Molluscan Zones.....	27
Carbon-Isotope Stratigraphy.....	29
Geochronology.....	31
Discussion.....	31
Tectonic Control on Deposition.....	31
Origin of Allomembers.....	41
Nature of Biozonal Boundaries.....	41
Conclusions.....	43
Acknowledgments.....	45
References.....	45
Appendix 1. Location of Measured Sections in this Study.....	49
Appendix 2 Results of Carbon Isotope Analyses of Samples from Cutpick Creek.....	50
<i>Figures 3–13.....</i>	<i>inserted after page 52</i>
Chapter 2.....	53
Abstract.....	53
Introduction.....	54
Geological Setting and Localities.....	54
Biostratigraphy.....	54
State and Substage Boundaries.....	59
Biogeography and Evolution.....	60
Terms and Repositories.....	61
Systematic Paleontology.....	61
<i>Inoceramus</i> Sowerby, 1814.....	61
<i>Tethyoceramus</i> (Sornay, 1980).....	69

<i>Cremnoceramus</i> Cox, 1969	69
<i>Volviceramus</i> Stoliczka, 1871	71
<i>Sphenoceramus</i> J. Böhm, 1915	89
Acknowledgments	98
References	98
Chapter 3	105
Abstract	105
Introduction	105
Geologic Background	106
Terminology	107
Taxonomic Background	110
Geographic Distribution	111
Stratigraphic Distribution	112
Paleoecology	115
Evolution	117
Repositories	120
Systematic Paleontology	120
<i>Scaphites</i> (<i>Scaphites</i>) <i>preventricosus</i> Cobban, 1952	120
<i>Scaphites</i> (<i>Scaphites</i>) <i>ventricosus</i> Meek and Hayden, 1862	127
<i>Scaphites</i> (<i>Scaphites</i>) <i>depressus</i> Reeside, 1927	139
<i>Clioscaphites saxitonianus</i> (McLearn, 1929)	159
Acknowledgments	168
References	169

Preface

NEIL H. LANDMAN, A. GUY PLINT, AND IRENEUSZ WALASZCZYK

This bulletin contains three closely integrated papers that treat Upper Cretaceous (Coniacian-Santonian) strata of the Western Canada Foreland Basin (WCFB). Our research is the culmination of the collective efforts of seven scientists from eight institutions in the United States, Canada, Poland, and the United Kingdom. It presents the results of 12 seasons of geological fieldwork in the Rocky Mountain Foothills of Alberta. As in many other high-latitude studies, some sites were difficult to access and required transport by helicopter, and fieldwork could be carried out only in July and August. The outcrops were measured in detail, with particular attention to depositional cycles and bounding surfaces that indicate relative changes in sea level. Fossils of molluscs were collected at each locality and placed precisely within each section. The results of these outcrop investigations were integrated with a public database comprising thousands of wireline logs, supplemented by cores, which provided the regional control to reconstruct the stratal geometry, facies relationships, and paleogeography of the basin in three dimensions.

The principal purpose of our research is to present a detailed allostratigraphic and biostratigraphic framework for the Coniacian and basal Santonian succession in the WCFB. The studied strata, approximately 100 m thick, comprise the lower part of the Wapiabi Formation (Coniacian to lower Campanian) that extends east from the Rocky Mountain Foothills and covers much of Alberta, and parts of Saskatchewan and Manitoba. Because of rapid flexural subsidence in the western foredeep, the Wapiabi Formation preserves an expanded record of terrestrial and shallow marine sedimentation. The rocks are dominated by mudstone and subordinate sandstone and were deposited on a very low-gradient, storm-dominated marine ramp. The rocks are organized into a series of upward-coarsening, upward-shoaling successions, bounded by marine flooding surfaces. These surfaces constitute proxy time planes that provide a framework within which to assess the temporal and spatial distribution of the molluscan fossils that furnish the basis for biostratigraphic correlation. The WCFB thus represents a natural laboratory in which to elucidate the interplay between the principal physical controls on sedimentation, namely tectonism, sediment supply, and eustasy, as well as the evolutionary patterns of the organisms that lived in the area during this time.

In the first paper of the bulletin, Plint et al. synthesize information from well-exposed sections in the fold-and-thrust belt of the Rocky Mountain Foothills and combine this information with data from a large correlation grid of wireline logs, supplemented by a few cores. In the Coniacian part of the section, they identify 24 flooding surfaces that can be traced for >750 km along strike in the subsurface. These flooding surfaces form the boundaries of 24 informal allomembers. Some of these surfaces are mantled with intra- or extrabasinal pebbles that imply a phase of shallowing and, potentially, subaerial emergence of the inner part of the ramp. Flooding surfaces represent small intervals of time relative to the rock units that they bound and, therefore, allow the subsidence history of the basin to be reconstructed in a series of relatively short time-steps. This new allostratigraphic framework emphasizes the importance of marine erosional surfaces, and their genetic relationship to relative changes in

sea level. Development of such a regional subsurface allostratigraphic framework helps resolve stratal geometry and facies distributions, from which paleogeography, paleobathymetry, subsidence patterns, relative sea-level changes, and overall depositional history can be reconstructed.

The allostratigraphic framework constitutes the physical and temporal matrix within which the vertical and lateral distribution of molluscan fossils, principally inoceramid bivalves and scaphitid ammonites, can be assessed. Regional mapping reveals that allomembers, which exhibit a near-tabular geometry, can be grouped into “tectono-stratigraphic units” that span hundreds of thousands of years and fill saucer-shaped, flexural depocenters. Successive depocenters are offset laterally by several hundred km, which probably reflects episodic lateral shifts in the locus of active thickening in the Cordilleran orogenic wedge, and a corresponding lateral shift in the locus of maximum isostatic subsidence.

As a complement to the allostratigraphic study, Plint et al. present preliminary carbon-isotope data from one section of Coniacian strata in Alberta, and compare the results to the reference curve from the UK Chalk succession, and to results from coeval rocks in Colorado. On the basis of shape-matching and biostratigraphic tie-points, the Light Point, East Cliff, and White Fall carbon-isotope events (CIE) of the UK Chalk succession appear to be present in Alberta. The astronomically calibrated succession of CIE in the English Chalk suggests that each of the 24 mapped allomembers in Alberta has an average duration of approximately 125,000 kyr. Because allomembers can be traced for hundreds of km, an allogenic control, probably eustasy, appears to be the most likely genetic mechanism responsible for sea-level cycles.

The WCFB yields a rich and well-preserved molluscan fauna dominated by inoceramid bivalves. This is treated by Walaszczyk et al. in the second paper in this volume. In the upper lower Coniacian to basal Santonian, six successive inoceramid zones are recognized. In ascending stratigraphic order, they are the *Cremnoceramus crassus crassus*-*deformis deformis* Zone, the *Inoceramus gibbosus* Zone, the *Volvicceramus koeneni* Zone, the *V. involutus* Zone, the *Sphenoceramus subcardisoides* Zone, and the *Sphenoceramus* ex gr. *pachti* Zone. The base of the middle Coniacian is marked by the lowest occurrence of the taxonomically variable *Volvicceramus* fauna including *V. koeneni* (Müller, 1888), *V. exogyroides* (Meek and Hayden, 1862), and *V. cardinalensis*, sp. nov., in association with *I. undabundus* Meek and Hayden, 1862. The base of the upper Coniacian is marked by the lowest occurrence of the characteristically northern inoceramid species *S. subcardisoides* (Schlüter, 1877). The lowest occurrence of *V. stotti* sp. nov., described for the first time from the Canadian sections, is also close to this boundary. The base of the Santonian is marked by the lowest occurrence of *S. ex gr. pachti* (Arkhangelsky, 1912). Several of the zonal assemblages are known widely from the Euramerican biogeographic region, although they are mostly representative of the northern boreal area. This new inoceramid-based zonation allows correlation with other parts of the Euramerican biogeographic region.

The lowest occurrence of each inoceramid species can be interpreted in the context of the relative sea-level framework developed by Plint et al. The lowest occurrences of *Cremnoceramus crassus crassus* (Petrascheck, 1903), various species of *Volvicceramus*, *Sphenoceramus subcardisoides*, and *S. ex gr. pachti* are immediately above major flooding surfaces, suggesting that the first appearances of these taxa are closely linked to episodes of relative sea-level rise. Thus, the boundaries of biozones appear to coincide with physical stratigraphic (flooding) surfaces. The generally rare species *Inoceramus gibbosus* Schlüter, 1877, is abundant in the upper part of the lower Coniacian. This species is usually absent in both Europe and North America due to a stratigraphic gap resulting from a eustatic lowstand. The preservation of this species in Canada is attributed to rapid subsidence of the foredeep, which outpaced the eustatic sea-level fall.

The WCFB also contains a rich record of scaphitid ammonites (scaphites), which are described by Landman et al. in the third paper in this issue. These species are widespread and restricted to higher latitudes and allow correlation with other parts of the Western Interior of North America, as well as with western Greenland. In ascending order, Landman et al. recognized four ammonite zones, the *Scaphites* (*S.*) *preventricosus* Zone, the base of which coincides with the base of the lower Coniacian, the *S.* (*S.*) *ventricosus* Zone, the base of which coincides with the base of the *Inoceramus gibbosus* Zone and marks the upper part of the lower Coniacian, the *S.* (*S.*) *depressus* Zone, the base of which coincides with the base of the upper Coniacian, and the *Clioscaphtes saxitonianus* Zone, the base of which coincides with the base of the Santonian. The lowest occurrence of each scaphite species can be interpreted in the context of the relative sea-level framework developed by Plint et al. The lowest occurrence of *S.* (*S.*) *preventricosus* Cobban, 1952, is just above an erosional surface that indicates the beginning of a major transgression that commenced in the very latest Turonian. The lowest occurrence of *S.* (*S.*) *ventricosus* Meek and Hayden, 1862, is just below an interpreted highstand and prior to a regression in the latest early Coniacian. The lowest occurrence of *S.* (*S.*) *depressus* Reeside, 1927, is in an overall regressive succession, which marks the base of the upper Coniacian, and the lowest occurrence of *Clioscaphtes saxitonianus* (McLearn, 1929) coincides with a major transgression at the base of the Santonian. All of these species exhibit some degree of stratigraphic overlap, which implies evolutionary episodes of cladogenesis rather than anagenesis, which was the mechanism previously postulated to explain the evolution of these scaphites.

The most distinctive feature in the ontogenetic development of these scaphites is the change in coiling during ontogeny. At the approach of maturity, the shell uncoils slightly, forming a shaft, which then recurves backward approaching the earlier secreted phragmocone. As a result, the aperture faces upward during the lifetime of the animal, so that the buccal apparatus can extend outward to collect small organisms in the water column. The sequence of species leading from *Scaphites* (*S.*) *preventricosus* to *Clioscaphtes saxitonianus* appears to form an evolutionary lineage, suggesting a long-term trend toward recoiling of the adult shell, while still maintaining the same position of the aperture during life. This trend is accompanied by an increase in adult size (possibly caused by a delay in the timing of maturation) and degree of shell depression. This tendency toward more recoiled shell shapes and larger adult sizes occurred against a background of changing environmental conditions in the Western Interior Seaway during the Coniacian that reflected an overall relative rise in sea level and the expansion of the seaway to cover nearly all of Alberta. This transgression resulted in an expansion of offshore habitats that may have promoted the evolutionary appearance of larger scaphite species with more closely coiled shapes and more depressed whorl sections, which were better adapted to these environments.

REFERENCES

- Arkhangelsky, A.D. 1912. Upper Cretaceous deposits of the eastern part of the European Russia. Reprinted in Akademik A.D. Arkhangelsky, *Izobrannyye Trudy*, vol. 1: 133–466. Moskva: Izdatelstvo Akademii Nauk SSSR. [in Russian]
- Cobban, W.A. 1952. Scaphitoid cephalopods of the Colorado Group. U.S. Geological Survey Professional Paper 239, 42 pp.
- Meek, F.B., and Hayden, F.V. 1862. Description of new Cretaceous fossils from Nebraska Territory, collected by the expedition sent out by the government under the command of Lieut. John Mullan, U.S. Topographical Engineers,

- for the location and construction of a Wagon Road from the sources of the Missouri to the Pacific Ocean. Proceedings of the Academy of Natural Sciences of Philadelphia 14: 21–28.
- Müller, G. 1888. Beitrag zur Kenntnis der oberen Kreide am nördlichen Harzrande. Jahrbuch des Preußischen Geologischen Landesanstalt 8: 372–456.
- McLearn, F.L. 1929. Cretaceous invertebrates: Mesozoic paleontology of Blairmore region, Alberta. Canada National Museum Bulletin 58: 73–79.
- Petrascheck, W. 1903. Ueber Inoceramen aus der Kreide Böhmens und Sachsens. Jahrbuch der Kaiserlich-Königlichen Reichsanstalt 53: 153–168.
- Reeside, J.B., 1927. Cephalopods from the lower part of the Cody Shale of Oregon Basin, Wyoming. U.S. Geological Survey Professional Paper 150-A: 1–19.
- Schlüter, C. 1877. Kreide-Bivalven. Zur Gattung *Inoceramus*. Palaeontographica 24: 250–288.

ACKNOWLEDGMENTS

This work reflects the efforts of many graduate students at the University of Western Ontario including B. Norris, J. McKay, and S. Donaldson. For able field assistance over the years, we thank O. Al-Mufti, P. Angiel, R. Buckley, S. CoDyer, R. Cotton-Barratt, P. Elliott, B. Hart, Y. Hu, S. Morrow, M. O'Driscoll, K. Pavan, T. Plint, J. Shank, K. Vannelli, and R. Vesely. Funding for A.G. Plint's regional stratigraphic studies was provided by the Natural Sciences and Engineering Research Council of Canada over numerous grant cycles. Supplementary funding was provided by Canadian Hunter Ltd, Home Oil Ltd., Imperial Oil Ltd., Texaco Ltd., and Unocal Canada, Ltd. Well-log data were donated by Imperial Oil Ltd. and Divestco Ltd. A gamma ray spectrometer was donated to the University of Western Ontario by Pan Canadian Petroleum Ltd.

I. Walaszczyk acknowledges the financial support of the Faculty of Geology of the University of Warsaw (BST grant No. 173502). For his final studies in Denver in November 2016, he acknowledges NCN Grant UMO-2015/17/B/ST10/03228. He also thanks Marcin Ploch, Warsaw, for his assistance in preparing the cover photograph. D.R. Gröcke and I. Jarvis acknowledge funding by UK Natural Environment Research Council (NERC) grants NE/H021868/1 and NE/H020756/1, respectively.

N.H. Landman thanks B. Hussaini, M. Conway, and K. Sarg (AMNH) for curation of fossils, S. Thurston (AMNH) for photographing specimens and preparing figures, M. Slovacek (AMNH) for preparation of specimens and illustrations, M. Wilson (College of Wooster, Wooster, Ohio) for identification of bryozoans, N. Larson (Larson Paleontology Unlimited, Keystone, South Dakota) for preparation of specimens, S. Butts (Yale Peabody Museum, New Haven, Connecticut) for providing access to collections in her care, and B. Strilisky (TMP) for facilitating the transfer of specimens to the Tyrell Museum of Paleontology. This research was funded in part by NSF Grant DEB-1353510.

We thank John A. Chamberlain, Jr. (Brooklyn College, Brooklyn, New York), Matt P. Garb (Brooklyn College, Brooklyn, New York), Ben Hathway (Alberta Geological Survey), Gregori López (Universitat Autònoma de Barcelona, Spain), Marcin Machalski (Institute of Paleobiology, Warsaw, Poland), and Royal H. Mapes (North Carolina Museum of Natural History, Raleigh, North Carolina) for carefully reviewing earlier drafts of these manuscripts. Their detailed and perceptive comments have significantly improved the final text and figures. The authors also thank Mary Knight and the publications committee at the AMNH for their help in shepherding these manuscripts through the review and editing process, ultimately leading to publication.

Chapter 1

Integrated, High-Resolution Allostratigraphic, Biostratigraphic and Carbon-Isotope Correlation of Coniacian Strata (Upper Cretaceous), Western Alberta and Northern Montana

A. GUY PLINT,¹ ELIZABETH A. HOOPER,¹
MERIEM D. GRIFI,² IRENEUSZ WALASZCZYK,³ NEIL H. LANDMAN,⁴
DARREN R. GRÖCKE,⁵ JOÃO P. TRABUCHO ALEXANDRE,⁶
AND IAN JARVIS⁷

ABSTRACT

Lower to upper Coniacian rocks in the foredeep of the Western Canada Foreland Basin are dominated by mudstone and subordinate sandstone and were deposited on a very low-gradient, storm-dominated marine ramp. The rocks are organized into several scales of upward-coarsening, upward-shoaling succession, bounded by marine flooding surfaces. Abundant, publicly available wireline log data permit flooding surfaces to be traced for hundreds of kilometers in subsurface. Flooding surfaces can be considered to approximate time surfaces that allow the subsidence history of the basin to be reconstructed. Particularly widely traceable flooding surfaces were chosen, on pragmatic grounds, as the boundaries of 24 informal allomembers, most of which can be mapped along the foredeep for >750 km. Allomembers can also be traced westward into the fold-and-thrust belt to outcrop in the Rocky Mountain Foothills. Some flooding surfaces are mantled with intra- or extrabasinal pebbles that imply a phase of shallowing and, potentially, subaerial emergence of part of the ramp.

The rocks yield a rich and well-preserved molluscan fauna dominated by inoceramid bivalves and scaphitid ammonites. Several major inoceramid speciation events are recognized. The lowest occurrence of *Cremnoceramus crassus crassus*, various species of *Volvicceramus*, *Sphenoceramus subcardisoides*, and *S. pachtii* all appear immediately above major flooding surfaces, suggesting that speciation,

¹ Department of Earth Sciences, The University of Western Ontario, London, Ontario, Canada.

² Husky Energy Inc., Calgary, Alberta, Canada.

³ Faculty of Geology, University of Warsaw, Poland.

⁴ Division of Paleontology, American Museum of Natural History.

⁵ Department of Earth Sciences, Durham University, Durham, U.K.

⁶ Department of Earth Sciences, Universiteit Utrecht, Utrecht, the Netherlands.

⁷ Department of Geography and Geology, Kingston University London, Kingston upon Thames, U.K.

and dispersal of new inoceramid taxa were closely linked to episodes of relative sea-level rise. Thus, the boundaries of biozones can be shown to coincide with physical stratigraphic (flooding) surfaces. The generally rare species *Inoceramus gibbosus* is abundant in the upper part of the lower Coniacian; the preservation of this zonal form may be attributed to rapid subsidence of the foredeep that outpaced a major eustatic? sea-level fall that took place at the end of the early Coniacian and that is marked by a hiatus in most epicontinental basins. Regional mapping shows that allomembers, which have a near-tabular geometry, can be grouped into “tectono-stratigraphic units” that fill saucer-shaped, flexural depocenters. Individual depocenters appear to have been active for ca. 0.5 to 1.5 m.y., and successive depocenters are offset laterally, probably reflecting episodic shifts in the locus of active thickening in the Cordilleran orogenic wedge and related subsidence in the foreland basin. Preliminary carbon-isotope results from one section are tentatively correlated, using biostratigraphic tie-points, to the English Chalk reference curve: the Light Point, East Cliff, and White Fall carbon-isotope events (CIE) are recognized with some degree of confidence. The astronomically calibrated succession of CIE in the English Chalk suggests that the 24 mapped allomembers in Alberta each had an average duration of about 125,000 yr. Because allomembers can be traced for hundreds of km, an allogenic control, probably eustasy, appears to be the most likely genetic mechanism.

INTRODUCTION

The Western Canada Foreland Basin (WCFB) contains a preserved stratigraphic succession, over 5 km thick, that forms an expanded record of terrestrial and shallow-marine sedimentation through much of the Late Jurassic, Cretaceous, and Paleocene (Wright et al., 1994). Well-exposed sections in the Rocky Mountain Foothills, coupled with a public database of tens of thousands of wireline logs and thousands of cores permit reconstruction of basin-scale stratal geometry, facies relationships, and paleogeography in a high-resolution allostratigraphic framework (e.g., Plint et al., 1986; Bhattacharya and Walker, 1991a, 1991b; Plint, 2000; Varban and Plint, 2008a, 2008b; Roca et al., 2008). Allostratigraphic units are mappable bodies of rock defined by bounding discontinuities (NACSN, 2005: Article 58). In the succession studied here, marine flooding or transgressive surfaces form the mappable bounding surfaces of allomembers. Such surfaces typically have low diachroneity relative to the time represented by the rock units that they bound, and hence can be considered to approximate time planes (e.g., Cross and Lessenger, 1988). In consequence, the WCFB provides an unparalleled natural laboratory in which to assess the principal physical controls on sedimentation, namely: sedi-

ment supply, tectonism, and eustasy. The temporal framework provided by physical, marine flooding surfaces also makes it possible to determine the temporal and spatial distribution of evolving lineages of molluscs that provide the principal basis for biostratigraphic correlation. It is then possible to address the question: Are biotic speciation and extinction events consistently associated with physical stratigraphic surfaces, and the relative sea-level changes that those surfaces are considered to represent?

The principal purpose of this paper is to present a very detailed allostratigraphic framework, developed for Coniacian strata across the foredeep of the Western Canada Foreland Basin. That framework then constitutes a physical, and near-temporal matrix in which to plot the vertical and lateral distribution of molluscan fossils, principally inoceramid bivalves and scaphitid ammonites. Full taxonomic documentation of the inoceramid and ammonite faunas is provided in companion papers (Landman et al. and Walaszczyk et al., this issue). A secondary objective is to present preliminary carbon-isotope data from Coniacian strata in Alberta, and to compare those results with the reference curve from the UK Chalk succession (Jarvis et al., 2006), and with results from coeval rocks in Colorado (Joo and Sageman, 2014). An interpretation of relative sea-

level changes is given in the companion papers by Landman et al. and Walaszczyk et al. (this issue).

TECTONIC AND PALEOGEOGRAPHIC OVERVIEW OF THE BASIN

Subsidence of the Western Canada Foreland Basin was initiated in the Jurassic as the result of isostatic flexure of underlying cratonic lithosphere under the load of the tectonically thickened Cordilleran fold-and-thrust belt to the west (Price, 1994; Evenchick et al., 2007). The earliest preserved foreland strata were deposited from the Late Jurassic (Kimmeridgian) to Early Cretaceous (Valanginian), when sediment was supplied to the Canadian portion of the basin by both local rivers and a continent-scale, north-flowing drainage system with headwaters in the southwestern and possibly also the southeastern United States (Williams and Stelck, 1975; Wright et al., 1994; Raines et al., 2013). In the Berriasian to Barremian, diminished tectonic activity in the Rocky Mountain Cordillera, resulted in widespread erosion and isostatic uplift of Upper Jurassic to Lower Cretaceous sediments in the foredeep (Leckie and Cheel, 1997; Leier and Gehrels, 2011). Subsidence of the Western Canada Foreland Basin resumed in the Aptian, accompanied by gradual marine flooding by a southward-advancing arm of the Polar Ocean. One or more continent-scale, north- and west-flowing river systems delivered sediment to the basin from headwaters in the Canadian Shield, the Appalachians, and the Cordillera (Benyon et al., 2014; Blum and Pecha, 2014).

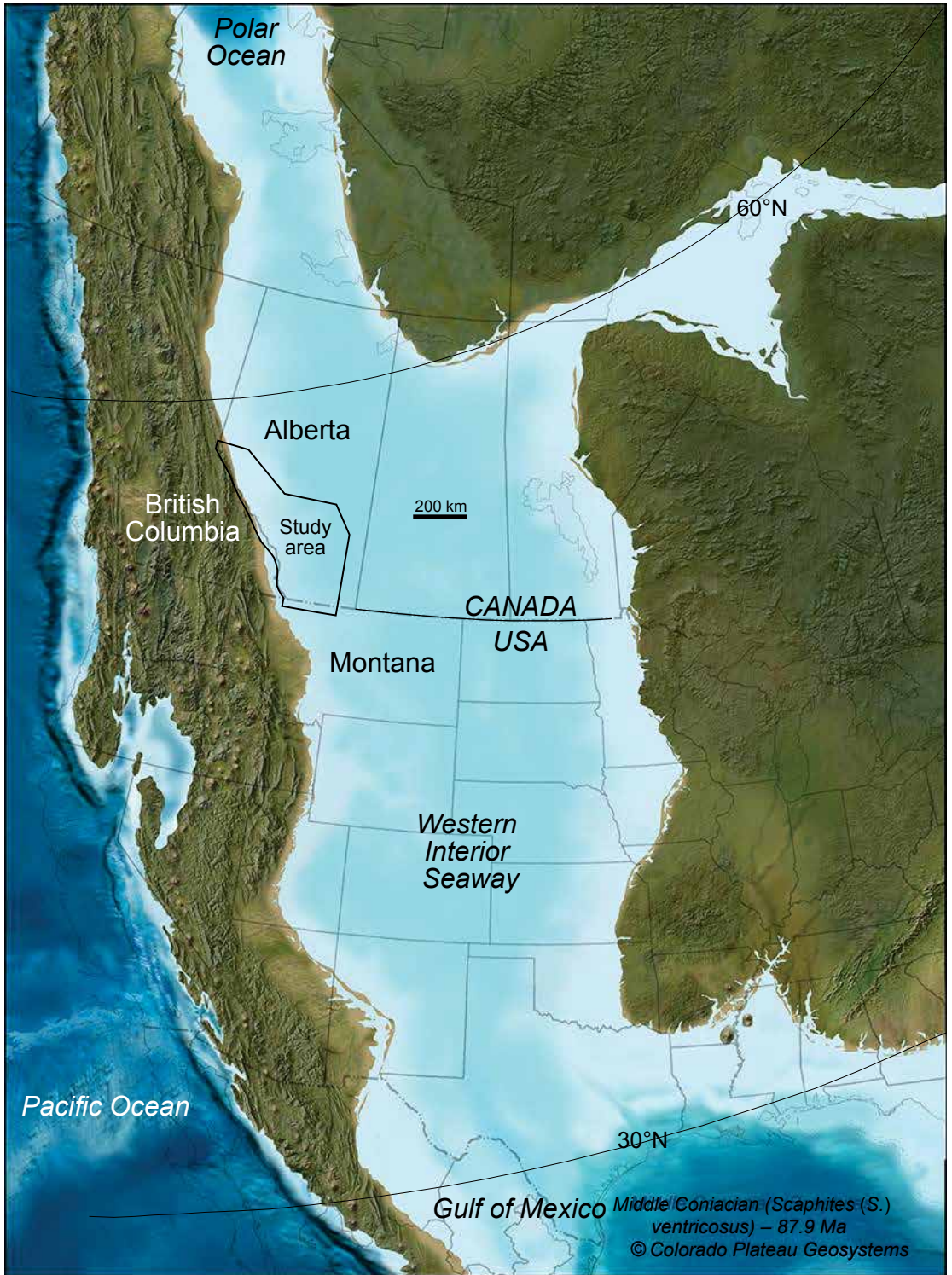
At about the Albian-Cenomanian boundary (about 100.5 Ma), a southward-encroaching embayment of the Polar Ocean (the Mowry Sea) merged with a northward-encroaching arm of the Gulf of Mexico to form the early Greenhorn Sea (Williams and Stelck, 1975). This seaway continued to widen through the late Cenomanian to a maximum extent in the early Turonian, before progressive eustatic sea-level fall caused the seaway to narrow to a minimum in the late Turonian and earliest Coniacian, as recorded by rocks of the Cardium Formation (e.g., Nielsen et al., 2008;

Shank and Plint, 2013; Walaszczyk et al., 2014). Earliest Coniacian regressive sandstones in the upper part of the Cardium Formation were buried by marine mudstone of the early to middle Coniacian Muskiki Member of the Wapiabi Formation. Muskiki strata record the onset of the Niobrara Cycle (Kauffman, 1977), which is expressed as a major transgression that drove the shoreline so far to the west that no near-shore deposits are preserved in outcrop sections exposed in the Alberta or British Columbia (BC) foothills (Stott, 1963, 1967; fig. 1). In late Coniacian time, the broadly regressive, siltstone- and sandstone-dominated Marshybank Member was deposited along the western margin of the basin. The slightly younger Bad Heart Formation was deposited in the north-eastern part of the basin, and is confined to the Peace River Plains (Stott, 1963, 1967; Plint et al., 1990; Donaldson et al., 1998). Late Coniacian regression was followed by major regional transgression in latest Coniacian and early Santonian time, leading to widespread deposition of marine mudstone across Alberta and BC; this transgression coincided with a period of renewed flexural subsidence of the foredeep of the foreland basin (Nielsen et al., 2008; Hu and Plint, 2009; Plint et al., 2012a).

PREVIOUS STRATIGRAPHIC STUDIES

LITHOSTRATIGRAPHY

The early history of stratigraphic investigation of Upper Cretaceous rocks in Alberta was thoroughly reviewed by Stott (1963, 1967). The present study is focused on Coniacian rocks that form part of the Wapiabi Formation, a unit that was originally recognized and named by Malloch (1911). The Wapiabi Formation comprises up to about 650 m of marine mudstone with minor intercalations of sandstone and siltstone. Stott (1956, 1963, 1967) showed that the Wapiabi Formation could consistently be divided into seven members, each characterized by a distinct suite of lithologies that could be traced along most of the Rocky Mountain Foot-



hills from NE BC to the Montana border (figs. 2, 3; fig. 3 inserted after p. 52). The lowest unit, the Muskiki Member, rests disconformably on the underlying Cardium Formation and comprises primarily offshore marine mudstone.

The boundary between the Muskiki and overlying Marshybank Member is typically a rapidly gradational to sharp contact between mudstone and siltstone and overlying, intensely bioturbated siltstone and silty sandstone. Toward the north, particularly north of the Athabasca River, the siltstone-dominated Marshybank Member undergoes a lateral facies change to include clean, well-sorted sandstone as well as siltstone and minor mudstone. Even further to the NW, in BC, the Marshybank includes not only near-shore sandstone but also a unit of terrestrial deposits (Plint and Norris, 1991). Stott (1967) did not extend the term “Marshybank” to describe these northern, sandstone-rich rocks, but instead chose to assign them to the “Bad Heart” Formation, inferring that sandy rocks in the foothills correlated with the type Bad Heart Formation that is exposed about 150 km to the NE on the Smoky River in the Peace River Plains. In the latter area, the Bad Heart Formation comprises fine-grained sandstone and ooidal ironstone with minor dark silty claystone.

A change of lithostratigraphic terminology occurs at the Canada–U.S. border: rocks of the Cardium and Wapiabi formations in Alberta being broadly correlative with the Ferdig and Kevin members of the Marias River Formation in Montana (Cobban et al., 1976; Nielsen et al., 2003; figs. 2, 3; figs. 3–13 inserted after p. 52).

BIOSTRATIGRAPHIC STUDIES

Stott (1963, 1967) summarized existing biostratigraphic information regarding the age of

the Wapiabi Formation. Stott reported that the lowest part of the Muskiki Member contained *Scaphites* (*S.*) *preventricosus* Cobban and *Inoceramus deformis* Meek. Stott used the stratigraphical interpretation of Jeletzky (who followed the traditional German subdivision) and dated these two taxa to the late Turonian, although he (Stott, 1963) did note that Jeletzky (personal commun.) considered that they might be of earliest Coniacian age (as treated at that time in the U.S.; see e.g., Seitz, 1959). The higher part of the Muskiki contained *Scaphites* (*S.*) *ventricosus* Meek and Hayden and *Inoceramus involutus* Sowerby, indicative of a Coniacian age. Neither *I. involutus* nor *S. (S.) ventricosus* were found to range up into the Marshybank Member (Stott, 1963). The Marshybank Member contained *Scaphites* (*S.*) *depressus* Reeside, which Stott did not find below the base of the member. At the time of Stott’s studies, *S. (S.) depressus* was considered by Jeletzky (see also discussion in Obradovich and Cobban, 1975) to indicate an early Santonian age, but that zone was later reassigned to the upper Coniacian (Kennedy and Cobban, 1991). Collom (2001) undertook a litho- and biostratigraphic study of the Wapiabi Formation and equivalent strata between Highwood River in the south and the lower Smoky River in the north. Collom’s correlation of depositional cycles along the Foothills was, however, made without reference to subsurface data, and his stratigraphic sections contain insufficient detail to be related to our own observations. Moreover, Collom’s inoceramid taxonomy, and consequently his stratigraphic interpretation, cannot be confirmed in most of the cases (see companion paper by Walaszczyk et al., this issue).

In Montana, Cobban et al. (1976) recognized ammonite and bivalve zones in the Fer-

FIG 1. Paleogeographic reconstruction of North America for the middle Coniacian (*Scaphites* (*S.*) *ventricosus* time). This map is representative of the paleogeography during deposition of the Muskiki Member of the Wapiabi Formation when the Coniacian transgression was at approximately its greatest extent. The study area in Alberta and Montana is indicated. (Map adapted from R. Blakey, <http://cpgeosystems.com>).

UPPER CRETACEOUS		Alberta and British Columbia ¹		N Alberta Plains ²		N Alberta Foothills ²		S Alberta Foothills ³		S Alberta Plains subsurface ⁴		N Montana ⁵	
		SANTONIAN		Puskaskau Fm		Puskaskau Fm		Puskaskau Fm		Wapiabi Fm		Milk River Fm	
CONIACIAN		Dowling M (part) Bad Heart Fm Marshybank Fm		Thistle M Dowling M Bad Heart Fm		Thistle M Dowling M Bad Heart Fm		Thistle M Dowling M Marshybank M		First White Specks M Medicine Hat M		Kevin M	
Muskiki Fm		Muskiki Fm		Muskiki Fm		Muskiki Fm		Muskiki M		Verger M			
TURONIAN		Cardium alloformation		Cardium Fm		Cardium Fm		Cardium Fm		Niobrara Fm		Marias River Fm	
Blackstone Fm (part)		Kaskapau Fm (part)		Kaskapau Fm (part)		Kaskapau Fm (part)		Blackstone Fm (part)		Cariile Fm (part)			

¹Plint et al., 1986, 1990, allostratigraphy.

²Stott, 1967, lithostratigraphy.

³Stott, 1963, lithostratigraphy.

⁴Nielsen et al., 2003, 2008.

⁵Cobban et al., 1976, lithostratigraphy.

Abbreviations: Fm = Formation; M = Member.

FIG. 2. Summary of stratigraphic schemes that have been applied to Upper Cretaceous strata in Alberta, British Columbia and northern Montana. The far left column shows the allostratigraphically defined limits of the Cardium alloformation, the base of which (surface E1) is placed below the lithostratigraphically defined position of Stott (1963, 1967).

dig and Kevin members of the Marias River Formation, allowing them to establish a broad correlation with the Cardium Formation and the Muskiki and Marshybank members of the Wapiabi Formation in Alberta. Cobban et al. (2005) made a detailed study of a thin (typically 10–20 cm) carbonate-cemented conglomerate bed (Bed 100 of the Kevin Member; Cobban et al., 1976) that, because it was so distinctive and widespread, was named by Cobban et al. (1959) the MacGowan Concretionary Bed. The bed contains small, well-rounded chert pebbles as well as reworked

phosphate nodules and molluscan fossils. This bed lies at, or just above, the boundary between middle and upper Coniacian strata. A second bed of green-stained phosphate nodules, some of which are bivalve steinkerns, is located 3.5 m above the MacGowan Bed at the Type Section of the Kevin Member (Bed 108 of Cobban et al., 1976). Cobban et al. (2005) speculated that the MacGowan Bed in Montana might be correlative with the erosion surface documented beneath the Bad Heart Formation in Alberta, 850 km to the NW (Plint et al., 1990; Donaldson et al., 1998, 1999).

ALLOSTRATIGRAPHIC STUDIES

PREVIOUS WORK

Regional allostratigraphic correlation of Coniacian rocks was initially conducted in northwestern Alberta and adjacent BC, where it was shown that upward-coarsening successions, bounded by marine flooding surfaces, could be traced for several hundred km in the subsurface, and also correlated into outcrop (Norris, 1989; Plint, 1990; Plint et al., 1990; Plint and Norris, 1991). These studies showed that the erosion surface that defined the *top* of the “Bad Heart” Formation in the foothills could be correlated with an erosion surface that defined the *base* of the type Bad Heart in the Peace River Plains. Plint et al. (1990) therefore proposed that Stott’s term “Marshybank” be applied to *all* siltstone and sandstone facies overlying the Muskiki mudstones, throughout the foothills (fig. 2). The sandy and ooidal Bad Heart Formation was shown to be restricted to the plains, where it onlaps westward onto the top of the Marshybank Member and pinches out before reaching outcrop (Donaldson et al., 1998, 1999). Subsequent study of additional outcrop and surface sections in the Peace River Plains, coupled with dinoflagellate biostratigraphy, confirmed the existence and significance of the erosional contact between the Bad Heart Formation and the underlying Muskiki Formation, or older strata (Kafle et al., 2013).

Within the Muskiki Member, Plint (1990) traced two regional flooding surfaces, informally termed M1 and M2 (equivalent to surfaces CS4 and CS15 in the present study), and also divided the Marshybank Member into 12 informal “units, termed A through L, bounded by erosion surfaces. Simple upward-coarsening “parasequences” in the offshore part of the basin could be traced westward (landward) to areas where the rocks became sandier and commonly included clean, well-sorted, hummocky- and swaley-cross-stratified sandstone deposited in a shoreface environment (Plint, 1991; Plint and Norris, 1991). Where exposed in the Rocky Mountain Foothills, most shoreface sand-

stone bodies have a sharp, erosional basal contact that was interpreted as evidence for deposition during relative sea-level fall (Plint, 1991; Plint and Norris, 1991). Thus it could be shown that upward-shoaling “parasequences” deposited offshore, passed laterally landward into “sequences” that preserved evidence for both relative sea-level rise and fall. The sharp-based shoreface sandbodies in the Marshybank Member provided some of the initial stimulus to develop the concept of “forced regression” (Plint, 1991), and ultimately, contributed to the establishment of the falling-stage systems tract (Plint and Nummedal, 2000), which is now the widely accepted “fourth component” of the standard depositional sequence model (e.g., Catuneanu, 2006).

A reconnaissance study by Durbano (2009), extended allostratigraphic correlations southward, enabling Grifi (2012) to establish an allostratigraphic scheme for Coniacian rocks over 60,000 km² of southern Alberta, extending from Township 26 southward into the most northerly Montana Plains (fig. 3, *inserted after p. 52*). Grifi (2012) extended correlations from the subsurface of Alberta and Montana to outcrop sections, including the Type Section of the Kevin Member of the Marias River Formation, and to various sections in the Alberta Foothills. It was shown that depositional sequences in the lower (Coniacian) part of the Kevin Member in the Type Section near Kevin, MT, could be correlated, via wireline logs, to the Muskiki and Marshybank rocks in Canada (Grifi et al., 2013). Current investigation (Hooper, in prep.) has now linked the correlations of Plint (1990) and Grifi (2012) in the area between townships 26 and 44 (fig. 3).

DATA AND METHODS

The results reported here are founded on a series of linked studies that, collectively, involved over 4800 wireline well logs, 74 outcrop sections, and 30 cores, spanning about 200,000 km² of the foredeep in Alberta and northern Montana (Norris, 1989; Plint, 1990; Plint and Norris, 1991; Donaldson, 1997; Donaldson et al., 1998, 1999; Durbano, 2009;

Grifi, 2012; Grifi et al., 2013; Hooper, Ph.D. in prep.; fig. 3, *after p. 52*). Allostratigraphic units were defined by marine flooding surfaces, recognizable in wireline logs by an abrupt increase in gamma-ray intensity and a decrease in resistivity, corresponding to an increase in clay content. These surfaces were traced and “looped” through grids of log cross sections to ensure that they were correlated consistently (figs. 4–13, *inserted after p. 52*). Outcrop sections in the foothills were palinspastically restored using balanced structural cross sections constructed by Rotenfusser et al. (2002) on the basis of outcrop mapping, drilling, and seismic data. On the base map (fig. 3), outcrop sections relevant to the present study are shown in their present and restored positions, and distances between wells and outcrop are noted on the cross sections (figs. 4–13, *after p. 52*).

Most major outcrop sections of Coniacian strata exposed in the Rocky Mountain Foothills were measured in detail, with particular attention paid to depositional cyclicity and bounding surfaces that were indicative of relative sea-level changes (appendix 1). A gamma-ray log was made for selected outcrop sections using an *Exploranium GR-130* portable gamma-ray spectrometer, with a sampling period of 30 seconds per site. Simultaneous collection of in situ molluscan macrofauna was conducted, with specimens located precisely in each measured section.

All fossil material collected during this investigation is archived at the Royal Tyrrell Museum of Palaeontology. Details of specimens and accession numbers are given in Walaszczyk et al. and Landman et al., in this issue.

ALLOSTRATIGRAPHIC TERMINOLOGY

In order to make an allostratigraphic description of the Muskiki and Marshybank strata, it is necessary to give names to both the stratigraphic *surfaces* that bound rock units as well as to the *rock units* themselves. In the following discussion, the regionally mappable flooding surfaces within Coniacian rocks have been designated as CS1 (Coniacian surface 1) to CS23. The erosion surface separating the Cardium Formation from the

overlying Muskiki Member is termed E7 following Plint et al. (1986), and the basal surface of Santonian strata is designated SS0 (Santonian surface 0). Allostratigraphically defined rock units are designated CA1 (Coniacian allomember 1) to CA24. Note that allomembers defined herein are considered to be informal stratigraphic units, designated by letters and numbers rather than formally defined names, and therefore are not capitalized in the text (NACSN, 2005).

CARBON-ISOTOPE ANALYSIS

Seven sections through Coniacian rocks (six outcrop, one core) were selected for carbon-isotopic analysis. Results of carbon-isotope analysis for the Cutpick Creek section (fig. 4) are reported here (appendix 2). At this site, 106 samples were collected at 1 m intervals from all lithologies except clean sandstone, in which the organic matter content was too low. Analyses were undertaken at the Stable Isotope Biogeochemistry Laboratory at the University of Durham. Rock samples were ground to a fine powder (ca. 10 μm) using a Retsch agate mortar grinder RM100. The bulk rock powders (ca. 5 mL) were decalcified overnight at room temperature (20° C) using a 3 M HCl solution in 50 mL centrifuge tubes. Insoluble residues were rinsed three or four times in deionized water, dried at 50° C, reground in an agate mortar, and stored in glass vials.

Organic carbon isotope ($\delta^{13}\text{C}_{\text{org}}$) measurements were performed on 2.5–3 mg splits of the insoluble residues using a Costech elemental analyser (ESC 4010) connected to a Thermo Scientific Delta V Advantage isotope ratio mass spectrometer via a Conflo III interface. Carbon isotope ratios are corrected for ^{17}O contribution and reported in standard delta (δ) notation in per mil (‰) relative to VPDB. Data accuracy was monitored through analyses of international and in-house standards calibrated against the international standards (viz., IAEA 600, USGS 24, and USGS 40). Analytical uncertainty for carbon isotope measurements was $\pm 0.1\text{‰}$ for replicate analyses of standards and $< 0.2\text{‰}$ on replicate sample analyses.

ESTABLISHING REGIONAL ALLOSTRATIGRAPHIC CORRELATIONS

A series of cross sections (figs. 4–13) that integrate wireline logs with outcrop sections, form the physical basis for the new allo- and biostratigraphic scheme presented here. To constrain the stratigraphic relationships between separate outcrop sections scattered along the Rocky Mountain Foothills, a summary, strike-oriented (NW–SE) well-log cross section was constructed (fig. 4), extending more than 750 km from Cutpick Creek, NW Alberta (in the vicinity of Grande Cache; Township 58, latitude 54° 5' N), to Kevin, Montana (latitude 49° 45' N; fig. 3). The correlations shown in the strike section are tightly constrained by a large grid of cross sections to the north and east, which are not shown on the base map (Plint, 1990; Grifi, 2012, Hooper, Ph.D. in prep.; fig. 3). Each principal section exposed in the Foothills between Cutpick Creek in the north, and Kevin in the south was correlated to this master cross section using wireline logs, some of which were from wells drilled in the deformed belt (figs. 3, 5–13).

Systematic tracing of marine flooding surfaces through the regional correlation grids of Plint, (1990), Grifi (2012) and Hooper (in prep.), showed that 24 flooding surfaces, designated CS1 to CS23 and SS0, were particularly robust, and could be traced through large parts, if not all of the study area (figs. 4–13).

THE CHARACTER AND SIGNIFICANCE OF FLOODING SURFACES

Although each of the studied allomembers is typified by one or more, upward-coarsening successions (e.g., fig. 14), the nature of the flooding surface that bounds each allomember is variable. Four categories of surface are recognized: either the surface lacks a coarse-grained lag, or one of three types of granule to pebble lag is present. It is important to appreciate that these lags, which may be up to about 20 cm thick, can also be very discontinuous across a given exposure, to the

extent that, on a lateral scale of a few meters, coarse grains may be *entirely absent* from some parts of the flooding surface (fig. 15). In some places, it is clear that lag deposits are confined to shallow erosional depressions on the flooding surface (fig. 16).

No coarse-grained lag: Flooding surfaces CS2, CS3, CS7, and CS9 have no coarse-grained lag and are characterized by an abrupt upward transition from coarser- to finer-grained sediment at which there is no evidence for concentration or winnowing of coarser grains, or formation of an irregular erosion surface. This type of flooding surface provides no evidence of relative sea-level fall and concomitant sea-floor erosion, and therefore is parsimoniously interpreted to record only relative sea-level rise and shoreline transgression, accompanied by a decrease in the volume and caliber of sediment supplied to the shelf.

Lag of intrabasinal clasts: Flooding surfaces CS6 and CS14 locally have a lag comprising intrabasinal phosphate and/or siderite pebbles that range in diameter up to about 100 mm. These clasts are indicative of some degree of erosion, probably to a depth of at least several dm, sufficient to expose early diagenetic nodules and to allow their concentration on the erosion surface. The presence of reworked intraclasts suggests that a phase of relative sea-level fall terminated deposition of the underlying allomember. The absence of extrabasinal pebbles suggests that erosion took place subaqueously, although subaerial emergence can not be ruled out. Subsequent relative sea-level rise reduced current energy at the bed, allowing the clasts to be buried in mud.

Lag of mixed extra- and intrabasinal clasts: In foothills exposures, flooding surfaces E7 and CS1, CS4, CS8, CS11, CS13 and CS15 to CS23 inclusive are, at least locally, mantled with a mixture of extrabasinal chert pebbles, typically 5–15 mm in diameter, and intrabasinal phosphate and siderite pebbles, typically 20 to 100 mm in diameter. Because of the asymmetry of wave-generated currents in shallow water, pebbles are not transported seaward across a marine shelf for

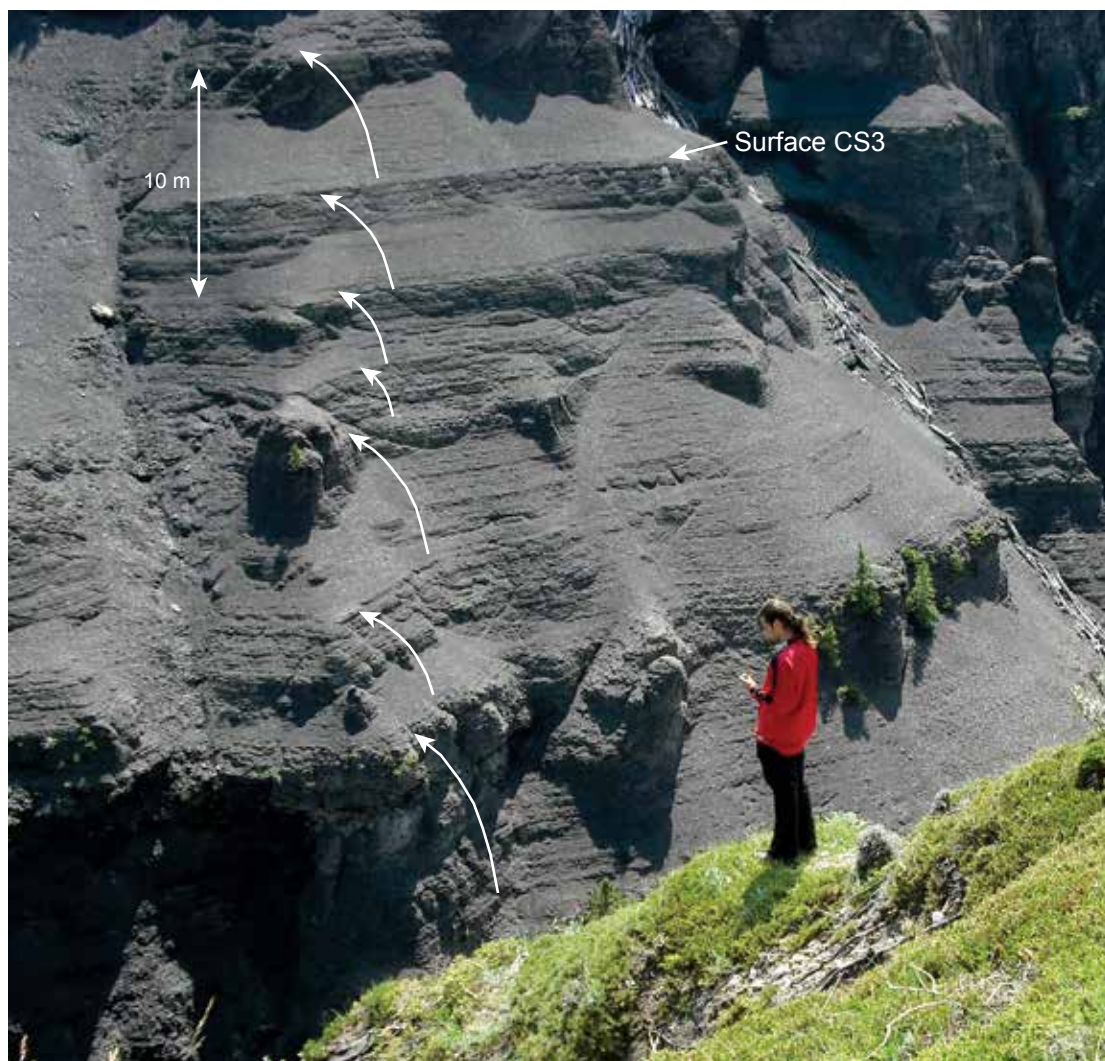


FIG. 14. A portion of the Muskiki Member exposed in Sheep River (fig. 11), illustrating typical sandier-upward successions (arrows) bounded by flooding surfaces. The regionally mappable surface CS3 is indicated.

more than a few hundred m to a few km from shore (e.g., Clifton, 2006), and it is not possible to concentrate chert pebbles by winnowing underlying sediment lacking such clasts. It is therefore concluded that the presence of chert pebbles on a flooding surface is an indication that the surface had previously been subaerially exposed, when extrabasinal pebbles were supplied by rivers flowing to a lowstand shoreline. This interpretation was initially advanced to

explain the extensive mantles of chert pebbles on erosion surfaces in the Cardium Formation (e.g., Plint et al., 1986). Applying similar reasoning, it is inferred that at least the more westerly parts of the chert pebble-bearing surfaces in the Muskiki and Marshybank members experienced a phase of subaerial exposure.

Lag of mixed extra- and intrabasinal clasts in a matrix of ferruginous clay ooids: In the southern portion of the study area, flooding surface



FIG. 15. **A.** Overview of surface CS1 exposed at river level at the mouth of Oldfort Creek (fig. 10). At right, a coarse-grained wave ripple composed of granules and small pebbles of chert and quartz rests sharply on regional erosion surface CS1. Traced laterally over only 3 m, the coarse lag pinches out and surface CS1 is manifest simply as a sharp mud-on-mud contact; scale bar = 20 cm. **B.** Detail of the coarse-grained wave ripple.

CS23 is overlain by 0.1 to 1.2 m of ooidal ironstone, the base of which is sharp but typically intensely burrowed by a *Glossifungites* ichnofauna (fig. 17). Well-rounded chert pebbles, typically 5–15 mm in diameter, and somewhat larger phosphate pebbles are distributed throughout the ooidal ironstone, which lacks stratification and appears to be highly bioturbated. Ooidal ironstone is commonly interpreted to form under conditions of protracted clastic sediment starvation, accompanied by repeated winnowing and erosion of the sea floor in shallow water (e.g., Donaldson et al., 1999, and references

therein). Regional correlation shows that the ooidal ironstone, which forms a patchy blanket across southern Alberta and northern Montana, is spatially coincident with a region of subtle stratal upwarp, across which Upper Coniacian strata are either very thin or absent (Griff, 2012; figs. 4, 9–11). Stratigraphic relationships therefore suggest that, for much of late Coniacian time, the region blanketed by ooidal ironstone was either subaerially emergent, or so shallowly submerged that no clastic sediment could be accommodated, leading to the formation of a regional unconformity. Deposition of ooidal



FIG. 16. Intraclastic pebble lag resting on surface SS0 at Thistle Creek west (fig. 5). **A.** General view of siderite pebbles seen from above; scale bar in each image = 20 cm. **B.** Detail of panel A showing pitted, bioeroded surface of a siderite pebble. **C.** Side view of conglomerate showing clasts filling a shallow erosional trough (arrows).

ironstone above the unconformity is interpreted to have taken place in shallow water across a clastic-starved ramp during the early stage of relative sea-level rise in latest Coniacian time. Toward the northwest, the ooidal ironstone appears to be stratigraphically equivalent to up to 20 m of sandy siltstone that forms allomember CA24; this wedge-shaped allomember accumulated in an area of active flexural subsidence.

USE OF DISTINCTIVE FLOODING SURFACES TO ESTABLISH CORRELATION TO OUTCROP

In order to establish, on a regional scale, the stratigraphic distribution of molluscan faunas collected at outcrop, it was necessary to trace flooding surfaces westward from the master

strike line (fig. 4), via well logs, to studied outcrop sections in the Rocky Mountain fold-and-thrust belt. For most sections, correlation to subsurface was relatively straightforward, based on matching upward-coarsening depositional successions, a process greatly facilitated by the outcrop gamma-ray log that provided an objective measure of lithology. It is emphasized that the process of outcrop to subsurface correlation was based, as far as was possible, on matching the scale and lithological character of depositional successions, and certain thick bentonites seen at outcrop, with those represented in the nearest wireline well logs; wherever possible, the distribution of molluscan fauna was not used as a basis for correlation. This approach was intended to provide an independent check

on the relationship between depositional cyclicality and the stratigraphic distribution of molluscan fossils. A number of distinctive physical stratigraphic markers helped to constrain correlations between outcrop and well log, as discussed below.

E7 surface. The E7 surface separates the Cardium Formation from the overlying Muskiki Member, and constitutes a prominent and robust stratigraphic marker across the basin. In the vicinity of the foothills and in the adjacent subsurface, E7 has up to several tens of meters of erosional relief in the form of NW–SE elongate, NE-facing “steps” (e.g., Wadsworth and Walker, 1991). In consequence, the thickness of rock between E7 and overlying surfaces CS1 and CS2 can vary dramatically, reflecting the progressive onlap and burial of preexisting topography by lower Muskiki sediments. The E7 surface has a ubiquitous mantle of extrabasinal chert and quartz pebbles, typically a few cm to a few dm thick.

Surface CS1. Surface CS1 is a robust log marker that caps a distinct, upward-coarsening succession of mudstone, siltstone, and very fine-grained sandstone. In most outcrop sections, CS1 is mantled by a few mm to a few cm of anomalously coarse-grained sediment that may range from medium-grained sand to granules or small siliceous pebbles that may be molded into large-scale wave ripples (fig. 15). This thin but distinctive, coarser-grained lag forms a consistent stratigraphic marker. In some sites (e.g., Oldfort Creek, fig. 10), the granule lag on CS1 was discontinuous across an exposure tens of meters wide (fig. 15), raising the possibility that the apparent absence of the lag at some sites (e.g., Blackstone River, fig. 6, Highwood River and Sullivan Creek, fig. 12) may be attributed simply to limited lateral exposure.

Surface CS4. Over much of the study area, surface CS4 caps a prominent, sandier upward heterolithic succession, typically 10–20 m thick, comprising cm-scale interbeds of wave-rippled, very fine-grained sandstone and mudstone in which the bioturbation index (BI) is very low (fig. 18A). In the more westerly foothills expo-

tures, such as Bighorn Dam, Bighorn River, Wapiabi Creek, and Sheep River (fig. 18B, C), CS4 is mantled by a mm to cm-scale lag of small phosphate and chert pebbles typically <5 mm in diameter, whereas in more eastern sections, this lag is absent.

Surface CS11. In the north, at Cutpick Creek (fig. 4) allomember CA11 is mantled by a few cm of chert and intraclastic pebbles dispersed through a sideritized mudstone matrix. Allomember CA11 has a distinctive log signature that can be traced southward in well logs (fig. 4). However, the upper surface, CS11 does not carry a pebble lag in the more southerly outcrop sections described here. Instead, at Chungo Creek, Bighorn Dam, Sullivan Creek, and Highwood River, CS11 is mantled by a sharp-based, cm-scale bed of clean, fine- to medium-grained sandstone that forms hummocky cross stratification (HCS) or combined-flow ripples, or fills gutter casts. This thin bed suggests some degree of storm-winnowing and erosion of the top of allomember CA11 that could be an expression of relative sea-level fall.

Surface CS14. Throughout the central foothills, between Thistle Creek (fig. 5) and Mill Creek (fig. 13), surface CS14 marks an abrupt facies boundary between underlying, cm-scale interstratified very fine-grained sandstone and mudstone, and overlying, intensely bioturbated siltstone and silty sandstone that characterizes the lithostratigraphic Marshybank Member (e.g., Stott, 1963; fig. 19A). In wireline logs, particularly toward the east, CS14 is manifest as a distinct “hot” spike on the gamma ray log, suggestive of an enrichment in clay and/or organic matter. Locally, as at Cardinal River (fig. 5), Burnt Timber Creek (fig. 9), and Sheep River (fig. 11), CS14 is mantled by a thin lag of siderite and phosphate pebbles. Toward the north, CS14 is truncated by CS15 (fig. 4).

Surface CS15. In the north at Cutpick Creek, CS15 is mantled by chert pebbles and lithic intraclasts. From north to south, CS15 progressively truncates allomembers CA11, 12, 13, 14, and 15 (fig. 4). Surface CS15 persists southward



as a distinctive flooding surface until Township 36, where it is truncated by surface CS23. Traced westward, CS15 is a subtle flooding surface, locally mantled with chert and/or intraclastic pebbles, seen at Bighorn Dam and Bighorn River (fig. 7), Burnt Timber Creek (fig. 9), and Sullivan Creek (fig. 12).

Surface CS16. This surface caps a very widespread sandier-upward succession that, in the north, includes dm-scale sandstone beds with HCS, (e.g., Cutpick Creek, fig. 4). Within allomember CA16, stratified sandstone in the north grades laterally into highly bioturbated silty sandstone toward the south (e.g., figs. 5, 6, 7). Surface CS16 is mantled in the north by chert pebbles whereas to the south, pebbles are absent and the surface may be marked by a subtle flooding surface, or simply a band of large siderite nodules.

Surfaces CS17 to CS22. Surfaces CS17 to 22 are either mantled with a veneer of chert pebbles, or have an irregular, eroded upper surface and/or deep burrows, including *Thalassinoides*, suggestive of a firm-ground and early lithification. This suite of surfaces is here represented only at Cutpick Creek (fig. 4), but most of these surfaces have been traced for at least 150 km further to the NW of the present study area (Plint, 1990; Plint and Norris, 1991).

Surface CS23. An overall upward-coarsening succession is evident in the lithostratigraphic Marshybank Member (i.e., those rocks above CS14). The upper boundary of that regressive succession (i.e., the maximum regressive surface) is surface CS23 (fig. 20). This is a regional-scale surface that has been traced for 150 km to the north of the present study area (Plint, 1990),

and for at least 300 km into Montana to the south of the study area (e.g., Cobban et al., 2005), for a minimum N–S extent of at least 1200 km (fig. 21). Surface CS23 is typically mantled by a lag of chert pebbles and/or intraclasts (phosphate, siderite) that form a layer that may range from a layer only one clast thick to a layer several dm (and exceptionally a few m) thick. South of about Township 26, and extending at least 170 km east to Range 13 W4, CS23 is overlain by 0.1 to 1.2 m of ooidal ironstone containing scattered small chert and phosphate pebbles, and typically pervasively cemented by siderite (Grifi, 2012; fig. 17). The basal surface of the ooidal ironstone is sharp, erosive, and typically highly burrowed (fig. 17). This pebbly ooidal ironstone is correlative with the MacGowan Concretionary Bed mapped over a large part of Montana by Cobban et al. (2005; fig. 4).

Surface SS0. Above CS23, bioturbated silty sandstone and siltstone form allomember CA24, which is an eastward-thinning unit up to about 20 m thick (e.g., fig. 8). CA24 comprises an overall upward-fining stack of meter-scale, upward-coarsening successions bounded by flooding surfaces that commonly are mantled by a mixture of chert, siderite and phosphate pebbles (e.g., fig. 16). Successive upward-coarsening successions show a gradual upward decrease in BI, with progressively better preservation of cm-scale primary stratification. The top of this relatively coarse-grained package is marked by a sharp or abruptly gradational (few cm) transition, at surface SS0, into dark grey, thinly bedded mudstone with a BI of 0–1, characterized by a much higher radioactivity than the underlying

FIG. 17. **A.** Ooidal ironstone containing small chert pebbles overlying a heavily bioeroded surface near the top of the Coniacian succession on Sullivan Creek (fig. 12). The base of the ironstone is flooding surface CS23. Flooding surface CS15 is mantled with cm scale rounded siderite and phosphate pebbles and surface CS14 marks the boundary between underlying, well-stratified sandstone and mudstone and overlying, highly bioturbated sandy siltstone. **B.** Detail of bioerosion on the base of the ooidal ironstone shown in (A). Arrows indicate cm scale *Thalassinoides*, whereas larger irregular erosional structures may also be attributed to *Thalassinoides*, but may be the result of burrowing by larger arthropods and are perhaps comparable to the “subway tunnels” described from the Cardium Formation (Pemberton et al., 1984); scale bar = 20 cm. **C.** Detail of the ooidal ironstone above surface CS23 at Mill Creek (fig. 13). A dense network of large *Thalassinoides* (arrows) penetrate up to 30 cm into the underlying sandy siltstone; hammer is 28 cm long.



FIG. 18. **A.** Overview of the lower part of the Coniacian succession at Burnt Timber Creek (fig. 9) illustrating depositional cyclicity and bounding surfaces E7 and CS1 to CS5. Note the prominent sandier-upward succession culminating in surface CS4. **B.** Overview of part of the Sheep River canyon (fig. 11). The CS4 surface caps an upward-coarsening package that, in this view, is repeated by a thrust fault; Walaszczyk (circled) provides an indication of scale. **C.** Detailed view of the subtle, but sharp CS4 surface that is mantled with a few mm of chert and phosphate pebbles and granules and separates bioturbated siltstone and very fine-grained sandstone below from silty clay above.

rock (fig. 19B). SS0 is particularly prominent in the western part of the study area where the contrast between under- and overlying lithologies is greatest; SS0 gradually becomes more subtle toward the east as allomember CA24 thins. Toward the north, SS0 gradually onlaps onto surface CS23 such that the two surfaces are indistinguishable at the scale of well logs (fig. 4). Where exposed at Cutpick Creek, CS23 lies at the base of a 1 m thick conglomerate capping the Marshybank Member, and SS0 may lie at the same surface, or possibly may be unrecognizable within, or at the top of the conglomerate.

CONTINUITY OF BOUNDING SURFACES

Figures 4 to 13 show that most of the flooding surfaces that bound allomembers can be traced as nearly parallel surfaces for at least 750 km along the strike of the proximal foredeep, and for many tens of km westward to outcrop. Locally, however, some allomembers do lap out. Allomembers CA1 and CA2 onlap locally against erosional topography on the underlying E7 surface (e.g., fig. 4 between wells 3-16-53-25W5 and 10-30-54-25W5). Allomembers CA3 to CA14 form a near-tabular set of strata, traceable throughout most of the strike section. However,

allomembers CA5 and CA9 lap out northward whereas CA6 and CA8 lap out southward (fig. 4). Allomembers CA16 to CA23 are confined to a northern depocenter (fig. 4), and extend beyond the northern limit of the present study area. To the east of the proximal foredeep, a number of disconformities have been recognized, across which various allomembers lap out, or are truncated (Hooper and Plint, 2016; Hooper, Ph.D. in prep.). These stratal terminations take place across narrow linear regions that might reflect differential subsidence and uplift across underlying structures (cf. Griff et al., 2013); discussion of this aspect of the stratigraphy is beyond the scope of the present study.

SEDIMENTOLOGY

The focus of this paper is on regional stratigraphy and, in consequence, only a brief account of the principal sedimentary facies is given here. The Muskiki Member is dominated by mudstone with a variable proportion of interstratified fine- to very fine-grained sandstone, whereas the Marshybank Member includes both bioturbated sandy siltstone and various types of clean, well-sorted sandstone. Five facies are distinguished here.

Stratified silty mudstone typically has a low BI (0–2) and consists of mudstone interstratified with mm-scale, sharp-based beds of coarse siltstone that may have planar or wave-rippled upper surfaces. The rock may have a rusty weathering appearance, and siderite nodules vary from absent to common (fig. 22A, B). Silt and clay are interpreted to have been transported seaward, primarily by storm-generated combined flows (cf. Plint et al., 2012b; Buckley et al., 2016). A low level of bioturbation indicates a sparse metazoan infauna, suggestive of stressed conditions, probably attributable to a low dissolved oxygen content (i.e., 2–5 mg/L⁻¹) in the bottom water (cf. Dashtgard et al., 2015; Dashtgard and MacEachern, 2016). Rusty weathering is an indication of abundant disseminated pyrite. Siderite nodules are a relatively early diagenetic mineral, precipitated from pore water with a

high bicarbonate (derived from organic matter), and low dissolved sulfide content, the latter having been removed by prior pyrite formation (McKay et al., 1995). This facies is interpreted to represent a relatively distal (order of 100 km or more) offshore environment, above storm wave-base for mud (?50–70 m water depth, cf. Plint et al., 2012b; Plint, 2014).

Bioturbated silty mudstone typically has a faintly stratified to rubbly appearance at outcrop as a result of intense bioturbation (BI 4–6; fig. 22C). Siderite nodules are common in this facies and may be scattered, or concentrated in bands. A high degree of bioturbation indicates a thriving metazoan infauna, suggesting a bottom water dissolved oxygen level of >5 mg/L⁻¹ (Dashtgard et al., 2015). Common siderite suggests that a higher level of oxygen in the pore water inhibited pyrite formation, allowing more iron to be available for siderite precipitation, which took place in the methanogenic zone, some distance below the sea floor (e.g., McKay et al., 1995). Sediment transport was primarily by storms and deposition took place closer to shore, and in somewhat shallower water than the stratified silty mudstone facies. The bottom water contained a higher dissolved oxygen content, promoting colonization by a benthic metazoan fauna.

Interstratified mudstone and very fine-grained sandstone is bedded on a cm scale (fig. 22A). Sandstone beds are always sharp-based, commonly with wave- or combined-flow ripples. The facies may have a red, rusty-weathering appearance, has a low BI (0–1) and generally lacks siderite nodules. The rusty-weathering appearance reflects abundant early diagenetic pyrite that formed in anaerobic pore fluids at a very shallow burial depth (McKay et al., 1995). Physical sedimentary structures indicate deposition from storm-generated combined flows above wave-base for very fine sand (?30–40 m). However, the low intensity of macroscopic bioturbation suggests that the bottom water had a low (i.e., 2–5 mg/L⁻¹) dissolved oxygen content that suppressed colonization by benthic macrofauna, resulting in well-preserved stratification.



Bioturbated sandy siltstone to silty sandstone characterizes the more southern portion of the Marshybank Member (e.g., at Cardinal River, Bighorn Dam, Ram River, Cripple Creek; figs. 5, 7, 8). This facies appears abruptly above surface CS14 and persists to surface SS0 (fig. 19A). Although cm-scale beds of very fine-grained sandstone are discernable at intervals, most of the rock lacks stratification as a consequence of intense bioturbation (BI 5-6) by infauna of the *Cruziana* ichnofacies. Rounded nodules of siderite, typically 10–30 cm in diameter, are commonly arranged in bands throughout the facies. In far western exposures, such as Bighorn River, dm-scale, sharp-based, moderately bioturbated, very fine-grained sandstone beds are preserved (fig. 20B). Overall, this facies is interpreted to represent an inner shelf to lower shoreface environment in perhaps 10–30 m of water. Preserved, sharp-based sandstone beds suggest deposition from storms. However, pervasive bioturbation has destroyed most primary sedimentary structures, indicating that the sediment hosted a thriving metazoan infauna, supported by well-oxygenated bottom water and an abundant supply of organic matter (e.g., MacEachern et al., 2010; Dashtgard et al., 2015). The overall upward-coarsening succession between surfaces CS14 and CS23 suggests long-term shoreline progradation, upon which numerous minor, higher-frequency transgressive-regressive events were superimposed. The great lateral extent (>>100 km) of these minor successions suggests an allogenic (sea-level) rather than autogenic control. Depositional successions from CS23 up-section to SS0 are also composed of this facies, but are organized in an overall back-stepping, upward-fining pattern suggestive of long-term

shoreline transgression, culminating in dark stratified mudstone above SS0 (fig. 19B).

Well-sorted sandstone with minor siltstone is confined to the northern portion of the Marshybank Member. The basic sedimentary motif comprises sandier-upward successions of siltstone and sandstone (fig. 23). Siltstones are commonly moderately to highly bioturbated (BI 3–6) whereas sandstones are well-sorted, well-stratified and generally weakly bioturbated. Sharp-based, cm- to dm-scale beds of very fine-grained sandstone commonly preserve wave ripples and hummocky cross stratification with a variable overprint of bioturbation. Meter-scale, sharp-based, fine-grained sandstone bodies show swaley cross stratification or planar lamination (fig. 23). Sandstone in this facies provides good evidence for deposition under the influence of storm waves in an inner shelf to shoreface setting (e.g., Cheel and Leckie, 1993; Plint, 2010). Swaley cross-stratified sandstone bodies are sharp-based, typically underlain by large gutter casts, and are assigned to the falling-stage systems tract, interpreted to have been deposited during relative sea-level fall (Plint and Nummedal, 2000). The stacked, upward-shoaling, shelf to shoreface successions can be mapped for 200 to 300 km along strike, suggesting that they record an allogenic, sea-level control, rather than a more localized autogenic effect such as delta-lobe switching.

PRINCIPAL MOLLUSCAN ZONES

Although physical allostratigraphic correlation provides a good basis for understanding regional stratigraphy, confidence in correlation is greatly strengthened by integration of key ele-

FIG. 19. **A.** Overview of the upper part of the Coniacian succession at Cardinal River, showing the sharp boundary at surface CS14 that separates well-stratified mudstone and sandstone below from intensely bioturbated silty sandstone above. **B.** Overview of the upper part of the Coniacian succession at Ram River, showing the transition from intensely bioturbated silty sandstone below 137.5 m level, into bioturbated siltstone up to 141 m, above which siltstone gradually becomes darker and contains more inter-stratified very fine-grained sandstone up to surface SS0, above which the first Santonian fauna is found.



FIG. 20. **A.** The upper part of the Marshybank Member at the Bighorn Dam section (fig. 7). Surface CS23, which is mantled with chert and siderite pebbles, marks a maximum regressive surface and is overlain by four subtle upward-coarsening successions culminating in surface SS0. **B.** Upper part of the Marshybank Member exposed on the Bighorn River (fig. 7) showing bioturbated sandy siltstone grading up into weakly stratified silty sandstone, the top of which is marked by surface CS23.

ments of the molluscan fauna. Five key biostratigraphic events have been identified based on inoceramids (fig. 24; see Walaszczyk et al., this issue, for detailed discussion):

1. *Cremnoceramus crassus crassus* appears immediately above the E7 surface, as documented by Walaszczyk et al. (2014). This fauna persists up to surface CS4.
2. *Inoceramus gibbosus* fauna is present only in allomembers CA2–CA4 and is not found above surface CS4. This fauna characterizes the uppermost zone of the lower Coniacian.
3. *Volvicceramus koeneni*, in association with *V. undabundus*, *V. exogyroides*, and *V. cardinalensis*, appears immediately above surface CS4, which marks the base of the middle Coniacian (see also Walaszczyk and Cobban, 2006). *V. involutus* appears slightly higher, above surface CS7.
4. *Sphenoceramus subcardissoides* appears in the upper part of allomember CA15, which is the basal unit of the upper Coniacian, defined by the first occurrence of *Scaphites* (*S.*) *depressus*.
5. *Sphenoceramus pachtii* coappears with *Clioscaphtes saxitonianus* immediately above surface SS0, and both mark the base of the Santonian.

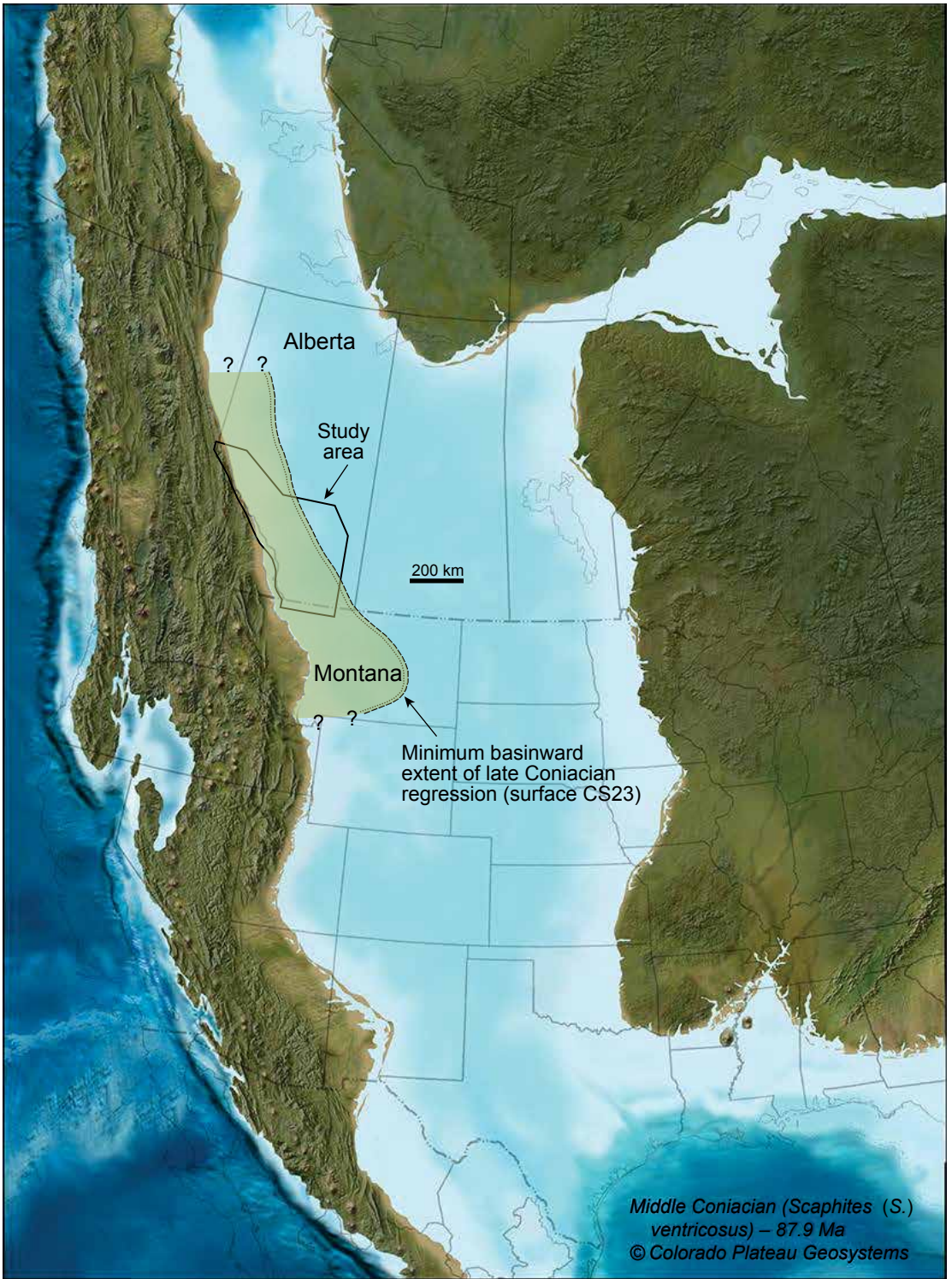
Four key biostratigraphic events have also been identified based on scaphitid ammonites (Landman et al., this issue):

1. The lowest occurrence of *Scaphites* (*S.*) *preventricosus* is just above erosional surface E5.5 in the Cardium alloformation, which marks the beginning of a major transgression, just below the base of the lower Coniacian (Walaszczyk et al., 2014).
2. The lowest occurrence of *S.* (*S.*) *ventricosus* is immediately above surface CS2 in allomember CA3, just below an interpreted highstand and prior to major regression that culminates at surface CS4 that marks the lower to middle Coniacian boundary.
3. The lowest occurrence of *S.* (*S.*) *depressus* is in allomember CA15, immediately above surface CS14 in an overall regressive succession that marks the base of the upper Coniacian.
4. The lowest occurrence of *Clioscaphtes saxitonianus* is at the base of the Santonian (surface SS0), coinciding with a major transgression and a marked change in facies to deeper-water, more offshore mudstone.

CARBON-ISOTOPE STRATIGRAPHY

Regional stratigraphic correlation (fig. 4) shows that the Cutpick Creek section contains six discontinuities at surfaces E7, CS4, CS8, CS11, CS15, and CS23. In representing the carbon-isotope stratigraphy for this section, it is necessary to accommodate these hiatuses. The stratigraphic log, as well as the corresponding carbon-isotope curve, is therefore presented in an “expanded” form to include gaps that are approximately proportional to the thickness of the missing parts of the section (fig. 25). Tie-points between Alberta and the UK Chalk succession (Jarvis et al., 2006), were established on the basis of: (1) The lowest occurrence of *Cremnoceramus crassus crassus* immediately above the E7 surface and (2) The lowest occurrence of *Volvicceramus koeneni* immediately above surface CS4. The lowest occurrence of *Clioscaphtes saxitonianus* was inferred, based on correlations in figures 4–13, to be at or immediately above surface SS0. Unfortunately, neither scaphitid ammonites, nor *Sphenoceramus subcardissoides* or *S. pachtii* are present in the UK Chalk succession and hence can not be used as biostratigraphic tie points.

The carbon-isotopic events recorded at Cutpick Creek are tentatively correlated to the English Chalk Reference curve (fig. 25). Greater confidence is placed in the correlation of the lower and lower-middle Coniacian strata where biostratigraphic control is good. The Light Point, East Cliff, and White Fall carbon-isotope events (CIE) appear to be recognizable with some degree of confidence. The carbon-isotope record at Cutpick Creek is also



tentatively correlated with the Coniacian record from hemipelagic sediments sampled in the USGS Portland core in central Colorado (Joo and Sageman, 2014). Biostratigraphic control is provided by the lowest occurrences of *Volviceras* and *Scaphites* (*S.*) *depressus*, allowing tentative correlation of the Light Point, East Cliff, and White Fall CIE.

Although a carbon-isotope curve was published for the upper Albian to Santonian succession in a core sampled at Cold Lake in eastern Alberta (Schröder-Adams et al., 2012), the location of that core, on the crest of the forebulge, has resulted in a very fragmentary stratigraphic record. The Lower Coniacian is not represented and the middle and upper Coniacian isotopic record has neither sufficient character nor biostratigraphic control to establish a correlation with the Cutpick Creek section.

GEOCHRONOLOGY

Nielsen et al. (2003, citing Obradovich, personal commun., 2000) reported argon-argon ages of 89.4 ± 0.31 and 89.19 ± 0.51 Ma for two bentonites located, respectively, 1.8 and 2.6 m above the E7 surface in well 13-20-17-7W4. Allostratigraphic correlation (Grifi, 2012; Grifi et al., 2013) showed that the dated bentonites were located near the base of the Muskiki Member, between surfaces CS1 and CS2 of the present study (i.e., within allomember CA2). On the basis of these dated bentonites, Grifi et al. (2013) inferred an age of about 89.5 Ma for the E7 unconformity. The succession of CIE in the English Chalk (Jarvis et al., 2006), calibrated to an astronomical time scale (Laurin et al., 2015; fig. 25), allows the Coniacian succession in Alberta to be calibrated in terms of absolute age. Figure 25 indicates that the lowest occurrence of *C. crassus crassus*, at the E7 surface, is close to 89.51 Ma, suggesting that the bentonite ages reported in Nielsen et al. (2003) are consistent, within error, with the astronomically calculated ages for allomember CA2. The calibrated Chalk reference curve indicates that the base of the

middle Coniacian (lowest occurrence of *Volviceras*) is at about 88.99 Ma, implying that Muskiki allomembers CA1–CA4 collectively span just over 500,000 yr. The Coniacian–Santonian boundary is placed at 86.49 ± 0.44 Ma by Sageman et al. (2014; fig. 25), implying that, collectively, the middle and upper Coniacian part of the Alberta succession (surfaces CA4–SS0) spans 2.5 m.y.

DISCUSSION

TECTONIC CONTROL ON DEPOSITION

Grifi et al. (2013) showed that, in southern Alberta, Coniacian rocks could be grouped into three distinct packages that had been deposited in three discrete depocenters. Allomember CA1 (equivalent to rocks between surfaces E7 and ME1 of Grifi et al., 2013) occupies an arcuate, westward-thickening basin centered at approximately Township 25, whereas allomembers CA2–CA10 (equivalent to rocks between surfaces ME1 and ME7 of Grifi et al., 2013) collectively occupy a SW-thickening basin with a center located south of the Alberta–Montana border. The abrupt along-strike shift in the locus of flexural subsidence was attributed to a corresponding shift in the region of active tectonic thickening in the adjacent orogenic wedge. Allomembers CA12–CA15 (equivalent to rocks between surfaces ME7 and DE1 of Grifi et al., 2013) form a thin tabular sheet over the present study area, but thicken markedly to the east where they fill an elongate trough interpreted to have subsided as result of forced folding above an actively extending normal fault in the Precambrian basement (Grifi et al., 2013).

The patterns of subsidence recognized by Grifi et al. (2013) in the south can be traced northward through the present study area. The larger perspective afforded by the present study, coupled with geochronological control (figs. 25, 26), shows that lower Coniacian rocks (allomembers CA1–CA4) occupy

FIG. 21. Paleogeographic map showing the minimum extent of the erosion surface CS23 that forms the maximum regressive surface in the Upper Coniacian succession, and which is overlain by chert pebbles in west-central Alberta and BC, and by ooidal ironstone in southern Alberta and Montana. Chert pebbles provide definite evidence of subaerial emergence. Compiled from present study, Donaldson et al. (1998) and Cobban et al. (2005).

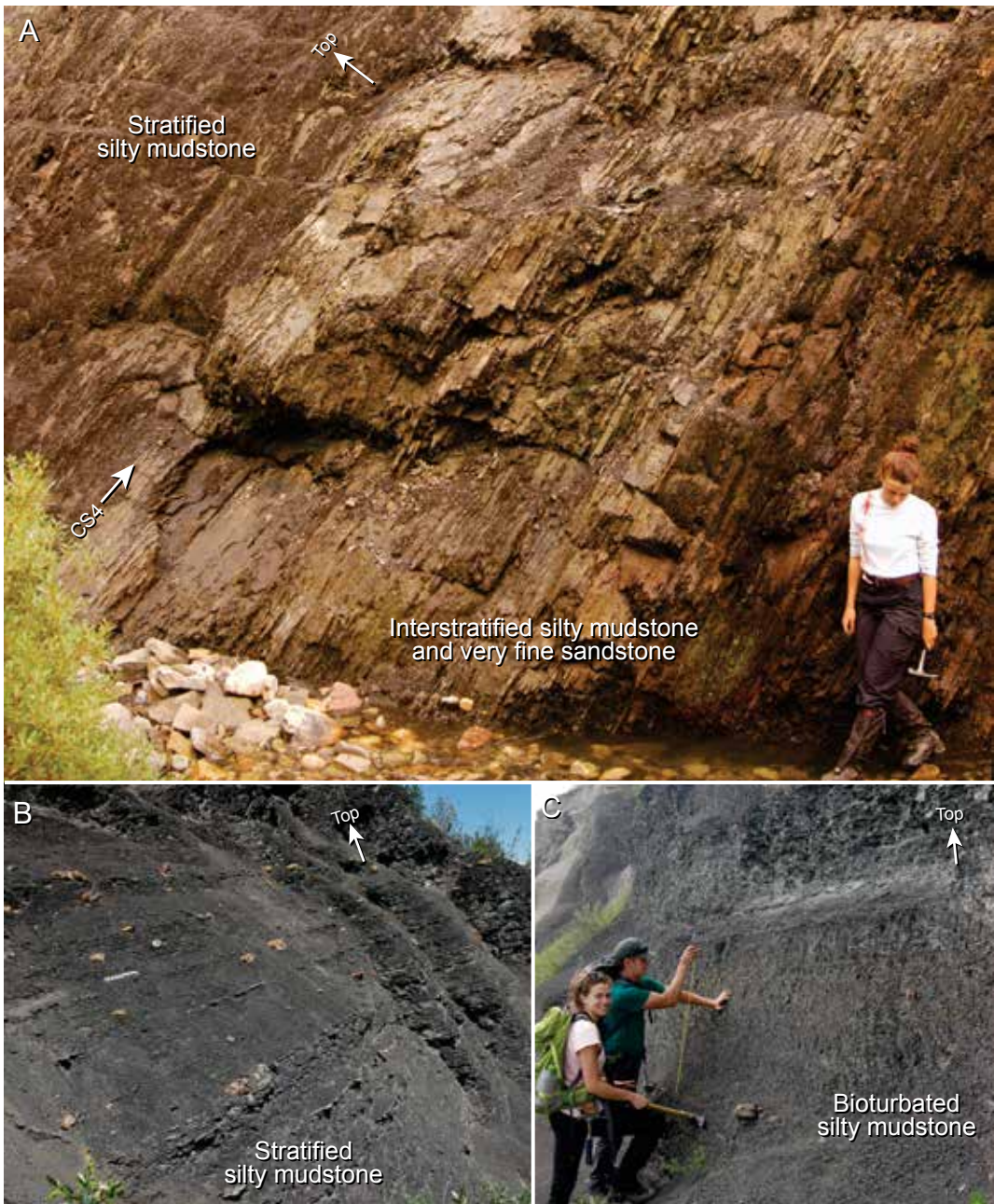


FIG. 22. Offshore facies typical of the Muskiki Member. **A.** Weakly bioturbated (BI 0-1) cm-scale beds of very fine-grained sandstone interstratified with mudstone forming an upward-coarsening succession culminating at flooding surface CS4. The rusty-weathering colour is typical of this facies and is due to abundant disseminated pyrite. Overlying rock comprises weakly bioturbated mudstone with mm-scale siltstone interbeds. Example: “Brown Creek” section (fig. 6, 11–19 m). **B.** Stratified mudstone (BI 1-2) with mm-scale coarse siltstone interbeds and abundant, dispersed siderite nodules; scale bar = 20 cm. Example: Oldfort Creek (fig. 10, 42–46 m). **C.** Heavily bioturbated (BI 4-5) sandy siltstone with dispersed siderite nodules. Example: Oldfort Creek (fig. 10, 49–52 m).



FIG. 23. Near-shore, sandstone-rich facies in the Marshybank Member in Cutpick Creek (fig. 4, 90–120 m). Bounding surfaces CS18 to CS23 and allomembers CA18 to CA23 are indicated. The upper part of CA18 contains fine-grained sandstone with hummocky cross stratification and the lower part of CA19 contains meter-scale, sandstone-filled gutter casts. The upper part of CA19 and most of CA20 consists of well-sorted, swaley cross-stratified, fine-grained sandstone. Centimeter-scale fine sandstone beds in CA21 to CA23 are planar laminated and wave rippled.

FIG. 24. Summary chart showing the stratigraphic distribution of fossils within the 24 allomembers mapped through the study area.

Bounding surfaces	Kevin (Montana)	Mill Creek	Highwood River	Sullivan Creek	Sheep River
SS0	<i>Clioscaphtes saxitonianus</i>	<i>Scaphites (S.) depressus</i>			
CS23					?
CS22					
CS21					
CS20					
CS19					
CS18					
CS17					
CS16					
CS15					<i>Sphenoceramus subcardissoides</i> <i>Volviceramus stotti</i> , sp. nov. <i>Scaphites (S.) depressus</i>
CS14	<i>Scaphites (S.) depressus</i>				<i>Scaphites (S.) depressus</i>
CS13					<i>Volviceramus cardinalensis</i> <i>Volviceramus involutus</i> <i>Volviceramus stotti</i> , sp. nov.
CS12				<i>Volviceramus exogyroides</i>	
CS11					
CS10	<i>Volviceramus involutus</i> <i>Volviceramus koeneni</i>	<i>Scaphites (S.) ventricosus</i>			
CS9				<i>Volviceramus koeneni</i>	
CS8					<i>Volviceramus exogyroides</i>
CS7					<i>Volviceramus</i> sp. A
CS6					
CS5					<i>Volviceramus undabundus</i> <i>Scaphites (S.) ventricosus</i>
CS4	<i>Cremnoceramus crassus</i>		<i>Cremnoceramus</i> sp.	<i>Cremnoceramus</i> sp.	<i>Inoceramus gibbosus</i>
CS3	<i>Cremnoceramus crassus</i>				
CS2		<i>Scaphites (S.) preventricosus</i>			
CS1		<i>C. crassus-inconstans</i> lineage <i>Tethyoceramus ernsti</i> <i>Tethyoceramus</i> sp. <i>S. (S.) preventricosus</i>	<i>Cremnoceramus crassus</i> <i>crassus</i>		<i>Cremnoceramus deformis</i> <i>deformis</i>
E7		<i>S. (S.) preventricosus</i>			

Shaded area represents section not deposited, or removed below various erosion surfaces, particularly surface CS23 (maximum regressive surface).

Oldfort Creek

Burnt Timber
Creek

James River

Ram River

Lynx Creek

		<i>Clioscaphites saxitonianus</i>			
?		<i>Sphenoceramus</i> sp. <i>Scaphites (S.) depressus</i>	<i>S. subcardissoides</i> <i>Sphenoceramus</i> sp. <i>Scaphites (S.) depressus</i>	<i>Sphenoceramus</i> sp.	
			<i>Scaphites (S.) depressus</i>		
			<i>Inoceramus stantoni</i> <i>Volviceramus involutus</i>		
			<i>S. subcardissoides</i> <i>Volviceramus involutus</i> <i>Scaphites (S.) depressus</i> <i>Scaphites (S.) ventricosus</i>		
?		<i>Volviceramus</i> sp.			
	<i>Inoceramus undabundus</i>	<i>Volviceramus</i> sp.			
<i>Volviceramus koeneni</i>					
<i>Scaphites (S.) ventricosus</i>		<i>Volviceramus exogyroides</i>			
<i>Volviceramus</i> sp.			<i>Volviceramus involutus</i>		
	<i>Volviceramus tenuirostratus</i>	<i>Scaphites (S.) ventricosus</i>	<i>Volviceramus involutus</i>		
<i>Volviceramus involutus</i>					
	<i>Scaphites (S.) ventricosus</i>				
<i>Scaphites (S.) preventricosus</i>					
			<i>Cremonoceramus crassus</i>		

Not exposed

Cripple Creek

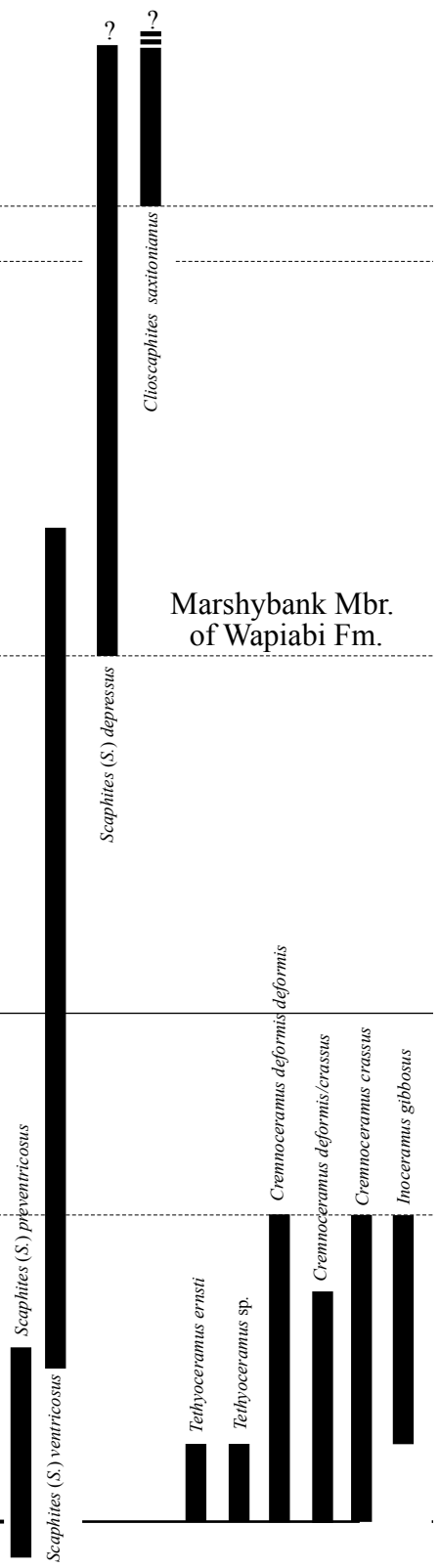
Bighorn Dam

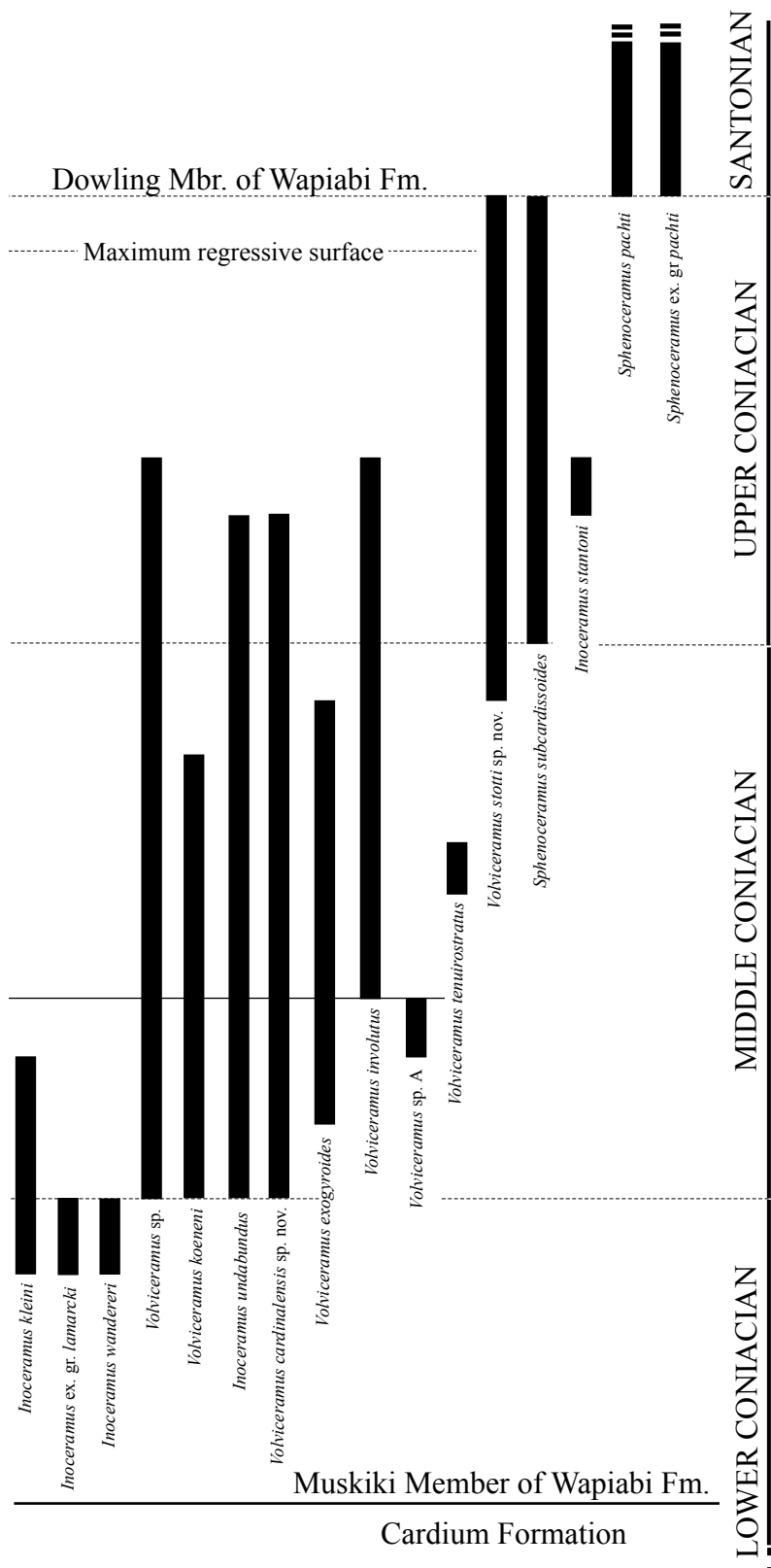
Bighorn River

Blackstone River

<i>Sphenoceras</i> ex. gr. <i>pachti</i> <i>Clioscapites saxitonianus</i>	<i>Sphenoceras</i> ex. gr. <i>pachti</i>			Not exposed
<i>Scaphites</i> (<i>S.</i>) <i>depressus</i>	<i>Volviceras</i> <i>stotti</i> , sp. nov.	<i>Scaphites</i> (<i>S.</i>) <i>depressus</i> <i>Baculites</i> sp.		
	<i>Scaphites</i> (<i>S.</i>) <i>depressus</i>	<i>Scaphites</i> (<i>S.</i>) <i>depressus</i>		
	<i>Volviceras</i> sp. <i>Scaphites</i> (<i>S.</i>) <i>depressus</i>	<i>Volviceras</i> sp.		
	<i>Volviceras stotti</i> , sp. nov. <i>Scaphites</i> (<i>S.</i>) <i>depressus</i> <i>Sphenoceras subcardissoides</i> <i>S</i> (<i>S.</i>) <i>ventricosus</i> <i>Volviceras cardinalensis</i> , sp. nov. <i>Inoceramus undabundus</i> <i>Volviceras</i> sp.	<i>Baculites</i> sp. <i>Scaphites</i> (<i>S.</i>) <i>depressus</i> <i>Scaphites</i> (<i>S.</i>) <i>ventricosus</i>		
Not exposed		<i>Scaphites</i> (<i>S.</i>) <i>ventricosus</i>	<i>Volviceras exogyroides</i> <i>Volviceras</i> sp.	
		<i>Volviceras exogyroides</i> <i>Scaphites</i> (<i>S.</i>) <i>ventricosus</i>		
		<i>Volviceras cardinalensis</i> , sp. nov. <i>Volviceras exogyroides</i>		
		<i>Volviceras exogyroides</i> <i>Inoceramus undabundus</i>		
		<i>Volviceras exogyroides</i>		
		<i>Volviceras exogyroides</i> <i>Inoceramus undabundus</i> <i>Volviceras involutus</i> <i>Scaphites</i> (<i>S.</i>) <i>ventricosus</i>		
		<i>Volviceras cardinalensis</i> , sp. nov. <i>S</i> (<i>S.</i>) <i>ventricosus</i> <i>Volviceras exogyroides</i> <i>Volviceras involutus</i>		
		<i>Volviceras cardinalensis</i> sp. nov. <i>Volviceras exogyroides</i> <i>Inoceramus undabundus</i> <i>Volviceras involutus</i> <i>Scaphites</i> (<i>S.</i>) <i>ventricosus</i>	<i>Volviceras exogyroides</i> <i>Volviceras involutus</i>	
		<i>Volviceras exogyroides</i>		
		<i>Volviceras cardinalensis</i> , sp. nov. <i>Volviceras exogyroides</i> <i>Inoceramus kleini</i>		
	<i>Volviceras cardinalensis</i> , sp. nov. <i>Inoceramus undabundus</i> <i>Scaphites</i> (<i>S.</i>) <i>ventricosus</i> <i>Volviceras</i> sp.			
	<i>Inoceramus wandereri</i> <i>Cremnoceras</i> sp.		<i>Inoceramus gibbosus</i>	
			<i>Cremnoceras deformis</i> / <i>crassus</i> <i>Cremnoceras</i> c. <i>inconstans</i> <i>Inoceramus gibbosus</i>	
<i>Tethyoceras</i> sp. <i>Cremnoceras crassus</i>	<i>Cremnoceras crassus</i> <i>Tethyoceras</i> sp. <i>Cremnoceras deformis</i> <i>deformis</i> <i>Scaphites</i> (<i>S.</i>) <i>preventricosus</i>		<i>Cremnoceras deformis</i> / <i>crassus</i> <i>Cremnoceras crassus</i> <i>inconstans</i>	

Thistle Creek West	Cutpick Creek	Allo- members
<i>Sphenoceramus</i> ex. gr. <i>pachti</i> <i>Clioscaphtes saxitonianus</i>		
<i>Volviceramus stotti</i> , sp. nov. <i>Scaphites</i> (S.) <i>depressus</i>		CA24
		CA23
		CA22
		CA21
		CA20
		CA19
		CA18
<i>Scaphites</i> (S.) <i>depressus</i>		CA17
<i>Sphenoceramus subcardissoides</i> <i>Volviceramus</i> sp. <i>Scaphites</i> (S.) <i>depressus</i>	<i>Sphenoceramus subcardissoides</i>	CA16
<i>Volviceramus</i> sp.		CA15
		CA14
<i>Volviceramus involutus</i> <i>Inoceramus undabundus</i>		CA13
	<i>Volviceramus</i> sp.	CA12
		CA11
	<i>Volviceramus</i> sp.	CA10
		CA9
<i>Inoceramus</i> sp. <i>Volviceramus</i> sp.	<i>Volviceramus involutus</i> <i>Volviceramus</i> sp.	CA8
<i>Volviceramus</i> sp.		CA7
<i>Inoceramus</i> sp. <i>Volviceramus</i> sp.		CA6
<i>Volviceramus</i> sp.		CA5
<i>Cremnoceramus deformis deformis</i> <i>Inoceramus gibbosus</i> <i>Inoceramus kleini</i> <i>Inoceramus</i> ex. gr. <i>lamarcki</i>		CA4
	<i>Cremnoceramus deformis</i> <i>Scaphites</i> (S.) <i>preventricosus</i>	CA3
		CA2
		CA1





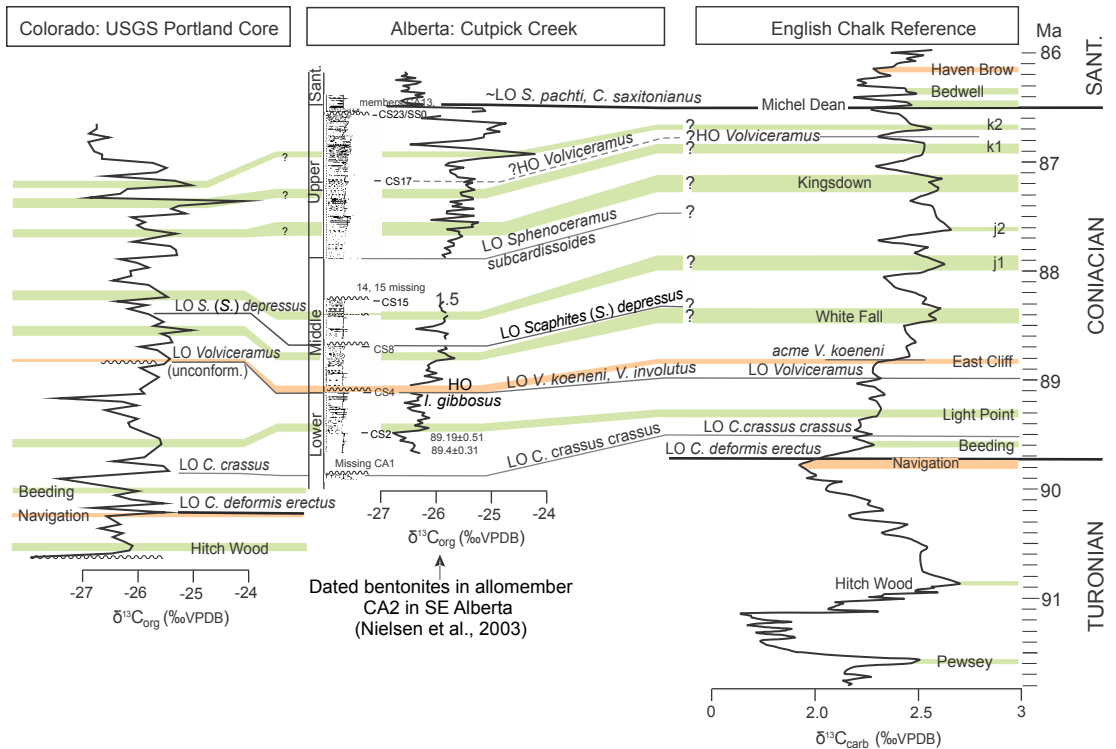


FIG. 25. Comparison of the organic carbon isotope stratigraphy at Cutpick Creek with the carbonate carbon isotope reference curve for the English Chalk succession (after Jarvis et al., 2006, recalibrated to GTS2012 after Laurin et al., 2015). The Cutpick section, and corresponding carbon-isotope curve, has been “expanded” to show the location of hiatuses determined on the basis of regional subsurface correlation (i.e., fig. 4). Biostratigraphic collections made in all the Coniacian sections included in this study (fig. 24), allow three tie-points to the UK Chalk to be established at the lowest occurrence (LO) of *Cremnoceramus crassus crassus*, and the lowest occurrence of *Volviceramus*. The base of the Santonian is defined at the co-appearance level of *Clioscaphtes saxitonianus* and *Sphenoceramus ex gr. pachti*, which corresponds to surface SS0 of this study. The lowest occurrence of *C. crassus*, *Volviceramus* and *Scaphites (S.) depressus* allows tentative correlation to the Portland core, which does not extend as high as the Coniacian–Santonian boundary (Joo and Sageman, 2014). The highest local occurrence of *Inoceramus gibbosus*, which is widely distributed in allomembers CA3 and CA4 in the western Alberta foredeep, is marked by the lag-strewn erosion surface CS4, suggestive of significant sea-level fall and subsequent transgression. The absence of the *I. ex gr. gibbosus* interval in most sections of topmost lower Coniacian strata in other parts of the world suggests that a significant hiatus exists at the base of the overlying *Volviceramus* Zone.

a broadly saucer-shaped, SW-thickening basin that thins toward both the NW and SE; this depocenter appears to have been active for about 500,000 yr. Middle Coniacian rocks (allomembers CA5–CA14) occupy a SW-thickening basin that underwent active subsidence for about 1.5 m.y. Toward the NW part of that basin, allomembers CA11–CA14 are progressively truncated by surface CS15 (fig. 4). Upper Coniacian rocks, constituting allomembers CA15–CA23, occupy a distinct northern basin that subsided for about 1 m.y.; Upper Coniacian strata are truncated toward the SE by surface CS23. It is clear, therefore, that during the Coniacian the location of the active flexural depocenter shifted episodically along strike by several hundred km. Each actively subsiding basin was rimmed by a corresponding peripheral region of subtle upwarp and stratal truncation. This pattern of shifting depocenters is directly analogous to that mapped in overlying Santonian–Campanian strata (Hu and Plint, 2009; Plint et al., 2012a). The episodic subsidence of discrete, arcuate depocenters may have been a response to the development of localized salients in the adjacent deformed belt. Such salients may have developed in response to a locally thicker sedimentary cover succession, a locally weaker detachment, or a localized indenter, amongst other reasons (cf. Macedo and Marshak, 1999).

ORIGIN OF ALLOMEMBERS

The excellent subsurface control available in the study area has allowed 24 Coniacian allomembers to be mapped with confidence. Allomembers are typically <10 m thick, and rarely exceed 20 m (figs. 4–13), yet can be traced along and across strike for hundreds of km. Given the ~3.0 m.y. represented by the studied interval of strata, each of the 24 allomembers can be inferred to have had an average duration of ~125,000 yr. The ubiquitous upward-coarsening signature of allomembers, coupled with the widespread presence of intra- or extrabasinal pebble lags on flooding surfaces, indicates that many allomembers can be interpreted as depositional sequences, each of which embodies evidence for initial relative sea-level rise, followed by shoal-

ing, and terminated by relative sea-level fall that led to erosion of the sea floor, and in some cases, to subaerial emergence. The lateral continuity, over hundreds of km, coupled with the extremely high aspect-ratio of each allomember suggests that depositional cyclicity was a response to allogenic forcing, rather than to localized autogenic effects such as delta lobe switching. It is possible that depositional cyclicity was the result of changes in the rate of clastic sediment supply that resulted in alternating coastal progradation and transgression, manifest as upward-shoaling successions bounded by flooding surfaces. However, extrabasinal pebble lags imply episodes of relative sea-level fall and subaerial exposure that can not be explained solely in terms of a changing rate of sediment supply.

Relative sea-level rise and fall can be effected by both tectonic and eustatic mechanisms. The stratigraphic data presented herein (figs. 4–13, 26), provide evidence that stratal packages composed of several allomembers form large-scale arcuate wedges that are most reasonably explained in terms of differential flexural subsidence and uplift on length scales of hundreds of kilometers. This pattern contrasts sharply with the relatively tabular geometry of individual allomembers. Given the evidence that tectonic subsidence due to static loading resulted in broad, saucer-shaped depocenters, it seems difficult to also attribute the tabular geometry of allomembers to the same mechanism. Allomembers are therefore most simply explained as a consequence of relatively high-frequency (order of 100,000 yr) eustatic sea-level cycles superimposed on relatively low-frequency (order of 0.5 to 1.5 m.y.), and spatially non-uniform pulses of tectonically driven subsidence.

NATURE OF BIOZONAL BOUNDARIES

Important biotic colonization events that mark the lowest occurrences of *Cremnoceramus crassus crassus*, *Volviceramus*, *Sphenoceramus subcardissoides*, and *S. pachtii*, all correspond to widely mappable erosion surfaces that indicate relative sea-level fall followed by transgression. Sea-level changes therefore appear to have played

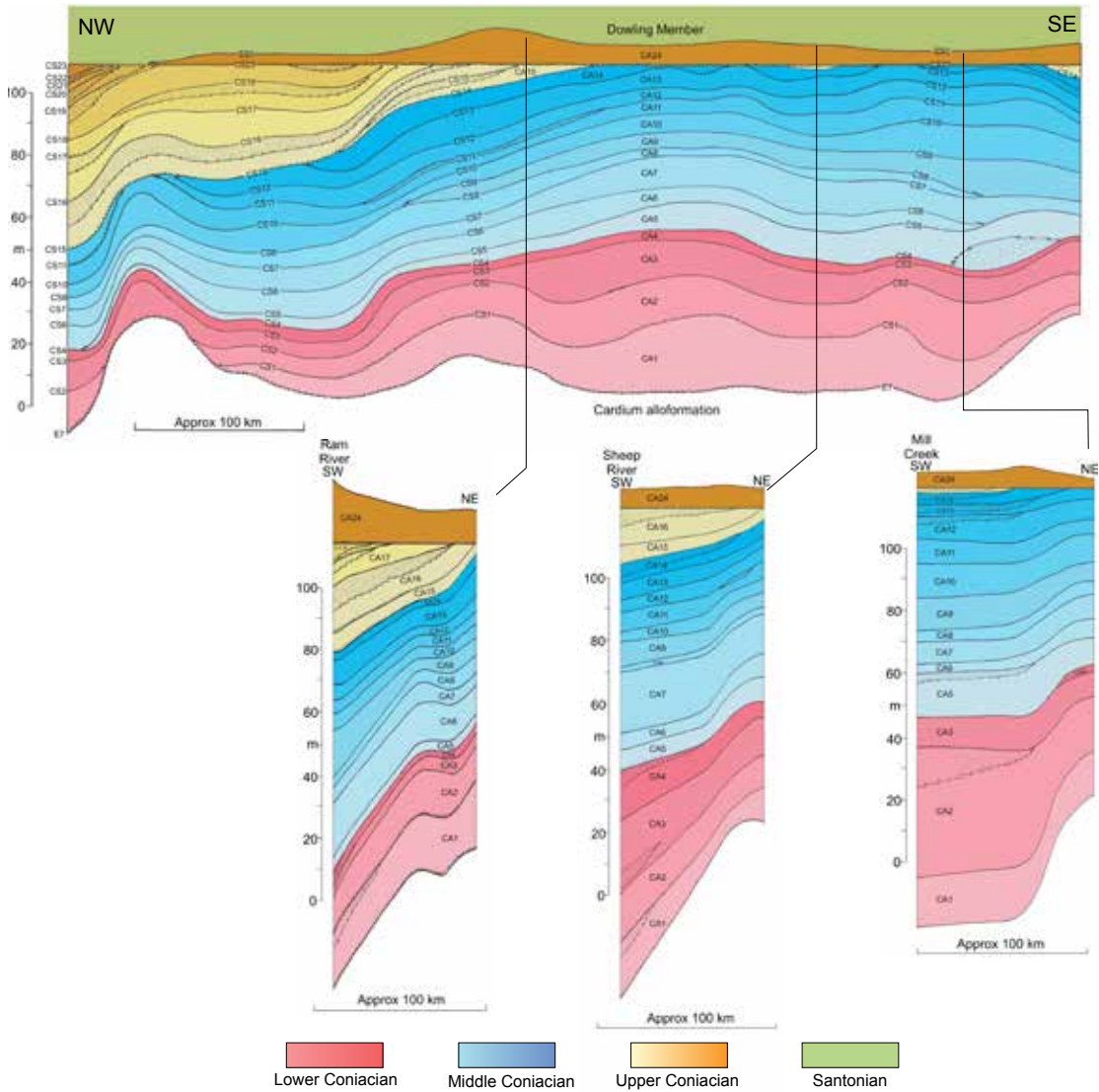


FIG. 26. Summary representation, to scale, of stratal geometry viewed in strike (NW-SE) and three dip (NE-SW) sections spanning the study area. Lower Coniacian strata fill a saucer-shaped depocenter that thins to both NW and SE, whereas Middle Coniacian strata are thickest in the south but are erosionally truncated toward the NW. Upper Coniacian strata fill a depocenter in the NW but are truncated toward the SE, and are largely absent over most of southern Alberta and northern Montana. Sections summarized from figures 4, 8, 11, and 13.

an important role in speciation and extinction events. Because marine flooding surfaces can be considered to have formed geologically instantaneously, it is also reasonable to interpret the boundaries of the inoceramid biozones to closely approximate time planes.

The coincidence between the lowest and highest occurrences of scaphitid ammonite species and erosional surfaces subsequently modified by transgression is less clear. The lowest occurrence of *Scaphites* (*S.*) *preventricosus* is just above erosional surface E5.5, which marks the beginning of a major transgression (Walaszczyk et al., 2014). However, the lowest occurrence of *S. (S.) ventricosus* is immediately above surface CS2, in allomember CA3, close to an interpreted highstand. The lowest occurrence of *S. (S.) depressus* is just above surface CS14, which marks a high-frequency flooding surface during a long-term shallowing trend that continued, punctuated by minor transgressions, through much of the late Coniacian. In contrast, the lowest occurrence of *Clioscaphtes saxitonianus* is at the base of the Santonian (surface SS0), coinciding with a major transgression and a marked change in facies to deeper-water, more offshore mudstones.

CONCLUSIONS

1. Coniacian marine rocks within a >750 km transect along the foredeep of the Western Canada Foreland Basin have been divided into a succession of 24 allomembers, bounded by marine flooding surfaces. Flooding surfaces have been correlated through a grid of ~4,800 wireline well logs, embracing an area of about 200,000 km², and have also been traced into equivalent strata exposed in the fold-and-thrust belt on the western margin of the basin.
2. Flooding surfaces probably formed on a time scale of only a few thousand years, and hence can be treated as proxy time lines. The allostratigraphic framework therefore provides a near-chronostratigraphic framework within which to analyze spatial and temporal patterns of molluscan evolution.
3. In the study area, Coniacian rocks are divided into five broad facies that represent a spectrum of offshore to shoreface environments. Offshore sediments are mudstones and siltstones with abundant wave ripples that indicate deposition above storm-wave base (probably only a few tens of m deep). Bioturbation intensity varies from 0 to 6. Low bioturbation index is attributed primarily to a low (2–5 mg/L⁻¹) dissolved oxygen content in bottom water, insufficient to support a benthic macrofauna; intensely bioturbated sediments indicate better oxygenated conditions. Sediments deposited closer to shore include variably bioturbated siltstones and sandstones with wave ripples and HCS, whereas mud-free sandstone with SCS represents a storm-influenced shoreface.
4. Flooding surfaces may lack a coarse-grained lag, or may bear anomalously coarse sand or pebbles. Pebbles may be intraformational clasts of siderite or phosphate or extrabasinal chert. Siderite and phosphate pebbles indicate erosion of the sea floor sufficient to exhume early diagenetic nodules, but do not prove subaerial emergence. Chert pebbles must have been supplied by rivers and imply a period of subaerial emergence of the shelf prior to transgressive reworking.
5. The more mudstone-rich facies contain abundant inoceramid bivalve and scaphitid ammonite fossils, preserved mainly as uncompressed siderite infills of the shell. Fossils were located precisely in measured outcrop sections, and subsequently were correlated into the regional subsurface allostratigraphic framework.
6. Several major speciation events among inoceramids are recognized. The lowest occurrence of *Cremnoceramus crassus crassus* coincides with the E7 surface at the base of the Muskiki Member; the fauna persists up to surface CS4. The *Inoceramus gibbosus* group is present only in allomembers CA2–

CA4 but is not found above surface CS4, which marks the Lower to Middle Coniacian boundary. Immediately above surface CS4 appear various species of *Volviceras*, which rapidly become abundant. *Sphenoceras subcardissoides* appears in allomember CA15 together with *Scaphites* (*S.*) *depressus* and hence marks the base of the upper Coniacian. *Sphenoceras pachti*, together with *Clioscaphtes saxitonianus* appear immediately above surface SS0 and mark the base of the Santonian.

7. The lowest occurrence of *Scaphites* (*S.*) *preventricosus* is just above Cardium Formation erosion surface E5.5, which lies just below the base of the Coniacian. The lowest occurrence of *S. (S.) ventricosus* is immediately above surface CS2 in allomember CA3, which is a short distance below the base of the Middle Coniacian. The lowest occurrence of *S. (S.) depressus* is in allomember CA15, immediately above surface CS 14, which marks both the onset of major regression and the base of the upper Coniacian. The lowest occurrence of *Clioscaphtes saxitonianus* is at transgressive surface SS0, which marks the local base of the Santonian.
8. The close correspondence between marine transgressive events and the appearance of new inoceramid (and sometimes ammonite) species suggests that the evolution and dispersal of new inoceramid species took place during episodes of relative sea-level rise that in some cases were preceded by a distinct lowstand.
9. A preliminary carbon-isotope record was obtained for Coniacian strata at Cutpick Creek in west-central Alberta. The succession of carbon-isotope events (CIE) are tentatively correlated to the English Chalk reference curve. The Light Point, East Cliff, and White Fall CIE appear to be recognizable with some degree of confidence. The carbon-isotope record at Cutpick Creek is also tentatively correlated with the Coniacian isotope record from hemipelagic sediments in Colorado, where biostratigraphic control from the lowest occurrences of *Volviceras* and *Scaphites* (*S.*) *depressus* allows tentative correlation of the Light Point, East Cliff, and White Fall CIE.
10. Mapping of allomembers along the strike of the foredeep shows that allomembers can be grouped into natural "tectono-stratigraphic" units that span ca. 0.5 to 1.5 m.y., and are bounded by low-angle beveling unconformities that truncate packages of nearly tabular allomembers. Each tectono-stratigraphic unit fills a broadly saucer-shaped depocenter, interpreted to have subsided in response to active tectonic loading in the adjacent sector of the fold-and-thrust belt.
11. The astronomically calibrated succession of CIE in the English Chalk provides an absolute time scale against which to interpret transgressive-regressive events in Alberta. The 24 mapped allomembers appear to span close to 3.0 m.y., suggesting that on average, each allomember represents about 125,000 yr. Because the flooding surfaces that bound allomembers can be mapped for hundreds of km (and in cases >1000 km), an at least regional-scale allogenic control is indicated: high-frequency eustatic change appears to provide the most likely driving mechanism.
12. Toward the south, upper Coniacian strata are progressively bevelled off such that south of about latitude 51° N, the succession comprises primarily lower and middle Coniacian strata, and most late Coniacian time is represented by an erosion surface, mantled by 0.1 to 1.2 m of chert-pebble bearing ooidal ironstone. This ironstone is correlative with the MacGowan Concretionary Bed mapped over much of western Montana. The region of late Coniacian uplift in southern Alberta probably constitutes a peripheral bulge related to a late Coniacian flexural depocenter located in NE British Columbia.

ACKNOWLEDGMENTS

The results reported here are based on 16 summers of fieldwork by the senior author and graduate students B. Norris, J. McKay, S. Donaldson, M. Grifi and E. Hooper, in collaboration with Dr. I. Walaszczyk. We were ably assisted in the field by O. Al-Mufti, P. Angiel, R. Buckley, S. CoDyer, R. Cotton-Barratt, P. Elliott, B. Hart, Y. Hu, S. Morrow, M. O'Driscoll, K. Pavan, T. Plint, J. Shank, K. Vannelli, and R. Vesely. Funding for A.G.P.'s regional stratigraphic studies was provided by the Natural Sciences and Engineering Research Council of Canada, over numerous grant cycles. Supplementary funding was provided by Canadian Hunter Ltd, Home Oil Ltd., Imperial Oil Ltd., Texaco Ltd., and Unocal Canada, Ltd. Well-log data were donated by Imperial Oil Ltd and Divestco Ltd. A gamma-ray spectrometer was donated by the former PanCanadian Petroleum Ltd. I.W. acknowledges the financial support of the Faculty of Geology of the University of Warsaw (BST grant No. 173502). D.R.G. and I.J. acknowledge funding by UK Natural Environment Research Council (NERC) grants NE/H021868/1 and NE/H020756/1, respectively.

N.H.L. thanks Mary Conway (AMNH) for curation of the specimens, Stephen Thurston (AMNH) for photographing the specimens and preparing the figures, Mariah Slovacek (AMNH), and Neal Larson (Larson Paleontology Unlimited, Keystone, SD) for preparation of the specimens, and Brandon Strilisky (TMP) for facilitating the accession of the specimens into the Tyrell Museum of Paleontology. We express our thanks to Ben Hathway and Matthew P. Garb for their detailed and perceptive comments that significantly improved the final text.

REFERENCES

- Benyon, C., et al. 2014. Provenance of the Cretaceous Athabasca Oil Sands, Canada: implications for continent-scale sediment transport. *Journal of Sedimentary Research* 84: 136–143.
- Bhattacharya, J.P., and R.G. Walker. 1991a. Allostratigraphic subdivision of the Upper Cretaceous Dunvegan, Shaftesbury and Kaskapau formations in the northwestern Alberta subsurface. *Bulletin of Canadian Petroleum Geology* 39: 145–164.
- Bhattacharya, J.P., and R.G. Walker. 1991b. River- and wave-dominated depositional systems of the Upper Cretaceous Dunvegan Formation, northwestern Alberta. *Bulletin of Canadian Petroleum Geology* 39: 165–191.
- Blum, M., and M. Pecha. 2014. Mid-Cretaceous to Paleocene North American drainage reorganization from detrital zircons. *Geology* 42: 607–610.
- Buckley, R.A., A.G. Plint, O.A. Henderson, J.R. Krawetz, and K.M. Vannelli. 2016. Ramp sedimentation across a middle Albian, Arctic embayment: influence of subsidence, eustasy and sediment supply on stratal architecture and facies distribution, Lower Cretaceous, Western Canada Foreland Basin. *Sedimentology* 63: 699–742.
- Catuneanu, O. 2006. Principles of sequence stratigraphy. Amsterdam: Elsevier, 375 p.
- Cheel, R.J., and D.A. Leckie. 1993. Hummocky cross-stratification. *Sedimentology Review* 1: 103–122. Oxford: Blackwell Scientific.
- Clifton, H.E. 2006. A reexamination of facies models for clastic shorelines. *In* H.W. Posamentier and R.G. Walker (editors), *Facies models revisited*. SEPM (Society for Sedimentary Geology) Special Publication 84: 293–337.
- Cobban, W.A., C.E. Erdmann, R.W. Lemke, and F.K. Maughan. 1959. Revision of Colorado Group on Sweetgrass Arch, Montana. *American Association of Petroleum Geologists, Bulletin* 43: 2786–2796.
- Cobban, W.A., C.E. Erdmann, R.W. Lemke, and E.K. Maughan, E.K. 1976. Type sections and stratigraphy of the Blackleaf and Marias River formations (Cretaceous) of the Sweetgrass Arch, Montana. United States Geological Survey, Professional Paper 974: 1–66.
- Cobban, W.A., T.S. Dyman, and K.W. Porter. 2005. Paleontology and stratigraphy of upper Coniacian–middle Santonian ammonite zones and application to erosion surfaces and marine transgressive strata in Montana and Alberta. *Cretaceous Research* 26: 429–449.
- Collom, C.J. 2001. Systematic paleontology, biostratigraphy, and paleoenvironmental analysis of the Wapiabi Formation (Upper Cretaceous), Alberta and British Columbia, Western Canada. Ph.D. dissertation, University of Calgary, Alberta, 834 pp.
- Cross, T.A., and M.A. Lessenger. 1988. Seismic stratigraphy. *Annual Review of Earth and Planetary Sciences* 16: 319–354.

- Dashtgard, S.E., and J.A. MacEachern. 2016. Unburrowed mudstones may record only slightly lowered oxygen conditions in warm, shallow basins. *Geology* 44: 371–374.
- Dashtgard, S.E., J.W. Snedden, and J.A. MacEachern. 2015. Unbioturbated sediments on a muddy shelf: hypoxia or simply reduced oxygen saturation? *Palaeogeography, Palaeoclimatology, Palaeoecology* 425: 128–138.
- Donaldson, W.S. 1997. The sedimentology, stratigraphy and diagenesis of the Upper Cretaceous Bad Heart Formation, NW Alberta. Ph.D. dissertation, University of Western Ontario, London, 492 pp.
- Donaldson, W.S., A.G. Plint, and F.J. Longstaffe. 1998. Basement tectonic control on the distribution of the shallow marine Bad Heart Formation: Peace River Arch area, NW Alberta. *Bulletin of Canadian Petroleum Geology* 46: 576–598.
- Donaldson, W.S., A.G. Plint, and F.J. Longstaffe. 1999. Tectonic and eustatic control on deposition and preservation of Upper Cretaceous ooidal ironstone and associated facies: Peace River Arch area, NW Alberta, Canada. *Sedimentology* 46: 576–598.
- Durbano, A. 2009. Stratigraphy of the Muskiki and Marshybank formations (Coniacian), west-central Alberta. B.Sc. thesis, University of Western Ontario, London, 48 pp.
- Evenchick, C.A., M.E. McMechan, V.J. McNichol, and S.D. Carr, S.D. 2007. A synthesis of the Jurassic-Cretaceous tectonic evolution of the central and southeastern Canadian Cordillera: Exploring links across the orogen. *In* J.W. Sears, T.A. Harms and C.A. Evenchick (editors), *Whence the mountains? Inquiries into the evolution of orogenic systems: a volume in honor of Raymond A. Price*. Geological Society of America, Special Paper 433: 117–145.
- Grifi, M.D. 2012. Stratigraphy and sedimentology of the Late Cretaceous (Coniacian) Muskiki and Marshybank members, southern Alberta and northwestern Montana. M.Sc. thesis, University of Western Ontario, London, 216 pp.
- Grifi, M.D., A.G. Plint, and I. Walaszczyk. 2013. Rapidly changing styles of subsidence revealed by high-resolution mudstone allostratigraphy: Coniacian of Sweetgrass Arch area, southern Alberta and northern Montana. *Canadian Journal of Earth Sciences* 50: 439–461.
- Hooper, E. In prep. Allostratigraphy and sedimentology of the Muskiki and Marshybank members (Late Cretaceous, Coniacian) in southwestern Alberta, Canada. Ph.D. dissertation, University of Western Ontario, London.
- Hooper, E., and A.G. Plint. 2016. Cryptic migrating depocentres in a mudstone-dominated succession: Coniacian Muskiki and Marshybank members, Central Alberta Plains and Foothills, Western Canada Foreland Basin. AAPG Annual Convention, Calgary, June 19–23, 2016. Poster, abstract on line.
- Hu, Y.G., and A.G. Plint, A.G. 2009. An allostratigraphic correlation of a mudstone-dominated syn-tectonic wedge: the Puskwaskau Formation (Santonian–Campanian) in outcrop and subsurface, Western Canada foreland basin. *Bulletin of Canadian Petroleum Geology* 57: 1–33.
- Jarvis, I., A.S. Gale, H.C. Jenkyns, and M.A. Pearce. 2006. Secular variation in Late Cretaceous carbon isotopes: a new $\delta^{13}\text{C}$ carbonate reference curve for the Cenomanian–Campanian (99.6–70.6 Ma). *Geological Magazine* 143: 561–608.
- Jarvis, I., J. Trabucho-Alexandre, D.R. Gröcke, D. Uličný, and J. Laurin. 2015. Intercontinental correlation of organic carbon and carbonate stable isotope records: evidence of climate and sea-level change during the Turonian (Cretaceous). *Depositional Record* 1: 53–90.
- Joo, Y.J., and B.B. Sageman. 2014. Cenomanian to Campanian carbon isotope chemostratigraphy from the Western Interior Basin, USA. *Journal of Sedimentary Research* 84: 529–542.
- Kafle, B., R.A. Olson, and O. Catuneanu. 2013. Stratigraphy of the Bad Heart Formation, Clear Hills and Smoky River areas, Alberta. *Bulletin of Canadian Petroleum Geology* 61: 253–282.
- Kauffman, E.G. 1977. Geological and biological overview: Western Interior Cretaceous Basin. *Mountain Geologist* 14: 75–99.
- Kennedy, W.J., and W.A. Cobban. 1991. Coniacian ammonite faunas from the United States Western Interior. *Special Papers in Palaeontology* 45: 1–96. [London]: Palaeontological Association.
- Laurin, J., S.R. Meyers, D. Uličný, I. Jarvis, and B.B. Sageman. 2015. Axial obliquity control on the greenhouse carbon budget through middle- to high-latitude reservoirs. *Paleoceanography* 30: 133–149.
- Leckie, D.A., and R.J. Cheel. 1997. Sedimentology and depositional history of Lower Cretaceous coarse-grained clastics, southwest Alberta and southeast British Columbia. *Bulletin of Canadian Petroleum Geology* 45: 1–24.
- Leier, A.L., and G.E. Gehrels. 2011. Continent-scale detrital zircon provenance signatures in Lower Cretaceous strata, western North America. *Geology* 39: 399–402.
- MacEachern, J.A., S.G. Pemberton, M.K. Gingras, and K.L. Bann. 2010. Ichnology and facies models. *In*

- R.W. Dalrymple and N.P. James (editors), *Facies models 4* (GEOtext 6): 19–58. St. John's, Newfoundland: Geological Association of Canada.
- Macedo, J., and S. Marshak. 1999. Controls on the geometry of fold-thrust belt salients. *Bulletin of the Geological Society of America* 111: 1808–1822.
- Malloch, C.S. 1911. Bighorn Coal Basin, Alberta. *Geological Survey of Canada Memoir* 9E: 1–66.
- McKay, J.L., F.J. Longstaffe, and A.G. Plint. 1995. Early diagenesis and its relationship to depositional environment and relative sea level fluctuations (Upper Cretaceous Marshybank Formation, Alberta and British Columbia). *Sedimentology* 42: 161–190.
- NACSN (North American Commission on Stratigraphic Nomenclature). 2005. North American Stratigraphic Code. *American Association of Petroleum Geologists Bulletin* 89: 1547–1591.
- Nielsen, K.S., C.J. Schröder-Adams, and D.A. Leckie. 2003. A new stratigraphic framework for the Upper Colorado Group (Cretaceous) in southern Alberta and southwestern Saskatchewan, Canada. *Bulletin of Canadian Petroleum Geology* 51: 304–346.
- Nielsen, K.S., C.J. Schröder-Adams, D.A. Leckie, J.W. Haggart, and K. Elberdak. 2008. Turonian to Santonian paleoenvironmental changes in the Cretaceous Western Interior Sea: the Carlile and Niobrara formations in southern Alberta and southwestern Saskatchewan, Canada. *Palaeogeography, Palaeoclimatology, Palaeoecology* 270: 64–91.
- Norris, B. 1989. The Upper Cretaceous Muskiki, Marshybank and Bad Heart formations (Smoky Group), Western Interior Seaway, northwestern Alberta, Canada: relative sea level control on stratigraphy and sedimentology. M.Sc. thesis, University of Western Ontario, London, 341 pp.
- Obradovich, J.D., and W.A. Cobban. 1975. A time-scale for the Late Cretaceous of the Western Interior of North America. *Geological Association of Canada Special Paper* 13: 31–54.
- Plint, A.G. 1990. An allostratigraphic correlation of the Muskiki and Marshybank formations (Coniacian–Santonian) in the foothills and subsurface of the Alberta Basin. *Bulletin of Canadian Petroleum Geology* 38: 288–306.
- Plint, A.G. 1991. High-frequency relative sea level oscillations in Upper Cretaceous shelf clastics of the Alberta Foreland Basin: evidence for a Milankovitch-scale glacio-eustatic control? *In* D.I.M. Macdonald (editor), *Sedimentation, tectonics and eustasy*. International Association of Sedimentologists Special Publication 12: 409–428. Oxford: Blackwell Science.
- Plint, A.G. 2000. Sequence stratigraphy and paleogeography of a Cenomanian deltaic complex: the Dunvegan and lower Kaskapau formations in subsurface and outcrop, Alberta and British Columbia, Canada. *Bulletin of Canadian Petroleum Geology* 47: 43–79.
- Plint, A.G. 2010. Chapter 8: Wave- and storm-dominated shoreline and shallow marine systems. *In* R.W. Dalrymple and N.P. James (editors), *Facies models 4* (GEOtext 6): 167–199. St. John's, Newfoundland: Geological Association of Canada.
- Plint, A.G. 2014. Mud dispersal across a Cretaceous prodelta: storm-generated, wave-enhanced sediment gravity flows inferred from mudstone microtexture and microfacies. *Sedimentology* 61: 609–647.
- Plint, A.G., and B. Norris. 1991. Anatomy of a ramp margin sequence: facies successions, paleogeography and sediment dispersal patterns in the Muskiki and Marshybank formations, Alberta Foreland Basin. *Bulletin of Canadian Petroleum Geology* 39: 18–42.
- Plint, A.G., and D. Nummedal. 2000. The falling stage systems tract: Recognition and importance in sequence stratigraphic analysis. *In* D. Hunt and R.L.G. Gawthorpe (editors), *Sedimentary responses to forced regressions*. Geological Society of London Special Publication 172: 1–17.
- Plint, A.G., R.G. Walker, and K.M. Bergman. 1986. Cardium Formation 6. Stratigraphic framework of the Cardium in subsurface. *Bulletin of Canadian Petroleum Geology* 34: 213–225.
- Plint, A.G., B. Norris, and W.S. Donaldson. 1990. Revised definitions for the Upper Cretaceous Bad Heart Formation and associated units in the foothills and plains of Alberta and British Columbia. *Bulletin of Canadian Petroleum Geology* 38: 78–88.
- Plint, A.G., et al. 2012a. Dynamic relationship between subsidence, sedimentation, and unconformities in mid-Cretaceous, shallow-marine strata of the Western Canada Foreland Basin: links to cordilleran tectonics. *In* C. Busby and A. Azor (editors), *Recent advances in the tectonics of sedimentary basins*: 480–507. Oxford: Wiley-Blackwell Publishing.
- Plint, A.G., J.H.S. Macquaker, and B.L. Varban. 2012b. Bedload transport of mud across a wide, storm-influenced ramp: Cenomanian-Turonian Kaskapau Formation, Western Canada Foreland Basin. *Journal of Sedimentary Research* 82: 801–822.
- Price, R.A. 1994. Chapter 2: Cordilleran tectonics and the evolution of the Western Canada Sedimentary Basin. *In* G. Mossop and I. Shetsen (compilers), *Geological atlas of the Western Canada Sedimentary Basin*: 13–24. Calgary: Canadian Society of Petroleum Geologists and Alberta Research Council.

- Raines, M.K., S.M. Hubbard, R.B. Kukulski, A.L. Leier, and G. Gehrels. 2013. Sediment dispersal in an evolving foreland: Detrital zircon geochronology from Upper Jurassic and lowermost Cretaceous strata, Alberta Basin, Canada. *Bulletin of the Geological Society of America* 125: 741–755.
- Roca, X., et al. 2008. An allostratigraphic correlation of Lower Colorado Group (Albian) and equivalent strata in Alberta and British Columbia, and Cenomanian rocks of the Upper Colorado Group in southern Alberta. *Bulletin of Canadian Petroleum Geology* 56: 259–299.
- Rottenfusser, B., et al. 2002. Regional evaluation of the coalbed methane potential in the plains and foothills of Alberta, stratigraphy and rank study (digital version). Alberta Geological Survey Special Report 7: 1–248. Calgary: Alberta Energy and Utilities Board.
- Sageman, B.B., et al. 2013. Integrating $^{40}\text{Ar}/^{39}\text{Ar}$, U-Pb, and astronomical clocks in the Cretaceous Niobrara Formation, Western Interior Basin, USA. *Bulletin of the Geological Society of America* 126: 956–973.
- Schröder-Adams, C.J., J.O. Herrle, and Q. Tu. 2012. Albian to Santonian carbon isotope excursions and faunal extinctions in the Canadian Western Interior Sea: Recognition of eustatic sea-level controls on a forebulge setting. *Sedimentary Geology* 281: 50–58.
- Seitz, O. 1959. Vergleichende Stratigraphie der Oberkreide in Deutschland und in Nordamerika mit Hilfe der Inoceramen. In L.B. Kellum (chairman), *El Sistema Cretacico. Un symposium sobre el Cretacico en el hemisferio occidental y su correlacion mundial*: vol. 1: 113–130. 20th International Geological Conference, Mexico City, Mexico.
- Shank, J.A. 2012. Sedimentology and allostratigraphy of the Cardium Formation (Turonian-Coniacian) in southern Alberta and equivalent strata in northern Montana. Ph.D. dissertation, University of Western Ontario, London, 374 pp.
- Shank, J.A., and A.G. Plint. 2013. Allostratigraphy of the Upper Cretaceous Cardium Formation in subsurface and outcrop in southern Alberta, and correlation to equivalent strata in northwestern Montana. *Bulletin of Canadian Petroleum Geology* 61: 1–40.
- Stott, D.F. 1956. The Alberta Group, Rocky Mountain Foothills, Alberta. Geological Survey of Canada Paper 56-1: 1–71.
- Stott, D.F. 1963. The Cretaceous Alberta Group and equivalent rocks, Rocky Mountain Foothills, Alberta. Geological Survey of Canada Memoir 317: 1–297 p.
- Stott, D.F. 1967. The Cretaceous Smoky Group, Rocky Mountain Foothills, Alberta and British Columbia. Geological Survey of Canada Bulletin 132: 1–133.
- Varban, B.L., and A.G. Plint. 2008a. Palaeoenvironments, palaeogeography, and physiography of a large, shallow, muddy ramp: Late Cenomanian-Turonian Kaskapau Formation, Western Canada foreland basin. *Sedimentology* 55: 201–233.
- Varban, B.L., and A.G. Plint. 2008b. Sequence stacking patterns in the Western Canada foredeep: Influence of tectonics, sediment loading and eustasy on deposition of the Upper Cretaceous Kaskapau and Cardium formations. *Sedimentology* 55: 395–421.
- Wadsworth, J.A., and R.G. Walker. 1991. Morphology and origin of erosion surfaces in the Cardium Formation (Upper Cretaceous, Western Interior Seaway, Alberta) and their implications for rapid sea-level fluctuations. *Canadian Journal of Earth Sciences* 28: 1507–1520.
- Walaszczyk, I., and W.A. Cobban. 2006. Palaeontology and biostratigraphy of the Middle-Upper Coniacian and Santonian inoceramids of the US Western Interior. *Acta Geologica Polonica* 56: 241–348.
- Walaszczyk, I., J.A. Shank, A.G. Plint, and W.A. Cobban. 2014. Inter-regional correlation of disconformities in Upper Cretaceous strata, Western Interior Seaway: biostratigraphic and sequence-stratigraphic evidence for eustatic change. *Bulletin of the Geological Society of America* 126: 307–316.
- Wall, J.H., and R.K. Rosene. 1977. Cretaceous stratigraphy and micropaleontology of the Crowsnest Pass-Waterton area, southern Alberta Foothills. *Bulletin of Canadian Petroleum Geology* 25: 842–867.
- Williams, G.D., and C.R. Stelck. 1975. Speculations on the Cretaceous palaeogeography of North America. In W.G.E. Caldwell (editor), *The Cretaceous System in the Western Interior of North America*. Geological Association of Canada Special Paper 13: 1–20.
- Wright, G.N., M.E. McMechan, and D.E.G. Potter. 1994. Chapter 3: Structure and architecture of the Western Canada Sedimentary Basin. In G. Mossop and I. Shetsen (compilers), *Geological Atlas of the Western Canada Sedimentary Basin*: 25–40. Calgary: Canadian Society of Petroleum Geologists and Alberta Research Council.

APPENDIX 1

Location of Measured Sections in this Study, Including Reference to Available Published Accounts

Locality Name	Published Description	Canadian NTS Grid Reference Latitude, Longitude	Access
Bighorn Dam	N/A	83C/8 462953 52°18'26.30"N, 116°19'06.49"W	Walk
Bighorn River	Stott, 1963, cross section 5-38	83C/8 366038 52°23'07.0"N 116°27'46.79"W	Helicopter
Blackstone River east	N/A	83C/9 472298 52°38'20.37"N, 116°18'17.76"W	Walk
"Brown Creek" (actually an un-named tributary of Brown Creek)	Stott, 1963, pl. 27, no description.	83C/10 214416 52°43'15.13"N 116°41'08.63"W	Helicopter
Burnt Timber Creek	Stott, 1963, cross section 6-9	82O/11 257108 51°32'06.01"N 115°11'12.22"W	Walk
Cardinal River	Stott, 1963, cross section 4-31	83C/15 221578 52°52'15.73"N 116°40'30.85"W	Walk
Chungo Creek	Stott, 1963, cross section 4-8	83C/9 375383 52°41'42.68"N 116°26'51.03"W	Walk
Cripple Creek	Stott, 1963, cross section 5-42	83B/4 705844 52°12'27.35"N 115°58'02.85"W	Walk
Cutpick Creek	Close to Stott, 1967, cross section 58-2	83L/3 605924 54°03'42.56"N 119°07'58.98"W	Helicopter
Highwood River	N/A (Stott, 1963, cross section 6-46 is faulted)	82J/9 849997 50°31'22.09"N 114°23'30.1"W	Walk
Kevin (Montana)	Cobban et al., 1976. Site 1A	48°47'36.3"N 111°56'27.83"W	Walk
	Site 1B	48°48'08.79"N 111°56'25.73"W	Walk
	Site 2	48°47'40.22"N 111°58'56.4"W	Walk
	Site 3A	48°49'04.54"N 111°59'50.66"W	Walk
	Site 3B	48°48'54.03"N 111°59'57.42"W	Walk
James River	Stott, 1963, cross section 6-5a	82O/14 291450 51°50'29.54"N 115°07'41.53"W	Walk
Mill Creek	Wall, 1967, Wall and Rosene, 1977	82G/8 074728 49°22'28.2"N 114°08'40.94"W	Walk
Mill Ck - tributary	N/A	82G/8 075727 49°22'26.79"N 114°08'38.03"W	Walk
Lynx Creek	Stott, 1963, cross section 6-4	83B/4 769759 52°07'48.59"N 115°52'36.17"W	Walk
Oldfort Creek	N/A	82O/2 401674 51°08'26.86"N 114°59'50.8"W	Walk
Ram River	N/A	83B/4 795777 52°04'58.47"N 115°50'27.99"W	Walk
Sheep River	Stott, 1963, cross section 6-34	82J/10 654118 50°38'15.69"N 114°39'40.33"W	Walk
Sullivan Creek	N/A	82J/9 845007 50°31'54.56"N 114°23'46.9"W	Walk
Thistle Creek West	Stott, 1963, cross section 4-52	83C/15 095493 52°47'41.68"N 116°51'37.4"W	Walk
Thistle Creek East	N/A	83C/15 118497 52°47'53.48"N 116°49'32.1"W	Walk
Wapiabi Creek	Stott, 1963, cross section 4-6	83C/9 415263 52°35'19.39"N 116°23'18.29"W	Walk

APPENDIX 2

Results of Carbon Isotope Analyses of Samples from Cutpick Creek

Sample Number	TOC (wt %)	$\delta^{13}\text{C}$ ‰ (VPDB)	Strat. Ht (m)
Cut 2 08-1	1.37	-26.26	0.2
Cut 2 08-2	1.09	-26.42	1.2
Cut 2 08-3	1.20	-26.37	2.2
Cut 2 08-4	1.13	-26.35	3.2
Cut 2 08-5	1.37	-26.38	4.2
Cut 2 08-6	1.38	-26.61	5.2
Cut 2 08-7	1.42	-26.51	6.2
Cut 2 08-8	1.39	-26.65	7.2
Cut 2 08-9	1.18	-26.74	8.2
Cut 2 08-10	1.31	-26.27	9.2
Cut 2 08-11	1.52	-26.10	10.2
Cut 2 08-12	1.27	-26.35	11.2
Cut 2 08-13	1.49	-26.21	12.2
Cut 2 08-14	1.38	-26.29	13.2
Cut 2 08-15	1.31	-26.08	14.2
Cut 2 08-16	1.21	-26.22	15.2
Cut 2 08-17	1.30	-26.17	16.2
Cut 2 08-18	0.87	-26.39	17.2
Cut 2 08-19	1.14	-26.48	18.2
Cut 2 08-20	1.37	-26.25	19.2
Cut 2 08-21	1.14	-26.53	20.2
Cut 2 08-22	1.24	-26.28	21.2
Cut 2 08-23	1.12	-26.30	22.2
Cut 2 08-24	1.12	-26.21	23.2
Cut 2 08-25	0.96	-26.42	24
Cut 2 08-26	1.14	-26.08	25.3
Cut 2 08-27	1.14	-25.84	26.6
Cut 2 08-28	0.83	-26.17	27.8
Cut 2 08-29	1.22	-25.95	29
Cut 2 08-30	0.97	-26.13	30.2
Cut 2 08-31	1.20	-26.07	31.2
Cut 2 08-32	1.06	-26.11	32.2
Cut 2 08-33	1.14	-26.05	33.2
Cut 2 08-34	1.21	-25.95	34.2
Cut 2 08-35	1.33	-25.62	35.2
Cut 2 08-36	1.33	-25.74	36.2

Sample Number	TOC (wt %)	$\delta^{13}\text{C}$ ‰ (VPDB)	Strat. Ht (m)
Cut 2 08-37	0.99	-25.79	37.2
Cut 2 08-38	1.05	-25.92	38.2
Cut 2 08-39	1.14	-25.76	39.2
Cut 2 08-40	1.02	-25.80	40.2
Cut 2 08-41	1.09	-25.82	41.2
Cut 2 08-42	1.27	-25.76	42.1
Cut 2 08-43	1.22	-25.94	43.1
Cut 2 08-44	0.73	-26.33	44
Cut 2 08-45	1.06	-26.02	45
Cut 2 08-46	1.06	-25.86	46
Cut 2 08-47	1.14	-25.81	47
Cut 2 08-48	1.08	-25.83	48
Cut 2 08-49	1.17	-25.77	49
Cut 2 08-50	0.97	-25.84	50
Cut 2 08-51	1.04	-25.84	51
Cut 2 08-52	1.07	-25.88	52
Cut 2 08-53	1.04	-25.86	53
Cut 2 08-54	0.90	-25.81	54
Cut 2 08-55	1.06	-25.86	55
Cut 2 08-56	1.14	-25.71	56
Cut 2 08-57	0.97	-25.73	57
Cut 2 08-58	1.03	-25.82	58
Cut 2 08-59	1.13	-25.65	59
Cut 2 08-60	1.14	-25.65	60
Cut 2 08-61	1.22	-25.75	61
Cut 2 08-62	1.11	-25.59	62
Cut 2 08-63	1.21	-25.49	63
Cut 2 08-64	1.07	-25.56	64
Cut 2 08-65	1.05	-25.55	65
Cut 2 08-66	0.78	-25.77	66
Cut 2 08-67	1.17	-25.30	67
Cut 2 08-68	1.22	-25.33	68
Cut 2 08-69	1.06	-25.21	69
Cut 2 08-70	0.73	-26.06	70
Cut 2 08-71	1.20	-25.29	71.8
Cut 2 08-72	0.87	-25.78	72.8
Cut 2 08-73	0.62	-25.77	73.8
Cut 2 08-74	1.38	-25.29	74.8
Cut 2 08-75	0.94	-25.68	75.8

Sample Number	TOC (wt %)	$\delta^{13}\text{C}$ ‰ (VPDB)	Strat. Ht (m)
Cut 2 08-76	0.94	-25.51	76.8
Cut 2 08-77	0.80	-25.71	77.8
Cut 2 08-78	1.01	-25.30	78.8
Cut 2 08-79	1.16	-25.31	79.5
Cut 2 08-80	0.71	-25.50	80.5
Cut 2 08-81	0.54	-25.53	81.7
Cut 2 08-82	0.78	-25.28	82.9
Cut 2 08-83	0.73	-25.37	83.9
Cut 2 08-84	0.72	-25.43	85
Cut 2 08-85	0.89	-25.31	85.9
Cut 2 08-86	1.20	-25.47	86.2
Cut 2 08-87	1.34	-25.27	87.5
Cut 2 08-88	1.15	-25.58	88.3
Cut 2 08-89	0.87	-25.62	89.3
Cut 2 08-90	0.77	-25.71	90.3
Cut 2 08-91	1.05	-25.72	91.3
Cut 2 08-92	1.16	-25.47	92.4
Cut 2 08-93	0.76	-25.80	93.4
Cut 2 08-94	0.65	-25.74	94.4
Cut 2 08-95	1.04	-25.48	95.4
Cut 2 08-96	1.57	-25.14	96.4
Cut 2 08-97	2.52	-24.19	98.2
Cut 2 08-98	1.10	-25.16	100.3
Cut 2 08-99	0.39	-26.44	102.3
Cut 2 08-100	0.88	-25.37	104.2
Cut 2 08-101	0.76	-25.11	105.3
Cut 2 08-102	1.42	-25.10	106.8
Cut 2 08-103	1.35	-24.82	107.8
Cut 2 08-104	1.35	-25.05	108.8
Cut 2 08-105	1.35	-24.86	110.5
Cut 2 08-106	2.51	-24.71	111.3
Cut 2 08-107	1.20	-26.24	113.5
Cut 2 08-108	1.19	-25.89	114.5

Chapter 2

Inoceramid Bivalves from the Coniacian and Basal Santonian (Upper Cretaceous) of the Western Canada Foreland Basin

IRENEUSZ WALASZCZYK,¹ A. GUY PLINT,² AND NEIL H. LANDMAN³

ABSTRACT

Inoceramid bivalves are the dominant invertebrate fauna of the Coniacian and basal Santonian of the Western Canada Foreland Basin in western Alberta. In the upper lower Coniacian through to basal Santonian, six successive faunas are recognized, which provide the basis for corresponding, formally defined inoceramid zones. From bottom upward these are the zones of: *Cremnoceramus crassus crassus* / *C. deformis deformis*, *Inoceramus gibbosus*, *Volvicceramus koeneni*, *Volvicceramus involutus*, *Sphenoceramus subcardissoides*, and *Sphenoceramus* ex gr. *pachti*. Particular faunas represent assemblages known widely from the Euramerican biogeographic region, although they characterize mostly its northern, boreal area. The inoceramid-based biostratigraphic scheme allows correlation with other parts of the North American Western Interior and with parts of the Euramerican biogeographic region.

The studied succession provides a good record of the *Inoceramus gibbosus* Zone, which characterizes the topmost lower Coniacian. This zone, first recognized from northern Germany, is usually absent, both in Europe and in North America, due to a stratigraphic gap resulting from a eustatic lowstand. The base of the middle Coniacian is marked by the abrupt appearance of the taxonomically variable *Volvicceramus* fauna (*V. koeneni* (Müller), *V. exogyroides* (Meek and Hayden)), with associated *Inoceramus undabundus* Meek and Hayden and *Volvicceramus cardinalensis*, newly described herein. *Scaphites* (*Scaphites*) *ventricosus* Meek and Hayden, the ammonite marker of the base of the middle Coniacian first appears in the late early Coniacian. The base of the upper Coniacian marks the first appearance of the characteristic northern inoceramid species *Sphenoceramus subcardissoides* (Schlüter), the appearance of which coincides with *Scaphites* (*Scaphites*) *depressus* Reeside, the ammonite marker of this boundary. Close to this boundary *Volvicceramus stotti* also appears, which is newly described from the Canadian sections. The base of the Santonian corresponds to the abrupt appearance of *Sphenoceramus* ex gr. *pachti* (Arkhangelsky).

The studied sections demonstrate that the appearance of new inoceramid faunas (lowest occurrence of *Cremnoceramus crassus crassus* (Petrascheck), of various species of *Volvicceramus*, *Sphenoceramus subcardissoides* (Schlüter) and of *S.* ex gr. *pachti*) takes place immediately above major marine flooding surfaces, suggesting a close correspondence between evolutionary and/or migration events and episodes of relative sea-level rise.

¹ Faculty of Geology, University of Warsaw, Warszawa, Poland.

² Department of Earth Sciences, University of Western Ontario, London, Ontario, Canada.

³ Division of Paleontology, American Museum of Natural History.

INTRODUCTION

The Coniacian and Santonian (Upper Cretaceous) succession of the Western Canada Foreland Basin is characterized by a rich molluscan (principally ammonites and inoceramids) record. Recent fieldwork on sections exposed in the foredeep in Alberta (see Plint et al., this volume) allowed the collection of fossils from the most complete sections of Coniacian strata in the basin. Each specimen was precisely located in a high-resolution allostratigraphic framework that extended throughout the foredeep (Plint et al., this issue). Consequently, the palaeontological material could be placed within a high-resolution stratigraphical, temporal, and spatial framework. This paper provides the description of the inoceramid faunas, including their taxonomy, biostratigraphy, and biogeographic characteristics. The details of the physical stratigraphy, sedimentary facies and tectono-stratigraphic evolution of the area are provided in a companion paper by Plint et al. (this issue); the ammonites are documented in a companion paper by Landman et al. (this issue).

GEOLOGICAL SETTING AND LOCALITIES

The studied area lies within the foredeep of the Western Canada Foreland Basin in western Alberta, embracing the area between the Cutpick Creek section in the north (close to the town of Grande Cache), south to Kevin, in northern Montana, spanning a distance of about 750 km (fig. 1). The Coniacian and basal Santonian strata studied herein are dominated by mudstone, with subordinate sandstone, and belong to the Muskiki and Marshybank members in the lower part of the Wapiabi Formation. The lower boundary of the studied interval is placed at the top of the underlying Cardium Formation, at disconformity surface E7 of Plint et al. (1986). The top of the studied interval is placed a short distance above surface SS0, that marks the base of the Santonian, as defined biostratigraphically by the first occurrence of the ammonite *Clioscaphtes saxitonianus*

(McLearn, 1929) (see Landman et al., this issue), the first occurrence of the inoceramid, *Sphenoceras* ex gr. *pachti* (Arkhangelsky, 1912), and in allostratigraphic terms by a major marine flooding surface (Plint et al., this issue).

The entire studied succession comprises a series of upward-coarsening, upward-shoaling packages, bounded by marine flooding surfaces. The regional correlation of marine flooding surfaces, based on data from abundant wireline well logs, numerous outcrop sections and a few cores, allowed the subdivision of the entire succession into 24 informal allomembers (CA1 through CA24), interpreted to be the result of high-frequency eustatic sea-level changes. The surfaces bounding allomembers are interpreted to approximate time lines and hence the allomembers can be considered to represent approximate chronostratigraphic subdivisions of the succession (Plint et al., this issue).

The material studied comes from 19 sections, located mostly in the Rocky Mountain Foothills (fig. 1). The graphic logs for each studied section, the stratigraphical location of the specimens studied herein, and their location within the informal allomembers are provided by Plint et al. (this issue). The summary chart showing the stratigraphic ranges of inoceramids in relation to the allostratigraphic framework is shown in figure 2.

BIOSTRATIGRAPHY

The biostratigraphic data are derived from allomembers CA1 to CA24 (bounded by surfaces E7, CS1 through CS24, and SS0), spanning the upper lower to upper Coniacian (fig. 1, and Plint et al., this issue). In all intervals where biostratigraphic data are available, both the bio- and physical stratigraphies form a consistent succession. Because the allomembers may be interpreted as chronounits (see Plint et al., this issue), then, strictly speaking, the biostratigraphic zones, as proposed herein, are chrono-biostratigraphic; the ranges of particular taxa given are composite ranges for the entire area, based on the allostratigraphic (physical) correlation of the

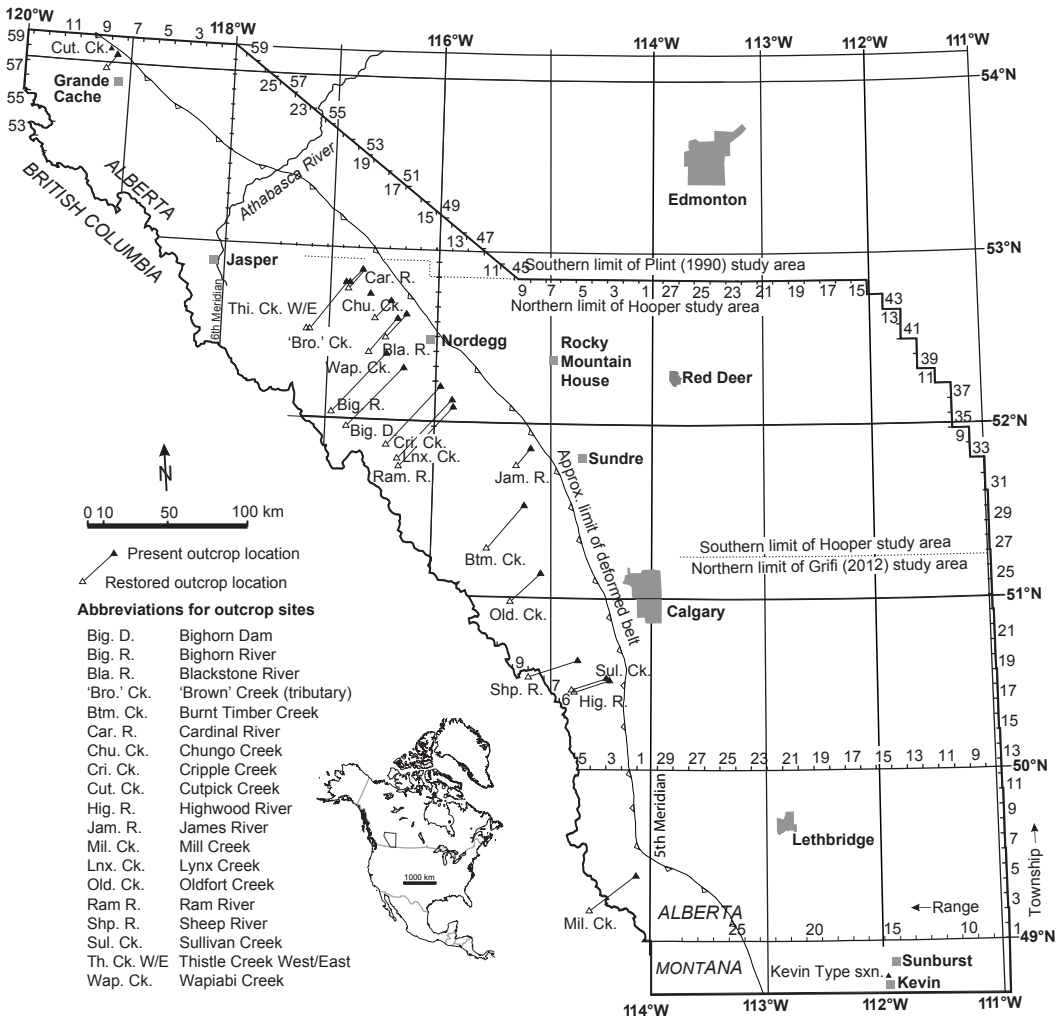


FIG. 1. Map of localities and the location of the study area with respect to the outline map of North America.

units that contain the fossils. In most cases the first appearance of taxa seem to correspond, as expected, to flooding surfaces that form the boundaries of allomembers.

Six biostratigraphic zones are distinguished within the studied interval (figs. 2, 3). All are defined as interval zones. They are characterized, in ascending order, below. The paleobiogeographic terms used are after Kauffman (1973). The correlation with previously proposed Western Interior inoceramid zonation (of Kauffman et al., 1993; and of Collom, 2001), as well as with

the European subdivision (as compiled by Tröger, 1989), are shown in figure 3.

CREMOCERAMUS CRASSUS CRASSUS–CREMOCERAMUS DEFORMIS DEFORMIS INTERVAL ZONE: The base of the zone is defined by the first occurrence of any of the index taxa, and its top is placed at the first occurrence of *Inoceramus gibbosus* Schlüter, 1877 as defined herein. In physical terms, the base coincides with surface E7, which marks the base of allomember CA1. As the lowest occurrence of *I. gibbosus* is recorded in allomember CA2, the top of the zone is placed at the base of

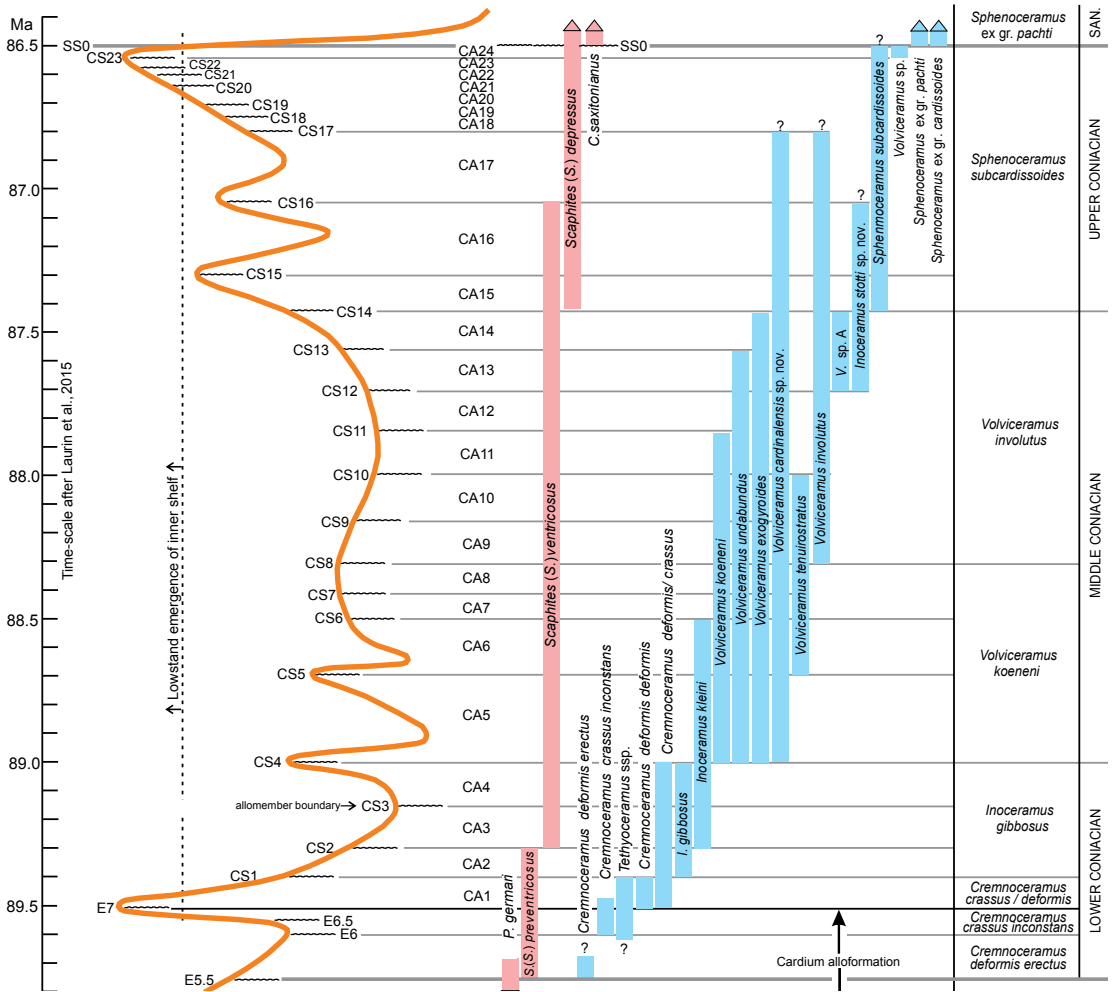


FIG. 2. Inoceramid ranges and zonation plotted against interpreted bathymetric changes in the interval studied. E5 through E7; CS1 through CS23, and SS0—erosional surfaces; CA1 through CA24—allomembers.

allomember CA2. The index taxa range higher, up to the middle part of allomember CA4. The other inoceramid taxa are: *Cremnoceramus crassus inconstans* (Woods, 1912) and *Tethyoceramus* spp.

The zone is widely recognizable within the entire Euramerican biogeographic region, northern Mediterranean Province, as well as in the South Atlantic Subprovince (e.g., Marcinowski et al., 1996; Walaszczyk and Wood, 1998; Kauffman and Bengtson, 1985; Walaszczyk et al., 2010, 2012, 2013).

In ammonite terms the zone corresponds to the uppermost part of the *Scaphites* (*Scaphites*) *preventricosus* Zone (figs. 2, 3; see also Landman et al., this issue).

The zone is well documented in all of the surface exposures that encompass the lower part of the succession: Wapiabi Creek, Chungo Creek, Blackstone River, Cutpick Creek, West Thistle Creek, and Bighorn Dam (fig. 1).

INOCERAMUS GIBBOSUS INTERVAL ZONE: The base of the zone is placed at the first occurrence

STAGE	substage	THIS PAPER	Ammonite subdivision LANDMAN ET AL., this volume	TROEGER 1989	KAUFFMAN ET AL. 1993	COLLOM 2001		
SANTONIAN	Lower	<i>Sphenoceramus</i> ex gr. <i>pachti</i>	<i>Clioscapites</i> <i>saxitonianus</i>	26 <i>Cladoceramus</i> <i>undulatoplicatus</i>	<i>Cladoceramus</i> <i>undulatoplicatus</i> <i>Platyceramus</i> <i>cycloides</i>	<i>Sphenoceramus</i> <i>pachti pachti</i>	<i>Platyceramus platinus</i> <i>Cordiceramus haenleini</i>	
	Upper	<i>Sphenoceramus</i> <i>subcardissoides</i>	<i>Scaphites</i> (S.) <i>depressus</i>	25 <i>Magadiceramus</i> <i>subquadratus</i> (without <i>Volvicceramus</i>) 24 <i>Magadiceramus</i> <i>subquadratus</i>	<i>Magadiceramus</i> <i>subquadratus</i> , <i>Magadiceramus</i> <i>austinensis</i>	<i>Magadiceramus</i> <i>subquadratus</i> <i>complicatus</i>	<i>Volvicceramus involutus</i> <i>Magadiceramus</i> <i>subquadratus</i>	
CONIACIAN	Middle	<i>Volvicceramus</i> <i>involutus</i>	<i>Scaphites</i> (S.) <i>ventricosus</i>	23 <i>Volvicceramus</i> <i>involutus</i>	<i>Volvicceramus</i> <i>koeneni</i>	<i>Cremnoceramus</i> <i>wandereri</i> <i>Cremnoceramus</i> <i>inconstans</i> n.ssp. (late form)	<i>Mytiloides</i> <i>stantoni</i>	<i>Cremnoceramus crassus</i> <i>Cremnoceramus brownei</i>
		<i>Volvicceramus</i> <i>koeneni</i>		22 <i>Volvicceramus</i> <i>koeneni</i>		<i>Cremnoceramus</i> <i>s. woodsii</i>		
	Lower (part)	<i>Inoceramus</i> <i>gibbosus</i>	<i>Scaphites</i> (S.) <i>preventricosus</i>	21 <i>Inoceramus</i> (<i>Cremnoceramus</i>) <i>schloenbachi</i>	<i>Cremnoceramus</i> <i>brownei</i> ; <i>Cr. trans.</i> <i>Cr. deformis</i> to <i>Cr. schloenbachi</i>	<i>Cremnoceramus</i> <i>deformis</i> s.ssp. (late form)	<i>Cremnoceramus</i> <i>schloenbachi</i> <i>schloenbachi</i>	<i>Cremnoceramus deformis</i> <i>Cremnoceramus inconstans</i>
		<i>Cremnoceramus</i> <i>crassus / deformis</i>						
		<i>Cremnoceramus</i> <i>crassus inconstans</i>						

FIG. 3. Inoceramid zonation of the Coniacian and basal Santonian as recognized herein, and its correlation with the zonations of Tröger, 1989, Kauffman et al., 1993, and Collom, 2001.

of the index taxon, as here defined, and its top is at the first occurrence of the inoceramid genus *Volvicceramus*. In allostratigraphic terms the zone corresponds to allomembers CA2, CA3, and CA4 (fig. 2).

Inoceramids are quite variable in the zone. In addition to the index taxon, sulcate forms of *Inoceramus* ex gr. *lamarcki* Parkinson, 1819, *Inoceramus* sp., *Tethyoceramus wandereri* (Andert, 1911), and various species of *Cremnoceramus* were noted, which continue from the zone below.

In ammonite terms, the zone corresponds to the basal part of the *Scaphites* (S.) *ventricosus* Zone (fig. 2; see Plint et al., this issue). The latter species appears earlier than hitherto assumed, in the latest early Coniacian. In the U.S. Western Interior sections, the apparent coincidence of the boundary between the zones of *S. (S.) preventricosus* and *S. (S.) ventricosus* with the first appear-

ance of *Volvicceramus* is because of an hiatus at this level that spans at least the *I. gibbosus* Zone (see remarks in Walaszczyk and Cobban, 2006).

The zone was first documented in the Staffhorst Mine section in northern Germany (Walaszczyk and Wood in Niebuhr et al., 1999). Based on inoceramid assemblages reported from Eastern Europe (e.g., Glazunova, 1972) it is apparently also present there. In other parts of Europe and North America, the zone seems to be missing due to nondeposition and/or subsequent erosion. The zone is best documented in the sections on Sheep River, Blackstone River, Wapiabi Creek, and Chungo Creek (fig. 1).

VOLVICERAMUS KOENENI INTERVAL ZONE: The lower boundary of the zone is defined by the first occurrence of the index taxon and its top by the first occurrence of *Volvicceramus involutus* (Sowerby, 1828), its evolutionary

successor (fig. 2). The base of the zone is provisionally accepted as the base of the middle Coniacian (e.g., Tröger, 1989; Kauffman et al., 1996). The presence of the zone of *Volviceramus koeneni* (Müller, 1888) below the first appearance of *V. involutus* was documented in a series of reports (Stille, 1909; Heinz, 1928a; Tröger, 1969, 1974), and appears regularly in compilations of inoceramid zonations (Tröger, 1981, 1989). In the studied sections, definite *V. involutus* appears in allomember CA9. Consequently, the top of the *V. koeneni* Zone is placed at the base of this allomember.

Besides the index taxon, the zone is characterized by *Volviceramus cardinalensis*, sp. nov., *Volviceramys exogyroides* (Meek and Hayden, 1862), *Inoceramus undabundus* Meek and Hayden, 1862, and *Inoceramus kleini* Müller, 1888. The zone is best documented in the sections on Chungo Creek and at the Bighorn Dam (fig. 1).

VOLVICERAMUS INVOLUTUS INTERVAL ZONE: The base of the zone is defined by the first occurrence of the index taxon, and its top by the first occurrence of *Sphenoceramus subcardissoides* (Schlüter, 1877). In the allostratigraphic scheme applied herein, it spans an interval from surface CS7 up to surface CS15. Because the first appearance of *S. subcardissoides* coincides with the first appearance of *Scaphites* (*S.*) *depressus* Reeside, 1927, which marks the base of the upper Coniacian, the *V. involutus* Zone characterizes the upper part of the middle Coniacian.

The zone is dominated by volviceramids. The index taxon is actually rare. The forms that dominate are: *V. exogyroides* and *V. cardinalensis*, sp. nov. The *V. involutus* Zone corresponds to the upper part of the *S.* (*S.*) *ventricosus* Zone. The zone is well documented in the sections at Bighorn Dam, Sheep River, and Chungo Creek (fig. 1).

SPHENOCERAMUS SUBCARDISSOIDES INTERVAL ZONE: The base of the zone is defined by the first appearance of the index taxon and its top by the first appearance of *Sphenoceramus*

ex gr. *pachti* (Arkhangelsky, 1912). In terms of the allostratigraphic scheme, the zone ranges between surface CS14 and the top of the Coniacian, marked by surface SS0 (fig. 2). Although the boundaries of the zone are well defined, its internal characteristics concerning inoceramid faunas and their evolution are poorly known. Starting with surface CS19 and ranging up to surface CS23, there is almost no inoceramid record. The reason is that most of the upper part of the upper Coniacian succession is preserved only to the north of our studied area, in northwestern Alberta and adjacent British Columbia. Because of differential subsidence to the northwest and flexural upwarp to the southeast, upper Coniacian strata were either not deposited, or were beveled off across much of the studied area (see Plint et al., this issue: figs. 4, 26). In addition to the index taxon, the zone is characterized by *V. involutus*, *V. cardinalensis*, and *Volviceramus stotti*, sp. nov. (fig. 2).

In ammonite terms the *S. subcardissoides* Zone spans approximately the zone of *Scaphites* (*S.*) *depressus*, defined as the interval zone, ranging between the first occurrences of *S.* (*S.*) *depressus* Reeside, 1927 and of *Clioscapites saxitonianus* (McLearn, 1929) (fig. 2). The lower part of the zone is documented in a number of sections.

SPHENOCERAMUS EX GR. PACTI INTERVAL ZONE: Only the basal part of the zone was studied. Consequently, only the lower boundary, marked by the first occurrence of the index taxon, is defined herein. In allostratigraphic terms, the base of the zone is placed at surface SS0, which is taken herein as the base of the Santonian. The part of the zone, studied herein, is invariably characterized by the index taxon. In ammonite terms, the base of the zone coincides with the base of the zone of *C. saxitonianus* (fig. 2). The zone is best represented in the sections on West Thistle Creek, Cardinal River, and Cripple Creek. It is also documented in the sections on Ram River, Bighorn Dam, James River, and Kevin MT (fig. 1).

STAGE AND SUBSTAGE BOUNDARIES

CONIACIAN SUBSTAGE SUBDIVISION: There is no formal subdivision of the Coniacian Stage into substages, and what is currently used is a proposal that was generally approved during the Second International Symposium on Cretaceous Stage Boundaries, Brussels 1995. Accordingly, the base of the middle Coniacian is taken at the first occurrence of the inoceramid genus *Volviceramus*, and specifically of the species *V. koeneni*, and the base of the upper Coniacian at the first occurrence of the inoceramid species *Magadiceramus subquadratus* (Schlüter, 1887) (see Kauffman et al., 1996). Actually, these definitions follow the former German subdivision of the stage as used at least since the 1980s (see Tröger, 1989).

The appearance and widespread occurrence of *Volviceramus*, including *V. koeneni*, in the studied Canadian sections allows for direct biostratigraphic recognition of the base of the middle Coniacian. More problematic however, is the recognition of the base of the upper Coniacian. *Magadiceramus subquadratus* (and the genus in general) is a more southern form, and no specimens of the genus were found during this study. In the U.S. Western Interior, the genus has not been reported north of Wyoming (see Cobban et al., 2005). In this context, it is noteworthy that Collom (2001) reported specimens, referred by him to *Magadiceramus*, from as far north as Bad Heart River in north-central Alberta. At least two of his specimens (Collom, 2001: pl. 12, fig. 8; pl. 13, fig. 3) appear to be reliable *Magadiceramus*. (However, his specimen from Ellesmere Island, referred by him to *Magadiceramus subquadratus* (Schlüter) (Collom, 2001, pl. 39, fig. 6), belongs to *Sphenoceramus*). Even accepting the presence of these two specimens, however, it seems that the occurrence of the genus in Alberta is accidental and cannot be used confidently in biostratigraphic study. In contrast to *Magadiceramus*, a very distinct biostratigraphic horizon contains *Sphenoceramus subcardisoides*, recorded from the entire studied area. Based on

allostratigraphic interpretation of the horizon at which *S. subcardisoides* is first found, it appears that this species forms a distinct isochronous event (first appearance event) across the area, immediately above surface CS14. Its record from the higher part of the succession is, however, poorly constrained, although it is known from Ram River and Cardinal River in allomember CA24 at the top of the Coniacian. *Sphenoceramus subcardisoides* was reported from various areas in Europe, and in well-dated sections it appears at, or very close to the base of the upper Coniacian, as defined by *Magadiceramus* (see Tröger, 1974, 1989; Tröger and Christensen, 1991; Walaszczyk and Wood in Niebuhr et al., 1999). Consequently, the species is treated as a good secondary marker of the base of the upper Coniacian. The location of its first appearance close to the base of the upper Coniacian, as currently defined, is also confirmed by its coappearance with the ammonite *Scaphites* (*S.*) *depressus* (Landman et al., this issue), and seems to be confirmed by the carbon-isotope correlations between the Alberta succession and the European standard curve (Jarvis et al., 2006; see Plint et al., this issue: fig. 25).

THE WESTERN INTERIOR SCAPHITES SUBDIVISION OF THE CONIACIAN: In the American Western Interior, the Coniacian substages have long been defined based on ammonites of the genus *Scaphites* (Cobban, 1951). The base of the middle and upper Coniacian (as defined by inoceramids) are currently defined by the first appearances of *Scaphites* (*S.*) *ventricosus* and of *Scaphites* (*S.*) *depressus* respectively (Kennedy and Cobban, 1991; Cobban et al., 2005, 2006; Walaszczyk and Cobban, 2006). Based on the record in the sections studied herein, this correlation between the ammonite and inoceramid zonations requires some amendment in the case of the lower/middle Coniacian boundary. Based on our data, it appears that *S. (S.) ventricosus* does not coappear with *Volviceramus*, but appears slightly earlier, in the latest early Coniacian. The apparent coincidence of first occurrences of both taxa seems to result from a gap at this boundary (spanning the

Inoceramus gibbosus Zone) in most of the sections south of Alberta (Walaszczyk and Cobban, 2006; Walaszczyk et al., 2014b). What is confirmed, however, is the coincidence of the first occurrence of *S. (S.) depressus* with the inoceramid species *S. subcardissoides*, which seems to be a good proxy for the base of the upper Coniacian, as defined by the first occurrence of *Magadiceramus subquadratus*.

CONIACIAN-SANTONIAN BOUNDARY: This boundary is defined by the first appearance of the inoceramid species *Cladoceramus undulatopticatus* (Roemer, 1852) and the boundary was recently formally approved by the International Stratigraphical Commission (Lamolda et al., 2014). However, *C. undulatopticatus*, like *Magadiceramus*, is a more southern form. In the North American Western Interior it has never been reported from north of southern Wyoming (Cobban et al., 2005). Another biostratigraphic proxy for this boundary, often used in the American Western Interior, is the ammonite species *C. saxitonicus* (see Scott and Cobban, 1964; Cobban et al., 2005, 2006; Walaszczyk and Cobban, 2006, 2007). This latter species occurs commonly in the studied area (see Landman et al. and Plint et al., this issue) and may be reliably used to locate the base of the Santonian. Additionally, in the studied sections, its first appearance coincides with the first occurrence of the inoceramid *Sphenoceramus* ex gr. *pachti*. Although the clade of *Sphenoceramus pachti/cardissoides* first appears slightly earlier than *C. undulatopticatus*, which is the basal Santonian boundary marker (see Seitz, 1962, 1965; Tröger, 1989; Remin, 2004), the form described herein differs from the typical representatives of Arkhangelsky's species and, based on the ammonite record, coappears with *C. saxitonicus* at the base of the Santonian Stage.

BIOGEOGRAPHY AND EVOLUTION

During the Late Cretaceous, the studied area was a part of the Western Interior Endemic Center, which belonged to the North American Province and, together with the North European

Province, formed the Euramerican Biogeographic Region (subdivision according to Kauffman, 1973). In terms of inoceramid faunas, the region was fluctuating between a highly provincial state (early-middle Cenomanian; middle-early late Turonian), to a state characterized by strong faunal unification (late Cenomanian-early Turonian; late late Turonian till early late Maastrichtian). However, even during the unification intervals, the region was an evolving and highly dynamic system, controlled mostly by climatic and eustatic changes.

The interval studied herein, i.e., the late early Coniacian to early Santonian, represented a time of inoceramid unification on a scale of the entire Euramerican Region. At the same time, however, the inoceramid assemblages were characterized by a high turnover rate. There was a total exchange of inoceramid faunas at the early to middle Coniacian boundary and at the Coniacian-Santonian boundary. Additionally, there was a marked faunal exchange at the middle to late Coniacian boundary (fig. 2). The former assumption of a lack of external (environmental) perturbations during that time (eustasy, climate) has made it difficult to identify the mechanism that triggered these changes. The studied sections have revealed, however, a close correlation between turnover/exchange intervals in inoceramid evolution and important bathymetric changes, reflected in marked facies changes and regional erosional discontinuities. New faunas typically (but not always), accompany transgressive episodes that follow the main regressive troughs (fig. 2; and discussion in Plint et al., this issue). The main exception to this seems to be the middle to upper Coniacian boundary, which in the short term coincides with a high-frequency flooding surface but in the long term marks the onset of what is interpreted as major shallowing, defined by a dramatic change from weakly bioturbated to intensely bioturbated sediment across surface CS14 (Plint et al., this issue). This could also coincide with an oceanographic change from poorly oxygenated to well-oxygenated bottom water. The time equivalency of the

recognized turning points in inoceramid evolution all over the Euramerican biogeographic region suggests that the bathymetric trends recognized herein were of a eustatic nature (see Plint et al., this issue).

The precise cause of the correlation between bathymetric fluctuations and faunal changes is, however, unclear. It seems clear that both in-place evolution and immigration/emigration events played a part. The other external factor in inoceramid evolution, which is difficult to assess at the moment, seems to be climate. In the studied interval, inoceramid assemblages were characterized by broad north-south biogeographic shifts, which at least in part, could have been climatically controlled. A profound change is noted at the early to middle Coniacian boundary. Whereas the early Coniacian inoceramid assemblages of the studied area ranged southward all over the Western Interior Basin, the middle to late Coniacian and early Santonian faunas demonstrate a clear north-south pattern, with two biogeographic bioheres present, with the boundary between them located in the northern part of the U.S. Western Interior. In the middle Coniacian, the southern biohere was characterized by the co-occurrence of *Volviceramus* and *Platyceramus*, with the eventual disappearance of *Volviceramus* in the far south. Conversely, *Platyceramus* is absent from the northern biohere, which included the Canadian portion of the basin. In the late Coniacian and early Santonian, the northern biohere, including the study area, was characterized by the Boreal genus *Sphenoceramus*. This genus is generally absent south of Montana. (Some short-lived *Sphenoceramus* excursion events to the south are noted later in the Santonian.) In contrast, the southern biohere was characterized by the genera *Magadiceramus*, *Cladoceramus*, *Platyceramus*, and *Cordiceramus*, which only occasionally are noted in the north.

This biogeographic pattern is not restricted to the American Western Interior but characterizes the entire Euramerican biogeographic region. The appearance of distinct zonal faunas among inoceramids may suggest climatic zoning in at least middle to late Coniacian and early Santo-

nian time, established after the breakdown of more equitable conditions that prevailed during early Coniacian time.

TERMS AND REPOSITORIES

Terminology and measurements of the external morphologic features of inoceramid shell are modified after Harries et al. (1996) and are shown in figure 4.

The specimens described in this paper are housed in the Royal Tyrell Museum, Drumheller, Alberta, Canada, and are prefixed TMP; some comparative material used here is from U.S. National Museum, Washington, D.C., and prefixed USNM. The geographic location of source localities are shown in figure 1 (modified from Plint et al., this issue). The geological logs of particular sections, with their allostratigraphic interpretation and specimen location are in Plint et al. (this issue).

SYSTEMATIC PALEONTOLOGY

BIVALVIA LINNÉ, 1758

PTERIOMORPHA BUERLEN, 1944

PTERIOIDA NEWELL, 1965

PTERIOIDEA GRAY, 1847

INOCERAMIDAE ZITTEL, 1881 (ICZN 473)

Genus *Inoceramus* Sowerby, 1814

TYPE SPECIES: *Inoceramus cuvieri* Sowerby, 1814, by subsequent designation of Cox, 1969: 315.

Inoceramus ex gr. *lamarcki* Parkinson, 1819
(sulcate variety)

Figures 5A, B, E, F

MATERIAL: Two single left valves; TMP 2016.041.0097 from Wapiabi Creek and TMP 2016.041.0233 from West Thistle Creek.

MEASUREMENTS: See table 1.

DESCRIPTION: TMP 2016.041.0097 (fig. 5A, B) is a moderately large (hmax = 84.5 mm) left-

TABLE 1

Measurements of species.

Abbreviations to measurements are shown in figure 4; n indicates the number of ribs counted along the growth axis at 20 to 50 mm from the beak.

	hmax	h	l	b	AM	s	H	L	α	δ	h/l	n
<i>Inoceramus ex gr. lamarcki</i> Parkinson												
TMP 2016.041.0097; LV	86	61	46.5	14	32	-	-	-	60	-	0.76	2
TMP 2016.041.0097; LV	102	78	56	20	56	-	-	-	58	-	0.72	2
<i>Inoceramus gibbosus</i> Schlüter, 1877												
TMP 2016.041.0172; LV	65	60	38*	15	-	-	-	-	-	-	-	3
TMP 2016.041.0110; RV	56.5	-	-	-	-	-	-	-	-	-	-	3
<i>Inoceramus kleini</i> Müller, 1888												
RTM 2016.041.0407; RV	45.5	28.5	21.5	10.5	18	14	26	21	95	75	0.75	5
RTM 2016.041.0407; LV	42	34	25.5	12	26	19	32	26	100	70	0.75	5
<i>Inoceramus undabundus</i> Meek and Hayden, 1862												
TMP 2016.041.0400; RV 64.0	47	40.5	14	17	-	42.5	40.5	105	60	0.86	2	
TMP 2016.041.0426; RV 97*	64	50	19*	14*	-	49.5	60	105	40	0.78	2	
TMP 2016.041.0426; LV 113*	80	60	19*	21*	-	48	70	105	35	0.75	3	
TMP 2016.041.0434; RV 103	-	-	-	-	-	-	-	-	-	-	3	
<i>Volviceramus koeneni</i> (Müller, 1888)												
RTM 2016.041.0184; LV	106	89	67	41	44	30*	-	-	115*	85	0.75	-
RTM 2016.041.0184; RV	88.5	75	52	34	42	20*	-	-	115*	90*	0.7	5
RTM 2016.041.0333; LV	63	57	52	20	24	-	-	-	-	-	0.9	-
<i>Volviceramus involutus</i> Sowerby, 1828												
TMP 2016.041.0243; LV	94.5	88	68	49.5	-	-	-	-	90	60	0.77	-
TMP 2016.041.0362; LV	54.5	46	35	30	-	-	-	-	90	60	0.76	-
TMP 2016.041.0423; LV	77	67	55	51	-	-	-	-	95	55	0.82	-
TMP 2016.041.0431; LV	65*	41	31	28	-	-	-	-	90	60	0.75	-
<i>Volviceramus exogyroides</i> (Meek and Hayden, 1862)												
TMP 2016.041.0415; LV	101	60.5	47	17	10*	35*	36.5	59	88	30	0.8	5
TMP 2016.041.0420; LV	71	52	36	15	13	35*	34	51	88	28	0.7	6
TMP 2016.041.0200; LV	100	56	42	18	13	-	42	50	80	30	0.75	-

TMP 2016.041.0417; LV	99	56	42	19	13	32	43	50.5	98	42	0.75	-
TMP 2016.041.0198; LV	122	70	53	17	18*	37*	53	60	90	35	0.75	-
<i>Volviceramus stotti</i> , sp. nov.												
TMP 2016.041.0245; LV	121	93	77	37	38	44*	82	78	105	65		
TMP 2016.041.0439; LV	90	60	49	20	27	-	-	-	120	75	0.82	3
<i>Volviceramus</i> morphotype sp. A												
RTM 2016.041.0195; LV	103	85	83	19	32	43*	80	80	115	70	1	-
RTM 2016.041.0334; LV	107	98	92	31	40	44*	85*	85*	115	75	0.94	-

valve (LV) internal mold, with the disc well preserved, but with the posterior auricle missing. The disc is triangular in outline, orthocline, with the beak curved anterodorsally, projecting slightly above the hinge line. The anterior margin is long, concave below the umbo, straight ventralward. The ventral margin is regularly rounded. The disc is weakly to moderately inflated, with maximum inflation in the umbonal part. The anterior wall is moderately high, steep, and almost perpendicular to the commissure below the umbo. The disc is ornamented with widely spaced, apparently regular (although deformed in our specimen) commarginal rugae, slightly asymmetrical with their leading edges slightly steeper, and with rounded edges and interrugae spaces.

TMP 2016.041.0233 (fig. 5E, F) is an internal mold of the moderately large LV (hmax = 100.5 mm), with its beak and most of its posterior auricle missing. The preserved fragment of the posterior auricle suggests, however, that it was extended and relatively large, of the type similar to *Inoceramus lusatae* Andert. This specimen differs from TMP 2016.041.0097 in possessing a less steep anterior wall below the umbo and in the presence of a better-developed radial sulcus, posteriorly of the disc axis. The sulcus is shallow and poorly developed; it begins at approximately 35 mm axial distance. The ornament is of the same type in both specimens.

DISCUSSION: The two specimens clearly belong to the *Inoceramus lamarcki* group. They may be

closely allied to *Inoceramus annulatus* Goldfuss, 1836, or *Inoceramus lusatae* Andert, 1911 (the latter is suggested by the type of the posterior auricle in the larger specimen). From both of these species, our specimens differ in possessing the radial sulcus. This feature appears in various lineages/clades of the “*lamarcki*” group (e.g., in the Turonian *Inoceramus hobetsensis* Nagao and Matsumoto, 1939, *Inoceramus flaccidus* White, 1879, or in Turonian representatives of *Inoceramus lamarcki* Parkinson, 1819, as known from the U.S. Western Interior; see Noda, 1975, Kauffman, 1977; Kauffman et al., 1978, Noda and Matsumoto, 1998, Walaszczyk and Cobban, 2000), but its taxonomic significance is not clear (Noda, 1975; Noda and Matsumoto, 1998).

OCCURRENCE: Both specimens are from the topmost part of the lower Coniacian.

Inoceramus gibbosus Schlüter, 1877

Figures 5C, D, G

1877. *Inoceramus gibbosus* Schlüter: 271.

1888. *Inoceramus percostatus* Müller: 413, pl. 17, fig. 3.

?non 1911. *Inoceramus percostatus* Müller. Andert: 56, pl. 5, fig. 4.

1929. *Inoceramus dankeri* Heinz var. *anderti* Heinz. Heinz: 686, figs. 4–5.

1929. *Inoceramus gibbosus* Schlüter. Heine: 50, pl. 4, figs. 20–22.

1929. *Inoceramus percostatus* Müller. Heine: 46, pl. 3, figs. 14–17.

1929. *Inoceramus bilobatus* Müller. Heine: 49, pl. 4, figs. 18–19.
- ?non 1934. *Inoceramus percostatus* Müller. Andert: 119, pl. 5, fig. 4.
1958. *Inoceramus russiensis* Nikitin. Bodylevski: 78, pl. 29, fig. 1; pl. 31, fig. 1.
1959. *Inoceramus percostatus* Müller. Drobrov and Pavlova: 145, pl. 12, fig. 3.
- non 1963. *Inoceramus percostatus* Müller. Assmus: 45, pl. 9, fig. 1.
- ?non 1969. *Inoceramus percostatus* Müller. Khalafova: 177, pl. 13, fig. 4; pl. 14, fig. 1 [pl. 13, fig. 4 = *deformis* group; pl. 14, fig. 1 = ?*Tethyoceramus* sp.]
1972. *Inoceramus percostatus* Müller. Glazunova: 59, pl. 2, figs. 1–2; pl. 3, fig. 2; pl. 9, fig. 1, pl. 13, fig. 6.
1972. *Inoceramus percostatus* Müller subsp. *gorenkaensis* subsp. nov., Glazunova: 60, pl. 4, figs. 1–2; pl. 6, figs. 1–2; pl. 7, fig. 1; pl. 9, fig. 2.
2006. *Inoceramus gibbosus* Schlüter, 1877. Walaszczyk and Cobban: 273; text-figs. 21, 12.11 and 13.5.

TYPE: The holotype, by monotypy, is the original of Schlüter (1877: 271) first illustrated by Heine (1929: pl. 4, figs. 20–22) from the upper Coniacian of Osterfeld Mine near Oberhausen, in Westphalia, northern Germany.

MATERIAL: Twenty-six specimens in total, most of which are fragmentarily preserved. TMP 2016.041.0110 through 2016.041.0127, from Blackstone River. TMP 2016.041.0236 from Thistle Creek. TMP 2016.041.0098, 2016.041.0089, 2016.041.0090, and 2016.041.0095, from Wapiabi Creek. TMP 2016.041.0170 and 2016.041.0172 from Chungo Creek. One unnumbered specimen from Sheep River.

MEASUREMENTS: See table 1.

DESCRIPTION AND REMARKS: Most of the specimens in our collection are small-sized, juvenile fragments from the Blackstone River section. They show, however, the upright form, pointed beak, and triangular outline, with well-developed, distinct rugae, covered with well-

developed, sharp-edged growth lines, typical for the species.

The best preserved is specimen TMP 2016.041.0110 from Blackstone River; the major part of the adult stage is well preserved (fig. 5D). Its umbonal part is poorly preserved (deformed), as is its anterior part. The disc, within the preserved part, is subrectangular in outline, and possesses a distinct radial sulcus posteriorly of the growth axis. The sulcus is shallow and does not deform the concentric rugae. The concentric rugae are regular to subregular, symmetrical, with rounded edges. They are covered with sharp-edged growth lines, which are evenly developed on the entire height of the disc.

The juvenile fragment from Sheep River (fig. 5C) possesses a well-preserved posterior auricle, which is extended and well separated from the disc, along a well-developed auricular sulcus. The disc is covered with subregular concentric rugae, superimposed by raised sharp-edged growth lines that are typical of the species.

The medium-sized incomplete specimen TMP 2016.041.0172 (fig. 5G), from Chungo Creek, demonstrates well the general outline of the species and type of ornament. The posterior part of its disc, with the posterior, radial sulcus, is deformed and partly missing.

OCCURRENCE: The species (as herein interpreted) is known from the Wapiabi Formation from localities on Blackstone River, Wapiabi Creek, West Thistle Creek, Sheep River, and Chungo Creek. It occurs invariably in the topmost part of the lower Coniacian, disappearing below the entry of the first *Volvicceramus*. The species, as herein understood, was first precisely located in the stratigraphic succession of the Staffhorst Mine section, in northern Germany (Walaszczyk and Wood in Niebuhr et al., 1999), where it occurs in an equivalent stratigraphic interval. Although the species was also reported from other regions (e.g., eastern part of European Russia; see, e.g., Nikitin, 1888; Glazunova, 1972), precisely located specimens have not been reported.

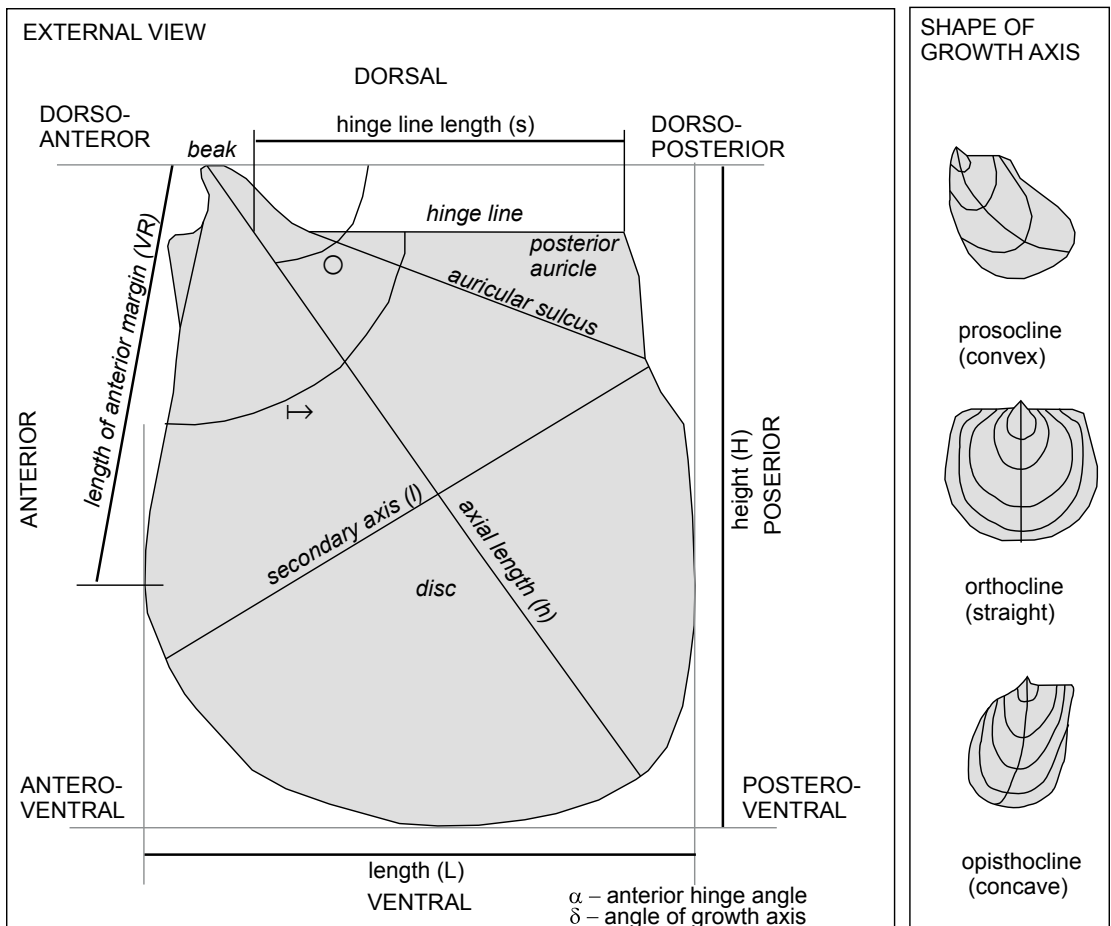


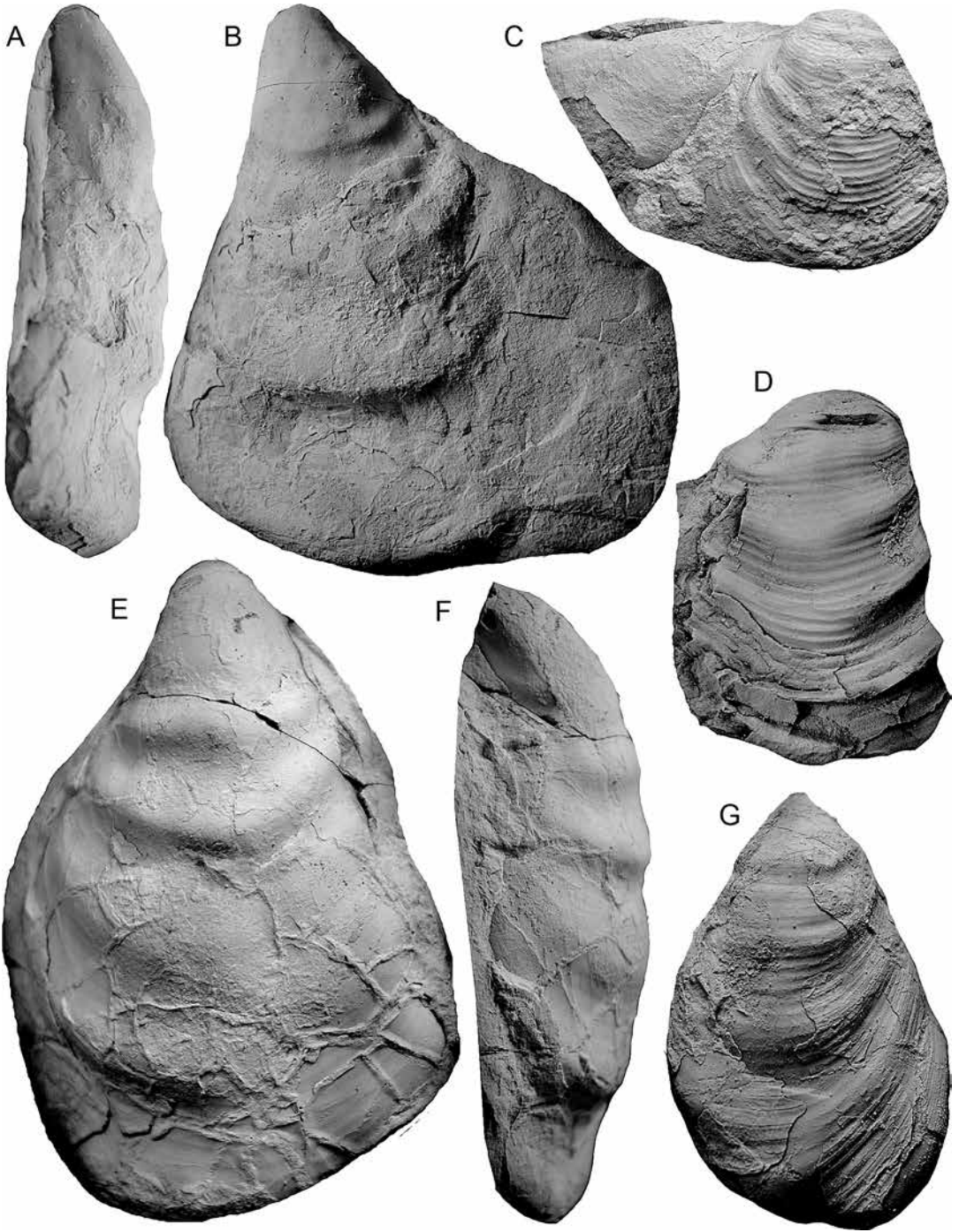
FIG. 4. Terminology and measurements of the external morphologic features of inoceramid shells as applied in this paper (partly after Harries et al., 1996).

Inoceramus kleini Müller, 1888

Figure 6

1888. *Inoceramus kleini*, sp. nov. G. Müller: 415, pl. 18, fig. 1a-b.
- ?pars 1911. *Inoceramus kleini* Müller. Andert: 48–50, pl. 2, fig. 6 [non pl. 1, fig. 7; pl. 2, figs. 3, 7–8].
- non 1934. *Inoceramus kleini* Müller. Andert: 115–117, text-figs. 10–12. pl. 4, figs. 9–10; pl. 5, figs. 1–2.
1929. *Inoceramus kleini* Müller. Heine: 44–46, pl. 2, figs. 10–11; pl. 3, figs. 12–13.
1969. *Inoceramus kleini* Müller. Radwanska: 709.
1979. *Inoceramus kleini* Müller. Ivannikov: 62, pl. 14, fig. 4; pl. 15, figs. 1–2; pl. 16, fig. 1; pl. 17, fig. 1.
- pars 1991. *Inoceramus kleini* Müller. Tarkowski: 109–110, pl. 13, fig. 7; pl. 14, fig. 2 [non pl. 14, fig. 3].
1992. *Inoceramus kleini* Müller. Walaszczyk: 37; pl. 38, fig. 3.
1992. *Inoceramus kleini* Müller. Cech and Sva-benicka, pl. 2, fig. 2.

TYPE: By monotypy, the holotype is the specimen figured by Müller (1888, pl. 18, fig. 1a-b) from the Spiegelsberge, south of Halberstadt



(Subhercynian Basin), Germany; from the middle Coniacian.

MATERIAL: Two specimens in total. Double-valve TM P 2016.041.0407, from Bighorn Dam, and one uncataloged, juvenile fragment of a single valve from West Thistle Creek.

MEASUREMENTS: See table 1.

DESCRIPTION: The double-valve specimen, TMP 2016.041.0407 (fig. 6A–C), is weakly deformed, almost complete, with posteroventral parts of valves missing. The specimen is equi-valve, inequilateral, small sized, and prosocline, with the disc subtriangular in outline and moderately inflated. The posterior auricle is small, moderately well separated from the disc. The beak is pointed, curved anterodorsally. Anterior margin is slightly concave below the umbo, then slightly convex; with the anterior margin steep. The ornament is composed of regularly spaced, symmetrical rugae, with interspaces growing gradually ventralward. The edges of the rugae are sharp. The rugae weaken on the posterior auricle and on the anterior wall, but are still visible.

REMARKS: The species is interpreted herein as the evolutionary precursor of *Inoceramus undabundus* Meek and Hayden. Early representatives of the latter species are similar in valve outline and type of ornament, however, the interspaces are much larger at equivalent axial length.

OCCURRENCE: The species spans the lower to middle Coniacian boundary. Although we have only two specimens (one from the topmost lower Coniacian in West Thistle Creek; and the second from the basal middle Coniacian at Bighorn Dam), this stratigraphic occurrence corresponds well with its occurrence in other areas. The species is known from Germany, Poland, Russia, Romania, and the Czech Republic.

Inoceramus undabundus Meek and Hayden, 1862

Figure 7A–D

1862. *Inoceramus undabundus* Meek and Hayden: 26.
1876. *Inoceramus undabundus* Meek and Hayden. Meek: 60, pl. 3, fig. 2.
1894. *Inoceramus undabundus* Meek and Hayden. Stanton: 84, pl. 16, figs. 1–2 [illustration and description after Meek, 1876].
1898. *Inoceramus undabundus* Meek and Hayden. Logan: 455, pl. 105, figs. 1–2. [illustration and description after Meek, 1876]
- ?1901. *Inoceramus undabundus* Meek and Hayden. Sturm: 92, pl. 10, fig. 4.
- pars* 1929. *Inoceramus undabundus* Meek and Hayden. Heine: 100, pl. 11, fig. 50; pl. 13, fig. 57 [non pl. 11, fig. 51; pl. 19, fig. 71, which are *Volviceramus exogyroides* Meek and Hayden]
- pars* 2006. *Inoceramus undabundus* Meek and Hayden, 1862. Walaszczyk and Cobban: 260; text-figs. 9.2, 9.4, 27.2, 28.2, 38.6 [only]

TYPE: The lectotype, designated by Walaszczyk and Cobban (2006: 260), is USNM 1909, which is the original of Meek (1876: pl. 3, fig. 2), from the Marias River Shale of Chippewa Point near Fort Benton, Chouteau County, Montana.

MATERIAL: Seven specimens; TMP 2016.041.0402, TMP 2016.041.0403, TMP 2016.041.0426, TMP 2016.041.0427, TMP 2016.041.0434; all from the Bighorn Dam section; TMP 2016.041.0244 from West Thistle Creek; and TMP 2016.041.0196 from Chungo Creek.

MEASUREMENTS: See table 1.

FIG. 5. **A, B**, *Inoceramus* ex gr. *lamarcki* Parkinson, 1819, sulcate form, TMP 2016.041.0097, Wapiabi Formation, Wapiabi Creek, 66.2 m: **A**, anterior view, **B**, left lateral view. **C**, *Inoceramus gibbosus* Schlüter, 1877, Wapiabi Formation, Sheep River, 76.0 m, right lateral view. **D**, *Inoceramus gibbosus* Schlüter, 1877, TMP 2016.041.0110, Wapiabi Formation, Blackstone River, 43.5 m, right lateral view. **E, F**, *Inoceramus* ex gr. *lamarcki* Parkinson, 1819, sulcate form, TMP 2016.041.0233, Wapiabi Formation, West Thistle Creek, 34.4 m: **E**, left lateral view, **F**, anterior view. **G**, *Inoceramus gibbosus* Schlüter, 1877, TMP 2016.041.0172, Wapiabi Formation, Chungo Creek, 42.0 m, right lateral view. All photographs are $\times 1$.

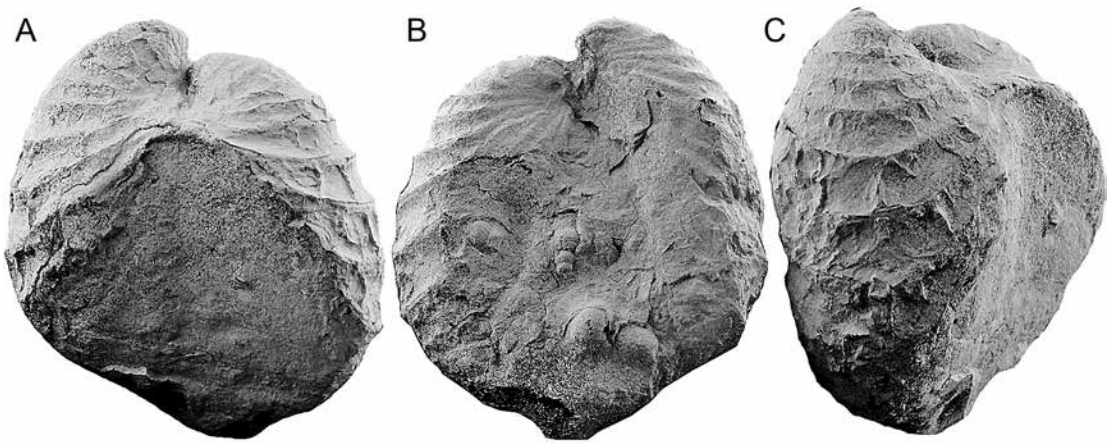


FIG. 6. *Inoceramus kleini* Müller, 1888, double-valve specimen, TMP 2016.041.0407, Wapiabi Formation, Bighorn Dam, 47.0 m: **A**, posterior view, **B**, anterior view, **C**, right lateral, view; the specimen is $\times 1$.

DESCRIPTION: The typical specimens of the species are TMP 2016.041.0426 (fig. 7A, D), TMP 2016.041.0427, TMP 2016.041.0434, and TMP 2016.041.0244. Based on these four specimens, the characteristic of the species is as follows. The shell is inequivalve, with LV larger and more inflated than the right valve (RV), with a general architecture typical for *Volviceramus*. Both valves grow obliquely, with δ angle ranging between 30° and 45° . The beaks in both valves pointed, only slightly coiled, not projecting above the hinge line. The oblique growth continues till ca. 10 cm in axial length, the obliquity is then markedly reduced. Both valves are ornamented with strong commarginal rugae, with distinct ventralward increase of interspaces. The details of the shell are not known; the rugae on internal molds are symmetrical to moderately asymmetrical, with leading edges steeper. The interspaces are distinctly wider than the rugae edges. The edges of the rugae are rounded.

The smallest specimen, which comes from the basal middle Coniacian and apparently phylogenetically the oldest (2016.041.0402; fig. 7B, C), is only slightly inequivalve. It already possesses, however, the typical ornament. TMP 2016.041.0403 from Bighorn Dam and TMP 2016.041.0196 from Chungo Creek, are fragments of LVs.

DISCUSSION: The material studied includes the first well-documented RVs of the species ever reported.

Although in our material the species is represented by only seven specimens, they demonstrate the evolution of the species from a relatively small-sized, weakly inequivalve morphotype (fig. 7B, C), in the earliest middle Coniacian, to moderate size, markedly inequivalve more advanced morphotype stratigraphically higher (fig. 7A, D). The phylogenetically oldest, weakly inequivalve specimens closely resemble *Inoceramus kleini*, from which they differ in having more robust ornament. The phylogenetically more advanced specimens possess features typical for volviceramids; this is particularly well seen on the RVs, in which the beak moves ontogenetically from its marginal position gradually inward (fig. 7A), as a consequence of inequivalve growth of the valve. Based on its evolutionary interpretation, the species (as a successor of *Inoceramus kleini*) is left in the genus *Inoceramus*, in spite of its close morphological resemblance to *Volviceramus*.

Walaszczyk and Cobban (2006) included into the synonymy of *Inoceramus undabundus* also *Inoceramus stantoni* (= *I. acuteplicatus* of Stanton, 1894) Sokolov, 1914. Based on the Canadian

material, however, it seems that phylogenetic changes of both species differ. In contrast to *I. undabundus*, *I. stantoni* remained only slightly inequivalve and preserved its more subtle ornament. Consequently we keep both species separate here. Both *I. undabundus* and *I. stantoni* seem to originate from *I. kleini*.

OCCURRENCE: *Inoceramus undabundus* is most abundant in the Bighorn Dam section, where it was found at levels 41.0, 60.0, and 73.0 m. The single specimen from West Thistle Creek is from 72.4 m, and the specimen from Chungo Creek is from 54.0 m. The species is known from the U.S. Western Interior and Gulf Coast of North America. It is convincingly documented from Poland (Sturm, 1901) and Germany (Heine, 1929).

Tethyoceramus (Sornay, 1980)

TYPE SPECIES: *Inoceramus* (*Tethyoceramus*) *basseae* Sornay (1980: pl. 1, figs. 1, 4, 6; pl. 2, figs. 1–3) by original designation.

DIAGNOSIS AND DISCUSSION ON THE GENUS: See Walaszczyk and Wood (1998).

Tethyoceramus sp.

Figure 8

MATERIAL: Six specimens in total. Single unnumbered specimen from Mill Creek, from 76.6 m; 4 specimens from Bighorn Dam: TMP 2016.041.0395 and TMP 2016.041.0391 from 8.5 m; TMP 2016.041.0398 from 10.5 m; and TMP 2016.041.0400 from 41.5 m. Single specimen from Highwood River, TMP 2016.041.0139.

REMARKS: The genus is relatively rare in the studied material, similar to the equivalent succession of the U.S. Western Interior (Walaszczyk and Cobban, 2000). Most of the specimens are poorly preserved, incomplete single valves. Two left valves of specimen TMP 2016.041.0395 (fig. 8) resemble *Tethyoceramus alpinus* (Heinz) (the smaller specimen) and *Tethyoceramus ernsti* (Heinz) (the larger one). To the latter species may also be referred the huge specimen from Highwood River (TMP 2016.041.0139). TMP 2016.041.0400 (not illustrated) is referred herein

to *Tethyoceramus wandereri* (Andert), based on its very slender form and strong inflation.

OCCURRENCE: The genus is known from the mid lower Coniacian in Europe and in the American Western Interior (see Walaszczyk and Wood, 1998; Walaszczyk and Cobban, 2000), and is well represented in Madagascar, where it apparently starts at the topmost Turonian and ranges through most of the lower Coniacian (Sornay, 1980; Walaszczyk et al., 2004, 2014a).

Cremnoceramus Cox, 1969

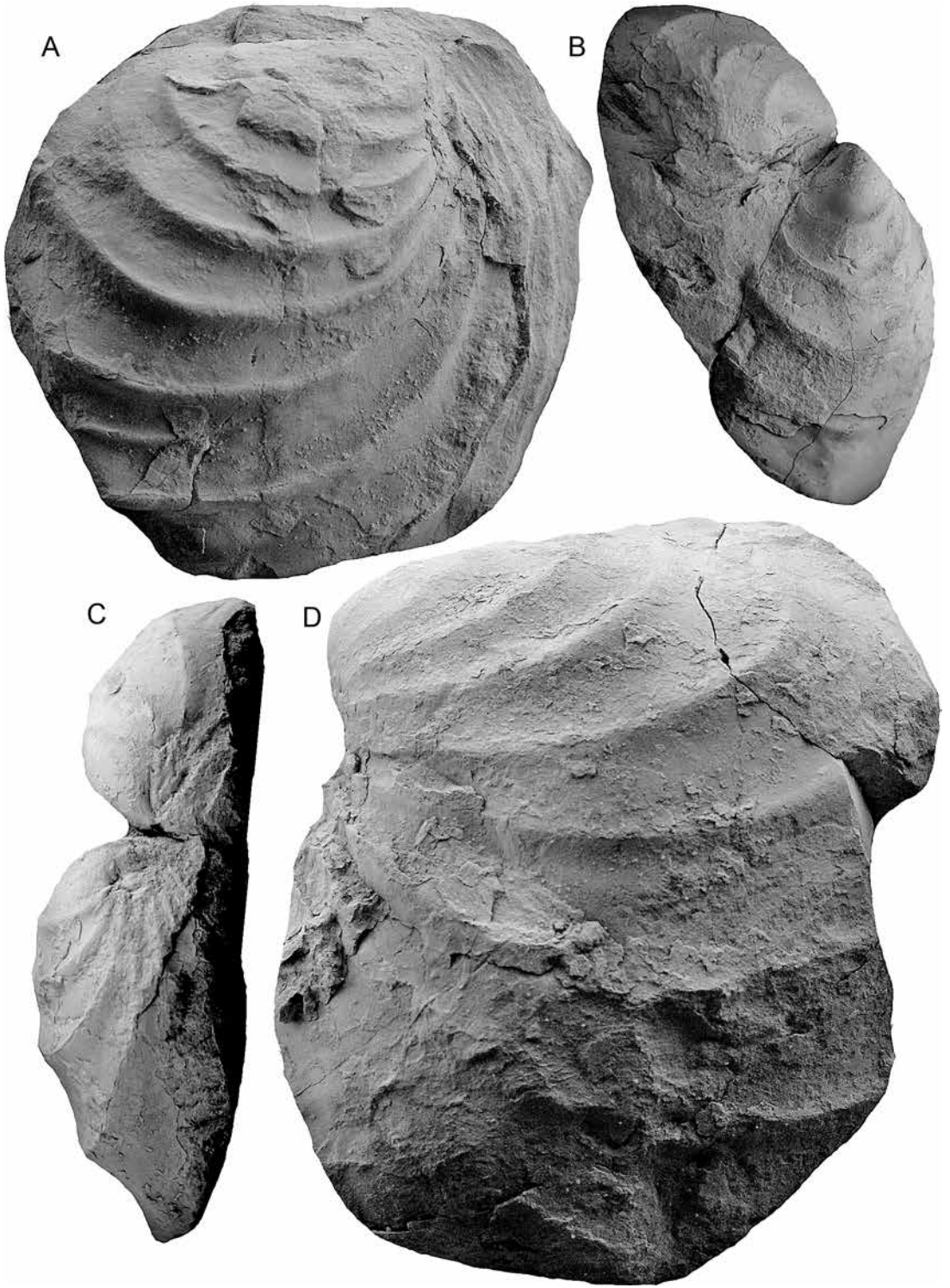
(*non Cremnoceramus* Heinz, 1932 (nomen nudum))

TYPE SPECIES: By original designation, *Inoceramus inconstans* Woods, 1912, from the lower Coniacian (Cox, 1969: N315).

Cremnoceramus sp.

Figures 9, 10

MATERIAL: Forty-one specimens in total. Seven specimens from Chungo Creek: TMP 2016.041.0176 through to TMP 2016.041.0180 from 33.5 m; TMP 2016.041.0175 from 34.5 m; and TMP 2016.041.0174 from 37 m. Two specimens from West Thistle Creek; TMP 2016.041.0239 and TMP 2016.041.0237, both from 28.5 m. Nine specimens from Blackstone River: TMP 2016.041.0102 from 6.5 m; TMP 2016.041.0103 from 13.6 m; TMP 2016.041.0132 from 20.5 m; TMP 2016.041.0133 from 38.2 m; TMP 2016.041.0134 from 39.4 m; and TMP 2016.041.0128 through to TMP 2016.041.0131, from 43.5 m. Four specimens from Wapiabi Creek: TMP 2016.041.0096 from 2.8 m; TMP 2016.041.0101 from 7.9 m; TMP 2016.041.0100 from 48.5 m; and TMP 2016.041.0089 from 54.7 m. Six specimens from Sullivan Creek: TMP 2016.041.0078 through to TMP 2016.041.0083, from the *inconstans* interval. Single, unnumbered specimen from Cutpick Creek. Eight specimens from Bighorn Dam: TMP 2016.041.0389 through to TMP 2016.041.0394 from 8.5 m; TMP 2016.041.0397 from 10.5 m; TMP 2016.041.0401



from 32.5 m; and TMP 2016.041.0396 from 34.0 m. Four specimens from Highwood River: TMP 2016.041.0141, TMP 2016.041.0142, TMP 2016.041.0143, and TMP 2016.041.0146.

REMARKS: The taxonomy and evolutionary interpretation of the genus, as applied herein, follows Walaszczyk and Wood (1998) and Walaszczyk and Cobban (2000), with slight modification, as discussed below.

The genus is well represented in the lowermost part of the Wapiabi Formation, up to surface CS4. The cremnoceramid assemblage is composed of *Cremnoceramus deformis deformis* (Meek, 1871), *Cremnoceramus crassus crassus* (Petrascheck, 1903), and *Cremnoceramus crassus inconstans* (Woods, 1912). This is the same assemblage as known from the southern part of the Western Interior Basin (see Walaszczyk and Cobban, 2000), and outside, in other areas of the Euramerican biogeographic region (e.g., Walaszczyk, 1992; Walaszczyk and Wood, 1998). The form that dominates the assemblage is *C. deformis deformis* (fig. 9A, D); less common is *C. crassus crassus* (fig. 9B). What is very interesting is the parallel occurrence of *C. crassus crassus* and typical forms of *C. crassus inconstans* (fig. 10). This may suggest that the change from *C. crassus inconstans* to *C. crassus crassus* was cladogenetic in character and both forms co-occurred subsequently. Consequently, both should be simply referred to as *C. crassus* and *C. inconstans*.

OCCURRENCE: The genus is well represented in all localities studied herein spanning the lower Coniacian: Cutpick Creek, West Thistle Creek, Bighorn Dam, Chungo Creek, Ram River, Sheep River, Wapiabi Creek, Blackstone River, and Highwood River (fig. 1). The genus is known from the Euramerican biogeographic region (western Central Asia, Europe, and the Atlantic and gulf coasts of North America; North Ameri-

can Western Interior) (Tröger, 1981, 1989; Walaszczyk, 1992; Kauffman et al., 1993; Walaszczyk et al., 1998; Walaszczyk and Cobban, 1998, 2000; Wood et al., 2004); North Pacific Province (Japan, Sakhalin) (Noda, 1996), New Zealand (Crampton, 1996), South America (Brazil) (Kauffman and Bengtson, 1985).

Volviceramus Stoliczka, 1871

TYPE SPECIES: *Inoceramus involutus* J. de C. Sowerby: 1828: 160, pl. 583, figs. 1–3, by original designation (Stoliczka, 1871: 394, 401).

REMARKS: Woods (1912) regarded *Volviceramus* as a successor of the *Inoceramus lamarcki* Parkinson group. However, as rightly pointed out by Tsagarély (1942), both the valve outline (particularly the RV) and the ornament of *Volviceramus* are close to *Cremnoceramus* (*Inoceramus inconstans* in Tsagarély, 1942). The single RV of various species, as well as the juveniles LV of *V. cardinalensis*, sp. nov., or *V. exogyroides* can very easily be mistaken for *Cremnoceramus*. Both *Volviceramus* and *Cremnoceramus* also show similar morphological variability in juvenile obliquity of growth. In the case of *Volviceramus* this is well seen in LVs; this feature is difficult to evaluate in case of RVs.

Through its distinct inequivalvness, the genus is very easily separated from other inoceramids. Some inequivalve representatives of the genus *Inoceramus*, as, e.g., *Inoceramus inaequivalvis* Schlüter, 1877, differ from *Volviceramus* in being distinctly less inequivalve (and they are never coiled) and in possessing more or less similar ornament on both valves.

Volviceramids appear abruptly above CS4, which caps a prominent, sandier-upward heterolithic succession of the lower Coniacian. Already within the lowest middle Coniacian allomembers (CA5-6) the variability of the genus is remark-

FIG. 7. *Inoceramus undabundus* Meek and Hayden, 1862. A, TMP 2016.041.0426, Wapiabi Formation, Bighorn Dam, 73.0 m, lateral view of RV. B, C, TMP 2016.041.0402, Wapiabi Formation, Bighorn Dam, 41.0 m: B, lateral view, C, anterior view. D, TMP 2016.041.0427, Wapiabi Formation, Bighorn Dam, 73.0 m, anterodorsal view of LV. All photographs are $\times 1$.

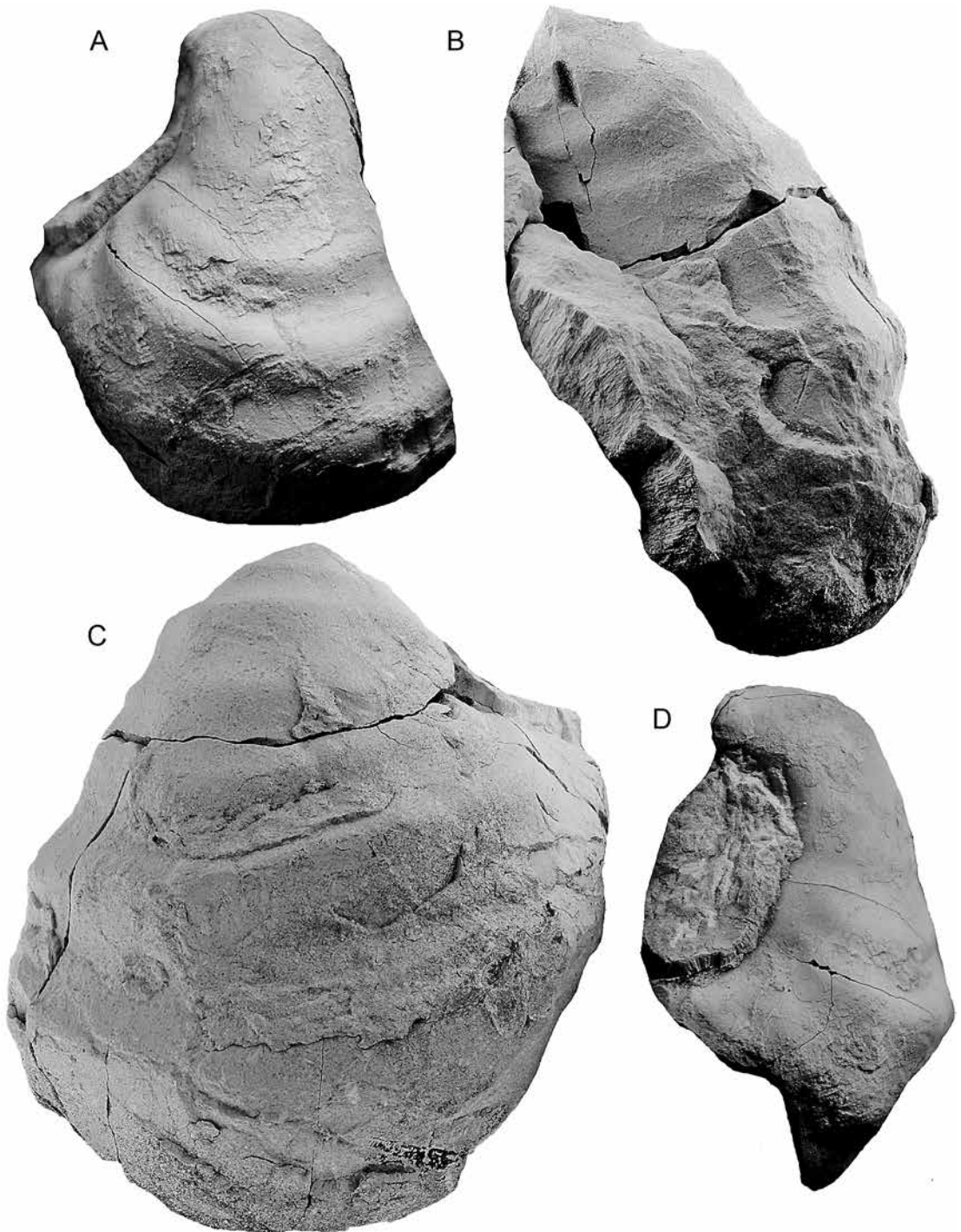


FIG. 8. *Tethyoceramus* sp., TMP 2016.041.0395 (two left valves), Wapiabi Formation, Bighorn Dam, 8.5 m: A, D, smaller specimen; A, lateral view; D, anterior view. B, C, larger specimen; B, anterior view, C, lateral view. All photographs are $\times 1$.

able. There appear: *Volviceramus koeneni* (Müller), *V. exogyroides* (Meek and Hayden), and *V. cardinalensis*, sp. nov. In addition to a single specimen, which shows a transitional character between *V. exogyroides* and *V. involutus*, the latter species was not noticed in this lowest interval; the first typical representatives of *V. involutus* are from allomember CA8.

The intraspecific variability within *Volviceramus* is caused mainly by the variability in the juvenile obliquity in their LVs. This allows the distinction of two morphogroups within the clade. The first group comprises low-obliquity forms (with high juvenile δ angle), characterized by a coiled or uncoiled, slender general outline. The group is represented by: *V. koeneni*, *V. involutus*, and *V. stotti*, sp. nov. The second group comprises forms growing obliquely in the juvenile stage (low juvenile δ angle), changing the direction of growth, to a less oblique one, later in ontogeny. This leads to a similar final architecture of the valve as the one observed in strongly inflated cremnoceramids. The oblique juvenile growth causes marked increase in valve length, and combined with subsequent geniculation and change to distinctly lower obliquity, gives a broad morphotype with massive appearance. The group is represented by *V. exogyroides* and *V. cardinalensis*, sp. nov. (see figs. 13–17). Whereas, however, the LVs in this second group resemble strongly geniculated valves in *Cremnoceramus*, their RVs are distinctly smaller, nongeniculated, with the typical *Volviceramus* RV geometry.

OCCURRENCE: The documented range of *Volviceramus* is middle to upper Coniacian. The genus is known from the Euramerican biogeographic region (western Central Asia, Europe, Gulf of Mexico area, American Western Interior).

Volviceramus koeneni (Müller, 1888)

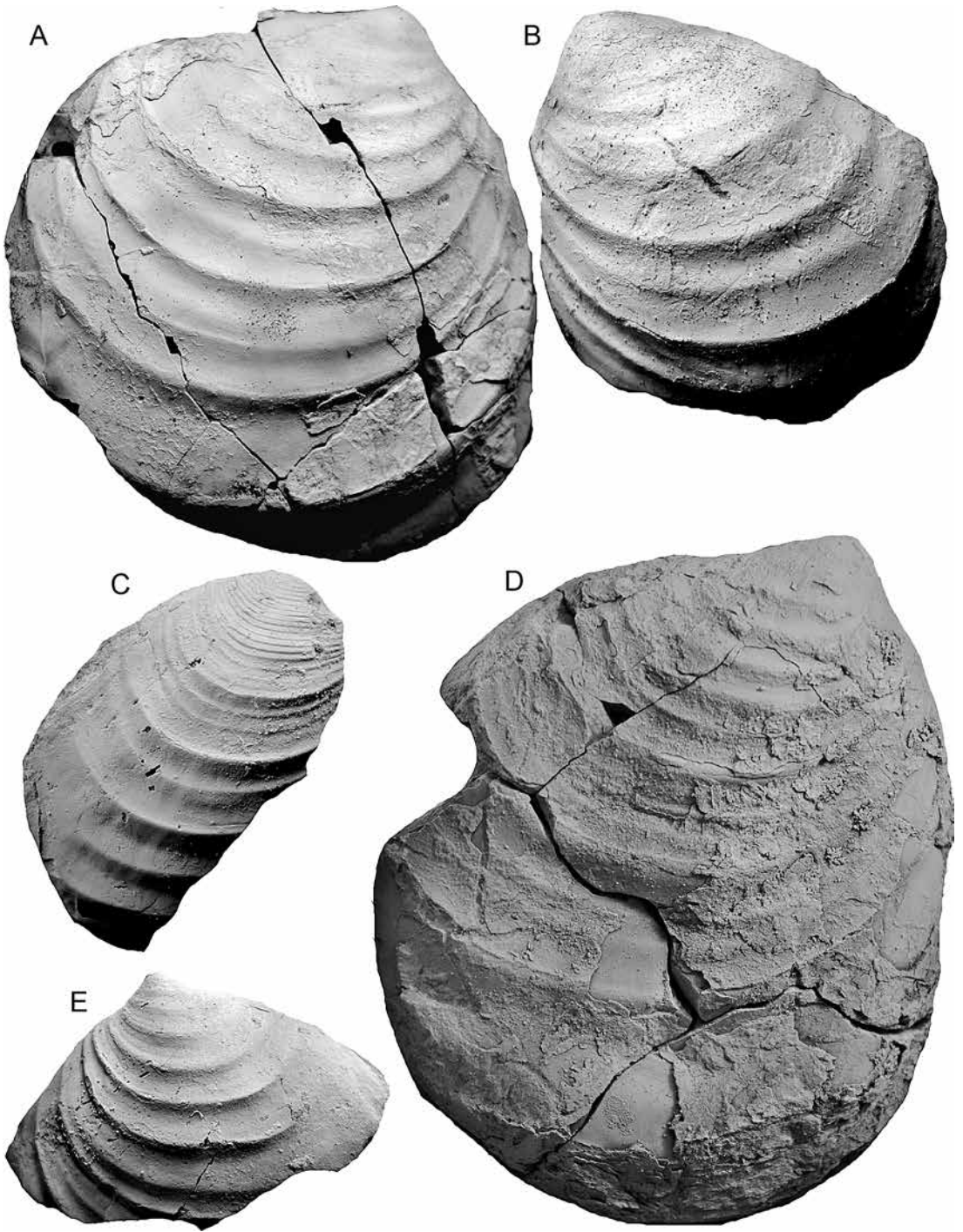
Figure 11

1888. *Inoceramus (Volviceramus) Koeneni* n.sp., Müller: 412, pl. 17, fig. 1.
 1891. *Inoceramus paradoxus* v. Haenlein. Langenhan and Grundey: 12, pl. 5, figs. 3–4.

1891. *Inoceramus varius* v. Haenlein. Langenhan and Grundey: 12, pl. 5, figs. 1; ?pl. 5, fig. 2.
 1913. *Inoceramus (Volviceramus)*(aff.?) *involutus* Sowerby. Scupin: 213, pl. 12, fig. 3.
 1928. *Inoceramus koeneni* Müller. Heinz: 37, pl. 3, fig. 2.
 1929. *Inoceramus koeneni* Müller. Heine: 98, pl. 15, fig. 63; pl. 17, fig. 66; pl. 18, fig. 67.
 1932. *Rhadinoceramus regalis*, sp. nov., Heinz: 21.
 non 1933. *Cymatoceramus (Cymatoceramus)* cf. *koeneni* Müller. Heinz: 253; pl. 19, fig. 3 [= *Tethyoceramus basseae* Sornay]
 1934. *Inoceramus koeneni* Müller. Andert: 132, text-figs. 16a–c; pl. 8, figs. 2–3.
 ?1959. *Inoceramus involutus* Sowerby. Dobrov and Pavlova: 153; pl. 10, fig. 1.
 ?1968. *Inoceramus koeneni* Müller. Kotsubinsky: 135; pl. 23, figs. 4, 5
 1969. *Inoceramus koeneni* G. Müller. Tröger: 68, pl. 1, figs. 1–6; pl. 2, figs. 1–5.
 1974. *Inoceramus koeneni* G. Müller. Tröger, pl. 5, figs. X4302, X4303, X4305, X4306.
 1991. *Inoceramus (Volviceramus) koeneni* Müller. Tröger and Christensen: 31, pl. 3, fig. 7; ?pl. 2, figs. 2–3.
 1994. *Volviceramus koeneni* (G. Müller, 1888). Tröger and Summesberger: 169, pl. 2, figs. 1–3.
 non 1994. *Inoceramus (Volviceramus)* cf. *koeneni* Müller. Malchus et al.: 116, text-fig. 4a, pl. 1, fig. 7 [= *Cordiceramus cordiforis*]
 ?non 1996. *Inoceramus (Volviceramus) koeneni* Müller, 1888. Noda: 566, fig. 10.
 ?non 1998. *Inoceramus (Volviceramus) koeneni* Müller, 1887. Noda and Matsumoto: 459, pl. 13, fig. 3. [reillustrated specimen of Noda, 1996: fig. 10]
 2006. *Volviceramus koeneni* (Müller, 1888). Walaszczyk and Cobban: 282; text-fig. 24, 25.2–25.4, 29.2.

TYPE: The lectotype, by subsequent designation of Tröger (1969), is the original of Müller (1888: pl. 17, fig. 1) from the middle Coniacian of Lehofsberg, near Quedlinburg, Germany.

MATERIAL: Nine specimens in total. Single specimen, TMP 2016.041.0076, from Sullivan



Creek. Eight specimens from Chungo Creek: complete, double-valve TMP 2016.041.0184; TMP 2016.041.0182, TMP 2016.041.0183 (2 specimens), and TMP 2016.041.0187, and TMP 2016.041.0189 (2 specimens). Single specimen (cf.) from Sheep River, TMP 2016.041.0333.

MEASUREMENTS: See table 1.

DESCRIPTION: TMP 2016.041.084 (fig. 11) is a well-preserved double-valved specimen, almost complete (a small fragment of the anterior part of the LV is missing), slightly deformed; with much of its shell intact. LV is 107 mm high; RV is 90 mm high. Both valves are slender (with b/h ration 0.56 and 0.63 in the RV and LV respectively), however, this is partly due to secondary deformation perpendicular to the commissure. The LV is more inflated than the RV; its h/b ratio being 0.54. The LV juvenile growth is slightly oblique, with δ angle c. 75°. At h = 60 mm, δ angle increases to 90°. Its beak is pointed and curved dorsally. The LV bears weak, poorly developed commarginal rugae. In the ventral part it is almost smooth. The RV is moderately inflated; its b/h ratio is 0.42. Its obliquity is almost constant, with δ approximating 90°. The anterior wall is steep, high, and slightly concave. The posterior auricle is well separated from the disc, with a distinct sulcus in the dorsal part. The beak is pointed, projecting above the hinge line. The disc is ornamented with well-developed commarginal rugae, superimposed by radial sulci in the axial part of the midadult stage (fig. 11D).

TMP 2016.041.082, TMP 2016.041.087, and TMP 2016.041.0333 are juvenile fragments of the LVs, undeformed; TMP 2016.041.0333 is with fragments of shell intact. They are referred to the Müller's species based on their ornamented valve.

The double valve specimen TMP 2016.041.0189 is complete, moderately large specimen (hmax of RV = 104 mm), strongly deformed. It is moderately inequivalve, with the

LV almost smooth, and with strong, typically ornamented RV.

REMARKS: *V. koeneni* is morphologically the closest to *V. involutus*. The differences are (see Tröger, 1969) that *V. involutus* exhibits: stronger inequivalvness, lack of undulation on the LV, and distinctly stronger inflation and coiling of LV. Transitional forms between both species occur. The stronger inflation of the RV in *V. koeneni* than in *V. involutus*, mentioned by Müller (1888), is difficult to evaluate; one would need two-valve specimens, which are extremely rare. *Volviceramus koeneni* is the oldest member of the *Volviceramus* clade.

Cymatoceramus (*Cymatoceramus*) cf. *koeneni* Müller from Madagascar, illustrated by Heinz (p. 253; pl. 19, fig. 3), is *Tethyoceramus basseae* (Sornay) as shown by Sornay (1980). To *Tethyoceramus* also belongs, most probably, the specimen of *Inoceramus* (*Volviceramus*) *koeneni* as reported from Japan by Noda (1996: fig. 10; see also Noda and Matsumoto, 1998: pl. 13, fig. 3). The Japanese specimen shows a regular pattern of concentric rugae, typical for *Tethyoceramus*/*Cremnoceramus*.

OCCURRENCE: *Volviceramus koeneni* spans the middle Coniacian. At the base of the middle Coniacian it forms a distinct interval zone, being followed by *V. involutus* (see also Müller, 1900; Stille, 1909; Heinz, 1928; Tröger, 1969). It is known from the Euramerican biogeographic region; neither the Madagascan report (Heinz, 1933) nor the Japanese one (Noda, 1996) can be confirmed.

Volviceramus involutus Sowerby, 1828

Figure 12

1828. *Inoceramus involutus* J. de C. Sowerby: vol. vi: 160, pl. 583, figs. 1–3

1846. *Inoceramus involutus* Sowerby. d'Orbigny, vol. iii: 520, pl. 413, figs. 1–3.

FIG. 9. **A**, *Cremnoceramus deformis deformis* (Meek, 1871), RV, Wapiabi Formation, Cutpick Creek, 19 m, lateral view. **B**, *Cremnoceramus crassus crassus* (Petrascheck, 1903), LV, TMP 2016.041.0175, Wapiabi Formation, Chungo Creek, 34.5 m. **C**, *Cremnoceramus* sp., TMP 2016.041.0100, RV, Wapiabi Formation, Wapiabi Creek, 48.5 m. **D**, *Cremnoceramus deformis deformis* (Meek, 1871), TMP 2016.041.0392, RV, Wapiabi Formation, Bighorn Dam, 8.5 m. **E**, *Cremnoceramus* sp., TMP 2016.041.0089, LV, Wapiabi Formation, Wapiabi Creek, 54.7 m. All photographs are $\times 1$.

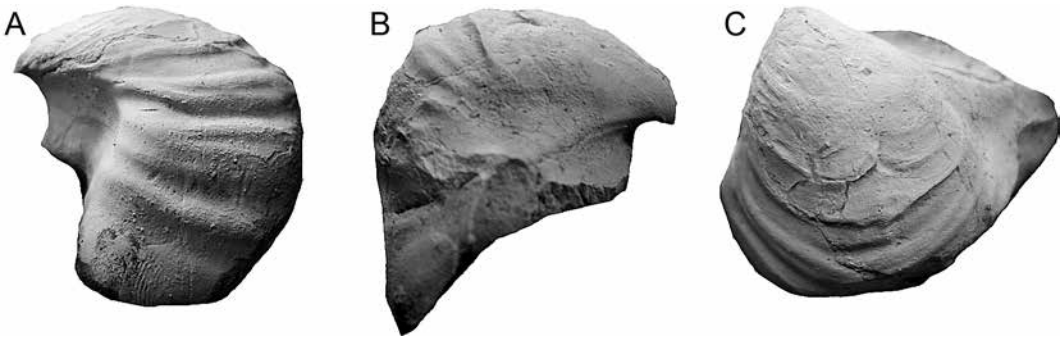


FIG. 10. *Cremonceramus crassus inconstans* (Woods, 1912), TMP 2016.041.0101, LV, Wapiabi Formation, Wapiabi Creek, 7.9 m, **A**, anterior view, **B**, oblique, posterodorsal view, **C**, lateral view of the juvenile stage. All photographs are $\times 1$.

1846. *Inoceramus lamarcki* d'Orbigny, vol. iii: 518, pl. 412.
1850. *Inoceramus involutus*. Dixon: pl. 28, fig. 32.[= *Volvicceramus anglo-germanicus* of Heinz, 1932; = *Inoceramus involutus belovodiensis* of Glasunova, 1972]
1858. *Inoceramus umbonatus* Meek and Hayden: 50.
1871. *Inoceramus (Volvicceramus) involutus* Sowerby. Stoliczka: 394, 401
1876. *Inoceramus umbonatus* Meek and Hayden. Meek: 44, pl. 3, fig. 1; pl. 4, fig. 1–2.
1888. *Inoceramus (Volvicceramus) involutus* Sowerby. Müller: pl. 16, figs. 3, 4,
1901. *Inoceramus involutus* Sowerby. Sturm: pl. 9, fig. 4.
1902. *Inoceramus involutus* Sowerby. Wolleemann: pl. 1, fig. 4; pl. 2, figs. 7, 8
1907. *Inoceramus umbonatus* Meek and Hayden. Veatch: pl. 10, fig. 2.
1912. *Inoceramus involutus* Sowerby. Woods: 327, text-figs. 88–94.
1932. *Volvicceramus anglo-germanicus* Heinz: 22. [= *Inoceramus involutus* Sowerby; Dixon, 1850, pl. 28, fig. 32]
- ?1959. *Inoceramus involutus* Sowerby. Dobrov and Pavlova: 153, pl. 10, fig. 1a, b.
1972. *Inoceramus involutus* Sowerby subsp. *belovodiensis* Glazunova, subsp. nov., Glazunova: 63; pl. 8, fig. 1; pl. 12, figs. 1, 2; pl. 13, fig. 5.
1974. *Inoceramus involutus* Sowerby. Kotsubinsky: 81, pl. 18.
2006. *Volvicceramus involutus* (J. de C. Sowerby, 1829). Walaszczyk and Cobban, text-figs. 9.3, 25.1, 26.1–26.3, 27.3–27.4, 28.3, 30.2.

TYPE: By subsequent designation of Woods (1912: 334) the lectotype is BM 43268, being the original of J. de C. Sowerby (1929: pl. 583, fig. 1) from the Upper Chalk, England; the locality is unknown.

DIAGNOSIS: Moderately large for genus, strongly inequivalve; LV coiled, growing moderately obliquely, almost smooth; RV weakly to moderately inflated, ornamented with well-developed rugae.

MATERIAL: Twelve specimens in total. Three specimens from Sheep River: TMP 2016.041.0321, TMP 2016.041.0329 and TMP 2016.041.0335, from 143 m. Two specimens from West Thistle Creek: TMP 2016.041.0243 from 72.5 m, and TMP 2016.041.0240 from 100.3 m. Single specimen from Bighorn River, TMP 2016.041.0362 from 51.8 m. Single specimen from Chungo Creek, TMP 2016.041.0188 from 75.7 m. Single specimen from James River, TMP 2016.041.0160 from 80.0 m. Single, unnumbered specimen from Cutpick Creek. Three specimens from Bighorn Dam: TMP 2016.041.0418 from 65.5 m, TMP 2016.041.0423 from 67.5 m, and TMP 2016.041.0431 from 67.5 m.

MEASUREMENTS: See table 1.

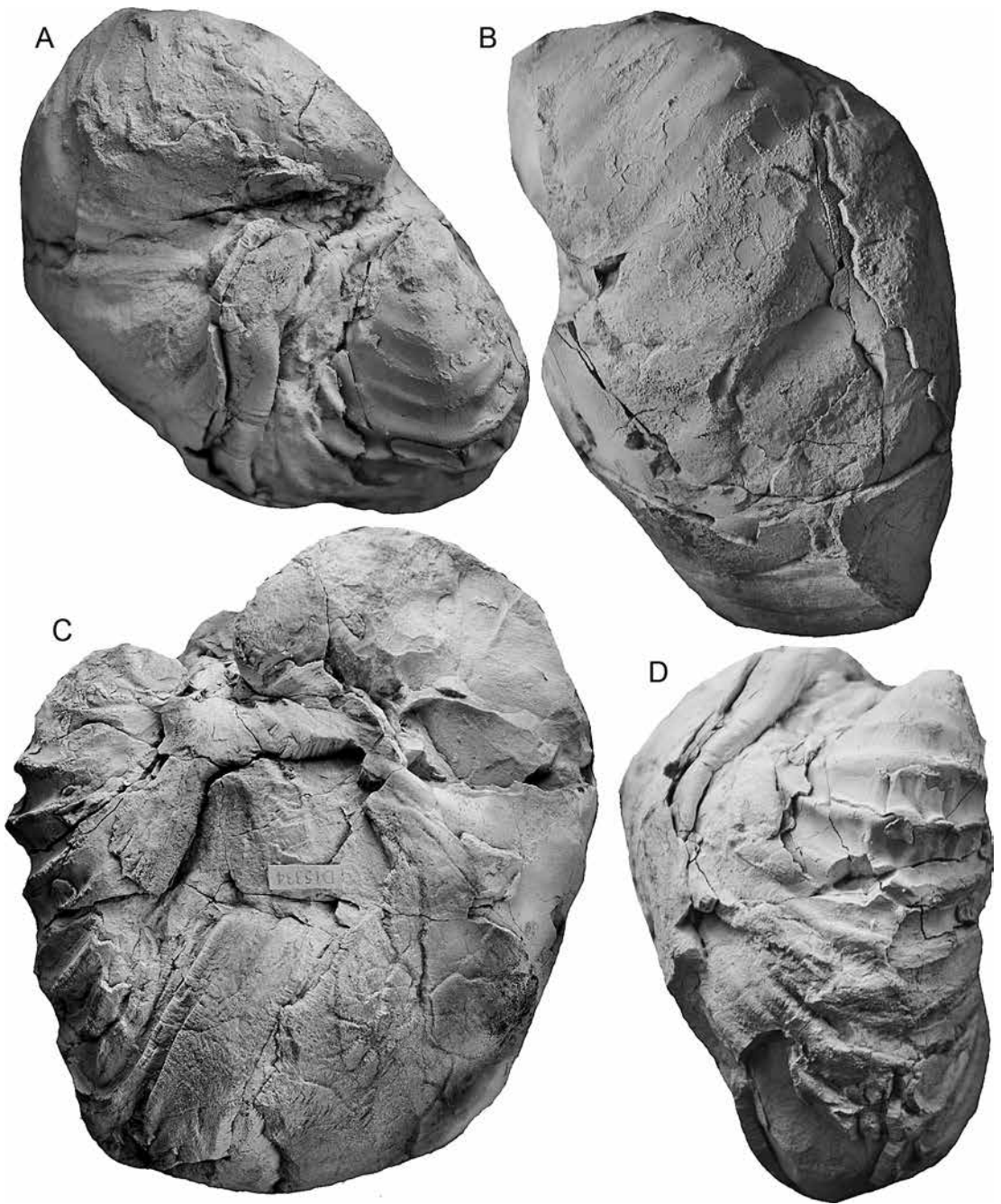


FIG. 11. *Volviceramus koeneni* (Müller, 1888), TMP 2016.041.0184, double-valve specimen, Wapiabi Formation, Chungo Creek, 45.5 m, A, dorsal view, B, lateral view of the LV, C, anterior view, D, lateral view of the RV. All photographs are $\times 0.95$.

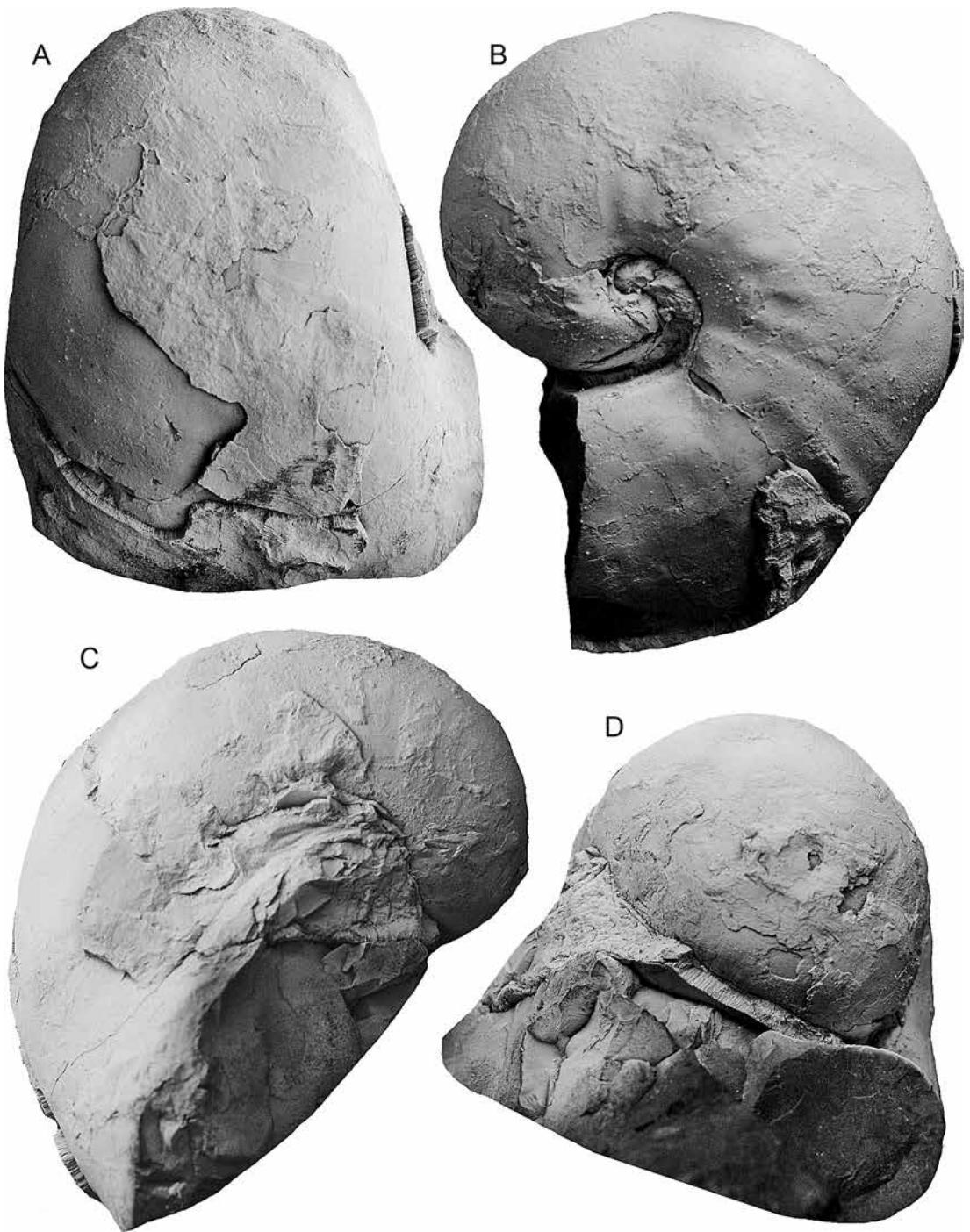


FIG. 12. *Volviceramus involutus* (Sowerby, 1828), TMP 2016.041.0243, LV, Wapiabi Formation, West Thistle Creek, 72.5 m, **A**, lateral view of the adult stage, **B**, anterior view, **C**, oblique, posterodorsal view, **D**, dorsal view, the photographs are $\times 1$.

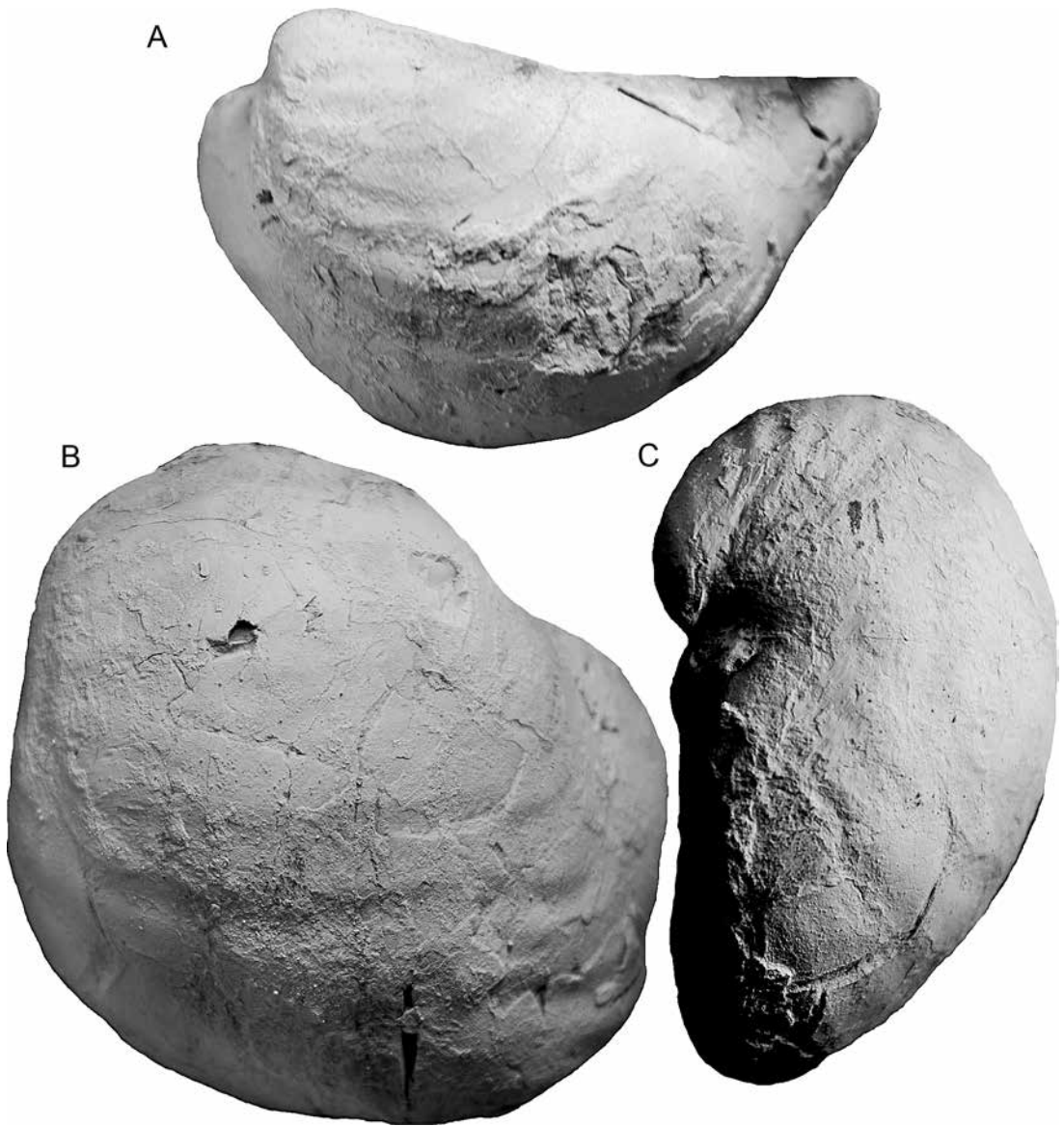
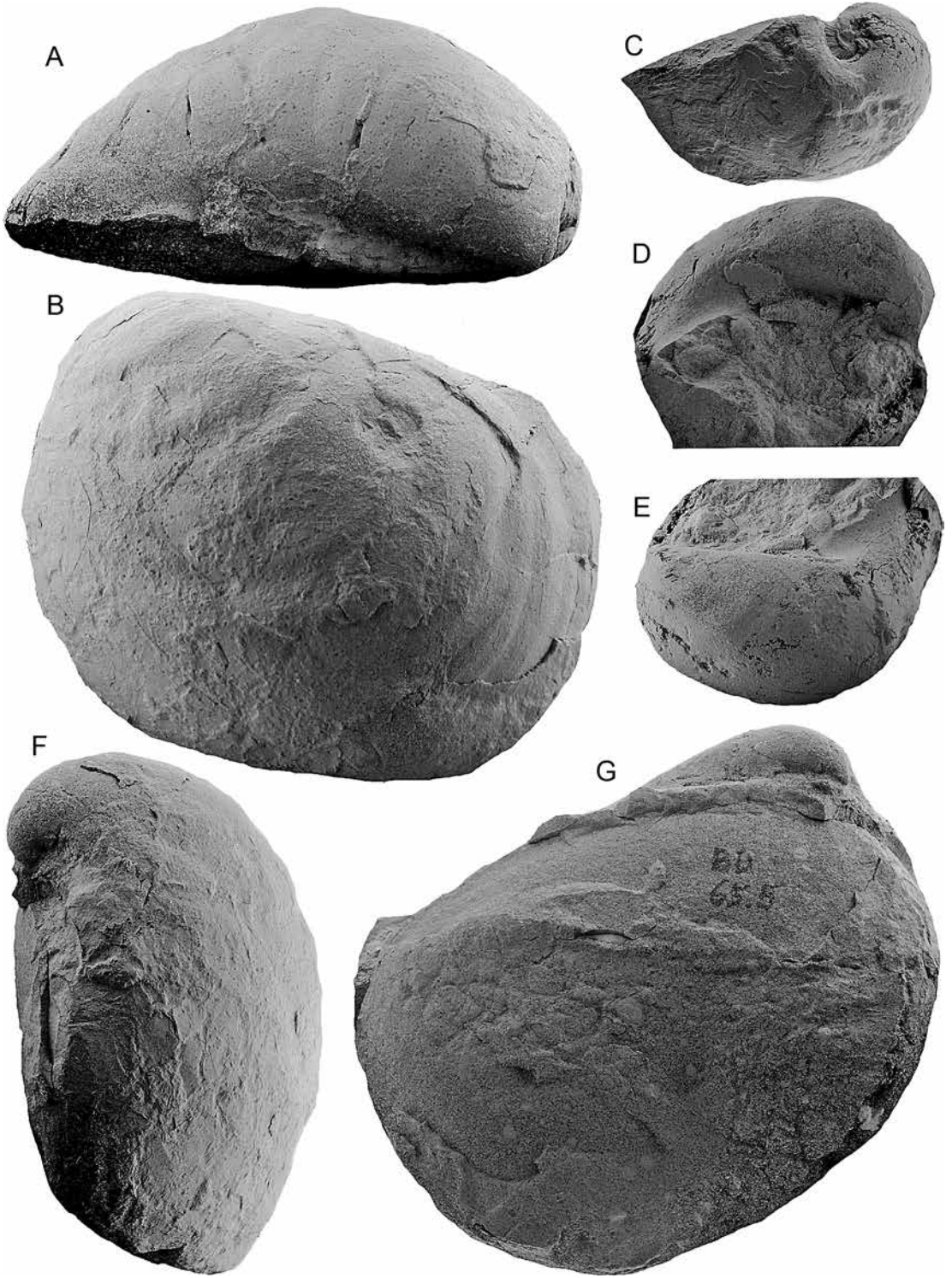


FIG. 13. *Volviceramus exogyroides* (Meek and Hayden, 1862), TMP 2016.041.0415, LV, Wapiabi Formation, Bighorn Dam, interval 50–60 m, **A**, lateral view of the juvenile stage, **B**, lateral view of the adult stage, **C**, anterior view. All photographs are $\times 1.0$.



DESCRIPTION: The species is small to medium size for the genus; inequilateral, strongly inequivalve. LV is strongly coiled, up to 1.5 whorls, tightly coiled, in the studied specimens (TMP 2016.041.0243; fig. 12). The LVs grow uniformly at $\delta = 60^\circ$, with strong inflation. The anterior margin gives a more or less consequent plane, and forms a well-developed planispiral coiling. The whorl in cross section is rounded in the lateral, anterior, and posterior parts; the “aperture” is oval. The LV is almost smooth. Only in the juvenile part may irregular, low, rounded rugae occur. Irregular rugae also occur in some specimens in the adult stage, usually at the anterior margin. The RV, when isolated, does not have any characteristic feature that allows it to be identified as belonging to a particular species of *Volviceramus*.

REMARKS: *Volviceramus involutus* is the only *Volviceramus* species with almost perfect coiling of the LV, as seen on the anterior wall of the valve, resembling *Nautilus* or some involute ammonites. The posterior, or lateral (which would be ventral in ammonoids), margin is certainly quite different. The species-level identification of the RV is at the moment impossible. Based on species, of which double-valved specimens are available, the variability of RVs is high, and more double-valved specimens of every species would be necessary to make a reliable assessment.

The infraspecific variability concerns mainly the l/h ratio, which results in more slender or more robust forms. The type species (Sowerby, 1828: pl. 583, figs. 1–3; see also Woods, 1912: text-fig. 88) is one of the robust forms, with high l/h ratio, well above 0.8. The slender form is best represented by Dixon’s specimen (1850: pl. 28, fig. 32; see also Woods, 1912, text-fig. 89), with l/h ration about 0.75. The slender form, with Dixon’s specimen as its type, was referred by Heinz (1932: 22) to a new species, *Volviceramus anglogermanicus*. Subsequently, the same speci-

men was chosen as the type of the new subspecies *Inoceramus involutus belovodiensis* by Glazunova (1972: 63), with the same diagnosis and the same aim to separate the slender morphotype of *Volviceramus involutus*. Based on our material it is clear, however, that both morphotypes are extreme variants of the same type and are, consequently, regarded as infraspecific variants (see also Walaszczyk and Cobban, 2006).

The American species *Volviceramus umbo-natus* (Meek and Hayden, 1858) is a typical representative of *V. involutus*, and consequently is a synonym of Sowerby’s species. *Volviceramus exogyroides* and *I. undabundus*, which have previously been considered as synonyms of *V. involutus*, are well defined, separate species (see discussion herein).

OCCURRENCE: *Volviceramus involutus* first appears in the middle part of the middle Coniacian and ranges into the upper Coniacian. It is well represented in the entire Western Interior Basin. The species is widely known from Europe and western Central Asia. It does not range south into the Mediterranean Province, although it was reported from Gosau in Austria (Tröger and Summesberger, 1994). The reports from Madagascar (Heinz, 1933) and from the western North Pacific Province (Pergament, 1971) have not been confirmed.

Volviceramus exogyroides (Meek and Hayden, 1862)

Figures 13–15

1862. *Inoceramus exogyroides* Meek and Hayden: 26.
 1876. *Inoceramus exogyroides* Meek and Hayden. Meek: 46, pl. 5, fig. 3.
 1893. *Inoceramus exogyroides* Meek and Hayden. Stanton: 83, pl. 17, figs. 1–2 [reillustration of Meek, 1876: pl. 5, fig. 3, specimen]

FIG. 14. *Volviceramus exogyroides* (Meek and Hayden, 1862), A, B, F, G, TMP 2016.041.0417, LV, Wapiabi Formation, Bighorn Dam, 65.5 m, A, dorsal view, B, lateral view, F, anterior view; G, apertural view. C–E, TMP 2016.041.0363, LV, Bighorn River, 51.8 m, C, anterior view, D, apertural view, E, dorsal view. All photographs are $\times 1$.

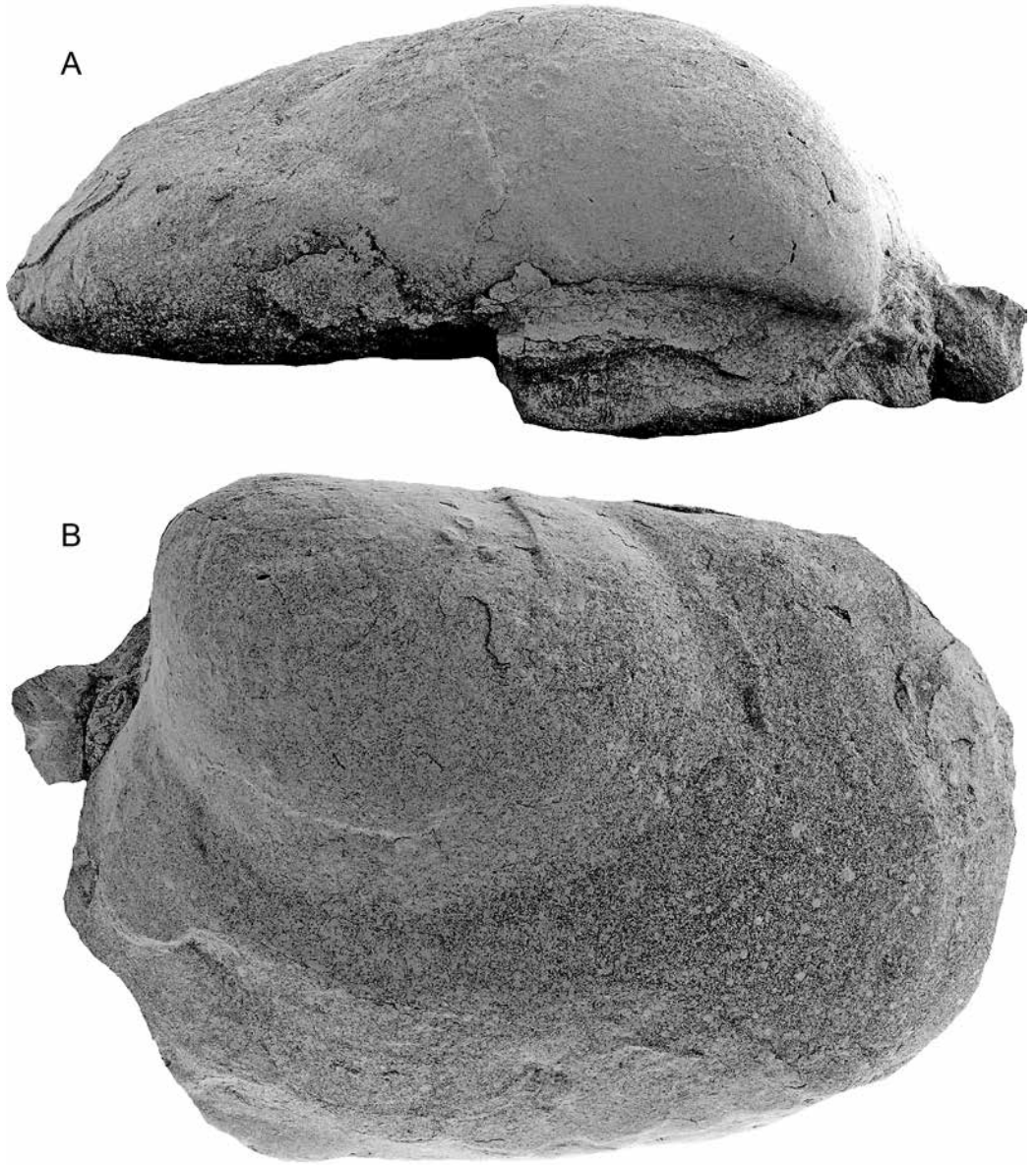


FIG. 15. *Volvicceramus exogyroides* (Meek and Hayden, 1862), TMP 2016.041.0198, Chungo Creek, 65.8 m; **A**, dorsal view, **B**, oblique lateral view. Both photographs are $\times 1$.

1898. *Inoceramus exogyroides* Meek and Hayden. Logan: 454, pl. 88, figs. 1–2 [reillustration of Meek, 1876: pl. 5, fig. 3, specimen].
1907. *Inoceramus exogyroides* Meek and Hayden. Veatch: pl. 11, fig. 1.
- pars* 1929. *Inoceramus undabundus* Meek and Hayden. Heine: 100, pl. 11, fig. 51; pl. 19, fig. 71 [non pl. 11, fig. 50; pl. 13, fig. 57, which are *Inoceramus undabundus* Meek and Hayden].
1972. *Inoceramus obliquus*, sp. nov., Glazunova: 63, pl. 8, figs. 2, 3.
2006. *Volviceramus exogyroides* (Meek and Hayden, 1862). Walaszczyk and Cobban: 291; text-figs. 27.1, 28.1, 29.1, 30.1.

TYPE: The holotype, by monotypy, is the original of Meek (1876: pl. 5, fig. 3) from the Marias River Shale (Fort Benton Group), 20 miles below “Fort Benton,” on the upper Missouri River, in north-central Montana.

MATERIAL: Nineteen specimens. Ten specimens from Bighorn Dam: TMP 2016.041.0404 and TMP 2016.041.0405 from 47.5 m; TMP 2016.041.0414, TMP 2016.041.0415 and TMP 2016.041.0416, from an interval 50–60 m; TMP 2016.041.0417 from 65.6 m; TMP 2016.041.0433 from 67.5 m; TMP 2016.041.0420 from 72.0 m; TMP 2016.041.0441 from 75.4 m; and TMP 2016.041.0438 from 81.0 m. Single specimen from Sheep River, TMP 2016.041.0332 from 110.5 m. Single specimen from West Thistle Creek, TMP 2016.041.0234 from 53.2 m. Four specimens from Chungo Creek: TMP 2016.041.0193, and TMP 2016.041.0194, from 65.8 m; TMP 2016.041.0200 from 65.9 m; and one unnumbered specimen from 65.8 m. Three specimens from Bighorn River: TMP 2016.041.0363, TMP 2016.041.0364, from 51.8 m, and TMP 2016.041.0357, from 93.6 m.

MEASUREMENTS: See table 1.

DESCRIPTION: The following description refers only to the LV; RVs are not represented in the studied material.

The shell is of small to moderate size, inequilateral. Its outline changes during ontogeny fol-

lowing the change of growth direction; its juvenile outline is triangular, strongly oblique, elongated parallel to the ligament; its adult outline is trapezoidal, due to the change of growth, to distinctly less oblique. The specimens vary between well-geniculated ones (see fig. 13) to forms with a gradual change from the juvenile to adult stage (fig. 14A, B, F, G). The beak is pointed, anteriorly terminal. The umbo is variably coiled, prosogyrate. The change from the oblique juvenile stage to less oblique adult stage is sometimes quite abrupt, geniculated. The juvenile stage is oblique, with δ angle ranging between 30° and 40° ; the adult stage growth at δ between 50° and 60° . The outline of the juvenile stage varies with variable inflation; the more inflated specimens have more coiled umbos and are more slender. Depending on the length of the juvenile stage, the adult stage is more or less subquadrate.

The valve is ornamented with regular to sub-regular commarginal rugae, with regular, ventralward increase of interspaces. The rugae are round topped, symmetrical to slightly asymmetrical. The ornament becomes less distinct in the adult stage, or it disappears completely.

DISCUSSION: Both the original material of Meek and Hayden (1862; also Meek, 1876) and the material recently described from the U.S. Western Interior by Walaszczyk and Cobban (2006) are represented exclusively by LVs. The only reports of the RV come from Europe. These are by Heine (1929) from northern Germany, who referred these forms to *Inoceramus undabundus* Meek and Hayden; and by Glazunova (1972), who described this species under the new name *Inoceramus obliquus* (actually, the name is the homonym of v. Haenlein’s species). Describing the RV Glazunova (1972) states that the RV is distinctly smaller than the LV and its outline is L-elongated. The beak is pointed, not projecting above the ligament, the umbo is weakly inflated. The valve is more evenly inflated than the LV. The ligamental plate is concave, covered with shallow resilifers intercalated with relatively narrower interresilifers.

Volviceramus exogyroides resembles closely *Volviceramus cardinalensis*, sp. nov. Both have a distinctly oblique juvenile stage and change to lower obliquity in the adult stage. The juvenile stage of *V. cardinalensis*, sp. nov., is, however, almost subrectangular, poorly inflated, and almost smooth.

The species has often been placed in synonymy with *Volviceramus involutus* (or its American synonym, *V. umbonatus*). Both species differ, however, in their ontogenetic development and consequent morphological characteristics.

The juvenile parts of LVs may easily be taken for a *Cremnoceramus*. The difference is clearly seen when the ligament plate is preserved, or when the specimen is preserved as with both valves. This may be the reason for reports of *Cremnoceramus* from the interval characterized otherwise by *Volviceramus* (see, e.g., Kauffman et al., 1993; Collom, 2001).

OCCURRENCE: *Volviceramus exogyroides* is known widely in the North American Western Interior. It is also known from Europe, where it was described as *Inoceramus obliquus* by Glazunova (1972). The species was reported (although without illustration) from the southern and eastern margins of the East European craton (e.g., Aliev and Kharitonov, 1981; Aliev and Pavlova, 1983), but it was never illustrated.

***Volviceramus cardinalensis*, sp. nov.**

Figures 16, 17

TYPE SPECIMENS: The holotype is TMP 2016.041.0317, upper middle Coniacian of the Sheep River section; paratypes: 14 specimens from various localities (see Material).

ETYMOLOGY: After Cardinal River, western Alberta, where one of the paratypes was collected.

MATERIAL: Fifteen specimens in total. Four specimens from Bighorn Dam: TMP 2016.041.0399, loose, but located approximately in the interval

50–60 m of the succession, TMP 2016.041.0413 from 43.0 m, TMP 2016.041.0406 from 47.5 m, and TMP 2016.041.0421 from 105.0 m. 10 specimens from Sheep River, from 144 m: TMP 2016.041.0310, TMP 2016.041.0314, TMP 2016.041.0315, TMP 2016.041.0316, TMP 2016.041.0317 (holotype), TMP 2016.041.0318, TMP 2016.041.0319, TMP 2016.041.0320, TMP 2016.041.0322, and TMP 2016.041.0323. Single, double-valved unnumbered specimen from Cardinal River, 96.8 m.

DIAGNOSIS. Noncoiled *Volviceramus* with LV strongly oblique and weakly inflated in juvenile stage, growing almost orthoclinally, with strong inflation in adult stage. RV strongly inflated for genus, with regular, widely spaced rugae, and shallow radial sulcus on its disc.

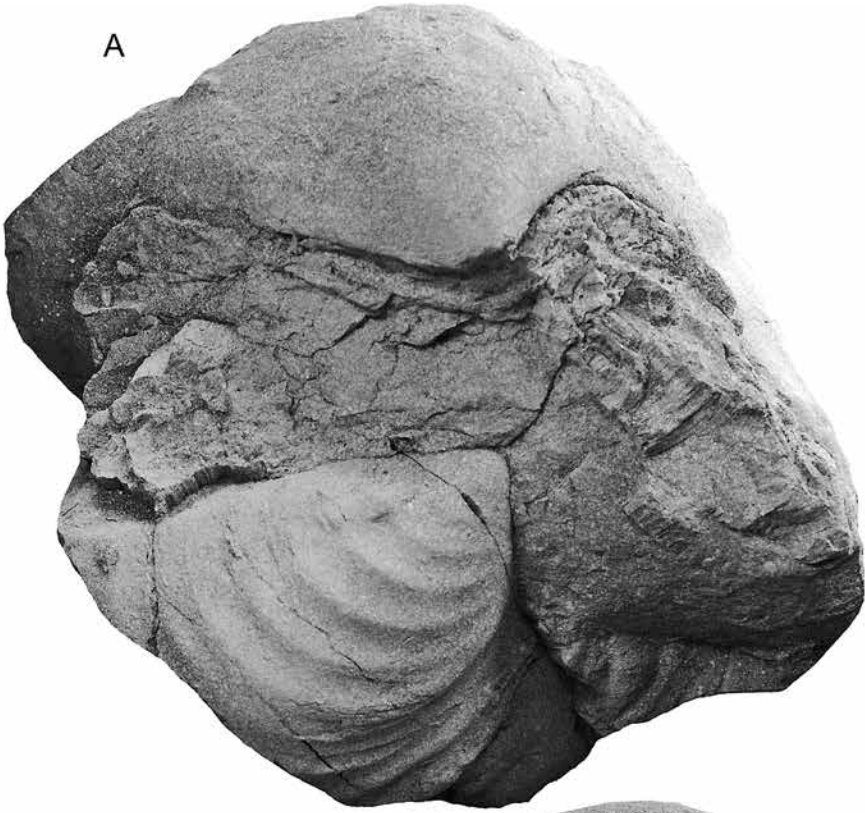
DESCRIPTION. The species is strongly inequivalve, noncoiled *Volviceramus*, attaining large size, with strongly inflated LV up to 30 cm in maximum h length. The LV shows characteristic change in growth direction, leading to the development of the juvenile and adult stages, sometimes, with well-developed geniculation. The juvenile valve, up to 100 mm of axial length, grows obliquely, with δ angle ca. 45° , then, in the adult stage, it changes its growth to markedly less oblique. The juvenile stage is subrectangular in outline, and moderately to weakly inflated. The strong inflation characterizes the adult stage. The adult stage varies in the L/H ratio, ranging from L-elongated, subrectangular specimens to subquadrate ones. The RV is relatively large, with strongly inflated disc, distinctly oblique. The disc is separated from the posterior auricle, along a well-developed auricular sulcus.

The juvenile stage of the LV is almost smooth; the adult stage is covered with subregular, widely spaced, low rugae. The RV is regularly, strongly rugate on the disc; the rugae do not continue over the posterior auricle. The rugae are distinctly narrower than interrugae spaces.

The holotype, TMP 2016.041.0317 (figs. 16, 17), is a huge (estimated maximum h is 180

FIG. 16. *Volviceramus cardinalensis*, sp. nov., TMP 2016.041.0317, Wapiabi Formation, Sheep River, 144 m, **A**, dorsal view, **B**, anterior view of the LV. Both photographs are $\times 0.7$.

A



B



A



B



mm), double-valved specimen, apparently undeformed, with parts of shell in the ligament area preserved. The L of the juvenile stage (fig. 17B) of the LV is ca. 110 mm, and its H is ca. 60 mm. This part is weakly inflated, with juvenile $b = 18$ mm, smooth, growing moderately obliquely, at $\delta = 45^\circ$. The beak is strongly prosogyrous, curved anteriorly. The α angle is 105° . Although there is no distinct geniculation, at $h = 120$ mm the valve starts growing perpendicularly to the juvenile stage. The adult stage is subrectangular, longer than high (H is only 110 mm at $L = 170$ mm).

REMARKS. *Volviceramus cardinalensis*, sp. nov., resembles *V. exogyroides*. It differs from the latter in its subrectangular juvenile outline, instead of suboval, and lower inflation. Moreover, the juvenile of *V. exogyroides* is usually regularly rugate, changing to almost smooth in adult stage. In contrary, *V. cardinalensis* is almost smooth in the juvenile stage, and changes its ornament to distinctly rugate in the adult.

OCCURRENCE: The species seems to appear very low in the middle Coniacian and ranges to the lower upper Coniacian.

***Volviceramus stotti*, sp. nov.**

Figure 18

pars 2001. *Volviceramus involutus* (Sowerby, 1828). Collom: 475, pl. 15, figs. 1, 2, 4, 5. [only]

2001. *Volviceramus* aff. *koeneni* [in text: *Volviceramus koeneni*] (Müller, 1888). Collom: 474, pl. 15, fig. 3.

TYPE SPECIMENS: Holotype is TMP 96.19.13, double valved, moderately large; well preserved (original to *Volviceramus involutus* (Soweby) in Collom, 2001: pl. 15, figs. 4, 5); paratypes: TMP 2016.041.0439, and TMP 2016.041.0245; both internal molds of LVs, with fragments of shell preserved; moreover: GSC 117324, LV, an origi-

nal to *Volviceramus involutus* (Soweby) in Collom 2001: pl. 15, fig. 1; TMP 96.53.1, LV, original to *Volviceramus involutus* (Soweby) in Collom 2001, pl. 15, fig. 2; and TMP 87.56.13, double-valved specimen, original to *Volviceramus* aff. *koeneni* (Müller) in Collom 2001: pl. 15, fig. 3.

TYPE LOCALITY: Bad Heart Formation, Kakut Creek (for details of location, see Collom, 2001).

MATERIAL: Our material consists of two specimens, both LVs: TMP 2016.041.0439 from Bighorn Dam, 91.5 m; TMP 2016.041.0245 from West Thistle Creek, 107.5 m. Two other specimens, TMP 2016.041.0313 and TMP 2016.041.0326, from Sheep River, are referred to herein as cf. *stotti*.

DIAGNOSIS: Moderately inflated and moderately inequivalve *Volviceramus*, of moderate size, rounded, prosocline, with ornament, composed of raised growth lines, with superimposed, low, widely spaced, subregular concentric rugae.

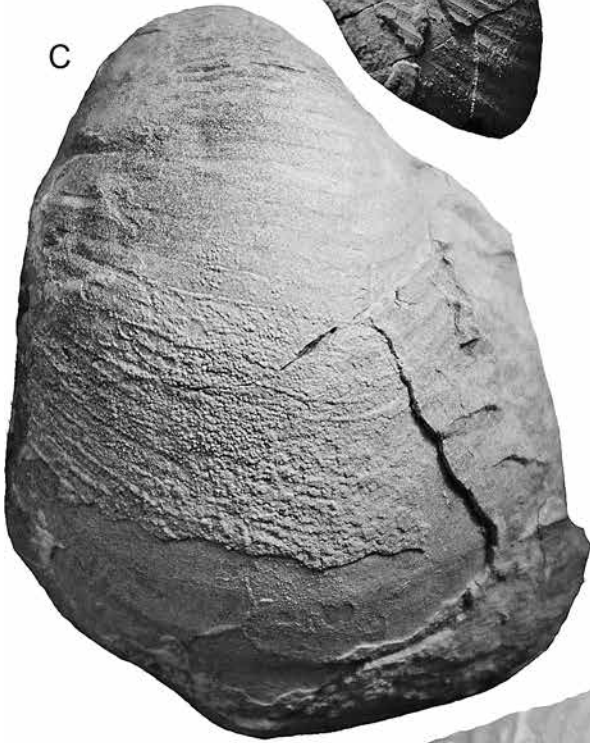
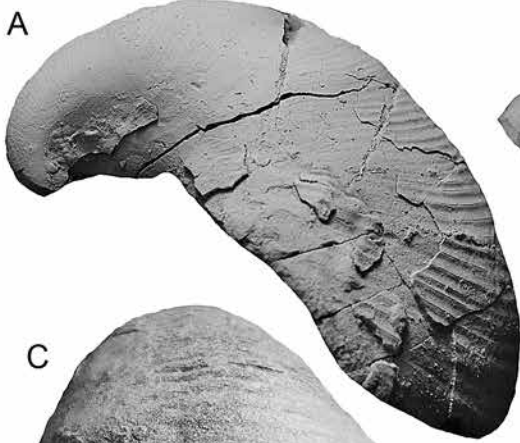
ETYMOLOGY: After Donald F. Stott, the preeminent Canadian geologist and researcher of the Cretaceous of the Canadian Western Interior.

MEASUREMENTS: See table 1.

DESCRIPTION: This is a moderately inequivalve *Volviceramus* species, with both valves regularly inflated, strongly prosocline, straight. LV is larger and more inflated, growing dominantly posteroventrally. The beak is pointed, curved anterodorsally; it projects above the hinge line. The valve outline is parabolical. The anterior margin is relatively short (AM/h between 0.40 and 0.45). The anterior wall is steep to overhanging, rounded. The anteroventral margin is rounded, broadly convex; ventral margin is rounded. The posterior auricle is small, well separated from the disc, particularly in the RV; less so in the LV. The ligament is strong; the resilifers as observed on one of the specimens illustrated in Collom (2001: pl. 15, fig. 1) are narrow and rectangular, with narrow interresilifer plates.

The ornament is composed of regular to subregular, round-edge rugae, superimposed by

FIG. 17. *Volviceramus cardinalensis*, sp. nov. TMP 2016.041.0317, Wapiabi Formation, Sheep River, 144 m, **A**, lateral view of the LV; **B**, lateral view of the juvenile part of the LV. Both photographs are $\times 0.7$.



sharp-edged growth lines, well visible both on outer shell surface and on internal mold.

REMARKS: The weak to moderate inequivalveness (the feature inferred from the characteristics of the ligamental plate), moderate to strong inflation of the LV, and a peculiar ornament, make this species different from any other *Volviceramus* species known. In general architecture *V. stotti*, sp. nov., resembles *V. koeneni*, however, the latter is distinctly inequivalve, with RV having a very distinct ornament, composed of sharp-edged, strong concentric rugae, with variably developed radial ribs.

OCCURRENCE: The species appears relatively high in the succession, close to the appearance level of *Sphenoceramus subcardissoides*, which marks the base of the upper Coniacian, and ranges to the top of CA16, in the middle part of the substage.

Volviceramus sp. A

Figures 19, 20

MATERIAL: Two specimens in total, both internal molds of LVs. Single specimen from Sheep River, TMP 2016.041.0334, from 106.5 m; single specimen from Chungo Creek, TMP 2016.041.0195, from 56.9 m.

MEASUREMENTS: See table 1.

DESCRIPTION: The valves are subrounded to suboval, weakly inequilateral, prosocline, moderately inflated. The beak is pointed, curved strongly dorsoanteriorly. The umbo is subtriangular. The umbonal part grows obliquely (umbonal δ is between 35° and 40°); then the valve becomes straight, growing at d between 70° and 75° . The posterior auricle apparently does not develop, or is very small (and not preserved on our specimen). The anterior margin is relatively short ($AM/h = 0.4$); it is concave below the umbo, then straight. The ventral margin is broadly and regularly rounded, long.

The posterior margin is not observed on our specimen; it apparently is very short.

The umbonal part is moderately to strongly inflated. The adult stage then becomes weakly or only moderately inflated, and becomes again strongly inflated in the ventral part (?gerontic stage). The valves are almost smooth, or bear only weakly developed, widely spaced, very low rugae; growth lines are not observed.

REMARKS: These two specimens resemble closely *Volviceramus exogyroides* and may easily be imagined as a morphotype of *V. exogyroides*, which very early in ontogeny changes its juvenile (very oblique) growth to the adult (almost straight). More material is needed to decide whether this morphotype is an extreme variant of *V. exogyroides* or it is an independent species.

OCCURRENCE: This morphotype is known from only two specimens from our collection. Both are from the lower middle Coniacian (both are from CA7) of Sheep River and Chungo Creek.

Sphenoceramus J. Böhm, 1915

TYPE SPECIES: *Inoceramus cardissoides* Goldfuss, 1835.

GENERIC CHARACTERS: The genus is obliquely wedge shaped in outline, weakly to moderately inflated, medium to large sized, equivalve and inequilateral. The disc is triangular in outline, with three growth axes (Schalenkante of Seitz: 1965, text-fig. 1), similar to the genus *Cordiceramus*, commonly with a more or less well-developed radial sulcus in the posterior part of the disc. The umbo is pointed, curved anteriorly, usually extending above the hinge line. The ornament is well developed over the disc, usually much weaker on the posterior auricle. Both concentric and radial ornament elements occur.

OCCURRENCE: *Sphenoceramus* appeared in the late Coniacian (see Heinz, 1926, 1928; Heine, 1929; Seitz, 1962; Tröger and Christensen, 1991;

FIG. 18. *Volviceramus stotti*, sp. nov. **A, B, D**, TMP 2016.041.0439, LV, **A**, anterior view; **B**, dorsal view, **D**, lateral view. Wapiabi Formation; Bighorn Dam, 91.5 m; the specimen is $\times 0.85$. **C, E**, TMP 2016.041.0245, LV, **C**, lateral view, **E**, posterodorsal view. Wapiabi Formation, West Thistle Creek, 107.5 m; the photograph is $\times 0.9$.

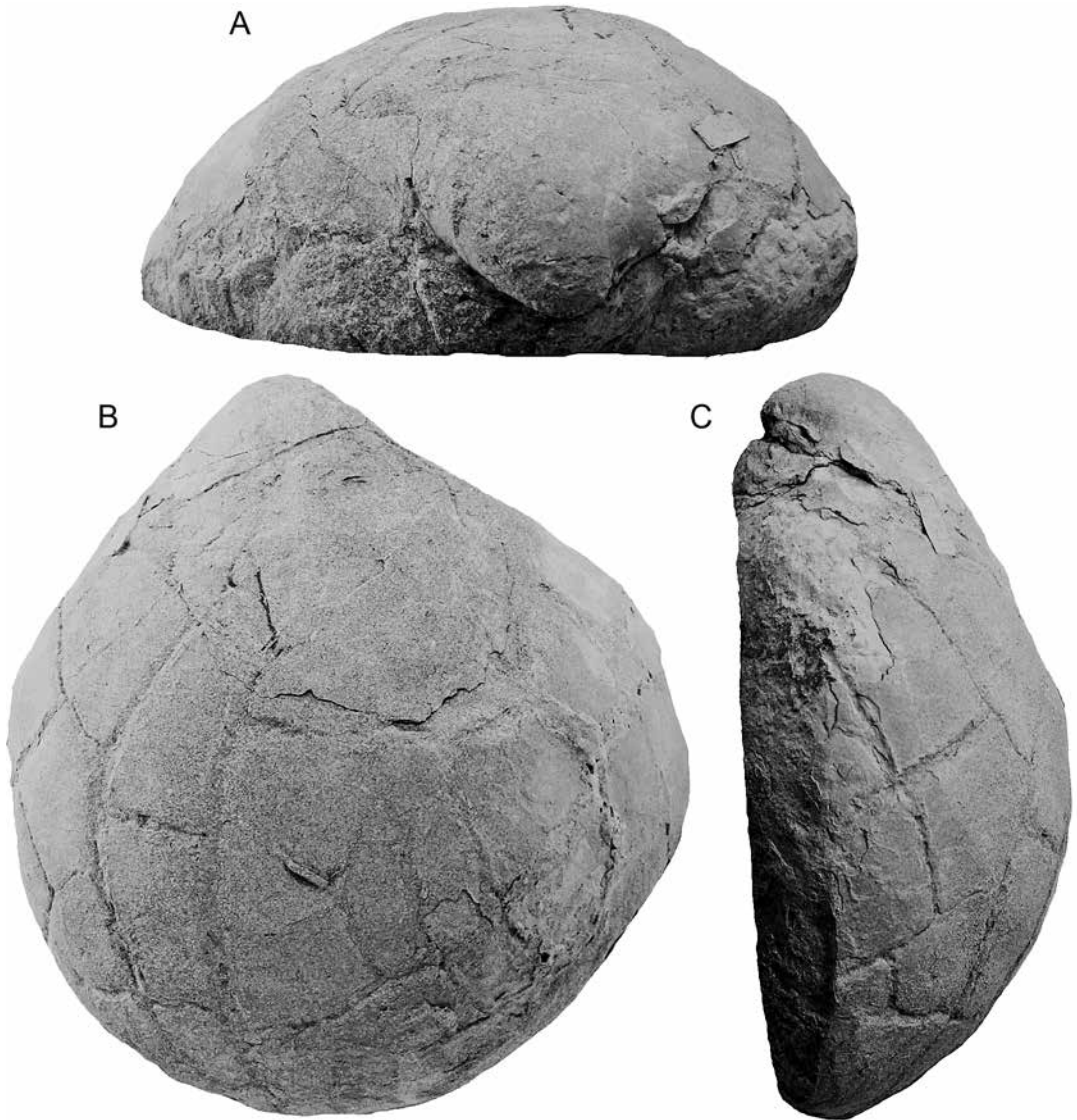


FIG. 19. *Volviceramus* sp. A, TMP 2016.041.0195, LV, Wapiabi Formation, Chungo Creek, 56.9 m, A, dorsal view, B, lateral view, C, anterior view. All photographs are $\times 1$.

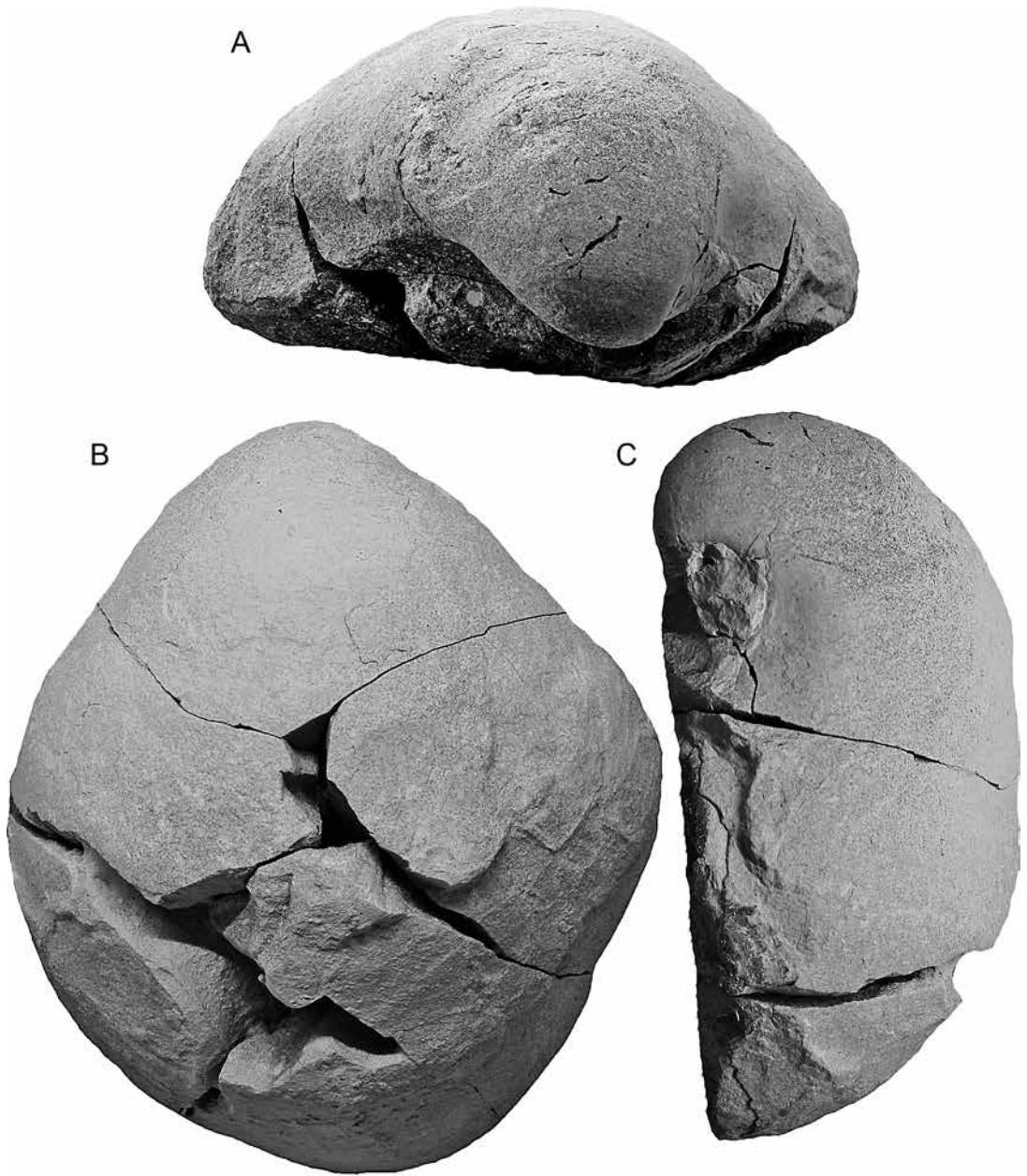


FIG. 20. *Volviceramus* sp. A, TMP 2016.041.0334, Wapiabi Formation, Sheep River, 106.5 m, A, dorsal view, B, lateral view, C, anterior view. All photographs are $\times 1$.



FIG. 21. *Sphenoceramus subcardissoides* (Schlüter, 1877), Wapiabi Formation, TMP 2016.041.0001, Ram River, 132 m, lateral view. The photograph is $\times 1$.

Walaszczyk and Wood in Niebuhr et al., 1999), and ranged up to the mid early Campanian (Seitz, 1965). It is a Boreal species, rarely reported in the Mediterranean area (see, e.g., Tröger and Summesberger, 1994). The genus seems to be limited to the Northern Hemisphere; reports from the Southern Hemisphere (Heinz, 1929; Kauffman in Kennedy et al., 1973) are not confirmed (see discussion in Walaszczyk and Cobban, 2006; Kennedy et al., 2008; Walaszczyk et al., 2014a). The genus is widely reported from the North Pacific Province, particularly from its western parts. How abundant the genus was in this province is, however, unclear. Of a wide variety of morphotypes referred to *Sphenoceramus* (e.g., Matsumoto et al., 1982; Toshimitsu, 1988; Noda, 1988), most should be referred to other genera (e.g., Glazunov, 1976; Zonova, 1992, 1993).

In the Western Interior Basin *Sphenoceramus* occurs regularly only in its northern part; probably ranging south to Montana. Further south the genus appears sporadically.

Sphenoceramus subcardissoides (Schlüter, 1877)

Figure 21

1877. *Inoceramus subcardissoides* Schlüter: 271, pl. 37
 1905. *Inoceramus subcardissoides* Schlüter. Wegner: 169
 1926. *Inoceramus subcardissoides* Schlüter. Heinz: 101
 1932. *Inoceramus subcardissoides* Schlüter. Heinz: 24.
 1953. *Inoceramus subcardissoides* Schlüter. Ødum: 12
 1956. *Inoceramus* ex gr. *subcardissoides* Schlüter. Soukup: pl. 13, figs. 1–3.
 1958. *Inoceramus subcardissoides* Schlüter. Kotsubinsky: 16, pl. 5, fig. 24.
 1968. *Inoceramus subcardissoides* Schlüter. Kotsubinsky: 137, pl. 24, fig. 3.
 non 1969. *Inoceramus subcardissoides soukupi* Mitura in Mitura et al.: 175, pl. 2, fig. 1

1974. *Inoceramus* cf. *subcardissoides* Schlüter. Tröger: pl. 6, figs. X4307, 4308

1991. *Inoceramus subcardissoides* Schlüter. Tröger and Christensen: 32, pl. 2, fig. 4.

pars 2001. *Euryceramus cardissoides* (Goldfuss). Collom: 489, pl. 13, fig. 5; pl. 14, figs. 1–2 [non pl. 13, fig. 6]

LECTOTYPE: The original to Schlüter (1877: pl. 37), from the Emchermergel of the rock-waste deposit of the Carnap I Mine Shaft near Horst in Westphalia, northern Germany.

MATERIAL: Seven specimens in total. Two fragments, TMP 2016.041.0443 from 92.5 m and TMP 2016.041.0444 from 92.0 m from Bighorn Dam. One fragmentary specimen, TMP 2016.041.0235 from 100.3 m in West Thistle Creek. Incomplete huge specimen TMP 2016.041.0201 from 96.5 m in Chungo Creek. One large incomplete specimen (internal and outer mold of the same), TMP 2016.041.0001, and TMP 2016.041.0002, from 132 m of Ram River. Incomplete fragment, TMP 2016.041.0338 from Sheep River.

DESCRIPTION: The best preserved is TMP 2016.041.0001 (fig. 21), the large fragmentary specimen from the Ram River section (and TMP 2016.041.0002, its outer mold). It is the medium stage part of the RV, with h = 190 mm. Its juvenile and the anterior parts are missing. Also, it is slightly deformed in the preserved anterior part. The disc is wide, moderately inflated, apparently triangular in outline, covered with widely spaced, round-topped rugae and strong radial ribs. The latter weaken when crossing concentric rugae to form weakly developed nodes. The specimen retained a well-preserved radial sulcus, which is relatively broad and deep in the posterior part of the disc. The posterior auricle is not preserved. The radial ornament disappears from the radial sulcus, and reappears on the disc, posterior to the sulcus.

TMP 2016.041.0235, from Thistle Creek, represents a much younger stage of the LV. It shows well, however, the tripartite disc and, although weak, clearly developed radial ribs.

TMP 2016.041.0444, from Bighorn Dam, is a juvenile stage, 75 mm h long fragment. The specimen does not have radial ornament yet, which appears later in ontogeny. The outline and structure of the disc fits the characteristics of the species.

DISCUSSION: Although incomplete, our specimens show well the characteristics of Schlüter's species: the presence of the strong, broad radial sulcus in the posterior part of the disc and the radial ornament, which crosses the concentric rugae, forming more or less well-developed nodes at crossings.

The best reported specimens, besides the illustrated type, are the ones photographed by Collom (2001: pl. 13, fig. 5; pl. 14), from the upper Coniacian of the Smoky River area. His specimen from the Puskwaskau Formation (Collom, 2001: pl. 13, fig. 6) has different ornament and character of the posterior auricle, and is a different species.

OCCURRENCE: *Sphenoceramus subcardissoides* first appears apparently at the base of the upper Coniacian (Tröger, 1989; Tröger and Christensen, 1991; Walaszczyk and Wood in Niebuhr et al., 1999). Heinz (1926) and Kotsubinsky (1958, 1968) reported the species from the upper Coniacian (upper *Involutus* Schichten in Heinz, 1926). Although quoted sometimes as ranging into the Santonian; no definite occurrence from this level can be confirmed. Consequently, it may be regarded as of late Coniacian age. In the studied area the species is common at the base of its range; its record higher in the succession is poorly known.

Sphenoceramus ex gr. *pachti*
(Arkhangelsky, 1912)

Figures 22, 23

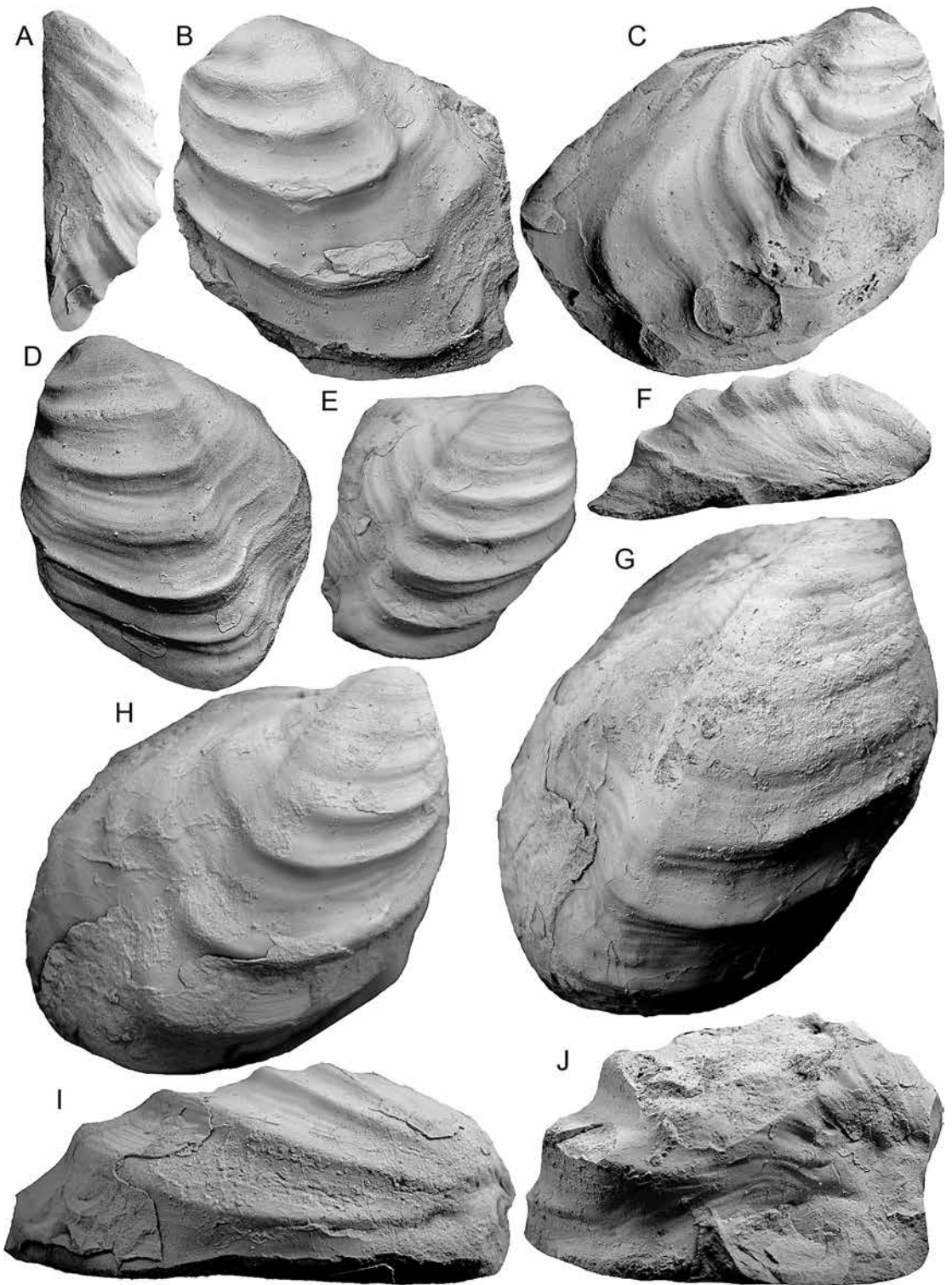
2006. *Sphenoceramus* ex gr. *pachti* (Arkhangelsky, 1912). Walaszczyk and Cobban: text-figs. 48.7, 48.10, 48.11.

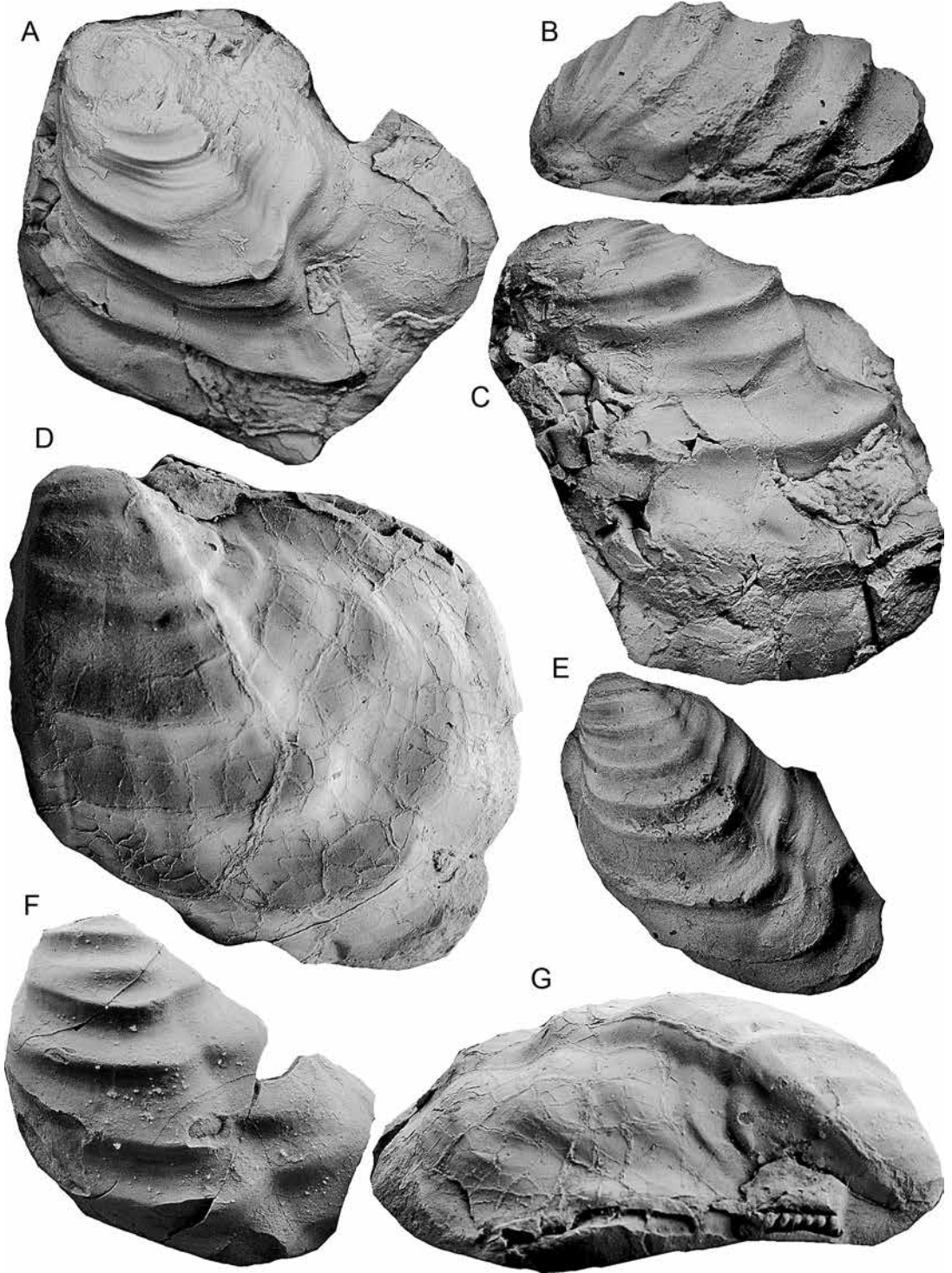
MATERIAL: Three specimens from Cripple Creek: TMP 2016.041.0152, TMP 2016.041.0153, and TMP 2016.041.0154. Twenty-six specimens from West Thistle Creek; TMP 2016.041.0246–TMP 2016.041.0271. Two specimens from Bighorn Dam, TMP 2016.041.0424 and TMP 2016.041.0430. Numerous uncataloged specimens from Cardinal River.

DESCRIPTION: The species is small to medium size for the genus, inequilateral, apparently equi-valve (?semiequivalve). The valve is weakly to moderately inflated, unless geniculated, quite oblique, with d between 45° and 50° . The valve outline is trapezoidal. The disc is trigonal in outline. The posterior auricle is usually well developed and well separated from the disc. The distinct auricular sulcus is visible in some specimens. The very distinct radial sulcus runs posteriorly of the growth axis. It starts at ca. 10 mm from the beak and becomes stronger with age. The beak is pointed, curved anterodorsally, projects slightly above the hinge line. The anterior margin is relatively short, usually slightly above 50% of the growth axis length, quite steep, may be slightly concave just below the umbo. The anterior margin passes into the long, broadly convex anteroventral margin. The ventral margin is narrowly rounded. The posterior margin is straight, almost parallel to the growth axis, being about 60% of the growth-axis length. The growth axis is straight in the juvenile and early adult part, then curves posteriorly. The ligament (dorsal) margin straight, relatively short, below 50% of the respective growth-axis length.

The general outline and shape changes in geniculated specimens. The geniculation appears usually at between 30 and 40 mm axial distance from the beak. The geniculation angle varies but is approximately 60° . Rarely, double geniculation is observed. The geniculated forms are character-

FIG. 22. *Sphenoceramus* ex gr. *pachti* (Arkhangelsky, 1912), Wapiabi Formation, West Thistle Creek, basal Santonian. **A, D, F**, TMP 2016.041.0248, LV, 125 m; **A**, anterior view, **D**, lateral view, **F**, posterior view. **B**, TMP 2016.041.0246, LV, lateral view. **C, J**, TMP 2016.041.0256, RV, 127.5 m, **C**, lateral view, **J**, anterior view. **E**, TMP 2016.041.0269, RV, 126.5 m, lateral view. **G**, TMP 2016.041.0270, RV, 126.5 m, lateral view. **H, I**, TMP 2016.041.0268, LV, 126.5 m, **H**, lateral view, **I**, anterior view. All photographs are $\times 1$.





ized by a steep (sometimes overhanging) anterior wall, and sharp anterior margin (fig. 22)).

The ornament is composed exclusively of commarginal rugae; very fine, discontinuous radial elements appear on some specimens (TMP 2016.041.0152, fig. 23D). Up to 20 mm of the axial length the rugae are poorly developed, and the ornament is composed almost entirely of raised, sharp-edged growth lines. In some specimens the rugae appear, however, much earlier, and the growth lines are poorly visible. In most of the specimens the rugae show a distinct step-wise change from rather closely spaced, round-topped ones, to widely spaced ones, with distinctly sharper edges. In the geniculated specimens, the change is associated with the change of growth plane. The growth lines become less and less regular with age. The rugae do not pass onto the posterior auricle. In the geniculated specimens they pass onto the anterior wall.

REMARKS: The studied material looks at first very variable. To a large extent this is, however, because of the geniculation; the geniculation causes changes in the character of the anterior margin and wall, and in the general shape of the whole specimens. Other than that, the specimens are quite stable with respect to general outline and ornament.

The general outline, ornament and ontogenetic changes make our specimens clearly representative of *Sphenoceramus pachtii*. The difference between the Arkhangelsky's types and the studied material is the lack of radial ornament. In this respect, our specimens correspond to *S. pachtii* subsp. indet. as described by Seitz (1965: pl. 9, figs. ?1, 3–4). Seitz suggested the possibility that his undescribed variety could represent juveniles of otherwise typical (i.e., radially ornamented) *S. pachtii*. Although this is also possible in the case of our material, no radially ribbed specimen of *S.*

pachtii has ever been reported from the Western Interior Basin, and our material also seems to include adult specimens. Consequently, our specimens are regarded as representing a sample of a nonradially ribbed natural population.

The geniculated, and particularly the small-sized specimens of *S. pachtii* described herein very closely resemble the type of *I. pontoni* McLearn (1926: pl. 20, fig. 1). The only differences that may be indicated, based on the limited material of McLearn's species, are: (1) weakening of the posterior radial sulcus and (2) general weakening of the ornament in the adult stages of *I. pontoni* (this is not the case in *S. pachtii*). The typical specimens of McLearn's species, collected from the Smoky River area, western-central Alberta, and from the Kevin section, northern Montana, come from beds slightly younger than *S. pachtii*. Consequently, it is suggested herein that *I. pontoni* may represent an evolutionary descendant of *S. ex gr. pachtii*.

OCCURRENCE: The material studied is from the lower Santonian of Alberta, Canada. Very similar specimens occur higher in the lower and middle? Santonian.

Sphenoceramus ex gr. cardissoides
(Goldfuss, 1835)

Figure 24

1965. *Inoceramus cardissoides* subsp. indet. Seitz: 47, pl. 4, figs. 1–4.

2006. *Sphenoceramus ex gr. cardissoides* (Goldfuss, 1835). Walaszczyk and Cobban: text-figs. 48.3–48.6.

MATERIAL: Single RV, RTM 2016.041.0272, from 126 m level of West Thistle Creek.

DESCRIPTION: The studied specimen (fig. 24) is the small-sized internal mold of the RV; its hmax = 48.5. The valve is strongly inflated as for *S. cardissoides*; its b/h = 0.45. The disc is subquadrate

FIG. 23. *Sphenoceramus ex gr. pachtii* (Arkhangelsky, 1912). Wapiabi Formation, basal Santonian. A, C, TMP 2016.041.0254, LV (geniculated), West Thistle Creek, 129.5 m, A, lateral view, C, anterior view. B, E, TMP 2016.041.0247, LV (geniculated), West Thistle Creek, 123 m, B, anterior view, E, lateral view. D, G, TMP 2016.041.0152, LV, Cripple Creek, 47.5 m, D, lateral view, G, oblique, dorsoposterior view. F, TMP 2016.041.0265, LV, West Thistle Creek, 125.3 m, lateral view. All photographs are $\times 1$.

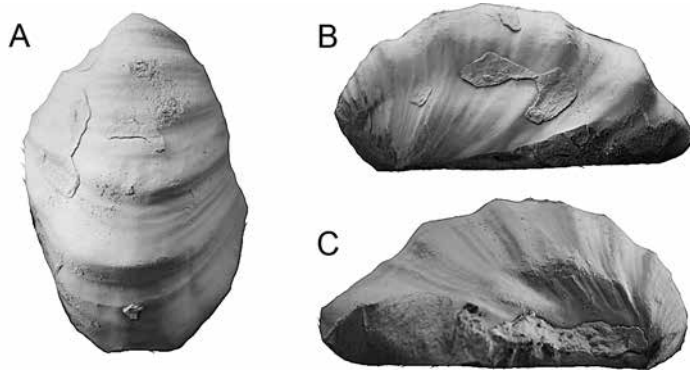


FIG. 24. *Sphenoceramus* ex gr. *cardissoides* (Goldfuss, 1835), TMP 2016.041.0272, RV, Wapiabi Formation, West Thistle Creek, 125.3 m, **A**, lateral view, **B**, posterior view, **C**, anterior view. The photograph is $\times 1$.

in outline, prosogyrate. The beak is pointed, curved anterodorsally, projecting above the hinge line. Its anterior margin is distinctly concave, relatively long, with $AM/h = 0.65$, which is distinctly higher than in *S. ex gr. pachtii* (ca. 0.5 or less). The anterior wall is steep to overhanging. The ventral margin is rounded. The radial sulcus is well developed. The posterior auricle is not preserved.

The valve is ornamented with strong commarginal rugae, sharp-edged, with flat, and relatively large interspaces. The rugae are superimposed by raised, sharp-edged growth lines. Traces of weak radial ribs are visible in the axial part of the valve.

REMARKS: The specimen clearly belongs to the *Sphenoceramus pachtii-cardissoides* group. Its relatively long anterior margin is a characteristic of *S. cardissoides*. The lack of radial ornament makes it close to forms referred by Seitz (1965: 47) to *Inoceramus cardissoides* subsp. indet. Similarly, as with nonradially ribbed variety of *S. pachtii*, Seitz did not name this variety, suggesting that it might comprise only the juvenile stages of other, radially ribbed species. The presence of this morphotype in the U.S. Western Interior suggests that the variety may represent a separate taxon.

OCCURRENCE: The studied specimen comes from the lower Santonian of the West Thistle Creek section; the US Western Interior specimens come from the Santonian. The morphotype is also known from the lower and middle Santonian of Germany (Seitz, 1965).

ACKNOWLEDGMENTS

The fossil material described here was collected during fieldwork between 2012 and 2014, with field assistance provided by O. Al-Mufti, P. Angiel, R. Buckley, S. CoDyer, M. Grifi, E. Hooper, S. Morrow, K. Pavan, T. Plint, and K. Vannelli. Funding for A.G.P.'s regional stratigraphic studies was provided by the Natural Sciences and Engineering Research Council of Canada over numerous grant cycles. Supplementary funding was provided by Canadian Hunter Ltd, Home Oil Ltd., Imperial Oil Ltd., Texaco Ltd., and Unocal Canada, Ltd. Funding for I.W., for final studies in Denver in November 2016, is from NCN Grant UMO-2015/17/B/ST10/03228. The remarks by journal reviewers, Gregori López, Barcelona, and an anonymous one, are warmly acknowledged.

REFERENCES

- Aliev, M.M., and V.M. Kharitonov. 1981. Stratigraphic distribution of *Inoceramus* in the Upper Cretaceous deposits of Azerbaijan. *Izvestia Akademii Nauk Azerbajanskoy SSR, Seria Nauk o Zemlie* (1981) 2: 3–13.
- Aliev, M.M., and M.M. Pavlova. 1983. Stratigraphic and paleoecologic peculiarities of inoceramides of the Upper Cretaceous of the south of the USSR. *Izvestia Akademii Nauk Azerbajanskoy SSR, Seria Nauk o Zemlie* (1983) 4: 97–102.

- Andert, H. 1911. Die Inoceramen des Kreibitz-Zittauer Sandsteingebirges. Festschrift des Humboldtvereins zur Feier seines 50 jährigen Bestehens: 33–64. Leipzig: M. Weg.
- Andert, H. 1934. Die Kreideablagerungen zwischen Elbe und Jeschken. Teil 3: Die Fauna der obersten Kreide in Sachsen, Böhmen und Schlesien. Abhandlungen der Preußischen Geologischen Landesanstalt, Neue Folge 159: 1–447.
- Arkhangelsky, A.D. 1912. Upper Cretaceous deposits of the eastern part of the European Russia. Reprinted in Akademik A.D. Arkhangelsky, *Izobrannye Trudy*, vol. 1: 133–466. Moskva: Izdatelstvo Akademii Nauk SSSR. [In Russian]
- Assmus, G. 1963. Stratigraphie und Petrographie des Coniac im östlichen Teil der Halberstädter Mulde. Diplomarbeit of the Freiberg Technical University, Germany.
- Böhm, J. 1915. Vorlage von Inoceramen aus dem subhercynen Emscher und Untersenen. Zeitschrift der Deutschen Geologischen Gesellschaft 67: 181–183.
- Bodylevski, W.I. 1958. Upper Cretaceous fauna from the lower reaches of the River Enisei. In Bodylevski, W.I. and N.I. Shulgina, Jurassic and Cretaceous faunas from the lower reaches of the Enisei. *Trudy Vsesoiuznovo Nauchnoissledovatel'skogo Instituta Geologii Arktiki* 93: 69–86. [In Russian]
- Cech, S., and L. Svabenicka. 1992. Macrofossils and nanofossils of the type locality of the Brezno Formation (Turonian-Coniacian, Bohemia). *Věstník Českého Geologického Ústavu* 67: 311–326.
- Cobban, W.A. 1951. Scaphitoid cephalopods of the Colorado Group. United States Geological Survey, Professional Paper 239: 1–42.
- Cobban, W.A., T.S. Dyman, and K.W. Porter. 2005. Paleontology and stratigraphy of upper Coniacian–middle Santonian ammonite zones and application to erosion surfaces and marine transgressive strata in Montana and Alberta. *Cretaceous Research* 26: 429–449.
- Cobban, W.A., I. Walaszczyk, J.D. Obradovich, and K.C. McKinney. 2006. A USGS zonal table for the Upper Cretaceous middle Cenomanian-Maastrichtian of the Western Interior of the United States based on ammonites, inoceramids, and radiometric ages. United States Geological Survey, Open-File Report 2006–1250: 1–46.
- Collom, C.J. 2001. Systematic paleontology, biostratigraphy, and paleoenvironmental analysis of the Wapiabi Formation (Upper Cretaceous), Alberta and British Columbia, Western Canada. Ph.D. dissertation, University of Calgary, Alberta: 834 pp.
- Cox, R.R. 1969. Family Inoceramidae Giebel, 1852. 314–321. In Moore, R.C. (editor), *Treatise on invertebrate paleontology. Part N. Mollusca* 6 (1), Bivalvia. 489 pp. Boulder: Geological Society of America and Kansas University Press.
- Crampton, J.S. 1996. Inoceramid bivalves from the Late Cretaceous of New Zealand. Institute of Geological & Nuclear Sciences, Monograph 14: 1–188.
- Dobrov, S. A. and M.M. Pavlova. 1959. Inoceramids. In M.M. Moskvina (editor), *Atlas of the Upper Cretaceous fauna of northern Caucasus and Crimea*: 130–165 Moscow: Gostoptechizdat. [in Russian]
- Glazunova, A.E. 1972. Paleontological bases of the stratigraphical subdivision of the Cretaceous deposits of Povolzhe. Upper Cretaceous. Moscow: Nedra, 202 pp. [in Russian]
- Glazunov, V.S. 1967. Systematics of Late Cretaceous Inoceramids of Sakhalin. *Paleontological Journal* (1967) 1: 35–44.
- Goldfuss, A. 1835. *Petrefacta Germaniae tam ea, quae in museo Universitatis Regiae Borussicae Fridericiae Wilhelmae Rhenanae servantur quam alia quaecunque in Museis Hoeninghusiano, Muensteriano aliisque extant, iconibus et descriptionibus illustrata* [1833–41], vol. 2: 69–140. Düsseldorf: Arnz and Co.
- Harries, P. J., E.G. Kauffman, and J.S. Crampton (redactors). 1996. Lower Turonian Euramerican Inoceramidae: a morphologic, taxonomic, and biostratigraphic overview. A report from the first workshop on Early Turonian inoceramids (Oct. 5–8, 1992) in Hamburg, Germany; organized by Heinz Hilbrecht and Peter Harries. *Mitteilungen aus dem Geologisch-Paläontologischen Institut der Universität Hamburg* 77: 641–671.
- Heine, F. 1929. Die Inoceramen des mittelwestfälischen Emschers und unteren Untersenen. *Abhandlungen der Preußischen Geologischen Landesanstalt, Neue Folge* 120: 1–124.
- Heinz, R. 1926. Beitrag zur Kenntnis der Stratigraphie und Tektonik der oberen Kreide Lüneburgs. *Mitteilungen aus dem Mineralogisch-Geologischen Staatsinstitut, Hamburg* 8: 3–109.
- Heinz, R. 1928. Das Inoceramen-Profil der Oberen Kreide Lüneburgs. Mit Anführung der neuen Formen und deren Kennzeichnung. *Beiträge zur Kenntnis der oberkretazischen Inoceramen* I. *Jahresbericht des Niedersächsischen geologischen Vereins zu Hannover* 21: 64–81.
- Heinz, R. 1929. Ueber Kreide-Inoceramen der Südafrikanischen Union (*Beiträge zur Kenntnis der ober-*

- kretazischen Inoceramen 11). *Compte Rendu, XV International Geological Congress, South Africa*, vol. 2: 681–687.
- Heinz, R. 1932. Aus der neuen Systematik der Inoceramen. Beiträge zur Kenntnis der oberkretazischen Inoceramen 14. Mitteilungen aus dem Mineralogisch-Geologischen Staatsinstitut, Hamburg 13: 1–26.
- Heinz, R. 1933. Inoceramen von Madagascar und ihre Bedeutung für Kreide-Stratigraphie. Beiträge zur Kenntnis der oberkretazischen Inoceramen 12. *Zeitschrift der Deutschen Geologischen Gesellschaft* 85: 241–259.
- Ivannikov, A.V. 1979. Inoceramids of the Upper Cretaceous in southwestern part of the East European Platform. Kiev: Akademia Nauk Ukrainskoy SSR, Institut Geologicheskich Nauk, 102 pp. [in Russian]
- Jarvis, I., A.S. Gale, H.C. Jenkyns, and M.A. Pearce. 2006. Secular variation in Late Cretaceous carbon isotope: a new $d^{13}C$ carbon reference curve for the Cenomanian–Campanian (99.6–70.6 Ma). *Geological Magazine* 143: 561–608.
- Kauffman, E.G. 1973. Cretaceous Bivalvia. In A. Hallam (editor) *Atlas of palaeobiogeography*: 353–383. Amsterdam: Elsevier Scientific Publishing Company.
- Kauffman, E.G. 1977. Illustrated guide to biostratigraphically important Cretaceous macrofossils, Western Interior Basin, USA. *Mountain Geologist* 14: 225–274.
- Kauffman, E.G., and P. Bengtson. 1985. Mid-Cretaceous inoceramids from Sergipe, Brazil: a progress report. *Cretaceous Research* 6: 311–315.
- Kauffman, E.G., et al. 1993. Molluscan biostratigraphy of the Cretaceous Western Interior Basin, North America. In W.G.E. Caldwell and E.G. Kauffman (editors), *Evolution of the Western Interior Basin*. Geological Association of Canada, Special Paper 39: 397–434.
- Kauffman, E.G. (compiler), W.J. Kennedy, and C.J. Wood. 1996. The Coniacian stage and substage boundaries. *Bulletin de l'Institut Royal des Sciences Naturelles de Belgique, Sciences de la Terre* 66 supp.: 81–94.
- Kennedy, W.J. and W.A. Cobban. 1991. Coniacian ammonite faunas from the United States Western Interior: *Special Papers in Palaeontology* 45: 96 pp.
- Kennedy, W.J., E.G. Kauffman, and H.C. Klinger. 1973. Upper Cretaceous invertebrate faunas from Durban, South Africa. *Transactions of the Geological Society of South Africa* 76: 95–111.
- Kennedy, W.J., I. Walaszczyk, and H.C. Klinger. 2008. *Cladoceramus* (Bivalvia, Inoceramidae)—ammonite associations from the Santonian of KwaZulu. *South Africa. Cretaceous Research* 29: 267–293.
- Khalafova, R.A. 1969. Fauna and stratigraphy of the Upper Cretaceous deposits of the SE part of the Small Caucasus and Nachitchevan area of ASSR. Erevan: ASS Academy of Sciences: 330 pp. [in Russian]
- Kotsubinsky, S.P. 1958. Inoceramids of the Cretaceous deposits of the Volhynian–Podolian Plate, 49 pp. Akademia Nauk Ukrainskoy SSR; Kiev. [in Ukrainian]
- Kotsubinsky, S.P. 1968. Inoceramidae. In S.I. Pasternak et al., *Fauna of the Cretaceous deposits of the Western Ukraine*: 115–148. Kiev: Naukova Dumka. [in Ukrainian]
- Kotsubinsky, S.P. 1974. *Inoceramus*. In G.J. Krymgoltz (editor), *Atlas of the Upper Cretaceous Fauna of Donbass*: 76–86. Moscow: Nedra. [in Russian]
- Lamolda, M.A., C.R.C. Paul, D. Peryt, and J.M. Pons. 2014. The Global Boundary Stratotype and Section Point (GSSP) for the base of the Santonian Stage, “Cantera de Margas,” Olazagutia, northern Spain. *Episodes* 37: 2–13.
- Langenhan, U., and M. Grundey. 1891. Das Kieslingsswalder Gestein und seine Versteinerungen. *Jahresbericht des Glatzer Gebirgs-Vereins* 10: 3–12.
- Logan, W.N. 1898. The invertebrates of the Benton, Niobrara and Fort Pierre groups. *University Geological Survey of Kansas 4 (Paleontology) (Upper Cretaceous 8)*: 431–518.
- Malchus, N., A.V. Dhondt, and K.-A. Tröger. 1994. Upper Cretaceous bivalves from the Glauconie de Lonzee near Gembloux (SWE Belgium). *Bulletin de l'Institut Royal des Sciences Naturelles de Belgique, Science de la Terre* 64: 109–149.
- Marcinowski, R., I. Walaszczyk, and D. Olszewska-Nejbert. 1996. Stratigraphy and regional development of the mid-Cretaceous (Upper Albian through Coniacian) of the Mangyshlak Mountains, Western Kazakhstan. *Acta Geologica Polonica* 46: 1–60.
- Matsumoto, T., M. Noda, and T. Kozai. 1982. Upper Cretaceous inoceramids from the Monobe Area, Shikoku. In *Multidisciplinary research in the upper Cretaceous of the Monobe area, Shikoku*. *Special Papers of the Palaeontological Society of Japan* 25: 53–68.
- McLearn, F. H. 1926. New species from the Coloradoan of lower Smoky and lower Peace Rivers, Alberta. *Contributions to Canadian Palaeontology; Geological Survey. Geological Survey of Canada, Museum Bulletin* 42: 117–126.

- McLearn, F.H. 1929. Palaeontology. *In* Mesozoic Palaeontology of Blairmore Region, Alberta. Bulletin of the Natural History Museum of Canada 58: 73–79.
- Meek, F.B. 1871. Preliminary paleontological report, consisting of lists of fossils, with description of some new types, etc. United States Geological Survey of Wyoming (Hayden), Preliminary Report 4: 287–318.
- Meek, F.B. 1876. A report on the invertebrate Cretaceous and Tertiary fossils of the upper Missouri country. United States Geological Survey of the Territories Report 9: 1–629.
- Meek, F.B., and F.V. Hayden. 1858. Descriptions of new organic remains collected in Nebraska Territory in the year 1857, by Dr. F.V. Hayden, Geologist to the Exploring Expedition under the command of Lieut. G.K. Warren, Top. Engr. U.S. Army, together with some remarks on the geology of the Black Hills and portions of the surrounding country. Proceedings of the Academy of Natural Sciences of Philadelphia 10: 41–59.
- Meek, F.B., and F.V. Hayden. 1862. Description of new Cretaceous fossils from Nebraska Territory, collected by the expedition sent out by the government under the command of Lieut. John Mullan, U.S. Topographical Engineers, for the location and construction of a Wagon Road from the sources of the Missouri to the Pacific Ocean. Proceedings of the Academy of Natural Sciences of Philadelphia 14: 21–28.
- Mitura, F., S. Ciesliński, and J. Milewicz. 1969. Upper Cretaceous inoceramids from the North Sudetic Basin. *Biuletyn Instytutu Geologicznego* 217: 169–181.
- Müller, G. 1888. (“1887”) Beitrag zur Kenntnis der oberen Kreide am nördlichen Harzrande. *Jahrbuch des Preußischen Geologischen Landesanstalt* 8: 372–456.
- Müller, G. 1900. Die Gliederung der *Actinocamax*-Kreide im nordwestlichen Deutschland. *Zeitschrift der Deutschen Geologischen Gesellschaft* 52: 38–39.
- Nagao, T. and T. Matsumoto. 1939. A monograph of the Cretaceous *Inoceramus* of Japan. Part I. *Journal of the Faculty of Science, Hokkaido Imperial University (Series 4)* 4: 241–299.
- Niebuhr, B., et al. 1999. The Upper Cretaceous succession (Cenomanian–Santonian) of the Staffhorst Shaft, Lower Saxony, northern Germany: integrated biostratigraphic, lithostratigraphic and downhole geophysical log data. *Acta Geologica Polonica* 49: 175–213.
- Nikitin, S. 1888. Les vestiges de la période crétacée dans la Russie centrale. *Memoires du Comité Géologique (St. Petersburg)* 5: 163 pp.
- Noda, M. 1975. Succession of *Inoceramus* in the Upper Cretaceous of Southwest Japan. *Memoirs of the Faculty of Science, Kyushu University, Series D, Geology* 23: 211–261.
- Noda, M. 1988. Notes on Cretaceous inoceramids from Sakhalin, held at Tohoku University, Sendai. *Saito Ho-on Kai Special Publication (Professor Tamio Kotaka Commemorative Volume)*: 137–175.
- Noda, M. 1996. Five inoceramids (Bivalvia) from the Upper Cretaceous of Hokkaido with some phylogenetic and taxonomic considerations, Part 1. Introductory remarks, method and systematic descriptions of one species of *Inoceramus* (*I.*) and one of *I.* (*Volvice-ramus*). *Transactions and Proceedings of the Palaeontological Society of Japan, N.S.* 184: 555–570.
- Noda, M., and T. Matsumoto. 1998. Palaeontology and stratigraphy of the inoceramid species from the mid-Turonian through upper Middle Coniacian in Japan. *Acta Geologica Polonica* 48: 345–482.
- Ødum, H. 1953. De geologiska resultaten från Borningarna vid Höllviken. De. V: the macro-fossils of the Upper Cretaceous. *Sverige Geologiska Undersökning, Ser. C* 527: 1–37.
- Orbigny, A. d’ 1843–1847. *Paléontologie française. Terrains crétacés 3 (Lamellibranches)*. Paris: Masson & Cie, 807 pp.
- Parkinson, J. 1819. Remarks on the fossils collected by Mr. Phillips near Dover and Folkstone. *Transactions of the Geological Society (London)* 5: 1–55.
- Pergament, M.A. 1971. Biostratigraphy and inoceramids of Turonian-Coniacian deposits of the Pacific regions of the USSR. *Transactions of the Academy of Sciences of the USSR, Geological Institute* 212: 1–196. [in Russian]
- Petrascheck, W. 1903. Ueber Inoceramen aus der Kreide Böhmens und Sachsens. *Jahrbuch der Kaiserlich-Königlichen Reichsanstalt* 53: 153–168.
- Plint, A.G., R.G. Walker, and K.M. Bergman. 1986. Cardium Formation 6. Stratigraphic framework of the Cardium in subsurface. *Bulletin of Canadian Petroleum Geology* 34: 213–225.
- Radwanska, Z. 1969. Kreda w otworze Sady IG-1. *Kwartalnik Geologiczny* 13: 709–710.
- Remin, Z. 2004. Biostratigraphy of the Santonian in the SW margin of the Holy Cross Mountains near Lipnik, a potential reference section for extra-Carpathian Poland. *Acta Geologica Polonica* 54: 587–596.

- Schlüter, C. 1877. Kreide-Bivalven. Zur Gattung *Inoceramus*. *Palaeontographica* 24: 250–288.
- Scott, G.R. and W.A. Cobban. 1964. Stratigraphy of the Niobrara Formation at Pueblo, Colorado. Professional Paper of the United States Geological Survey 454-L: 1–30.
- Scupin, H. 1912–1913. Die Löwenberger Kreide und ihre Fauna. *Palaeontographica* (Suppl. 6): 1–276.
- Seitz, O. 1962. Über *Inoceramus* (*Platyceramus*) *mantelli* Mercey (Barrois) aus dem Coniac und die Frage des Byssus-Ausschittes bei Oberkreide-Inoceramen. *Geologisches Jahrbuch* 79: 353–386.
- Seitz, O. 1965. Die Inoceramen des Santon und Unter-Campan von Nordwestdeutschland. II. Teil. Biometrie, Dimorphismus und Stratigraphie der Untergattung *Sphenoceramus* J. Böhm. Beihefte zum Geologischen Jahrbuch 69: 1–194.
- Sokolov, D.V. 1914. Kreideinoceramen des Russischen Sachalin. *Memoires du Comité Geologique, Nouvelle Série* 83: 1–95.
- Sornay, J. 1980. Revision du sous-genre d'inocerame *Tethyoceramus* Heinz 1932 (Bivalvia) et de ses représentants Coniaciens à Madagascar. *Annales de Paléontologie* 66: 135–150.
- Soukup, J. 1956. Das Vorkommen von Inoceramen aus der Gruppe *subcardissoides* in der böhmischen Kreide. *Sborník Ústředního Ústavu Geologického* 22: 103–122.
- Sowerby, J. 1814. In Article 6. Proceedings of philosophical societies—Linnaean Society. *Annals of Philosophy* 4: 448.
- Sowerby, J. de C. 1826–1829. The mineral conchology of Great Britain; or, Coloured figures and descriptions of those testaceous animals or shells, which have been preserved at various times and depths in the earth, vol. 6. London: Meredith, 230 pp.
- Stanton, T.W. 1894. The Colorado Formation and its invertebrate fauna. *Bulletin of the United States Geological Survey* 106: 3–189. [1893 imprint]
- Stille, H. 1909. Die Zone der *Inoceramus koeneni* G. Müller bei Paderborn. *Zeitschrift der Deutschen Geologischen Gesellschaft* 61: 194–196.
- Stoliczka, F. 1871. Cretaceous fauna of southern India, vol. 3. The Pelecypoda, with a review of all known genera of this class, fossils and recent. *Memoirs of the Geological Survey of India. Palaeontologica Indica*: 1–507.
- Sturm, F. 1901 (“1900”). Der Sandstein von Kieslingwalde in der Grafschaft Glatz und seine Fauna. *Jahrbuch der Königlich Preussischen Geologischen Landesanstalt und Bergakademie* 21: 39–98.
- Tarkowski, R. 1991. Stratigraphy, macrofossils and palaeogeography of the Upper Cretaceous from the Opole Trough. *Biuletyn Naukowy Akademii Górniczo-Hutniczej* 51: 3–156.
- Toshimitsu, S. 1988. Biostratigraphy of the Upper Cretaceous Santonian Stage in northwestern Hokkaido. *Memoires of the Faculty of Science of the Kyushu University D, Geology* 26: 125–192.
- Tröger, K.-A. 1969. Bemerkungen zur Variabilität von *Inoceramus koeneni* G. Müller aus der subhercynen Kreide. *Freiberger Forschungshefte C245*: 68–81.
- Tröger, K.-A. 1974. Zur Biostratigraphie des Ober-Turon bis Unter-Santon aus dem Schahtaufschluss der Zeche Grimberg IV bei Bergkamen (BRD). *Freiberger Forschungshefte C298*: 109–138.
- Tröger, K.-A. 1981. Zu Problemen der Biostratigraphie der Inoceramen und der Untergliederung des Cenomans und Turons in Mittel- und Osteuropa. *Newsletters on Stratigraphy* 9: 139–156.
- Tröger, K.-A. 1989. Problems of Upper Cretaceous Inoceramid biostratigraphy and paleobiogeography in Europe and Western Asia. In J. Wiedmann (editor), *Cretaceous of the Western Tethys. Proceedings 3rd International Cretaceous Symposium, Tübingen 1987*: 911–930. Stuttgart: E. Schweizerbart'sche Verlagsbuchhandlung.
- Tröger, K.-A., and W.K. Christensen. 1991. Upper Cretaceous (Cenomanian-Santonian) Inoceramid bivalve fauna from the island of Bornholm, Denmark. *Danmarks Geologiske Undersøgelse. DGU Serie A* 28: 1–47.
- Tröger, K.-A., and H. Summesberger. 1994. Coniacian and Santonian bivalves from the Gosau-Group (Cretaceous, Austria) and their biostratigraphic and palaeobiogeographic significance. *Annalen des Naturhistorischen Museum in Wien* 96A: 161–197.
- Tsagarély, A. 1942. Les inocérames crétacés de la Géorgie. *Académie des Sciences de la RSS Géorgienne, Travaux de l'Institut Géologique, Série Géologique* 1 (6), 90–205.
- Veatch, A.C. 1907. Geography and geology of a portion of southwestern Wyoming with special reference to coal and oil. Professional Paper of the Department of the Interior, United States Geological Survey 56.
- Walaszczyk, I. 1992. Turonian through Santonian deposits of the Central Polish Uplands; their facies development, inoceramid paleontology and stratigraphy. *Acta Geologica Polonica* 42: 1–122.
- Walaszczyk, I., and W.A. Cobban. 2000. Inoceramid faunas and biostratigraphy of the Upper Turonian–Lower Coniacian of the Western Interior of the

- United States. Special Paper in Palaeontology 64: 1–118.
- Walaszczyk, I., and W.A. Cobban. 2006. Palaeontology and biostratigraphy of the Middle–Upper Coniacian and Santonian inoceramids of the US Western Interior. *Acta Geologica Polonica* 56: 241–348.
- Walaszczyk, I., and W.A. Cobban. 2007. Inoceramid fauna and biostratigraphy of the upper Middle Coniacian–lower Middle Santonian of the Pueblo section (SE Colorado, US Western Interior). *Cretaceous Research* 28: 132–142.
- Walaszczyk, I., and C.J. Wood. 1998. Inoceramids and biostratigraphy at the Turonian/Coniacian boundary; based on the Salzgitter-Salder Quarry, Lower Saxony, Germany, and the Słupia Nadbrzeźna section, Central Poland. *Acta Geologica Polonica* 48: 395–434.
- Walaszczyk, I., R. Marcinowski, T. Praszkiel, K. Dembicz, and M. Bieńkowska. 2004. Biogeographical and stratigraphical significance of the latest Turonian and Early Coniacian inoceramid/ ammonite succession of the Manasoa section on the Onilahy River, south-west Madagascar. *Cretaceous Research* 25: 543–576.
- Walaszczyk, I., et al. 2010. The Salzgitter-Salder Quarry (Lower Saxony, Germany) and Słupia Nadbrzeźna river cliff section (central Poland): a proposed candidate composite Global Boundary Stratotype Section and Point for the Coniacian Stage (Upper Cretaceous). *Acta Geologica Polonica* 60: 445–477.
- Walaszczyk, et al. 2012. Testing the congruence of the macrofossil versus microfossil record in the Turonian–Coniacian boundary succession of the Wagon Mound–Springer composite section (NE New Mexico, USA). *Acta Geologica Polonica* 62: 581–594.
- Walaszczyk, I., L.F. Kopaevich, and V.N. Beniamovskii. 2013. Inoceramid and foraminiferal record and biozonation of the Turonian and Coniacian (Upper Cretaceous) of the Mangyshlak Mts., western Kazakhstan. *Acta Geologica Polonica* 63: 469–487.
- Walaszczyk, I., et al. 2014a. Ammonite and inoceramid biostratigraphy and biogeography of the Cenomanian through basal Middle Campanian (Upper Cretaceous) of the Morondava Basin, western Madagascar. *Journal of African Earth Sciences* 89: 79–132.
- Walaszczyk, I., J.A. Shank, A.G. Plint, and W.A. Cobban. 2014b. Inter-regional correlation of disconformities in Upper Cretaceous strata, Western Interior Seaway: Biostratigraphic and sequence-stratigraphic evidence for eustatic change. *Geological Society of America, Bulletin* 126: 307–316.
- Wegner, T. 1905. Die Granulaten-Kreide des Westfälischen Münsterlandes. *Zeitschrift der Deutschen Geologischen Gesellschaft* 57: 112–232.
- Westermann, G.E.G. 2000. Biochore classification and nomenclature in paleobiogeography: an attempt at order. *Palaeogeography, Palaeoclimatology, Palaeoecology* 158: 1–13.
- White, C.A. 1879. Contributions to invertebrate paleontology, no. 1: Cretaceous fossils of the Western States and Territories. Department of the Interior. United States Geological Survey, 11th Annual Report of the Survey for the year 1877: 273–319.
- Wood, C.J., I., Walaszczyk, R. Mortimore, and M. Woods. 2004. New observations on the inoceramid biostratigraphy of the higher part of the Upper Turonian and the Turonian–Coniacian boundary transition in Poland, Germany and the UK. *Acta Geologica Polonica* 54: 541–549.
- Woods, H. 1912. A monograph of the Cretaceous Lamellibranchia of England, vol. 2, part 8. Monographs of the Palaeontographical Society (for 1911): 285–340.
- Zonova, T.D. 1992. Cretaceous Inoceramids of eastern USSR. In T.D. Zonova, and K.O. Rostovtsev (editors), Atlas of the Mesozoic guide fossil faunal groups of southern and eastern USSR: 172–191. Transactions of VSEGEI, New Series 350: 375 pp. [in Russian]
- Zonova, T.D. 1993. Inoceramidae. In T.D. Zonova and A.I. Zhamoyda (editors), Atlas of the key paleontological groups of the Upper Cretaceous of Sakhalin: 85–143. Nedra; Sankt-Peterburg. [in Russian]

Chapter 3

Scaphitid Ammonites from the Upper Cretaceous (Coniacian-Santonian) Western Canada Foreland Basin

NEIL H. LANDMAN,¹ A. GUY PLINT,² AND IRENEUSZ WALASZCZYK³

ABSTRACT

The Upper Cretaceous (Coniacian-Santonian) of the Western Canada Foreland Basin, contains a rich record of scaphitid ammonites (scaphites). We describe four species: *Scaphites* (*Scaphites*) *pre-ventricosus* Cobban, 1952, *Scaphites* (*S.*) *ventricosus* Meek and Hayden, 1862, *Scaphites* (*S.*) *depressus* Reeside, 1927, and *Clioscapites saxitonianus* (McLearn, 1929). These are widespread index fossils that demarcate the upper lower-middle, middle, and upper Coniacian, and the lower Santonian, respectively. They occur in the lower part of the Wapiabi Formation, Alberta. The Coniacian part of the section has been divided into 24 informal allomembers based on the recognition of marine flooding surfaces, most of which can be traced through the >750 km extent of the study area. The most distinctive feature in the ontogenetic development of scaphites is the change in coiling during ontogeny. At the approach of maturity, the shell uncoils slightly, forming a shaft, which then recurves backward approaching the earlier secreted phragmocone. However, this sequence of scaphites shows an evolutionary trend toward recoiling, accompanied by an increase in size and degree of depression. These changes occurred against a background of changing environmental conditions resulting from the expansion of the Western Interior Seaway during the Niobrara transgression. This resulted in an increase in the area of offshore habitats, which may have promoted the appearance of larger species with more depressed whorl sections. Scaphites probably lived at depths of less than 100 m, and may have fed on small organisms in the water column.

INTRODUCTION

The Western Canada Foreland Basin (WCFB) comprises a stratigraphic succession of mudstones and sandstones approximately 5 km thick (Wright et al., 1994). The basin extends approximately 1000 km to the east of the Rocky Mountain Foothills. This succession yields a rich record of Late Cretaceous scaphitid ammonites (hereafter referred to as scaphites) ranging from the Turonian to the early Maastrichtian. In this paper, we document the stratigraphic and geographic distribution of the early Coniacian and lower Santonian scaphites, which, together with the co-occurring inoceramid bivalves, permit a subdivision of the Canadian succession into biostratigraphic units (Walaszczyk et al., this issue). Examination of the distribution of the scaphites also allows an evaluation of their biogeography and evolutionary patterns through time.

¹ Division of Paleontology, American Museum of Natural History, New York

² Department of Earth Sciences, University of Western Ontario, London, Ontario Canada.

³ Faculty of Geology, University of Warsaw, Warszawa, Poland.

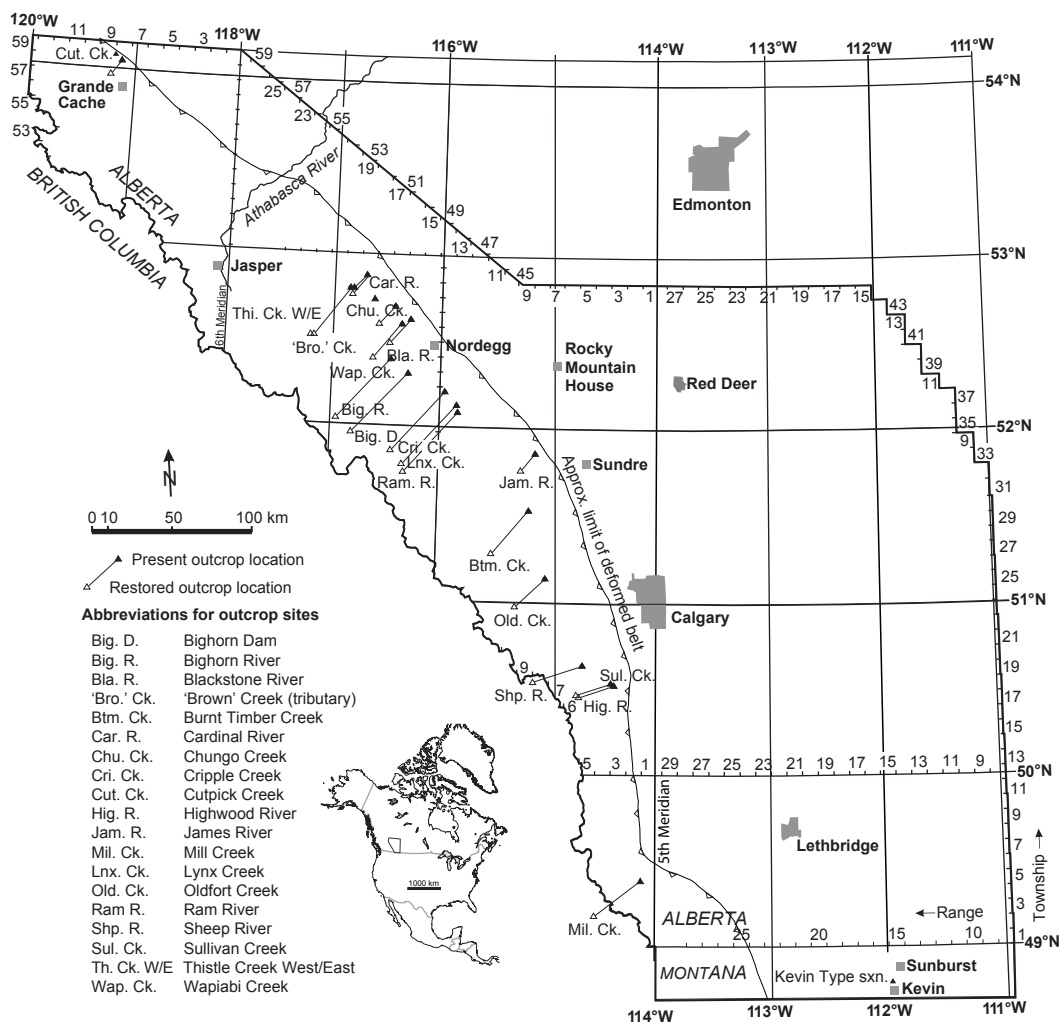


FIG. 1. Map of southwestern Alberta, Canada, showing localities mentioned in the text (for more details, see Plint et al., this issue).

GEOLOGIC BACKGROUND

The fossils described in this report were collected at 18 localities in the Rocky Mountain Foothills of Alberta. The localities are plotted in figure 1. They cover the western part of Alberta and extend from approximately 49°N to 54°N. The outcrop sections were correlated using a large database of publicly available wireline logs that permitted both lithostratigraphic and allostratigraphic relationships to be established, as described in more detail by Plint et al. (this issue).

The Wapiabi Formation consists of Coniacian to lower Campanian rocks and is divided into seven members, each with a distinctive succession of lithologies (Stott, 1963, 1967). The lowest unit is the Muskiki Member, which is dominated by mudstones and rests unconformably on the Cardium Formation. The Muskiki Member is overlain by the Marshybank Member, which is represented by offshore facies in the south and nearshore sandstones and terrestrial deposits in the north. Beneath the Peace River Plains in the Northeast, the Marshybank Member is uncon-

formably overlain by an upper Coniacian unit called the Bad Heart Formation, which consists of very fine-grained sandstones and ooidal ironstones and is exposed along the Smoky River (Plint et al., 1990; Donaldson et al., 1998, 1999). The Cardium and Wapiabi formations in Alberta correlate with the Ferdig and Kevin members of the Marias River Formation in Montana (Cobban et al., 1976; Shank, 2012; Shank and Plint, 2013; Walaszczyk et al., 2014).

Plint et al. (this issue) divided the Coniacian and lowermost Santonian rocks of the Wapiabi Formation into 24 informal allomembers based on the recognition of marine flooding surfaces. These surfaces are identified by an abrupt transition from coarser- to finer-grained sediments, and in many instances, the surfaces are marked by a veneer of intra- or extrabasinal pebbles that imply an episode of shallowing and possibly subaerial emergence. Plint et al. (this issue) interpreted these flooding surfaces as approximate time lines that allow a reconstruction of the subsidence history of the basin. The flooding surfaces in Coniacian rocks are designated CS1 (Coniacian Surface 1) to CS23. The allostratigraphically defined units of rock bounded by these flooding surfaces are designated CA1 (Coniacian Allomember 1) to CA24. In addition, the boundary between the Cardium Formation and the overlying Muskiki Member is designated E7 (after Plint et al. 1986), and the basal surface of the Santonian strata is designated SS0 (Santonian Surface 0).

TERMINOLOGY

Landman et al. (2010) reviewed the terms used to describe scaphites of the genus *Hoploscaphites*. These terms equally apply to the species described herein: *Scaphites* (*S.*) *preventricosus* Cobban, 1952, *S.* (*S.*) *ventricosus* Meek and Hayden, 1862, *S.* (*S.*) *depressus* Reeside, 1927, and *Clioscaphites saxitonianus* (McLearn, 1929). The adult shell consists of two parts, a closely coiled phragmocone and a slightly to strongly uncoiled body chamber (fig. 2). The part of the phragmocone that is exposed in the adult shell (as compared to the part that is

concealed inside) is called the adult phragmocone. The most adapical point of the adult phragmocone is called the point of exposure. The body chamber consists of the shaft, beginning near the last septum, and a hook terminating at the aperture. The point at which the hook curves backward is called the point of recurvature.

Measurements of the adult shell are the same as those described and illustrated in Landman et al. (2013: 9, fig. 3). All measurements were made using electronic calipers on actual specimens, rather than on photos, with the exception of the apertural and septal angles. The following sequence follows the order of the measurements such that H_p is linked to W_p , etc.

L_{MAX} = maximum length from the venter of the phragmocone to the venter of the hook

UD = umbilical diameter through the center of the umbilicus parallel to the line of maximum length

W_p = whorl width of the phragmocone along the line of maximum length

H_p = whorl height of the phragmocone along the line of maximum length

W_s = whorl width of the body chamber at mid-shaft

H_s = whorl height of the body chamber at mid-shaft

W_H = whorl width of the hook at the point of recurvature

H_H = whorl height of the hook at the point of recurvature

AA = in macroconchs, the angle of intersection (in degrees) between two lines (a line drawn along the umbilical shoulder and another line drawn along the apertural margin), extending from approximately the point of recurvature to the aperture

SA = in macroconchs, the angle of intersection (in degrees) between two lines (a line drawn along the umbilical shoulder coinciding with the line of maximum length and a line drawn through the position of the last septum); negative values are

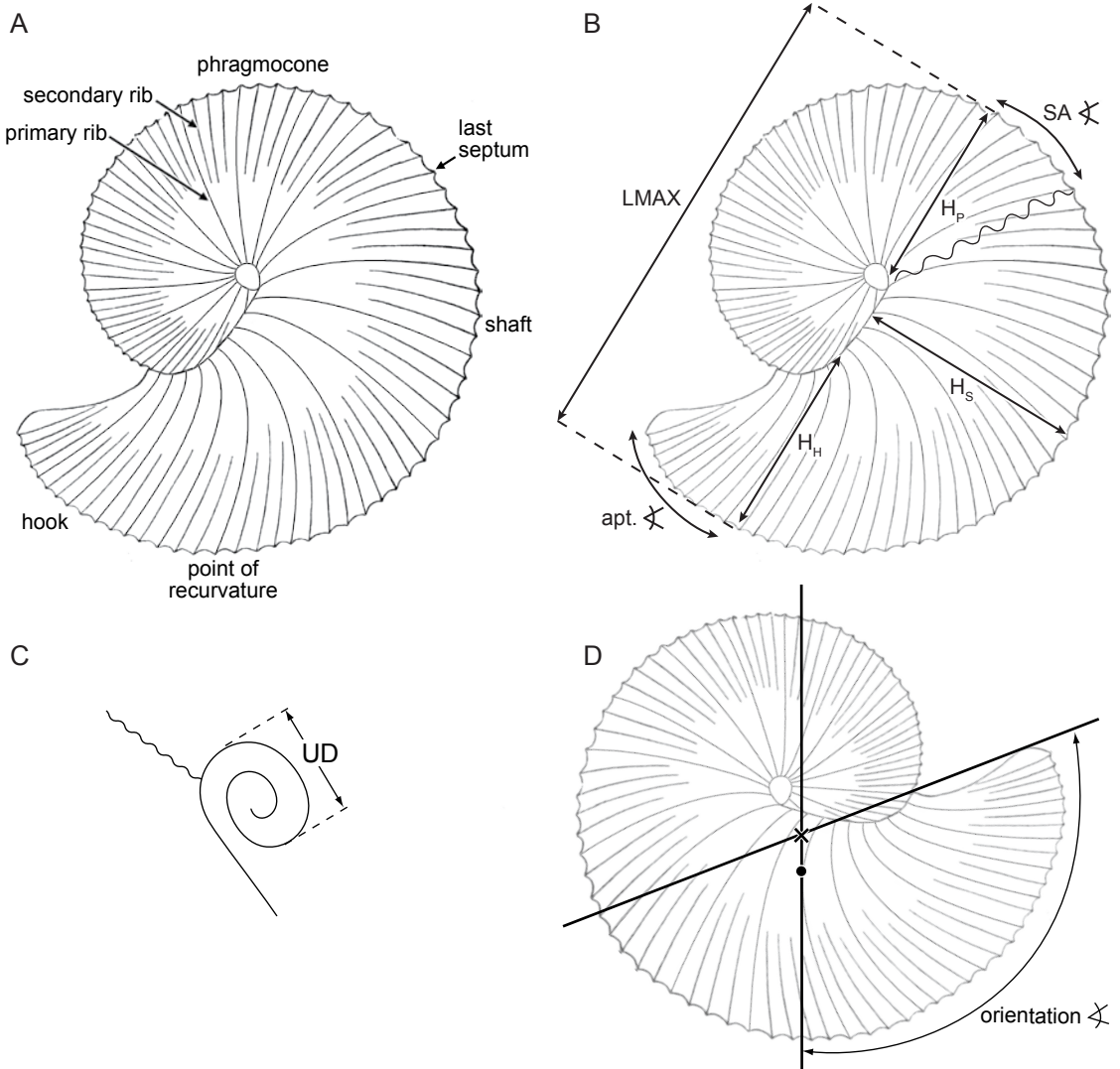


FIG. 2. Scaphite terminology. **A, B, D.** Macroconch, left (A, B) and right (D) lateral views. The position of the last septum marks the base of the body chamber. The umbilical seam of the shaft is straight in macroconchs. **C.** Close-up of the umbilicus; the umbilical diameter is measured parallel to the long axis of the specimen. **D.** Angle of orientation of the aperture with respect to the vertical (orientation). Abbreviations: H_p = whorl height of the phragmocone along the long axis; H_s = whorl height at midshaft; H_h = whorl height of the hook at the point of recurvature; LMAX = maximum length along the long axis; apt. \sphericalangle = apertural angle; SA \sphericalangle = septal angle; UD = umbilical diameter; X = center of buoyancy; • = center of mass.

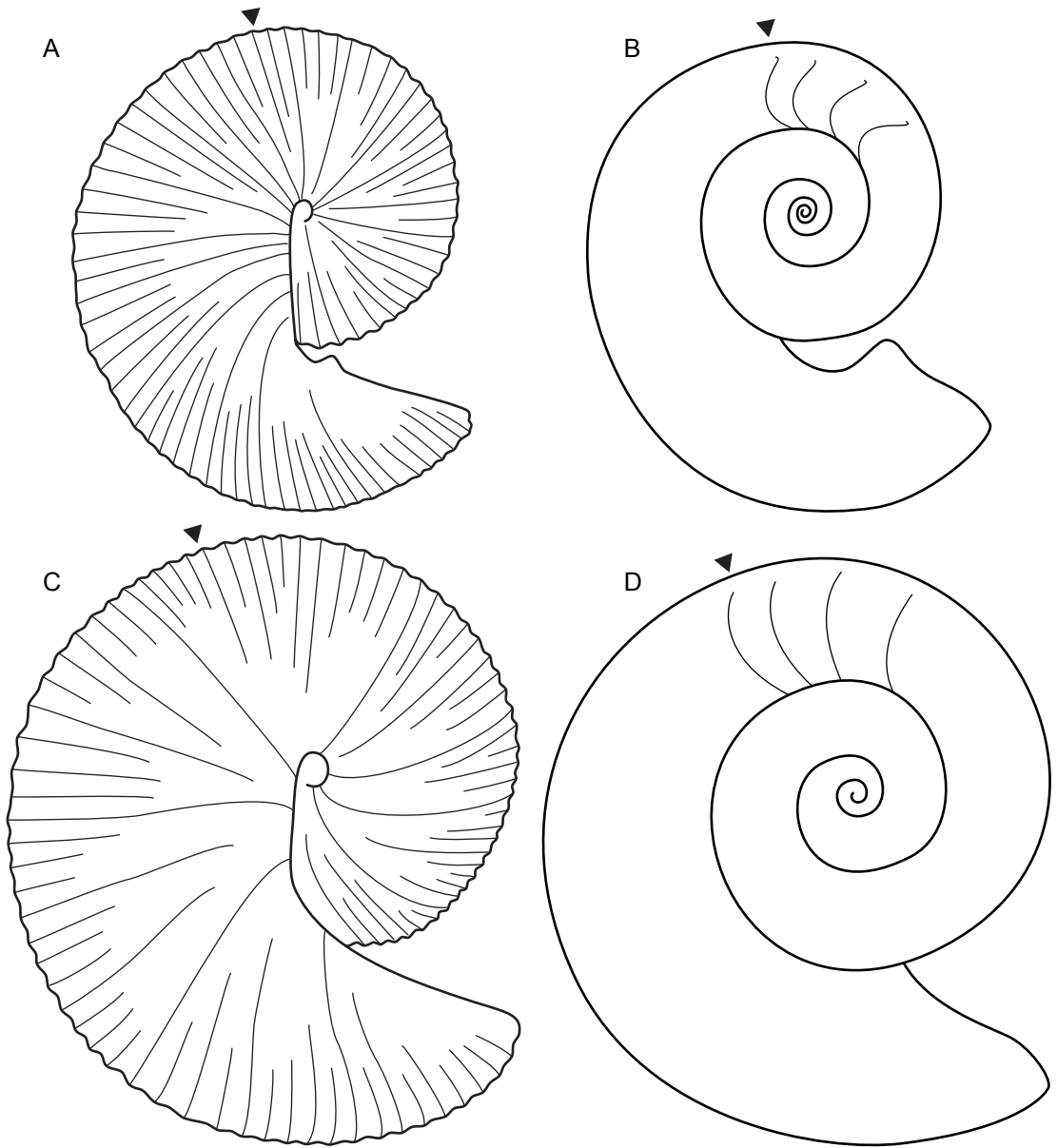


FIG. 3. Comparison of macroconch (C, D) and microconch (A, B) of *Scaphites* (*S.*) *depressus* Reeside, 1927, in lateral view (A, C) and median cross section (B, D). The tick marks indicate the base of the body chamber. A, B. $\times 1.5$; C, D. $\times 1$.

defined as above (adapical of) the line of maximum length; positive values are defined as below (adoral of) the line of maximum length

Several ratios were calculated to describe the shape of the adult shell and facilitate comparisons among specimens:

W_p/H_p = the ratio of whorl width to whorl height of the phragmocone along the line of maximum length

W_s/H_s = the ratio of whorl width to whorl height of the body chamber at midshaft

W_H/H_H = the ratio of whorl width to whorl height of the hook at the point of recurvature

$LMAX/H_p$ = the ratio of maximum length to whorl height of the phragmocone along the line of maximum length

$LMAX/H_s$ = in macroconchs, the ratio of maximum length to whorl height of the body chamber at midshaft

A number of terms are used to describe ornamentation:

primary ribs = ribs that originate near the umbilicus

secondary ribs = ribs that originate on the flanks or venter, either by branching or intercalation

rib density = number of ribs/cm on the venter as measured on the adapical and adoral parts of the phragmocone, the midshaft, and the hook

tubercles = small conical swellings

Photographs of adult shells are natural size. Small black tick marks on the photos mark the base of the body chamber, where visible. The base of the body chamber is defined as the position of the median saddle in the ventral lobe. Specimens are photographed in lateral, apertural, and ventral views. The suture terminology is that of Wedekind (1916), as reviewed by Kullmann and Wiedmann (1970).

TAXONOMIC BACKGROUND

Cobban (1952) revised the taxonomy of the Turonian-Santonian scaphites of the U.S. West-

ern Interior in his classic monograph in which he described 27 new species. He placed most of these species in the genus *Scaphites* but also introduced the genera *Clioscaphtes* for species that are closely coiled at maturity with trifold lateral lobes and *Desmoscaphtes* for species that develop constrictions in their early ontogeny. These species were subsequently studied by Birkelund (1965), Crick (1978), Landman (1987, 1989), Kennedy and Cobban (1991), Cooper (1994), Braunberger (1994), Braunberger and Hall (2001), Collom (2001), Landman and Cobban (2007), and Cobban et al. (2006). Cooper (1994: 176) introduced the new genera *Anascaphites* and *Billcobbanoceras* and reassigned several of the species that Cobban (1952) had previously included in *Scaphites* and *Clioscaphtes* to these new genera; these changes have not been followed by any subsequent workers (e.g., Braunberger and Hall, 2001; Cobban et al., 2006; Landman and Cobban, 2007). Until a thorough phylogenetic revision of all these species is undertaken, we prefer to follow the simplified taxonomy outlined by Kennedy and Cobban (1991) in their recent treatment of these forms.

The taxonomic discrimination of scaphite species mostly relies on features of the mature shell. Throughout most of ontogeny, the shell is closely coiled, similar to so-called normal ammonites. However, at the approach of maturity, the shell uncoils slightly, forming a shaft, which then recurves backward approaching the earlier secreted phragmocone. This change in shape is usually accompanied by a change in ornamentation affecting the coarseness and spacing of ribs and the appearance of ventrolateral tubercles. Internally, these changes are associated with a reduction in spacing of the last few septa, known as septal approximation.

Dimorphism is present in all scaphites, but usually is apparent only at maturity (fig. 3). It is generally interpreted as sexual in nature (Cobban, 1969; Landman and Waage, 1993; Davis et al., 1996). The dimorphs are referred to as the macroconch (M), presumably the female, and the microconch (m), presumably the male. In the scaphite species

described in this report, dimorphism is expressed by size, robustness, and degree of uncoiling, with macroconchs larger, more robust, and more tightly coiled. The body chamber is more inflated in macroconchs than in microconchs, possibly due to the expansion of the female reproductive organs. In both dimorphs, the whorl width and height decrease at the end of ontogeny, so that the adult aperture is smaller than that at midshaft (Collom, 2001: pl. 45, figs. 4–8).

As documented in other scaphites, macroconchs are larger than microconchs (Makowski, 1962; Cobban, 1969; Machalski, 2005). Dimorphs of the same species overlap in size, but the largest macroconch is usually larger than the largest microconch. For example, in our sample of *Scaphites* (*S.*) *depressus*, the extent of size overlap is 14% of the total combined size range of both dimorphs. The average size of microconchs is 72% that of macroconchs (or conversely, the average size of macroconchs is 139% that of microconchs). The difference in size between the two dimorphs in this species amounts to less than one whorl (Collom, 2001).

The dimorphs of the Turonian-Santonian scaphites were previously described as separate species or varieties of the same species (Cobban, 1952). In *Scaphites* (*Scaphites*) *preventricosus*, the microconch was originally designated as *S.* (*S.*) *preventricosus* var. *sweetgrassensis*, in *S.* (*S.*) *ventricosus*, it was originally designated as *S.* (*S.*) *tetonensis*, in *S.* (*S.*) *depressus*, it was originally designated as *S.* (*S.*) *depressus* var. *stantoni*, and in *Clioscapites saxitonianus*, it was originally designated as *C. saxitonianus* var. *keytei*. We follow the current systematic practice of combining the dimorphs (to the extent that we can recognize them) into the same species.

GEOGRAPHIC DISTRIBUTION

The Coniacian and Santonian scaphites described in this report are widely distributed in the Western Interior of North America (fig. 1). In addition, Birkelund (1965) described several of these species from western Greenland, supporting

a connection between this area and the Interior Seaway. However, none of these species has been reported from either the Gulf of Mexico and Atlantic Coastal Plains or Europe. Their absence there may represent a taphonomic bias, but more likely, it reflects their preference for boreal seas.

Scaphites (*S.*) *preventricosus* is present in the Cardium Formation at Highwood River, Alberta, and in the Wapiabi Formation at Mill Creek, Cutpick Creek, Oldfort Creek, Wapiabi Creek, and Bighorn Dam, Alberta (fig. 1). It is present in the United States in the Kevin Member of the Marias River Shale in north-central Montana and in the uppermost part of the Frontier Formation in Wyoming. Outside North America, it has been reported from Umivik, Svartenhuk, western Greenland (Birkelund, 1965). *Scaphites* (*S.*) *ventricosus* is present in the Wapiabi Formation at Ram River, East Thistle Creek, James River, Blackstone River, Chungo Creek, Mill Creek, Sheep River, Bighorn Dam, and Bighorn River, Alberta. It is present in the United States in the Kevin Member of the Marias River Shale in north-central Montana, the Cody Shale in western Wyoming, and the Mancos Shale in New Mexico. Outside North America, it has been reported from Alianaitsúnuaq, Nügssuaq, western Greenland (Birkelund, 1965). *Scaphites* (*S.*) *depressus* is present in the Wapiabi Formation at Ram River, East Thistle Creek, West Thistle Creek, James River, Sheep River, Bighorn Dam, Bighorn River, Cardinal River, and Mill Creek, Alberta. In the United States, it is present in the Kevin Member of the Marias River Shale in north-central Montana and the Cody Shale in western Wyoming. It is rare in the Smoky Hill Chalk Member of the Niobrara Formation in southwestern Colorado and the Mancos Shale in western Colorado and eastern Utah. *Clioscapites saxitonianus* is present in the Wapiabi Formation at James River, West Thistle Creek, Cardinal River, Cripple Creek, Lynx Creek, and above the measured section at Ram River, Alberta. In the United States, it is present in the Apishapa Shale of southeastern Colorado and the Kevin Member of the Marias River Shale on the east flank of the Sweetgrass Arch of north-central

Stages and Substages		Stage Boundaries (Ma)	Scaphite Zones	Age (Ma)	Inoceramid Zones
Santonian	upper	83.50 ± 0.70	<i>Desmoscaphites bassleri</i>	84.30 ± 0.34	<i>Sphenoceramus lundbreckensis</i>
			<i>Desmoscaphites erdmanni</i>		
	middle		<i>Clioscaphtes choteauensis</i>		<i>Cordiceramus bueltensis</i>
Coniacian	lower	85.80 ± 0.70	<i>Clioscaphtes vermiformis</i>		<i>Cladoceramus undulatoplicatus</i>
	upper		<i>Clioscaphtes saxitonianus</i>		<i>Magadiceramus crenulatus</i>
			<i>Scaphites (S.) depressus</i>	87.14 ± 0.39	<i>Magadiceramus subquadratus</i>
	middle	<i>Scaphites (S.) ventricosus</i>		<i>Volviceramus involutus</i>	
	lower	<i>Scaphites (S.) preventricosus</i>	88.55 ± 0.59	<i>Volviceramus koeneni</i>	
				<i>Cremnoceramus crassus crassus</i>	
<i>Cremnoceramus crassus inconstans</i>					
			<i>Cremnoceramus deformis dobrogensis</i>		
			<i>Cremnoceramus deformis erectus</i>		
		89.30 ± 1.00			

FIG. 4. Ammonite zonation of the Coniacian and Santonian of the U.S. Western Interior (modified from Cobban et al., 2006).

Montana. Outside North America, it has been reported from western Greenland (Birkelund, 1965).

STRATIGRAPHIC DISTRIBUTION

Based on the extensive biostratigraphic research summarized in Cobban et al. (2006), the Upper Cretaceous of the U.S. Western Interior was subdivided into 66 zones using ammonites and co-occurring inoceramid bivalves (fig. 4). According to this scheme, the Coniacian was subdivided, in ascending order, into the lower Coniacian *Scaphites (S.) preventricosus* Zone, the middle Coniacian *S. (S.) ventricosus* Zone, and the upper Coniacian *S. (S.) depressus* Zone. This succession is confirmed by the Canadian material studied here. However, the base of the *Scaphites (S.) ventricosus* Zone is lower down in the section than previously thought and occurs in the upper part of the lower Coniacian. The base of the middle Coniacian is defined by the lowest occurrence of the inoceramid genus *Volviceramus*. The apparent coincidence of the lowest occurrences of *S. (S.) ventricosus* and *Volviceramus* is probably the result of a pan-regional stratigraphic gap (e.g., Walaszczyk and Cobban

2000, 2006). The overlying Santonian consists, in ascending order, of the lower Santonian *Clioscaphtes saxitonianus* Zone, the middle Santonian *C. vermiformis* Zone, and the upper Santonian *C. choteauensis*, *Desmoscaphites erdmanni*, and *D. bassleri* Zones. The *S. (S.) preventricosus* Zone is dated at 88.55 ± 0.59 Ma, the *S. (S.) depressus* Zone at 87.14 ± 0.39 Ma, and the *D. bassleri* Zone at 84.30 ± 0.34 Ma, so that our study interval spans approximately 4 Myr (Sage-man et al., 2014).

Scaphites are present in all outcrop sections examined in our study (fig. 1). They occur as isolated specimens preserved as internal molds composed of siderite. The biostratigraphic distribution of the various species conforms to the established zonation. The stratigraphic position of each species is recorded in table 1 (for more details about this stratigraphic distribution, see Plint et al., this issue). The ranges of several of the species overlap. For example, at Bighorn Dam, a specimen of *Scaphites (S.) ventricosus* occurs in the lower part of the *S. (S.) depressus* Zone at a height of 107.5 m. At Cardinal River, two specimens of *S. (S.) depressus* occur in the lower part of the *Clioscaphtes saxitonianus* Zone at a height of 141.5–143.5 m. Similarly, at West Thistle Creek, two specimens of *S. (S.) depressus* occur in the lower part of the *C.*

TABLE 1
Height (m) of species in the measured section at each locality.
X = present, but height unknown.

Locality	<i>S. (S.) preventricosus</i>	<i>S. (S.) ventricosus</i>	<i>S. (S.) depressus</i>	<i>C. saxitonianus</i>
Bighorn Dam	8.5	42.6, 50–60, 69.5, 84.2, 87.6, 107.5	96.7, 103.4, 107.3, 108.0, 109.6, 112.8, 113.0, 115.3, 115.8, 116.0, 133.0	
Bighorn River		99.4	109.4, 132.4, 142.2, above measured section	
Blackstone River		37.4		
Cardinal River			90.4, 96.8, 121.0, 139.0, 141.5– 143.5	141.5–143.5
Chungo Creek		41.4, 48.9, 51.3		
Cripple Creek				47.0, 48.6
Cutpick Creek	9.0			
Highwood River	Cardium Fm.			
James River		52.1	92.7	105.7
Lynx Creek				x
Mill Creek	70.0, 90.0, 139.0, 141.0	191.0	230	
Oldfort Ck.	13.2			
Ram River		108.7	110.7, 111.4, 112.7, 119.6, 127.3, 132.5, 132.9	Above measured section
Sheep River		78	147.5, 149.0, 158.8	
Sullivan Creek				
E. Thistle Ck.		18.2	83.3	
W. Thistle Ck.			100.3, 100.9, 101.3, 102.0, 105.8, 106.7, 107.0, 110.7, 113.8, 114.9, 118.7, 121.0, 123.6	121.0, 123.6, 123.6, 125.9, 130.2
Wapiabi Ck	14.5, 51.0			

saxitonianus Zone at a height of 121.0 and 123.6 m. Cobban et al. (2005) also noted the co-occurrence of *S. (S.) depressus* and *C. saxitonianus*. These overlaps in stratigraphic range imply evolutionary episodes of cladogenesis rather than anagenesis, which was the pattern previously envisioned by Cobban (1952).

The lowest occurrences of each scaphite species can be interpreted in the context of the relative sea-level curve (fig. 5) based on the allostratigraphic scheme developed by Plint et al. (this issue). The lowest occurrence of *Scaphites (S.) preventricosus* is just above erosional

surface E5.5, which marks the beginning of a major transgression that commenced in the very latest Turonian (Walaszczyk et al., 2014). The lowest occurrence of *S. (S.) ventricosus* is immediately above surface CS2 in allomember CA3 just below an interpreted highstand and prior to a major regression that culminated at surface CS4, which marks the boundary between the lower and middle Coniacian. It is just below the lowest occurrence of *Volviceramus*, which marks the base of the middle Coniacian. The lowest occurrence of *S. (S.) depressus* is in allomember CA15, immediately above surface CS14 in an

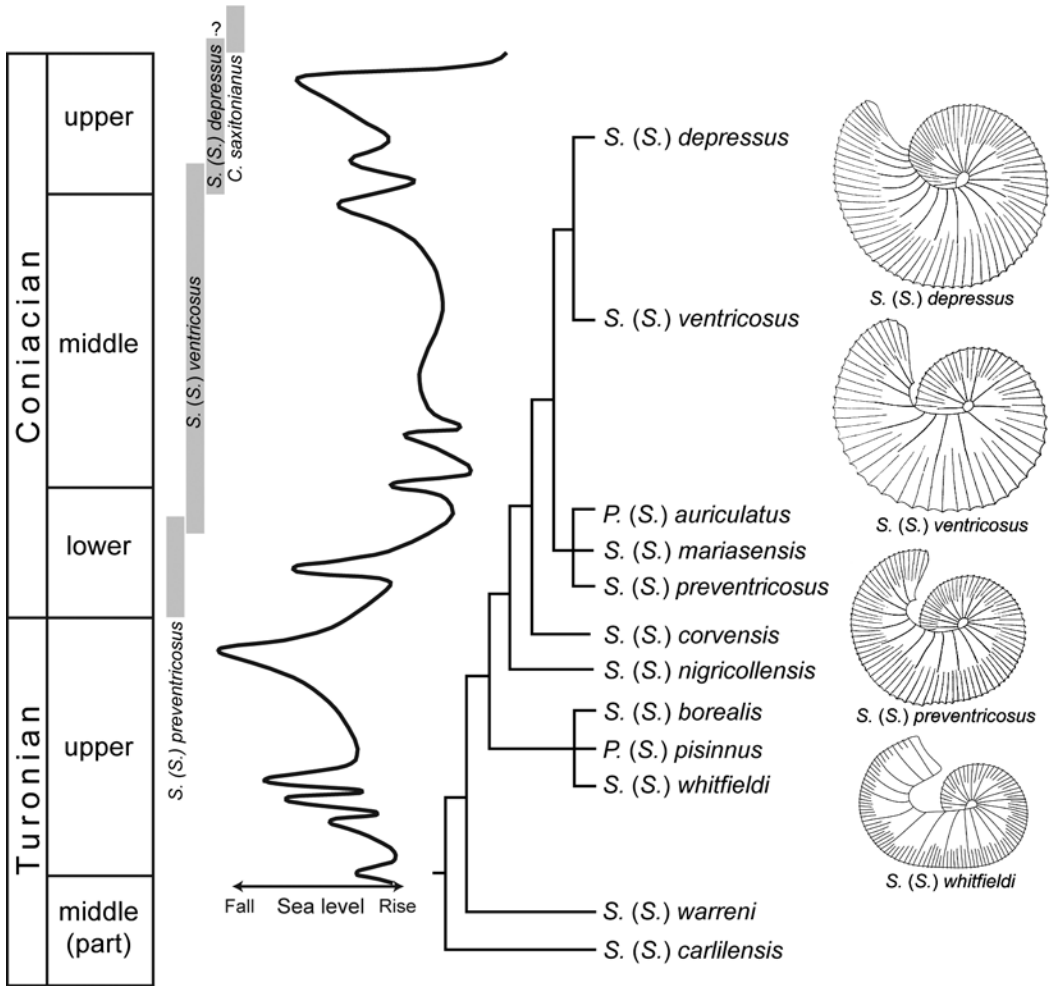


FIG. 5. Stratigraphic ranges of *Scaphites* (*S.*) *preventricosus*, *S. (S.) ventricosus*, *S. (S.) depressus*, and *Clioscaphtes saxitonianus* (plotted on the left side) next to a curve of the changes in relative sea level during the Turonian-Santonian based on analysis of stratigraphic sections in the Western Foreland Basin (Plint et al., this issue). The evolutionary relationships proposed by Cobban (1952) are presented as a cladogram showing the trend toward recoiling at maturity.

overall regressive succession, which marks the base of the upper Coniacian. The increase in abundance of this species above surface CS14 is possibly coupled with a change in water chemistry (oxygen level?) that is expressed by an abrupt increase in the intensity of bioturbation. The lowest occurrence of *Clioscaphtes saxitonianus* is at the base of the Santonian (surface SS0), and coincides with a major transgression that is expressed by a gradual change from bioturbated

sandy siltstones to dark mudstones with a very low level of bioturbation, indicative of a transition to a more offshore setting with more oxygen-deficient bottom water.

PALEOECOLOGY

One of the most important clues about the mode of life of ammonites is the angle of orien-

TABLE 2

Angle of orientation of the aperture with respect to the vertical in Turonian-Santonian scaphites. See figure 2 for description of measurements ;angles are reported to the nearest 0.5°.

Species	Sample No,	TMP No.	Dimorph	Angle (°)
<i>S. (S.) preventricosus</i>	30	2016.041.0038	Macroconch	125.0
<i>S. (S.) preventricosus</i>	26	2016.041.0034	Microconch	123.0
<i>S. (S.) preventricosus</i>	28	2016.041.0036	Microconch	135.0
<i>S. (S.) preventricosus</i>	31	2016.041.0039	Microconch	128.5
<i>S. (S.) ventricosus</i>	19	2016.041.0021	Macroconch	128.0
<i>S. (S.) ventricosus</i>	63	2016.041.0164	Macroconch	134.0
<i>S. (S.) ventricosus</i>	66	2016.041.0167	Macroconch	140.5
<i>S. (S.) ventricosus</i>	141	2016.041.0379	Macroconch	135.0
<i>S. (S.) ventricosus</i>	62	2016.041.0163	Microconch	121.0
<i>S. (S.) depressus</i>	9	2016.041.0011	Macroconch	122.0
<i>S. (S.) depressus</i>	37	2016.041.0069	Macroconch	122.0
<i>S. (S.) depressus</i>	78	2016.041.0212	Macroconch	128.5
<i>S. (S.) depressus</i>	85	2016.041.0219	Macroconch	113.5
<i>S. (S.) depressus</i>	115	2016.041.0303	Macroconch	141.5
<i>S. (S.) depressus</i>	121	2016.041.0350	Macroconch	114.0
<i>S. (S.) depressus</i>	150	2016.041.0388	Macroconch	122.5
<i>S. (S.) depressus</i>	3	2016.041.0005	Microconch	122.5
<i>S. (S.) depressus</i>	89	2016.041.0223	Microconch	126.5
<i>S. (S.) depressus</i>	144	2016.041.0382	Microconch	120.0
<i>C. saxitonianus</i>	105	2016.041.0279	Macroconch	116.0

tation of the aperture with respect to the vertical. Assuming that scaphites maintained near neutral buoyancy during life, this parameter can be calculated based on the positions of the centers of mass and buoyancy, using the same approach as Trueman (1941). We used photos of specimens in lateral view and “cut out” the whole specimen and body chamber separately. In incomplete specimens, we filled in the missing portions of the shell. Using a computer program (Image J), the centers of the areas of the whole specimen and of the body chamber were determined and treated as proxies for the centers of buoyancy and mass, respectively. We drew two lines: one through the center of mass and buoyancy constituting the vertical and another line through the apertural margin. The

angle of orientation of the aperture is defined as the angle between the apertural margin and the vertical.

The above method involves as least three simplifying assumptions: (1) the phragmocone is completely filled with air, with no cameral liquid present; (2) the soft tissues are uniformly distributed in the body chamber, thus neglecting the weight of the aptychus (jaws) at the adoral end; and (3) the thickness of the shell is uniform (for more details about these assumptions, see Landman et al., 2010).

We examined the angle of orientation of the aperture in four specimens of *Scaphites* (*S.*) *preventricosus* (one macroconch and three microconchs), five specimens of *S. (S.) ventricosus* (four macroconchs and one microconch),



FIG. 6. Hypothetical reconstruction of a macroconch (female) of *Scaphites* (*S.*) *preventricosus* with small delicate arms joined together by a thin web. The shell is covered by a thin periostracum. Artist: Mariah Slovacek (AMNH).

10 specimens of *S. (S.) depressus* (seven macroconchs and three microconchs), and one specimen of *Clioscaphtes saxitonianus* (macroconch). The angle of orientation is nearly the same in all four species (table 2). It averages 127.0° and ranges from 114.0° to 141.5° . It averages 128.0° in *S. (S.) preventricosus*, 132.0° in *S. (S.) ventricosus*, 123.5° in *S. (S.) depressus*, and 116.0° in *C. saxitonianus* (table 2). In addition, the angle of orientation of the aperture is approximately the same in dimorphs within the same species. In *S. (S.) preventricosus*, it averages 125.0° in macroconchs and 129.0° in microconchs; in *S. (S.)*

ventricosus, it averages 134.5° in macroconchs and 121.0° in microconchs; and in *S. (S.) depressus*, it averages 123.5° in macroconchs and 123.0° in microconchs.

These high values indicate that the aperture of these scaphites faced upward during life. This orientation is incompatible with feeding on the bottom, as in modern *Nautilus*. In addition, the aperture at maturity is smaller in size relative to that at midshaft, especially in macroconchs, further impeding access to the bottom. Instead, these scaphites may have fed on small organisms in the water column. To facilitate the capture of small prey, the soft body may have extended

weblike out of the aperture with the jaws protruding forward (fig. 6).

Collom (2001) reached a similar conclusion about the mode of life of scaphites based on the orientation of the aperture. However, he argued that these animals lacked jaws altogether based on the absence of jaws in the large collection of *Scaphites* (*S.*) *depressus* at his disposal. This is extremely unlikely given the presence of jaws in closely related species such as *S.* (*S.*) *mariasensis*, as documented by Landman et al. (2012). Indeed, the preservation of jaws is relatively rare and depends on many factors including whether the shells floated into the site after death or immediately fell to the sea floor in the same area in which they lived (Wani et al., 2005). It also depends on whether the animals were buried rapidly or remained at the sediment water interface for some time. As a clue to the circumstances surrounding the burial of the specimens in our study, two macroconchs of *S.* (*S.*) *depressus* in our collection bear bryozoan colonies that cover the inside surfaces of the body chambers (exposed on the outside surfaces of the internal molds), suggesting that these specimens remained on the sea floor long enough for epizoids to colonize them.

The preservation of jaws also depends on the length and shape of the body chamber. The short, depressed body chambers of *Scaphites* (*S.*) *depressus* do not seem to favor in situ jaw preservation. Landman et al. (2017) reported similar findings for fossil nautilids with short, depressed body chambers. They studied a collection of approximately 300 specimens belonging to the genus *Eutrephoceras*, and despite the abundance and excellent preservation of the shells, they did not find a single in situ jaw. Further studies could shed additional light on the relationship between body chamber size and shape and the incidence of in situ jaw preservation (for more details about the taphonomy of jaws in externally shelled cephalopods, see Wani, 2007).

Most investigations of the habitat of scaphites suggest that they lived a few meters above the

bottom. This inference is based on several lines of evidence, including incidence and kinds of injuries on the shells, facies and faunal associations, and isotopic analyses (Landman et al., 2012; Landman and Klofak, 2012). For example, in the Campanian Pierre Shale of the U.S. Western Interior, scaphites are associated with a rich benthic and nektic fauna (Tsujita and Westermann, 1998; Landman et al., 2010). Such associations suggest that the same factors (elevated levels of oxygen?) that favored the development of benthic communities also promoted an increase in the number of scaphites. The habitat depths of scaphites have been estimated based on investigations of the mechanical strength of the shell and septa. According to Hewitt (1996), the implosion depth of *Scaphites* (*S.*) *whitfieldi*, *S.* (*S.*) *preventricosus*, and *Clioscapites vermiformis* averages 170 m. In analogy with modern *Nautilus*, the ammonites would probably have lived at shallower depths, “to be on the safe side.” These values are consistent with depth estimates of the Alberta portion of the Western Interior Seaway during the Coniacian (Plint et al., this issue).

EVOLUTION

The evolutionary relationships among Coniacian and Santonian scaphites in the Western Interior of North America have not yet been resolved through rigorous phylogenetic analysis. However, based on his studies, Cobban (1952) assembled a detailed record of the stratigraphic succession of species in the U.S. Western Interior. This succession provides a biostratigraphic framework as well as a hypothesis of evolutionary relationships from more primitive to more advanced species (fig. 5). Cobban (1952) noted a succession of endemic species starting in the late Turonian and extending to the end of the Coniacian. In ascending biostratigraphic order, they are *Scaphites* (*S.*) *whitfieldi* Cobban, 1952, *S.* (*S.*) *nigricollensis* Cobban, 1952, *S.* (*S.*) *corvensis* Cobban, 1952, *S.* (*S.*) *preventricosus* and the closely related species *S.* (*S.*) *mariasensis* Cobban, 1952, *S.* (*S.*) *ventricosus*, and *S.* (*S.*) *depressus*. He also noted two micromorph

species, *S. (Pteroscaphites) pisinnus* (Cobban, 1952) and *S. (P.) auriculatus* (Cobban, 1952), which co-occur with *S. (S.) whitfieldi* and *S. (S.) preventricosus*, respectively. Since then, a “macro-morph” species, *S. (S.) borealis* Cobban and Kennedy, 1991, has also been described, which co-occurs with *S. (S.) whitfieldi*.

The evolutionary relationships proposed by Cobban (1952) are presented as a phylogenetic tree in figure 5. If these relationships are valid, they suggest a directional change in morphology from more loosely to more closely coiled shells at maturity, with the most marked change occurring between *Scaphites (S.) preventricosus* and *S. (S.) ventricosus*. The degree of uncoiling of macroconchs at maturity is expressed by the ratio of L_{MAX}/H_p (the ratio of maximum length to whorl height of the phragmocone along the line of maximum length, fig. 2). The value of this ratio is lower in more tightly coiled shells (Landman, 1987: fig. 74). In the present study, the value of this ratio averages 3.07 in *Scaphites (S.) preventricosus*, 2.55 in *S. (S.) ventricosus*, and 2.55 in *S. (S.) depressus*. The degree of uncoiling of macroconchs at maturity is also expressed by the apertural angle (fig. 2), not to be confused with the angle of orientation of the aperture with respect to the vertical during the lifetime of the animal. The value of the apertural angle is lower in more tightly coiled shells. In the present study, the value of this angle averages 100.0° in *S. (S.) preventricosus*, 82.5° in *S. (S.) ventricosus*, and 70.2° in *S. (S.) depressus*.

The change in the degree of uncoiling of the shell correlates with three other variables: position of the last septum, degree of whorl compression, and adult size (as observed in macroconchs). The position of the last septum relative to the line of maximum length of the shell is expressed by the septal angle (fig. 2). Negative angles are defined as above (adapical of) the line of maximum length whereas positive angles are defined as below (adoral of) the line of maximum length. The position of the last septum shifts toward the apex in more closely coiled shells. In the present study, the

value of the septal angle averages 52.0° in *Scaphites (S.) preventricosus*, 12.0° in *S. (S.) ventricosus*, and -2.5° in *S. (S.) depressus*. The degree of whorl depression is also higher in more closely coiled shells. The degree of whorl depression at maturity is expressed by the ratio of W_s/H_s (the ratio of whorl width to height at midshaft). In the present study, the value of this ratio averages 1.27 in *S. (S.) preventricosus*, 1.31 in *S. (S.) ventricosus*, and 1.39 in *S. (S.) depressus*. Finally, the adult size (L_{MAX}) is correlated with the degree of shell coiling, with larger shells more tightly coiled. Based on the measurements in the present study, the average value of L_{MAX} equals 70.1 mm in *S. (S.) preventricosus*, 85.4 mm in *S. (S.) ventricosus*, and 90.6 mm in *S. (S.) depressus*.

The degree of uncoiling, the size at maturity, and the degree of whorl compression are also linked together within species. For example, in *Scaphites (S.) depressus*, adult macroconchs are larger, more depressed, and more closely coiled than adult microconchs (fig. 3; Collom, 2001: pl. 7, figs. 5, 6). The adult body chamber in macroconchs remains in contact with the phragmocone whereas in microconchs, it uncoils slightly, so that a space develops between the body chamber and the phragmocone.

The position of the last septum and the apertural angle are also linked together within species. Landman et al. (2010) documented this relationship in adults of *Hoploscaphites nodosus* (Owen, 1851) and *H. brevis* (Meek, 1876) from the upper Campanian Pierre Shale. They discovered that the apertural angle is higher in specimens in which the last septum occurs below the line of maximum length. Based on calculations of the centers of mass and buoyancy in these scaphites, they argued that the covariation between the position of the last septum and the apertural angle guarantees that the angle of orientation of the aperture with respect to the vertical remains nearly the same.

The fact that the degree of shell uncoiling, position of the last septum, degree of whorl compression, and adult size vary within species suggests that this variation was available for

evolutionary modification. However, the additional fact that these features covary within species further implies that they formed an integrated whole, as expressed by the concept of morphological integration (Olson and Miller, 1958; for another example of covariation between morphological features in ammonites, see Yacobucci, 2004). This suggests that the same selective forces that acted on individuals may also have played a role in fashioning the shape of new species; any changes during evolution were constrained by interdependent interactions, so that, for example, the development of a larger shell invariably entailed a reduction in the degree of uncoiling with associated changes in the apertural angle and position of the last septum.

The reduction in the degree of uncoiling also affected the hydrostatic and hydrodynamic properties of the shell. It decreased the distance between the centers of mass and buoyancy, thus reducing stability. However, it improved the efficiency of horizontal swimming and maneuverability while maintaining the same orientation of the aperture (Landman et al., 2012).

The driving force for all these trends may have been an evolutionary increase in adult size. This increase was accommodated by the secretion of additional whorls rather than an increase in the degree of whorl expansion (Landman, 1987). If the rate of shell secretion and chamber formation remained the same in all species, this increase in size implies a delay in the timing of maturation or, in terms of heterochrony, hypermorphosis (McKinney and McNamara, 1991). Thus, the evolutionary sequence from *Scaphites* (*S.*) *whitfieldi* to *S.* (*S.*) *depressus* represents a peramorphocline in which more derived species were larger and longer lived than more primitive species. However, maturation entails its own set of morphological modifications starting at the point at which the shell departs from the spiral coil and develops into the shaft (Landman, 1989).

This evolutionary increase in adult size and associated reduction in the degree of uncoiling occurred against a backdrop of changing envi-

ronmental conditions due to changes in the extent of the Western Interior Seaway, as reflected in transgressive-regressive curves (fig. 5) and paleogeographic reconstructions (Williams and Stelck, 1975; Nielsen et al., 2008; Schröder-Adams et al., 2012). The overall expansion of the seaway during this time is associated with the Niobrara transgression (Kauffman and Caldwell, 1993). In the late Turonian, the *Scaphites* (*S.*) *whitfieldi* Zone was deposited in the middle of an overall regressive succession (fig. 5). The seaway was a narrow strait several hundred kilometers wide (Nielsen et al., 2008: fig. 10C). In the northern United States, it extended from central Wyoming to eastern South Dakota and, in Canada, it covered most of Alberta. It was characterized by an axial belt of calcareous muds flanked on either side by noncalcareous muds to muddy silts with sands along the margins. In contrast, in the middle Coniacian, the *S.* (*S.*) *ventricosus* Zone was deposited during a major transgression, and, as a result, the seaway was much wider. In the northern United States, it extended from western Wyoming to central Minnesota and, in Canada, it extended from eastern British Columbia to eastern Manitoba. The seaway was characterized by broad swatches of calcareous muds and noncalcareous muds to muddy silts (Nielsen et al., 2008: fig. 13A).

Because of the much larger size and depth of the seaway (but never exceeding the depth limits of scaphites), it may have been less susceptible to environmental perturbations affecting the habitat where the scaphites lived. According to current ecological theory, more stable environments promote the evolution of longer-lived species (e.g., Hone and Benton, 2005). In addition, the increase in the areal extent of muddy facies associated with quieter water conditions in the middle Coniacian may have favored the evolution of species with more depressed whorl shapes. Such shapes permit more efficient lower speed locomotion in lower energy, more offshore environments (Jacobs et al., 1994). In addition, such lower-energy environments make fewer demands

on the shell shapes of ammonites, so that streamlining is not as critical (Chamberlain, personal commun., 2017). Nevertheless, even in the most globose forms such as *Scaphites* (*S.*) *depressus*, the flanks are relatively flat to broadly rounded, suggesting good horizontal mobility.

Interestingly, once the maximum size and close degree of coiling were attained in *Scaphites* (*S.*) *depressus*, more derived species did not become more loosely coiled again even though the adult size decreased, as in *Clioscapites saxitsonianus*. This pattern of irreversible shape change follows the predictions of “Dollo’s Law,” as recently elaborated on by Collin and Cipriani (2003). Evidently, once a size threshold was attained, a return to more openly coiled shells was not possible. This evolutionary tendency to irreversibly reduce the degree of uncoiling in scaphites has also been noted in other lineages. In the U.S. Western Interior, Landman et al. (2010) documented that the most primitive (geologically oldest) members of *Hoploscapites* such as *H. nodosus* from the upper Campanian are more loosely coiled than the most derived (geologically youngest) members of this genus such as *H. nebrascensis* from the upper Maastriichtian. This same evolutionary tendency has also been documented during the geologic history of a single scaphite species from the middle Turonian of Japan (Tanabe, 1975).

REPOSITORIES

The repository of specimens described in the text is indicated by a prefix: **AMNH**, Division of Paleontology (Invertebrates), American Museum of Natural History, New York; **BMNH**, British Museum (Natural History), London; **NMC**, Canadian Museum of Nature, Ottawa, Ontario; **TMP**, Royal Tyrell Museum, Drumheller, Alberta, Canada; **YPM**, Yale Peabody Museum, New Haven, Connecticut; and **USNM**, U.S. National Museum, Washington, D.C. The localities of the specimens from Alberta are shown in figure 1 (modified from Plint et al., this issue).

SYSTEMATIC PALEONTOLOGY

Class Cephalopoda Cuvier, 1797

Order Ammonoidea Zittel, 1884

Suborder Ancyloceratina Wiedmann, 1966

Superfamily Scaphitoidea Gill, 1871

Family Scaphitidae Gill, 1871

Subfamily Scaphitinae Gill, 1871

Scaphites (*Scaphites*) *preventricosus*
Cobban, 1952

Figures 7–9A

1952. *Scaphites preventricosus* Cobban: 26, pl. 9, figs. 1–16.
1952. *Scaphites preventricosus* var. *sweetgrassensis* Cobban: 27, pl. 10, figs. 18–25.
- non 1952. *Scaphites preventricosus* var. *artilobus* Cobban: 27, pl. 8, figs. 1–6 (= *S.* (*S.*) *marinasensis* Cobban, 1952).
1955. *Scaphites preventricosus* Cobban. Cobban: 201, pl. 1, fig. 9; pl. 2, fig. 5.
1965. *Scaphites* (*Scaphites*) *preventricosus svarthenhukensis* Birkelund: 83, pl. 16, fig. 3; pl. 18, figs. 2, 3; pl. 19, fig. 1; text-figs. 75–77.
1968. *Scaphites* cf. *preventricosus* Cobban. Cobban: L3, pl. 1, fig. 15.
1970. *Scaphites preventricosus* Cobban. Casanova: fig. 79.
1976. *Scaphites preventricosus* Cobban. Cobban: 124, pl. 1, figs. 8, 9.
1977. *Scaphites preventricosus* Cobban. Kauffman: pl. 24, figs. 1, 2.
1983. *Scaphites preventricosus* Cobban. Cobban: 10, pl. 8, figs. 11–13.
1987. *Scaphites preventricosus* Cobban. Landman: 227.
1989. *Scaphites preventricosus* Cobban. Landman: fig. 1 (6a, b).
1991. *Scaphites* (*Scaphites*) *preventricosus* Cobban, 1952. Kennedy and Cobban: 84, text-figs. 28C, D.
1994. *Anascaphites preventricosus* (Cobban). Cooper: 176.

TABLE 3

Measurements of *Scaphites (S.) preventricosus* macroconchs.

See figure 2 for description of measurements. All measurements are in mm, except for apertural angle (AA) and septal angle (SA), which are in degrees. Rib density is reported to the nearest 0.25 ribs/cm on the adapical and adoral parts of the phragmocone, the midshaft, and the hook, depending upon the preservation of the specimen. The specimens from Highwood River are from the Cardium Formation. Height (m) is the height in the measured stratigraphic section.

Study No.	TMP No.	Locality	Height (m)	LMAX	LMAX/HP	LMAX/HS	AA	SA	UD	WP/HP	WS/HS	WH/HH	Rib density		
													Adoral	Shaft	Hook
29	2016.041.0037	Mill Ck.	90	-	-	-	-	-	-	-	-	-	-	-	-
30	2016.041.0038	Mill Ck.	115	72.0	3.18	2.02	104.0	56.5	3.4	-	1.03	1.64	6	6	6
42	2016.041.0085	Wapiabi Ck.	14.5	-	-	-	-	51.0	-	-	1.20	1.56	-	3.75	5
44	2016.041.0087	Wapiabi Ck.	51.0	-	-	-	104.0	53.0	-	1.31	1.43	-	-	-	-
50	2016.041.0135	Highwood Riv.	Cardium	68.2	2.95	2.19	-	43.0	-	1.06	-	-	5	5	-
51	2016.041.0136	Highwood Riv.	Cardium	-	-	-	-	-	-	-	-	-	-	-	-
73	2016.041.0207	Cutpick Ck.	9.0	-	-	-	-	55.0	6.3	1.49	1.30	-	-	4.5	4
74	2016.041.0208	Cutpick Ck.	9.0	-	-	-	92.0	55.0	-	-	1.37	1.66	-	4	5
151	TMP2 016. 041.0473	Oldfort Ck.	13.2	-	-	-	-	-	-	-	-	-	-	4	-
Average				70.1	3.07	2.10	100.0	52.0	4.8	1.29	1.27	1.65	5.5	4.5	5

1994. *Scaphites preventricosus* Cobban. Braunberger: 107–110, pl. 1, figs. 9–12; pl. 2, figs. 1–5; pl. 3, figs. 1–6; pl. 4, figs. 1–9; pl. 5, figs. 1–5; pl. 6, figs. 1–3.

2001. *Scaphites preventricosus* Cobban, 1951. Braunberger and Hall: 340–342, pl. 2, figs. 8–12; pl. 2, figs. 1–10.

DIAGNOSIS: Macroconchs large and stout with an oval outline in lateral view; body chamber loosely uncoiled with a reduced aperture; apertural angle approximately 100°; ornamented by fairly straight primary and secondary ribs that are uniformly spaced on the body chamber; microconchs smaller, more slender, with a more

loosely uncoiled body chamber; suture complex with asymmetrically bifid lateral lobes.

TYPE: The holotype is USNM 106675 from a bed of calcareous concretions in the Kevin Member of the Marias River Shale, 514 to 525 feet below the top, in the north bank of the Marias River, 5.5 miles south of Shelby, Toole County, Montana.

MATERIAL: The collection consists of 15 specimens, all of which are incomplete. They are divided into nine macroconchs and six microconchs.

MACROCONCH DESCRIPTION: LMAX averages 70.1 mm (table 3). Adults are robust with an oval outline in side view. The exposed phragmocone occupies approximately one whorl and terminates below the line of maximum length. The

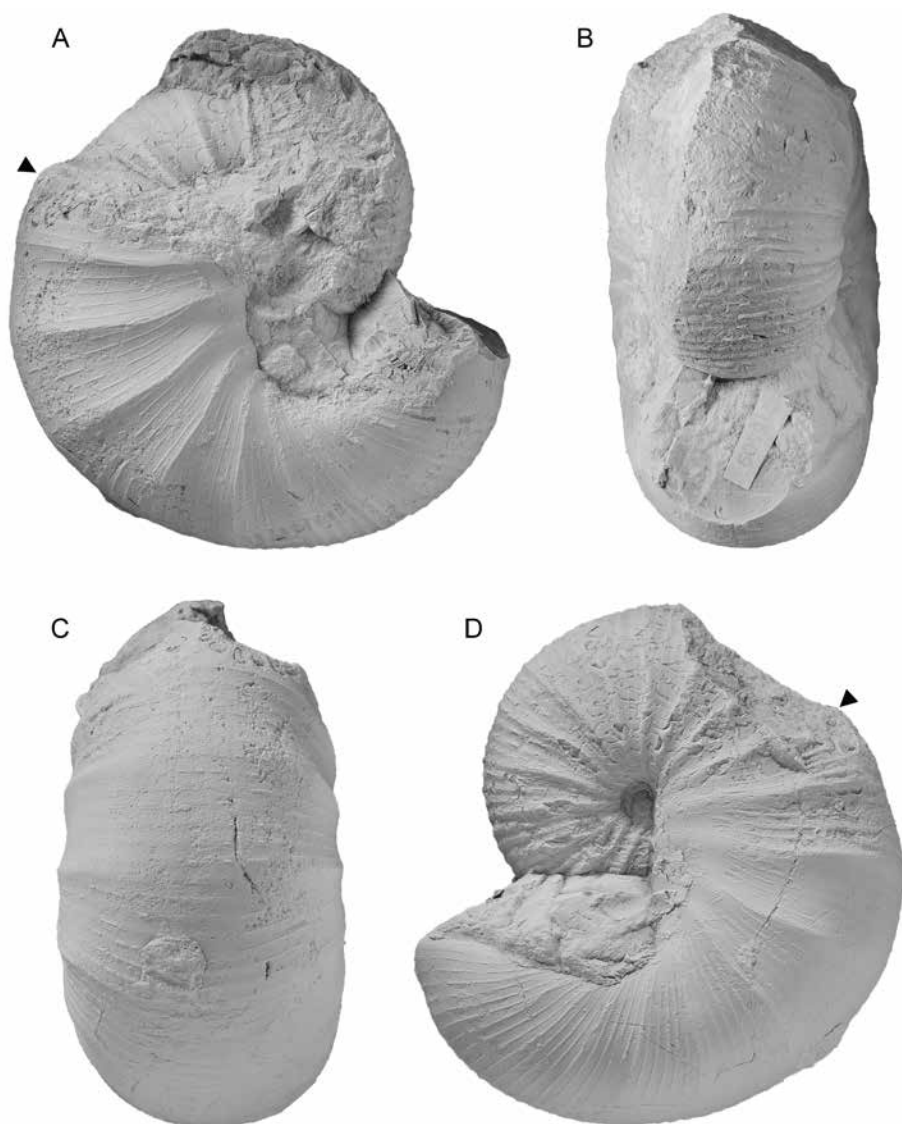


FIG. 7. *Scaphites* (*S.*) *preventricosus* Cobban, 1952, macroconch, TMP2016.041.0038, 115 m, Wapiabi Formation, Mill Creek, Alberta. **A.** Right lateral; **B.** apertural; **C.** ventral; **D.** left lateral.

septal angle averages 52° . The umbilical diameter of the phragmocone is small; it averages 4.8 mm (table 3). The body chamber consists of a shaft and recurved hook. The umbilical shoulder of the shaft is straight in side view. In TMP2016.041.0038, L_{MAX}/H_s and L_{MAX}/H_p equal 2.02 and 3.18, respectively. The body chamber is slightly uncoiled producing a small gap between the phragmocone and hook, with a

constricted aperture. The apertural angle equals 104° in TMP2016.041.0038.

The whorl section of the phragmocone along the line of maximum length, as shown in TMP2016.041.0207, is depressed and subovoid with maximum whorl width at one-third whorl height. The umbilical wall is steep and subvertical, the flanks are sharply rounded, and the venter is broadly rounded. W_p/H_p equals 1.49 in

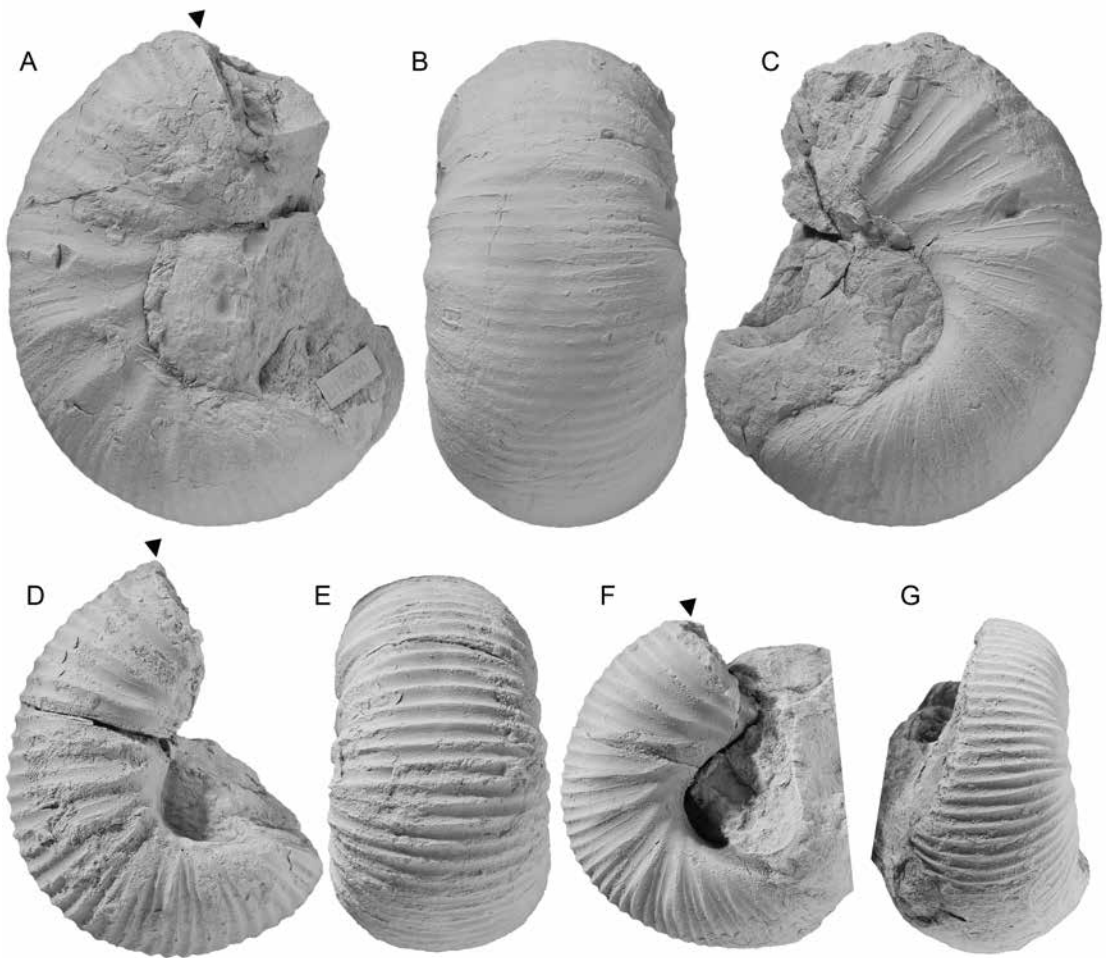


FIG. 8. *Scaphites* (*S.*) *preventricosus* Cobban, 1952, microconchs. A–C. TMP2016.041.0036, 139 m, Wapiabi Formation, Mill Creek, Alberta. A. Right lateral; B. ventral; C. left lateral. D, E. TMP2016.041.0034, 141 m, Wapiabi Formation, Mill Creek, Alberta. D. Right lateral; E. ventral. F, G. TMP2016.041.0039, 70 m, Wapiabi Formation, Mill Creek, Alberta. F. Right lateral; G. ventral.

this specimen. As the shell passes from the phragmocone into the body chamber in this specimen, both the whorl width and height increase slightly, and the whorl section at midshaft is nearly the same as that along the line of maximum length. It is depressed and subvoid with maximum whorl width at one-quarter whorl height. The umbilical wall is steep and subvertical, the flanks are sharply rounded, and the venter is broadly rounded. W_S/H_S equals 1.30 in TMP2016.041.0207. In contrast, in TMP2016.041.0038, the whorl section at mid-

shaft is nearly equidimensional with broadly rounded flanks; W_S/H_S equals 1.03. Adoral of the midshaft, as shown in this specimen, both the whorl width and especially the whorl height abruptly decrease. As a result, the whorl section at the point of recurvature is more depressed than that at midshaft. The umbilical wall is flat and slopes outward, the flanks are sharply rounded, and the venter is broadly rounded. W_H/H_H equals 1.64 in TMP2016.041.0038. The shell culminates in a constricted aperture with a dorsal lappet.

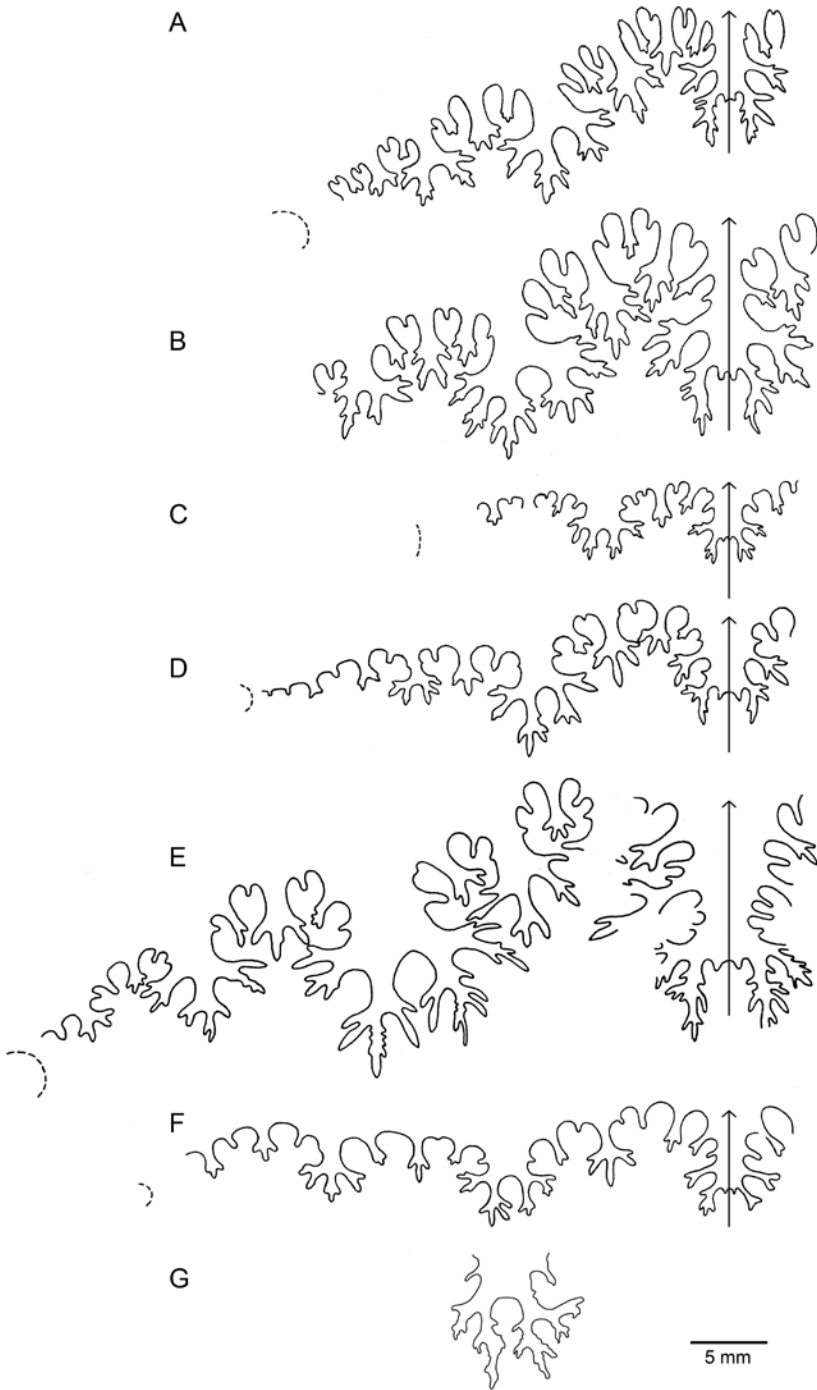


TABLE 4

Measurements of *Scaphites (S.) preventricosus* microconchs.

See figure 2 for description of measurements. All measurements are in mm. Rib density is reported to the nearest 0.25 ribs/cm on the adapical and adoral parts of the phragmocone, the midshaft, and the hook, depending upon the preservation of the specimen. * = measurements were taken at the base of the body chamber because the phragmocone was missing. The specimens from Highwood River are from the Cardium Formation. Height (m) is the height in the measured stratigraphic section.

Study No.	TMP No.	Locality	Height (m)	LMAX	LMAX/HP	UD	WP/HP*	WS/HS	WH/HH	Rib density		
										Adoral	Shaft	Hook
26	2016.041.0034	Mill Ck.	141	–	–	–	1.18	1.28	1.68	–	4.5	4
28	2016.041.0036	Mill Ck.	139	–	–	–	1.09	1.36	1.73	–	5	5
31	2016.041.0039	Mill Ck.	70	–	–	–	–	–	–	–	5.5	6
52	2016.041.0137	Highwood Riv.	Cardium	–	–	–	–	–	1.56	–	–	5.5
53	2016.041.0138	Highwood Riv.	Cardium	–	–	–	–	–	–	–	4	45
127	2016.041.0365	Bighorn Dam	8.5	–	–	–	1.24	1.38	1.49	–	6	5
Average				–	–	–	1.17	1.34	1.62	–	5	5.25

The ornamentation is well preserved in TMP2016.041.0038. On the phragmocone, primary ribs emerge at the umbilical seam and are slightly rursiradiate on the umbilical wall and shoulder. They develop into broad, elongate swellings that swing gently forward and then backward again before subdividing into three thin ribs, with another two thin ribs in between. They are sharp and uniformly strong on the venter, which they cross with a slight adoral projection. The ribs are equally and closely spaced, with a rib density of 6 ribs/cm on the adoral part of the phragmocone.

The same pattern of ribbing persists onto the body chamber. Primary ribs develop into broad elongate swellings on the flanks that swing gently

forward and then backward again, before subdividing into three thin secondary ribs, with as many as four thin ribs in between. Ribs are uniformly strong and closely spaced on the venter of the shaft, with a rib density of 6 ribs/cm. They are equally closely spaced on the venter of the hook, but exhibit a stronger adoral projection.

The suture is complex with asymmetrically bifid lateral lobes (fig. 9A).

MICROCONCH DESCRIPTION: Microconchs are elongate in lateral view. Because all of our specimens are incomplete, it is difficult to estimate LMAX. However, the body chambers of all of the microconchs are smaller than those of the macroconchs. The body chambers are also more loosely uncoiled leaving a larger gap between the

FIG. 9. Sutures (except for G, reproduced from Cobban, 1952). **A.** *Scaphites (S.) preventricosus* Cobban, 1952, sixth from last suture (flipped), USNM 106675, Marias River Shale, Toole County, Montana. **B.** *Scaphites (S.) ventricosus* Meek and Hayden, 1862, USNM 106698, Marias River Shale, Toole County, Montana. **C.** *Scaphites (S.) ventricosus* Meek and Hayden, 1862 (formerly *Scaphites (S.) tetonensis* Cobban, 1952), last suture, USNM 106707, Cody Shale, Teton County, Wyoming. **D.** *Scaphites (S.) depressus* Reeside, 1927, last suture, USNM 106695, Cody Shale, Park County, Wyoming. **E.** *Scaphites (S.) depressus* Reeside, 1927, second from last suture, USNM 106693, Cody Shale, Park County, Wyoming. **F.** *Clioscaphtes saxitonianus* (McLearn, 1929), last suture, USNM 106739a, Marias River Shale, Toole County, Montana. **G.** *Clioscaphtes saxitonianus* (McLearn, 1929), first lateral saddle, third from last suture, TMP2016.041.0229, Wapiabi Formation, West Thistle Creek, Alberta.

phragmocone and hook. In addition, the umbilical shoulder of the shaft is slightly more concave in microconchs than in macroconchs.

The whorl section at the base of the body chamber (we measured the whorl section at the base of the body chamber because the phragmocone was missing) is depressed and subvoid. W_p/H_p averages 1.17 and ranges from 1.09 to 1.24 (table 4). The umbilical wall is steep and nearly vertical, the flanks are broadly to sharply rounded, and the venter is broadly rounded. Whorl width increases gradually from the phragmocone into the body chamber and reaches its maximum value at the point of recurvature. Whorl height, on the other hand, decreases such that, together, the whorl section at midshaft is much more depressed than that at the base of the body chamber. The umbilical wall slopes outward and the flanks are broadly rounded. W_s/H_s averages 1.34 and ranges from 1.28 to 1.38. The whorl section at the point of recurvature is even more depressed than that at midshaft. W_H/H_H averages 1.62 and ranges from 1.49 to 1.73.

Primary ribs are prorsiradiate on the umbilical wall and shoulder of the shaft. They develop into broad straight or slightly concave swellings on the flanks, which reach their maximum strength at two-thirds whorl height. In TMP2016.041.0034, which is a coarsely ornamented specimen, each primary rib subdivides into two thin ribs, with another one or two thin ribs intercalating between them. In contrast, in TMP2016.041.0036, which is a more finely ornamented specimen, each primary rib subdivides into three thin ribs, with as many as four thin ribs intercalating between them. Ribs are sharp and uniformly strong on the venter of the shaft, which they cross with a slight adoral projection. The density of ribs on the venter of the shaft ranges from 4.5 to 6 ribs/cm among the specimens in our sample. Ribs are equally closely spaced on the venter of the hook, which they cross with a stronger adoral projection. The density of ribs on the venter of the hook ranges from 5 to 6 ribs/cm.

The suture of the microconchs is the same as that of the macroconchs.

REMARKS: Dimorphism is present in *Scaphites* (*S.*) *preventricosus*. Cobban (1952) initially segregated out microconchs as the variety *sweetgrassensis*. Macroconchs are larger and more robust, with a more closely coiled body chamber. In the present collection, all the microconchs are incomplete, but even so, the body chambers of the microconchs are smaller than those of the macroconchs.

Scaphites (*S.*) *preventricosus* can be distinguished from the overlying species *S.* (*S.*) *ventricosus* by its smaller size, more closely spaced ribbing, and more loosely uncoiled body chamber. The degree of uncoiling of the body chamber in macroconchs is expressed by the apertural angle. Based on our data, the apertural angle ranges from 92.0° to 104° in *S.* (*S.*) *preventricosus* whereas it ranges from 72° to 89° in *S.* (*S.*) *ventricosus*. The degree of uncoiling of the body chamber in macroconchs is also expressed by the ratio L_{MAX}/H_p . Based on our data, this value averages 3.07 in *S.* (*S.*) *preventricosus* whereas it averages 2.55 in *S.* (*S.*) *ventricosus*.

OCCURRENCE: In the Upper Cretaceous of the Western Interior of North America, this species demarcates the lower Coniacian *Scaphites* (*S.*) *preventricosus* Zone. In the study area, the lowest occurrence of this species is just above erosional surface E5.5, which marks the beginning of a major transgression just above the base of the lower Coniacian (Walaszczyk et al., 2014). It is present in the Cardium Formation at Highwood River (TMP2016.041.0136–.0138) and in the Wapiabi Formation at Mill Creek (TMP2016.041.0034, .0036–.0039), Cutpick Creek (TMP 2016.041.0207 and .0208), Oldfort Creek (TMP2016.041.0473), Wapiabi Creek (TMP2016.041.0085 and .0087), and Bighorn Dam (TMP2016.041.0365), Alberta. Elsewhere, this species is abundant in the Kevin Member of the Marias River Shale in north-central Montana and the uppermost part of the Frontier Formation in Wyoming. Outside North America, it has been reported from Umivik, Svartenhuk, Greenland (Birkelund, 1965).

Scaphites (Scaphites) ventricosus

Meek and Hayden, 1862

Figures 9B, C, 10–16

1862. *Scaphites ventricosus* Meek and Hayden, 1862: 22.
1876. *Scaphites (Scaphites) ventricosus* Meek and Hayden. Meek: 425, pl. 6, figs. 7, 8.
1894. *Scaphites ventricosus* Meek and Hayden. Stanton: 44, figs. 8, 9; pl. 43, fig. 1; non pl. 44, fig. 10.
1898. *Scaphites ventricosus* Meek and Hayden. Logan: 476, pl. 104, figs. 8, 9; pl. 105, fig. 1; non pl. 104, fig. 10.
1900. *Scaphites ventricosus* Meek and Hayden. Herrick and Johnson: pl. 45, figs. 8–10; pl. 46, fig. 1.
- 1927a. *Scaphites ventricosus* Meek and Hayden. Reeside: 6, pl. 3, figs. 11–18; pl. 4, figs. 1–4.
- non 1927a. *Scaphites ventricosus* var. *depressus*. Reeside: 7, pl. 5, figs. 6–10 [= *S. (S.) depressus*].
- non 1927a. *Scaphites ventricosus* var. *interjectus*. Reeside: 7, pl. 5, figs. 1–5 [= *Clioscapites interjectus*].
- non 1927a. *Scaphites ventricosus* var. *oregonensis*. Reeside: 7, pl. 6, figs. 11–15 [= *S. (S.) depressus*].
- non 1927a. *Scaphites ventricosus* var. *stantoni*. Reeside: 7, pl. 3, figs. 19, 20; pl. 4, figs. 5–10 [= *S. (S.) depressus*].
- 1927b. *Scaphites ventricosus* Meek and Hayden. Reeside: 35, pl. 10, figs. 1, 2.
- non 1929. *Scaphites ventricosus* var. *saxitonianus*. McLearn: 77, pl. 18, figs. 1–3; pl. 19, figs. 1, 2 [= *Clioscapites saxitonianus*].
1942. *Scaphites* cf. *ventricosus* Meek and Hayden. Rosenkrantz: 38, pl. 1.
1952. *Scaphites ventricosus* Meek and Hayden. Cobban: 31, pl. 12, figs. 1–10; pl. 13, figs. 11–13.
1952. *Scaphites tetonensis* Cobban, 1952: 31, pl. 14, figs. 1–10.
1952. *Scaphites ventricosus* Meek and Hayden. Basse: 607, fig. 14.
1955. *Scaphites ventricosus* Meek and Hayden. Cobban: 201, pl. 1, fig. 6.
1960. *Scaphites ventricosus* Meek and Hayden. Easton: fig. 11.28–3a, b.
1965. *Scaphites (Scaphites) ventricosus* Meek and Hayden. Birkelund: 87, pl. 19, figs. 2, 3; text-fig. 78.
1976. *Scaphites ventricosus* Meek and Hayden. Kennedy and Cobban: text-fig. 17 (part).
1977. *Scaphites ventricosus* Meek and Hayden. Kauffman: pl. 24, figs. 3, 4.
1989. *Scaphites ventricosus* Meek and Hayden. Landman: fig. 1 (7a, b).
1991. *Scaphites (Scaphites) ventricosus* Meek and Hayden, 1862. Kennedy and Cobban: 85, text-fig. 28A, B.
1991. *Scaphites (Scaphites) tetonensis* Cobban, 1952. Kennedy and Cobban: 87, text-fig. 30A–C.
1994. *Scaphites ventricosus* Meek and Hayden. Braunberger: 115–117, pl. 13, figs. 1–4.
1994. *Anascaphites ventricosus* (Meek and Hayden). Cooper: 176, fig. 1A, B.

DIAGNOSIS: Macroconchs large and stout with slightly uncoiled body chamber producing a small gap between the phragmocone and hook; cross section of shaft depressed and subovoid; apertural angle averaging 82.5°; ribbing coarse and widely spaced; microconchs smaller with more loosely uncoiled body chamber; suture complex with asymmetrically bifid lateral lobes.

TYPES: The holotype is USNM 1903 from the upper part of the Colorado Shale, about 20 miles northeast of Fort Benton, Montana.

MATERIAL: A total of 24 specimens, all of which are incomplete. They consist mostly of the body chamber without the phragmocone. All of them are adult, comprising 16 macroconchs and 8 microconchs. The collection also contains fragments of body chambers and phragmocones, but they are difficult to identify to species level.

MACROCONCH DESCRIPTION: In the measured sample, LMAX averages 85.4 mm and ranges from 70.4 to 101.1 mm (table 5). The ratio of the size of the largest specimen to that of the smallest

TABLE 5

Measurements of *Scaphites (S.) ventricosus macroconchs*.

See figure 2 for description of measurements. All measurements are in mm, except for apertural angle (AA) and septal angle (SA), which are in degrees. Rib density is reported to the nearest 0.25 ribs/cm on the adapical and adoral parts of the phragmocone, the midshaft, and the hook, depending upon the preservation of the specimen. Height (m) is the height in the measured stratigraphic section.

Study No.	TMP No.	Locality	Height (m)	LMAX	LMAX/ HP	LMAX/ HS	AA	SA	UD	WP/ HP	WS/ HS	WH/ HH	Rib density		
													Adoral	Shaft	Hook
19	2016.041.0021	Ram Riv.	108.7	93.4	2.43	2.2	72	-17	-	1.18	1.37	1.74	2	3.5	4
27	2016.041.0035	Mill Ck.	191.0	86.9	2.45	2.01	80	20.5	4.2	-	-	-	4.25	3.25	4
46	2016.041.0106	Black-stone Riv.	37.4	101.1	2.79	2.23	83	34.5	4.4	-	-	-	4	3.5	4
63	2016.041.0164	Chungo Ck	48.9	93.6	2.53	2.08	88	-2	-	1.40	1.29	1.8	3	2.75	3.25
64	2016.041.0165	Chungo Ck.	48.9	-	-	-	-	-	-	-	-	1.76	3	3.25	4
65	2016.041.0166	Chungo Ck.	48.9	76.2	2.52	-	83	8	-	-	-	1.61	3.75	3.75	4
66	2016.041.0167	Chungo Ck.	51.3	89.7	2.46	1.97	87	12	-	1.30	1.11	1.63	3.25	3.25	4.25
67	2016.041.0168	Chungo Ck	51.3	90.0	-	2.34	-	20	-	-	1.36	1.68	-	3	-
108	2016.041.0296	Sheep Riv.	78.0	-	-	-	-	-	-	-	-	-	3.5	3.25	-
128	2016.041.0366	Bighorn Dam	42.6	70.4	-	2.21	-	-11.5	-	-	1.35	-	-	3.25	4
130	2016.041.0368	Bighorn Dam	60.0	86.7	-	-	78	-	-	-	-	-	-	-	4.5
132	2016.041.0370	Bighorn Dam	69.5	78.5	2.54	2.05	-	-	-	1.46	1.25	1.64	3	3	4.25
133	2016.041.0371	Bighorn Dam	69.5	77.4	-	2.08	-	-	-	-	1.24	1.63	3.5	3	4.75
135	2016.041.0373	Bighorn Dam	87.6	68.8	2.95	2.23	-	-	-	-	-	1.47	-	4	5
136	2016.041.0374	Bighorn Dam	87.6	91.4	-	-	-	-	-	-	-	-	-	3.5	-
141	2016.041.0379	Bighorn Dam	107.5	91.0	2.26	2.32	89	-18	-	1.36	1.51	1.45	3	2.75	4
Average				85.4	2.55	2.16	82.5	12	4.3	1.34	1.31	1.64	3.25	3.25	4

TABLE 6

Measurements of *Scaphites* (*S.*) *ventricosus* microconchs.

See figure 2 for description of measurements. All measurements are in mm. Rib density is reported to the nearest 0.25 ribs/cm on the adapical and adoral parts of the phragmocone, the midshaft, and the hook, depending upon the preservation of the specimen. Height (m) is the height in the measured stratigraphic section.

Study No.	TMP No.	Locality	Height (m)	LMAX	LMAX/HP	UD	WP/HP	WS/HS	WH/HH	Rib density		
										Adoral	Shaft	Hook
34	2016.041.0066	E. Thistle Ck.	18.2	61.2	-	-	-	-	-	-	4	4
35	2016.041.0067	E. Thistle Ck.	18.2	-	-	-	1.38	-	-	-	5	-
57	2016.041.0155	James Riv.	52.1	-	-	-	-	-	-	-	5	6
60	2016.041.0161	Chungo Ck.	41.4	41.8	-	-	-	-	-	5	4	5
62	2016.041.0163	Chungo Ck.	41.4	50.7	-	-	-	-	-	-	4	3.75
120	2016.041.0349	Bighorn Riv.	99.4	-	-	-	1.49	-	-	-	-	9
129	2016.041.0367	Bighorn Dam	50-60	67.1	-	-	-	-	-	4.25	3.5	5
134	2016.041.0372	Bighorn Dam	84.2	-	-	-	-	-	-	-	4.5	7
Average				55.2	-	-	1.44	-	-	4.25	4	5.5

is 1.44. Adults are robust with an oval outline in side view. The exposed phragmocone occupies approximately one whorl and terminates slightly below the line of maximum length. The septal angle averages 12.0° . The umbilical diameter of the phragmocone is small and averages 4.3 mm (table 5). The body chamber consists of a shaft and recurved hook. The umbilical shoulder of the shaft is straight or slightly concave in side view. $LMAX/H_S$ averages 2.16 and ranges from 1.97 to 2.34. The body chamber is slightly uncoiled. $LMAX/H_P$ averages 2.55 and ranges from 2.26 to 2.95. As a result, a small gap appears between the phragmocone and hook, and is usually filled with sediment. The apertural angle averages 82.5° and ranges from 72.0° to 89.0° .

The whorl section of the phragmocone along the line of maximum length is depressed and subovoid with maximum whorl width at one-third whorl height. The umbilical wall is steep and subvertical, the flanks are sharply rounded, and the venter is broadly rounded. W_P/H_P aver-

ages 1.34 and ranges from 1.18 to 1.46. As the shell passes from the phragmocone into the body chamber, both the whorl width and height increase slightly, and the shape of the whorl section at midshaft is nearly the same as that along the line of maximum length. It is depressed and subovoid with maximum whorl width at one-quarter whorl height. The umbilical wall is steep and subvertical, the flanks are sharply rounded, and the venter is broadly rounded. W_S/H_S averages 1.31 and ranges from 1.11 to 1.51. Adoral of the midshaft, both the whorl width and especially whorl height abruptly decrease. As a result, the whorl section at the point of recurvature is more depressed than that at midshaft. The umbilical wall is flat and slopes outward, the flanks are sharply rounded, and the venter is broadly rounded. W_H/H_H averages 1.64 and ranges from 1.45 to 1.80. The shell culminates in a constricted aperture with a dorsal lappet.

Because none of our specimens preserves the adapical part of the phragmocone, our observa-

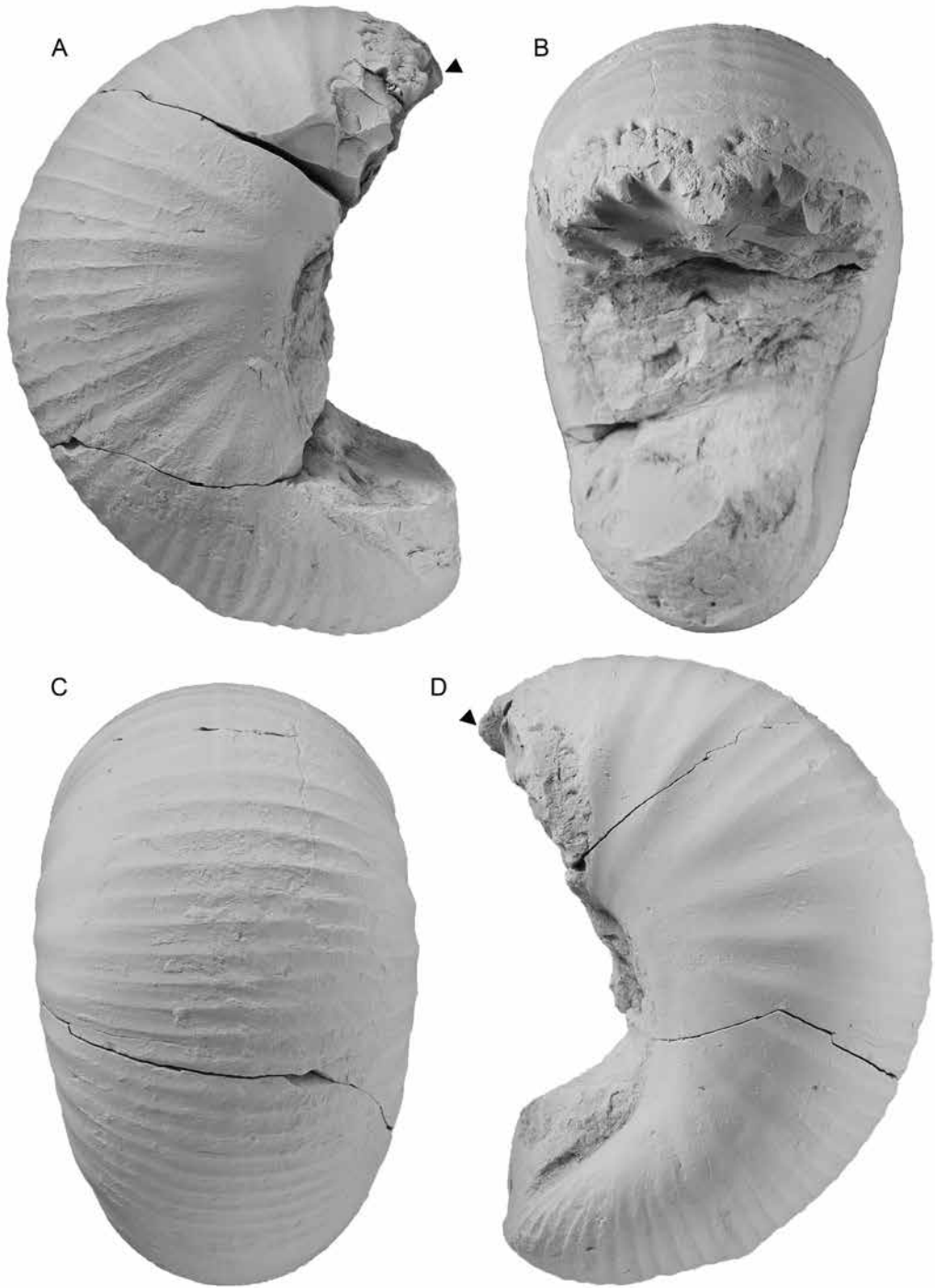


FIG. 10. *Scaphites* (*S.*) *ventricosus* Meek and Hayden, 1862, macroconch, TMP2016.041.0021, 108.7 m, Wapiabi Formation, Ram River, Alberta. **A.** Right lateral; **B.** apertural; **C.** ventral; **D.** left lateral.

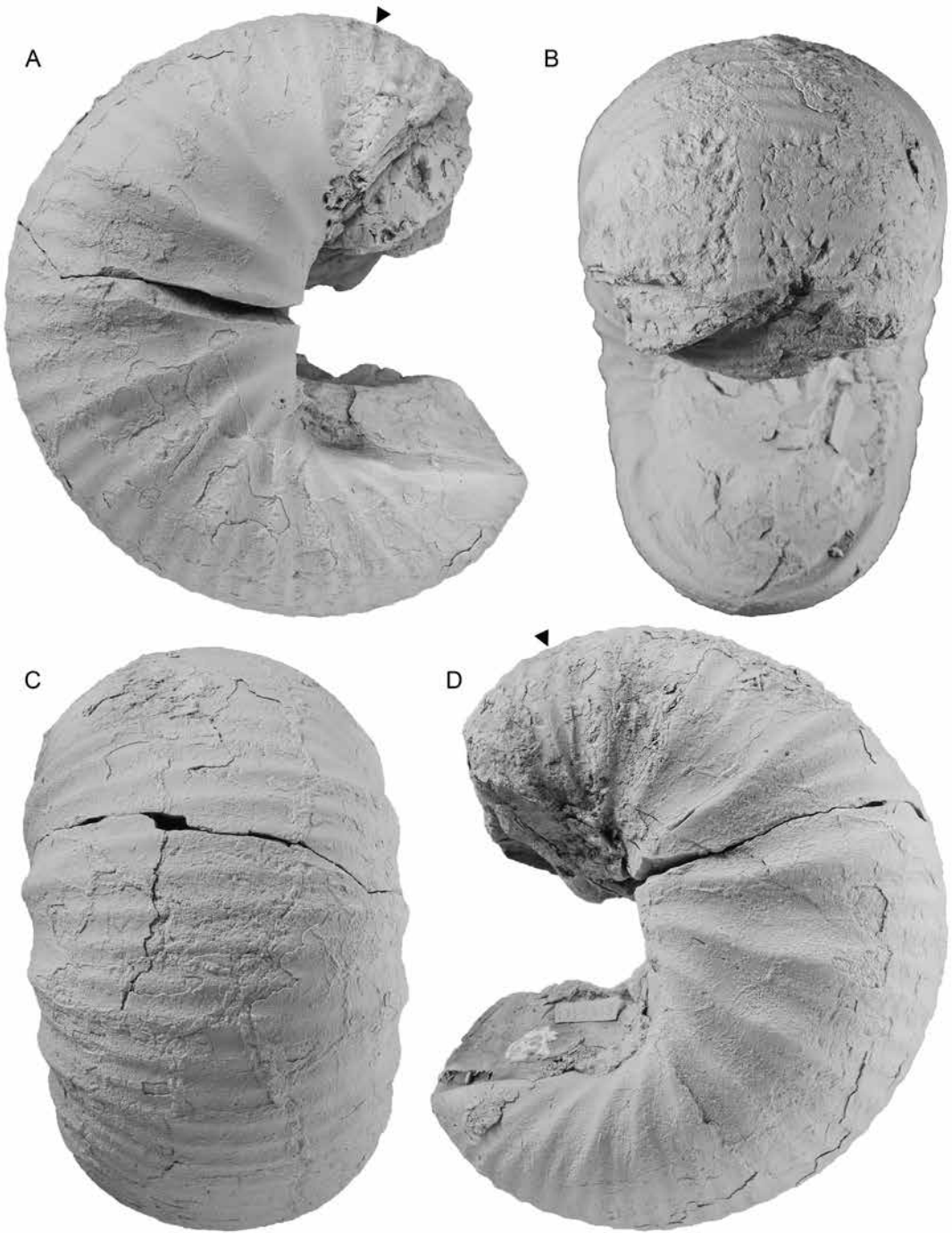


FIG. 11. *Scaphites* (*S.*) *ventricosus* Meek and Hayden, 1862, macroconch, TMP2016.041.0164, 48.9 m, Wapiabi Formation, Chungo Creek, Alberta. **A.** Right lateral; **B.** apertural; **C.** ventral; **D.** left lateral.

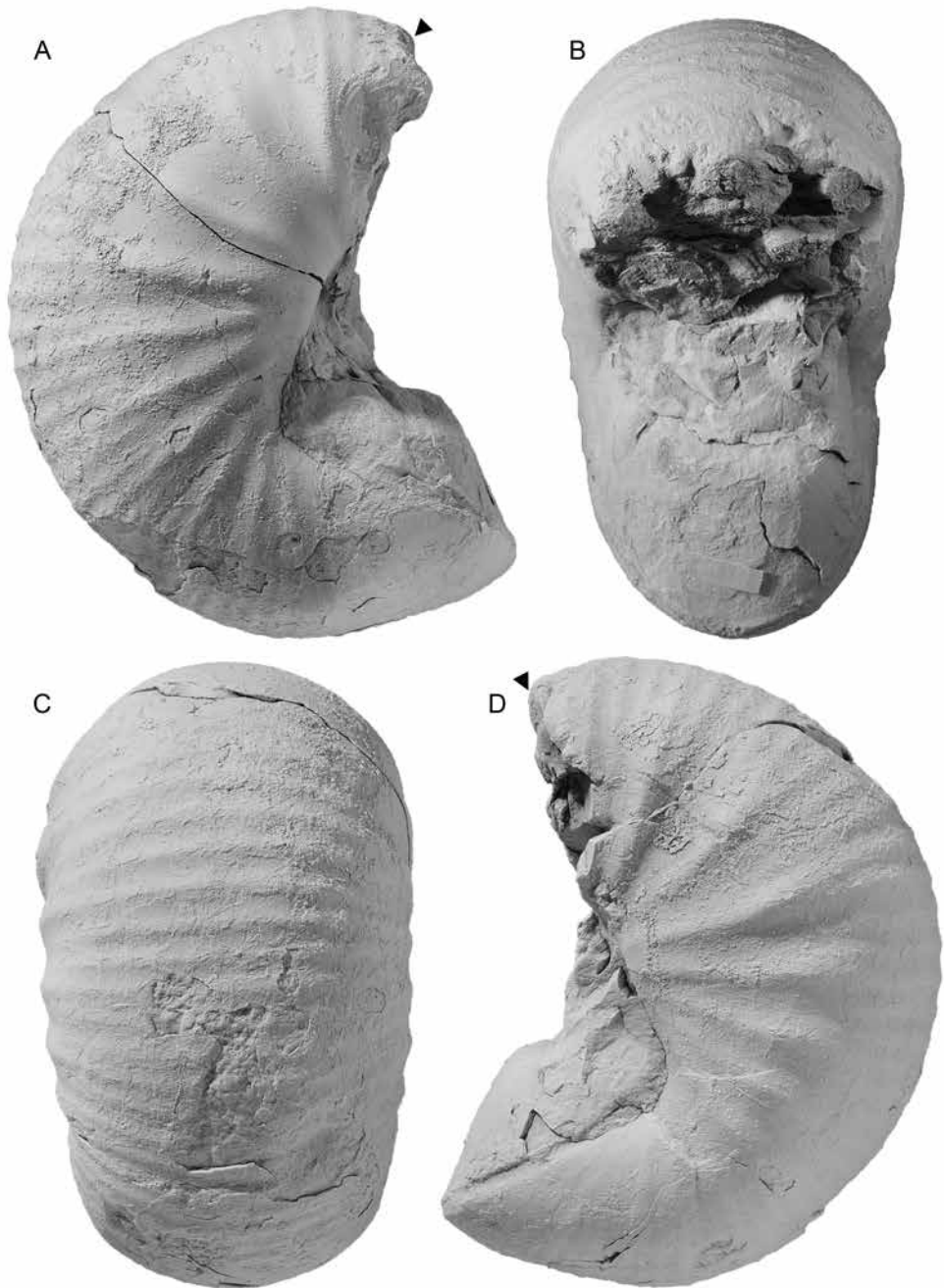


FIG. 12. *Scaphites (S.) ventricosus* Meek and Hayden, 1862, macroconch, TMP2016.041.0167, 51.3 m, Wapiabi Formation, Chungo Creek, Alberta. A. Right lateral; B. apertural; C. ventral; D. left lateral.

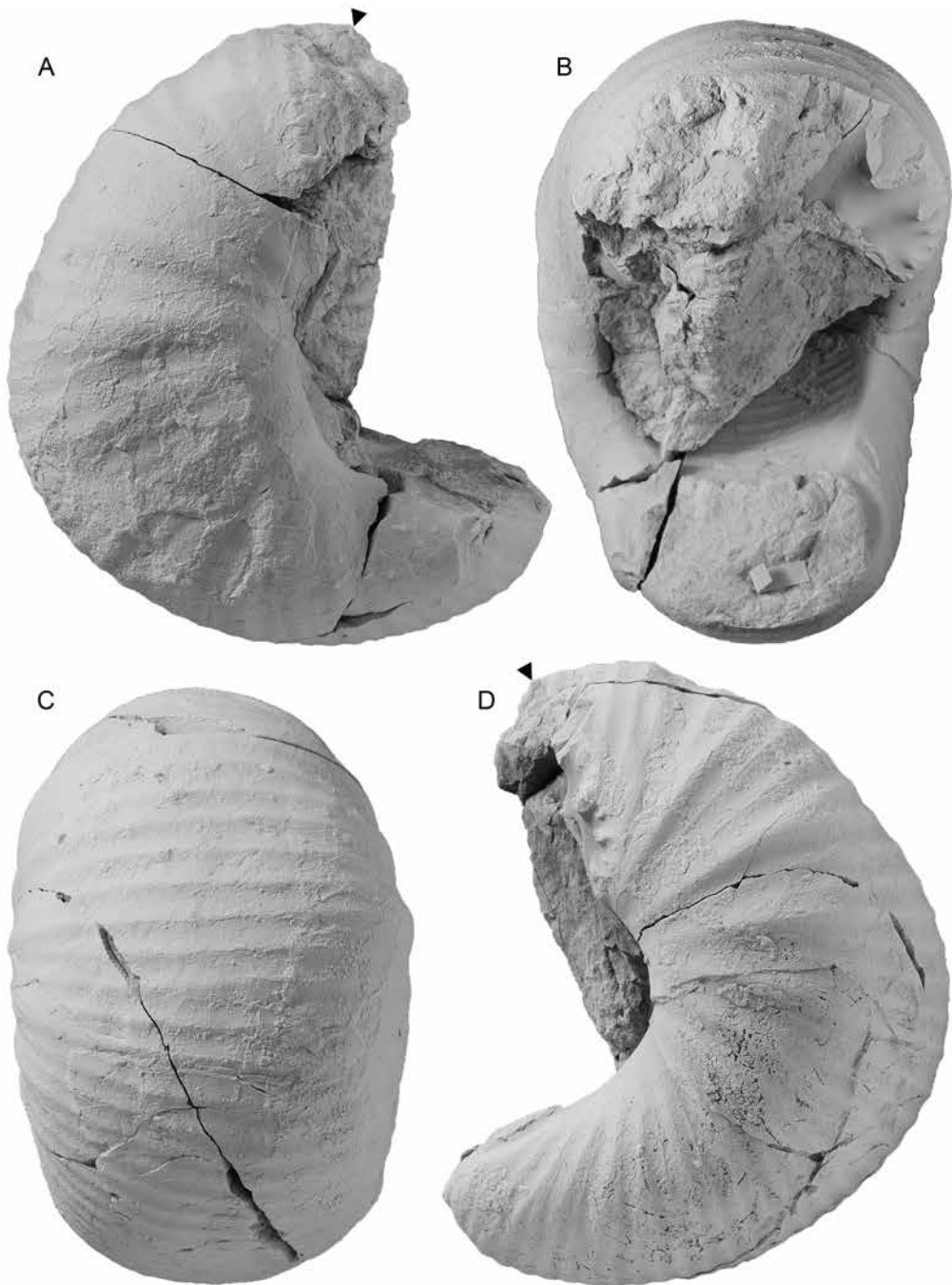


FIG. 13. *Scaphites* (*S.*) *ventricosus* Meek and Hayden, 1862, macroconch, TMP2016.041.0379, 107.5 m, Wapiabi Formation, Bighorn Dam, Alberta. **A.** Right lateral; **B.** apertural; **C.** ventral; **D.** left lateral.

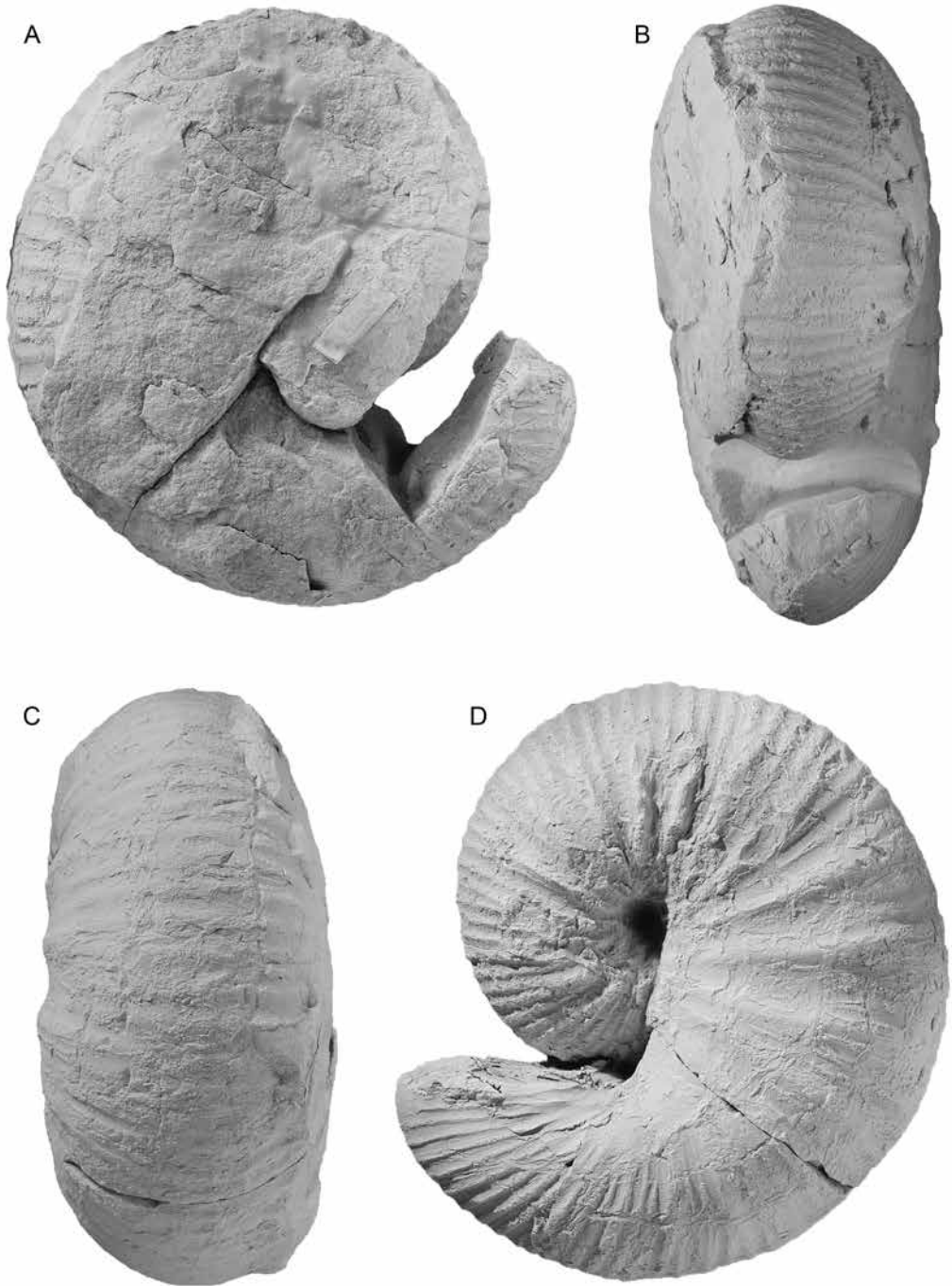


FIG. 14. *Scaphites* (*S.*) *ventricosus* Meek and Hayden, 1862, macroconch, TMP2016.041.0035, 191.0 m, Wapiabi Formation, Mill Creek, Alberta. **A.** Right lateral; **B.** apertural; **C.** ventral; **D.** left lateral.

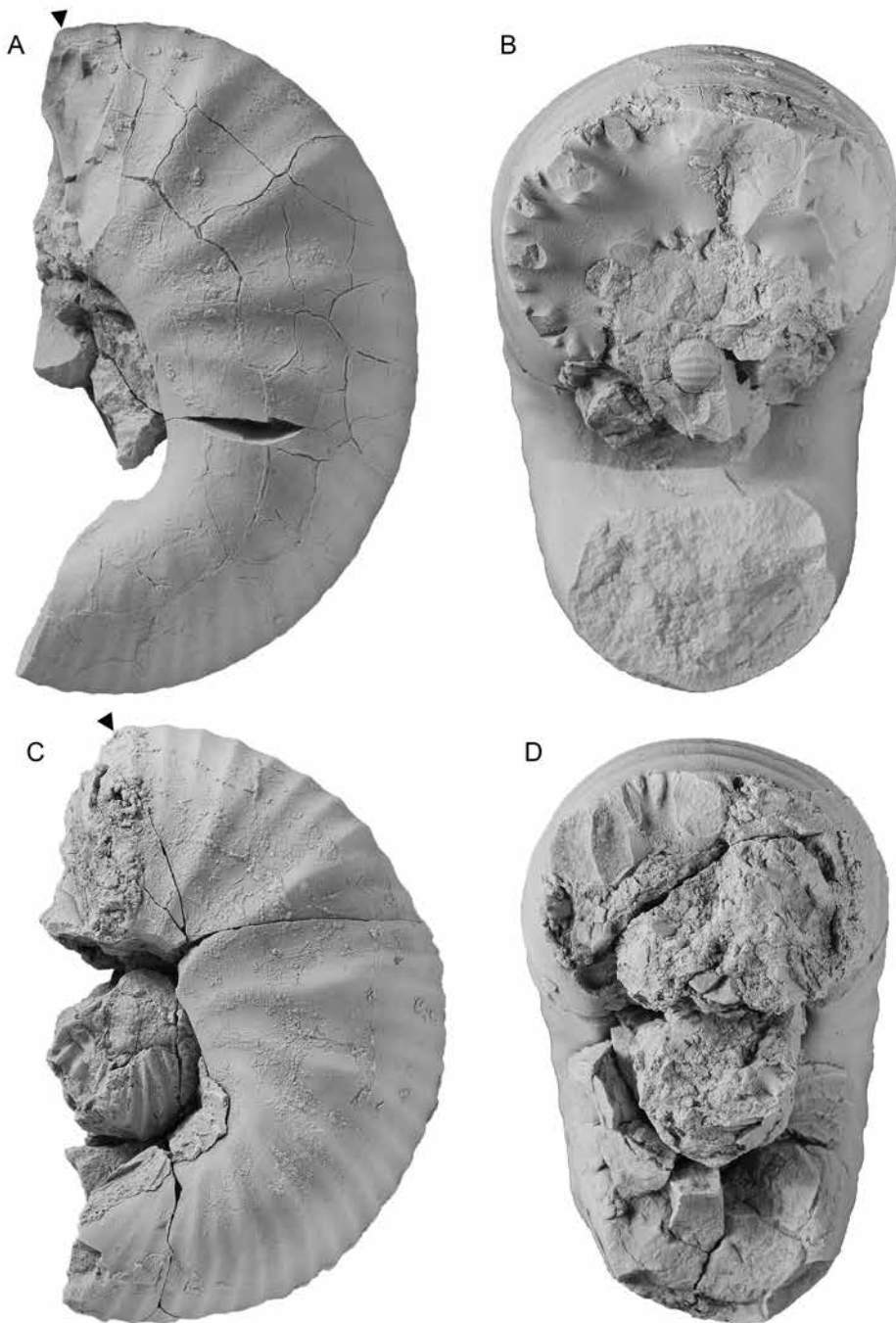
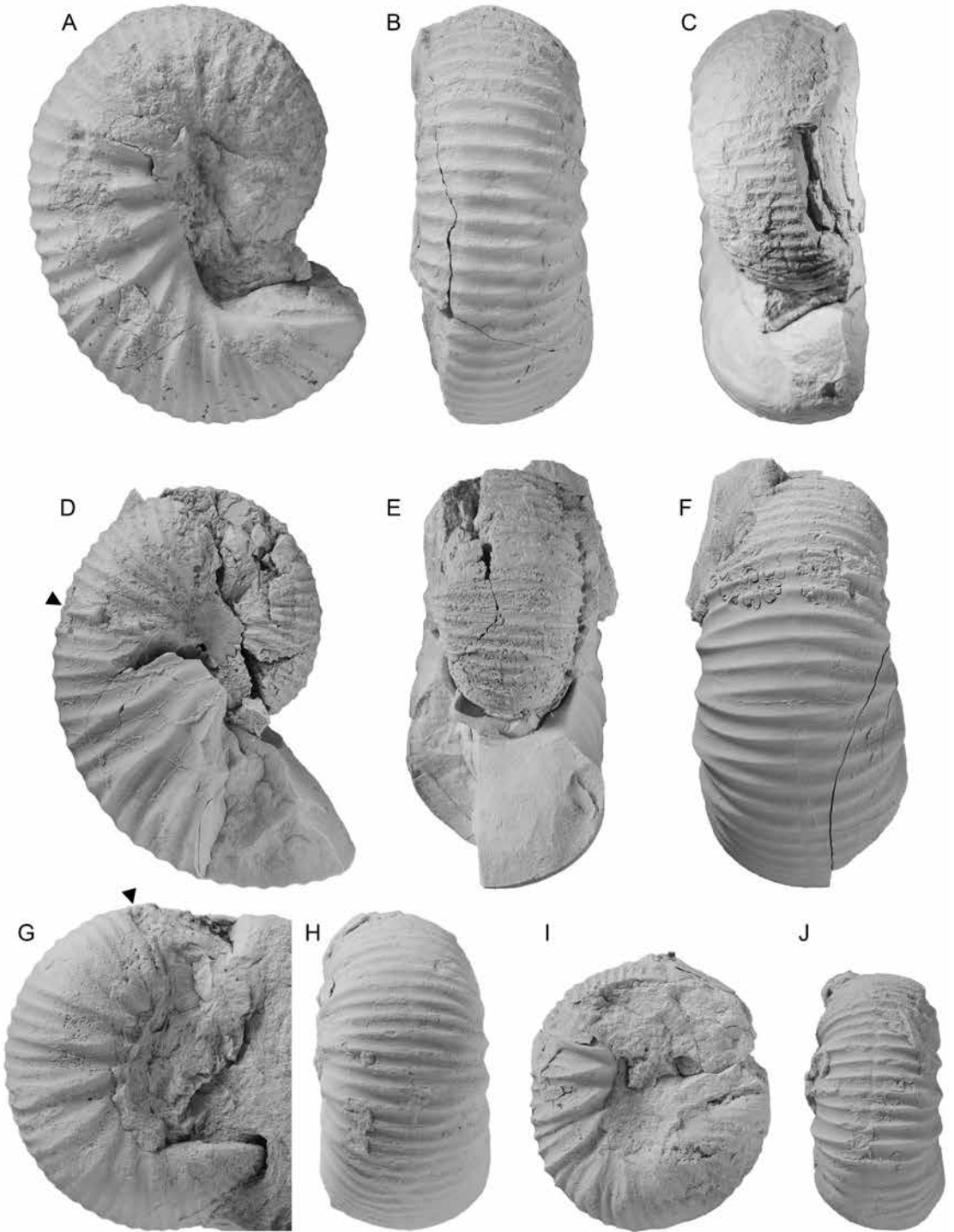


FIG. 15. *Scaphites* (*S.*) *ventricosus* Meek and Hayden, 1862, macroconchs, Montana. **A, B.** AMNH 108451, Kevin Member, Marias River Shale, Toole County, Montana. **A.** Left lateral; **B.** apertural. **C, D.** AMNH 91921, Kevin Member, Marias River Shale, Toole County, Montana. **C.** Left lateral; **D.** apertural.



tions are restricted to the adoral part. Primary ribs emerge at the umbilical seam and are straight and rectiradiate on the umbilical wall and shoulder. They develop into broad elongate swellings that reach their maximum strength at one-half whorl height, approximately coinciding with the ventrolateral shoulder. They each subdivide into two thin ribs, with another one or two thin ribs intercalated between them. Ribs are sharp and uniformly strong on the venter, which they cross with a slight adapical or adoral projection. They are equally and widely spaced. Rib density ranges from 2 to 4.25 ribs/cm among the specimens in our sample.

The same pattern of ribbing persists onto the body chamber. Primary ribs are rectiradiate on the umbilical wall and shoulder. They develop into broad elongate swellings that reach their maximum strength at one-half whorl height. They are prominent, rectiradiate, and equally spaced on the shaft, becoming weaker, prorsiradiate, and closely spaced on the hook. Each rib subdivides into two thin secondary ribs, with one or two thin ribs intercalating between them. Ribs are uniformly strong and widely spaced on the venter of the shaft, which they cross with a slight adoral projection. The density of ribs on the shaft ranges from 2.75 to 4 ribs/cm among the specimens in our sample. Ribs are more closely spaced on the venter of the hook, which they cross with a strong adoral projection. For example, in TMP2016.041.0379, the rib density is 2.75 ribs/cm at midshaft versus 4 ribs/cm on the hook.

A suture is not well enough preserved in any of the specimens in our study, but according to Cobban (1952), it is complex with asymmetrically bifid lateral lobes (fig. 9B, C).

MICROCONCH DESCRIPTION: Microconchs are elongate in lateral view. The most notable features of the microconchs relative to the

macroconchs are their smaller size and more loosely uncoiled body chamber, leaving a larger gap between the phragmocone and hook. In addition, the umbilical shoulder of the shaft is concave in microconchs whereas it is straight in macroconchs.

LMAX averages 55.2 mm and ranges from 41.8 to 67.1 mm (table 6). The whorl section of the phragmocone along the line of maximum length is depressed and subovoid. W_p/H_p averages 1.44 and ranges from 1.38 to 1.49. The umbilical wall is steep and nearly vertical, the flanks are sharply rounded, and the venter is broadly rounded. Whorl width increases gradually from the phragmocone into the body chamber and reaches its maximum value at midshaft. Whorl height also increases gradually from the phragmocone into the body chamber and attains its maximum value at the point of recurvature. The whorl section at midshaft is nearly the same as that along the line of maximum length. It is depressed and subovoid with maximum whorl width at one-half whorl height. The umbilical wall is steep and subvertical, the flanks are sharply rounded, and the venter is broadly rounded. The whorl section at the point of recurvature is more depressed than that at midshaft. The umbilical wall is flat and slopes outward, the flanks are sharply rounded, and the venter is broadly rounded.

At the base of the body chamber, primary ribs emerge at the umbilical seam and are rectiradiate on the umbilical wall and shoulder. They develop into broad, straight or slightly concave swellings on the flanks, which reach their maximum strength at one-half whorl height. They each subdivide into two thin ribs, with another one or two thin ribs intercalating between them. Ribs are sharp and uniformly strong on the venter,

FIG. 16. *Scaphites* (*S.*) *ventricosus* Meek and Hayden, 1862, microconchs. A–C. TMP2016.041.0367, Wapiabi Formation, Bighorn Dam, Alberta. A. Right lateral; B. ventral; C. apertural. D–F. AMNH 108452, 50–60 m, Kevin Member, Marias River Shale, Toole County, Montana. D. Right lateral; E. apertural; F. ventral. G, H. TMP2016.041.0163, 41.4 m, Wapiabi Formation, Chungo Creek, Alberta. G. Right lateral; H. ventral. I, J. TMP2016.041.0161, 41.4 m, Chungo Creek, Alberta. I. Right lateral; J. ventral.

which they cross with a slight adoral projection. The ribs are equally and widely spaced, with, for example, 5 ribs/cm on the adoral part of the phragmocone in TMP2016.041.0161.

The same pattern of ribbing persists onto the body chamber. Primary ribs are prominent and equally spaced on the shaft, becoming weaker and more closely spaced on the hook. They are straight or weakly flexuous on the flanks, swinging slightly backward on the inner flanks, slightly forward on the midflanks, and slightly backward again on the outer flanks. Each rib subdivides into two thin secondary ribs, with one or two thin ribs intercalating between them. Ribs are uniformly strong and widely spaced on the venter of the shaft, with, for example, 4.5 ribs/cm in TMP2016.041.0372. Ribs are more closely spaced on the venter of the hook, which they cross with a stronger adoral projection. The rib density ranges from 3.75 to 9 ribs/cm.

The suture of the microconchs is the same as that of the macroconchs.

REMARKS: Although *Scaphites* (*S.*) *ventricosus* is well established in the literature, it is rare to find complete specimens. Most specimens lack the phragmocone although, interestingly, the holotype retains the phragmocone but not the hook. The specimens in our collection closely match those from the U.S. Western Interior. For example, YPM 26721 is a macroconch illustrated by Reeside (1927b: pl. 4, fig. 1–4) from the Cody Shale of Wyoming. It is approximately the same size as the macroconchs in our collection (LMAX = 83 mm). It also displays the same pattern of ribs, with more widely spaced ribs on the midshaft than on the phragmocone (5 ribs/cm on the phragmocone versus 3 ribs/cm on the midshaft).

Dimorphs in this species are distinguished on the basis of size. The larger microconchs correspond to the macroconchs in our collection. However, two smaller microconchs (TMP2016.041.0161 and .0163) would previously have been referred to as *Scaphites* (*Scaphites*) *tetonensis*. This form occurs in the same

beds as *S.* (*S.*) *ventricosus*, and we argue that it simply represents a small microconch of this species. Other than size, dimorphs are distinguished by the outline of the umbilical shoulder of the shaft in side view. It is straight or slightly concave in macroconchs whereas it is markedly concave in microconchs. This is related to the fact that the body chamber is slightly more tightly coiled in macroconchs than in microconchs, although a small gap is present between the phragmocone and hook in both dimorphs.

Several closely related scaphite species occur in the Coniacian of the Western Interior of North America. *Scaphites* (*S.*) *ventricosus* is distinguished from the underlying species *S.* (*S.*) *pre-ventricosus* by its larger size, more tightly coiled shell, and more widely spaced ribs. It is distinguished from the overlying species *S.* (*S.*) *depressus* by its less tightly coiled shell and more widely spaced ribs.

OCCURRENCE: In the Upper Cretaceous of the Western Interior of North America, this species demarcates the upper lower and middle Coniacian *Scaphites* (*S.*) *ventricosus* Zone. In the study area, the lowest occurrence of this species is immediately above surface CS2 in allomember CA3, just below an interpreted highstand and prior to a major regression that culminates at surface CS4, which marks the boundary between the lower and middle Coniacian. It is present in the Wapiabi Formation at Ram River (TMP2016.041.0021), East Thistle Creek (TMP2016.041.0066 and .0067), James River (TMP2016.041.0155), Blackstone River (TMP2016.041.0106), Chungo Creek (TMP2016.041.0161–.0168), Sheep River (TMP2016.041.0296), Bighorn Dam (TMP2016.041.0366–.0368, .0370–.0374, and .0379), Mill Creek (TMP2016.041.0035), and Bighorn River (TMP2016.041.0349), Alberta. Elsewhere, it is abundant in the Kevin Member of the Marias River Shale in north-central Montana, the Cody Shale in western Wyoming, and the Mancos Shale in New Mexico. Outside North America, it has been reported

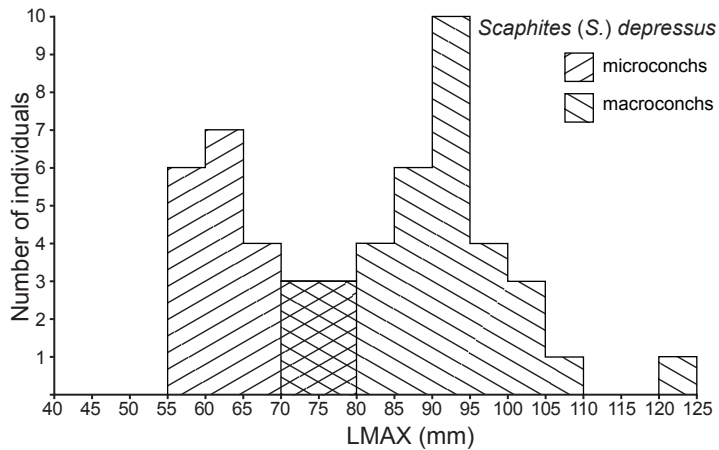


FIG. 17. Size-frequency histogram of *Scaphites (S.) depressus* Reeside, 1927, based on the samples in tables 7 and 8.

from Alianaitšunguaq, Nūgssuaq, Greenland (Birkelund, 1965).

Scaphites (Scaphites) depressus Reeside, 1927

Figures 9D, E, 17–32

1894. *Scaphites ventricosus* Meek and Hayden. Stanton: 186 (*pars*), pl. 44, fig. 10 only.
1898. *Scaphites ventricosus* Meek and Hayden. Logan: 476, pl. 104, fig. 10 only.
- 1927a. *Scaphites ventricosus* Meek and Hayden var. *depressus* Reeside: 7, pl. 5, figs. 6–10.
- 1927a. *Scaphites ventricosus* Meek and Hayden var. *stantoni* Reeside: 7, pl. 3, figs. 19, 20; pl. 4, figs. 5–10.
- 1927a. *Scaphites ventricosus* Meek and Hayden var. *oregonensis* Reeside: 7, pl. 6, figs. 11–15.
1952. *Scaphites depressus* Reeside. Cobban: 32, pl. 15, figs. 6–8.
1952. *Scaphites depressus* Reeside var. *stantoni* Reeside. Cobban: 33, pl. 15, figs. 1–5.
1952. *Scaphites depressus* Reeside var. *oregonensis* Reeside. Cobban: 33.
1964. *Scaphites depressus* var. *stantoni* Reeside. Scott and Cobban, pl. 5, fig. 2.
1970. *Scaphites depressus* Reeside. Jeletzky, pl. 26, fig. 2.

non 1976 *Scaphites* ex. gr. *ventricosus* Meek and Hayden. Szász: 204, pl. 3, fig. 2.

1976. *Scaphites depressus* Reeside. Kennedy and Cobban, pl. 7, fig. 4.

1977. *Scaphites depressus* Reeside. Kauffman: 263, pl. 24, figs. 9, 10.

1994. *Scaphites depressus* Reeside. Braunberger: 117–118, pl. 14, figs. 1–4; pl. 15, figs. 1–3; pl. 16, figs. 1–3.

1994. *Scaphites depressus* Reeside. Hills et al.: 735, pl. 1, figs. 2, 4.

DIAGNOSIS: Macroconchs globular and massive, with closely coiled body chamber and broadly rounded to flattened flanks, with a reduced aperture; apertural angle averaging 70°; ornament consisting of numerous, straight, closely spaced primary and secondary ribs; microconchs smaller with more loosely uncoiled body chamber; suture complex with asymmetrically bifid first lateral lobes.

TYPES: Holotype YPM 6417 from 244 m above the base of the Cody Shale on the Oregon Basin Oil Field in sec. 6, T.51N., R.100W., Park County, Wyoming.

MATERIAL: Approximately 77 specimens, all of which are adult specimens, comprising 45 macroconchs and 32 microconchs.

TABLE 7

Measurements of *Scaphites (Scaphites) depressus* macroconchs.

See figure 2 for description of measurements. All measurements are in mm, except for apertural angle (AA) and septal angle (SA), which are in degrees. Rib density is reported to the nearest 0.25 ribs/cm on the adapical and adoral parts of the phragmocone, the midshaft, and the hook, depending upon the preservation of the specimen. Height (m) is the height in the measured stratigraphic section.

Study No.	TMP No.	Loc.	Height (m)	LMAX	LMAX/HP	LMAX/HS	AA	SA	UD	WP/HP	WS/HS	WH/HH	Rib density			
													Adap.	Adoral	Shaft	Hook
2	2016.041.0004	Ram Riv.	132.5	89.9	-	-	-	-	-	-	-	-	-	4	4	5
5	2016.041.0007	Ram Riv.	132.5	88.8	-	-	-	-	-	-	-	-	-	3	4	4.5
7	2016.041.0009	Ram Riv.	132.5	91.4	2.38	2.51	-	-	-	1.32	1.48	1.32	-	3.25	4	4
8	2016.041.0010	Ram Riv.	132.5	76.8	2.50	2.33	-	-	-	1.38	1.44	1.42	-	4	4.5	4.5
9	2016.041.0011	Ram Riv.	132.5	95.5	2.34	2.14	77	-7	-	1.41	1.34	1.69	-	3.25	3.25	3.5
10	2016.041.0012	Ram Riv.	132.5	-	-	-	-	-	-	-	-	-	-	-	3	4
12	2016.041.0014	Ram Riv.	110.7	89.7	-	-	-	-	-	-	-	1.49	-	3	3	4
14	2016.041.0016	Ram Riv.	112.7	92.0	-	-	-	-	-	-	-	-	-	3	4	4
17	2016.041.0019	Ram Riv.	132.9	-	-	-	-	-	-	-	-	-	-	-	4	5
18	2016.041.0020	Ram Riv.	132.9	-	-	-	-	-	-	-	-	-	-	4.25	3	5
21	2016.041.0023	Ram Riv.	132.9	78.6	-	-	-	-	-	-	-	-	-	5	-	5
22	2016.041.0024	Ram Riv.	127.3	81.7	-	-	-	-	-	-	-	-	4.75	4.25	4	4.75
23	2016.041.0025	Ram Riv.	127.3	-	-	-	-	2	5.1	1.35	1.27	-	5	4.5	3.25	4
24	2016.041.0026	Ram Riv.	127.3	-	-	-	-	-	-	-	-	-	-	4	-	-
25	2016.041.0027	Ram Riv.	119.6	74.5	-	-	-	-	-	-	-	-	5	5	4.5	5.25
37	2016.041.0069	E. Thistle Ck.	83.3	90.1	2.40	2.10	79	0	4.9	1.39	1.31	1.35	5.5	4	3.75	4
38	2016.041.0070	E. Thistle Ck.	83.3	74.4	-	2.11	-	-12.5	-	-	-	-	-	-	3.5	-
39	2016.041.0071	E. Thistle Ck.	83.3	82.1	2.85	2.17	-	-	-	1.60	1.40	-	5	-	-	3.5
58	2016.041.0156	James Riv.	92.9	-	-	-	-	-	-	-	-	-	-	5	4	5
76	2016.041.0210	W. Thistle Ck.	100.9	102	2.76	2.38	-	-16	-	1.54	1.42	-	-	4	3.5	3.5
77	2016.041.0211	W. Thistle Ck.	101.3	93.3	-	-	-	-	-	-	-	-	4.5	4	-	4

Study No.	TMP No.	Loc.	Height (m)	LMAX	LMAX/HP	LMAX/HS	AA	SA	UD	WP/HP	WS/HS	WH/HH	Rib density			
													Adap.	Adoral	Shaft	Hook
78	2016.041.0212	W. This-tle Ck.	102.0	94.1	-	2.44	72	12	-	-	1.57	1.85	-	3.5	4	4
79	2016.041.0213	W. This-tle Ck.	106.7	98.1	2.64	2.06	-	-	-	1.44	1.25	1.36	4.5	4	3.25	-
80	2016.041.0214	W. This-tle Ck.	105.5	-	-	-	-	-	-	-	-	-	-	3.75	4	5
81	2016.041.0215	W. This-tle Ck.	105.8	-	-	-	-	-	-	-	1.37	-	-	4	3.5	4
82	2016.041.0216	W. This-tle Ck.	107.0	97.9	-	2.28	-	-	6.1	-	1.42	-	5	4	3.5	4.5
83	2016.041.0217	W. This-tle Ck.	110.7	94.6	2.54	2.30	-	-	-	1.38	1.36	1.48	3.75	3.75	3.5	5
84	2016.041.0218	W. This-tle Ck.	113.8	100.9	2.80	2.32	-	-	-	1.74	1.47	-	5	3.5	3.5	3.75
85	2016.041.0219	W. This-tle Ck.	114.9	84.2	2.61	2.25	61	11	-	1.52	1.40	1.43	-	4	4	5
99	2016.041.0273	Cardinal Riv.	90.4	122.7	-	-	-	-	-	-	-	-	-	-	-	-
101	2016.041.0275	Cardinal Riv.	96.8	76.7	-	-	-	-	-	-	-	-	5	4	3.75	-
110	2016.041.0298	Sheep Riv.	147.5	92.1	2.39	2.40	-	-	-	1.40	1.58	-	6	4	2	-
111	2016.041.0299	Sheep Riv.	147.5	99.4	-	2.16	-	-	-	-	1.36	1.48	4	3	3	4.25
112	2016.041.0300	Sheep Riv.	147.5	-	-	-	-	-	-	-	-	-	-	-	-	-
115	2016.041.0303	Sheep Riv.	158.8	105.6	-	2.01	81	-2.5	-	-	1.43	1.57	-	3	2.75	3.25
116	2016.041.0304	Sheep Riv.	158.8	104.8	-	-	-	-	-	-	-	-	-	4.5	-	4.5
121	2016.041.0350	Bighorn Riv.	109.4	88.6	-	2.08	68	-9.5	-	-	1.28	-	-	4.5	3.5	4
122	2016.041.0351	Bighorn Riv.	132.4	89.5	-	2.38	-	-	-	-	-	1.67	-	3.5	3.25	4.25
137	2016.041.0375	Bighorn Dam	96.7	92.2	-	-	-	-	-	-	-	-	-	3	-	-
138	2016.041.0376	Bighorn Dam	103.4	-	-	-	-	-	-	-	-	-	-	-	4	-
140	2016.041.0378	Bighorn Dam	107.3	74.3	2.51	2.01	-	-	-	1.56	1.40	-	6	4	2.25	4
142	2016.041.0380	Bighorn Dam	108.0	89.0	2.40	2.04	-	-	-	1.47	1.37	1.64	-	3.25	3	4
148	2016.041.0386	Bighorn Dam	115.3	92.7	2.60	2.28	-	-	-	1.47	1.36	1.87	-	4	3.5	4.5
150	2016.041.0388	Bighorn Dam	133.0	82.2	-	-	69	-	-	-	-	-	4.75	4	3.75	5
200	2016.041.0472	Mill Ck.	230.0	-	-	-	-	-	-	-	-	-	-	-	-	-
Average				90.6	2.55	2.23	70.2	-2.5	5.4	1.46	1.39	1.54	5	3.75	3.5	4.25

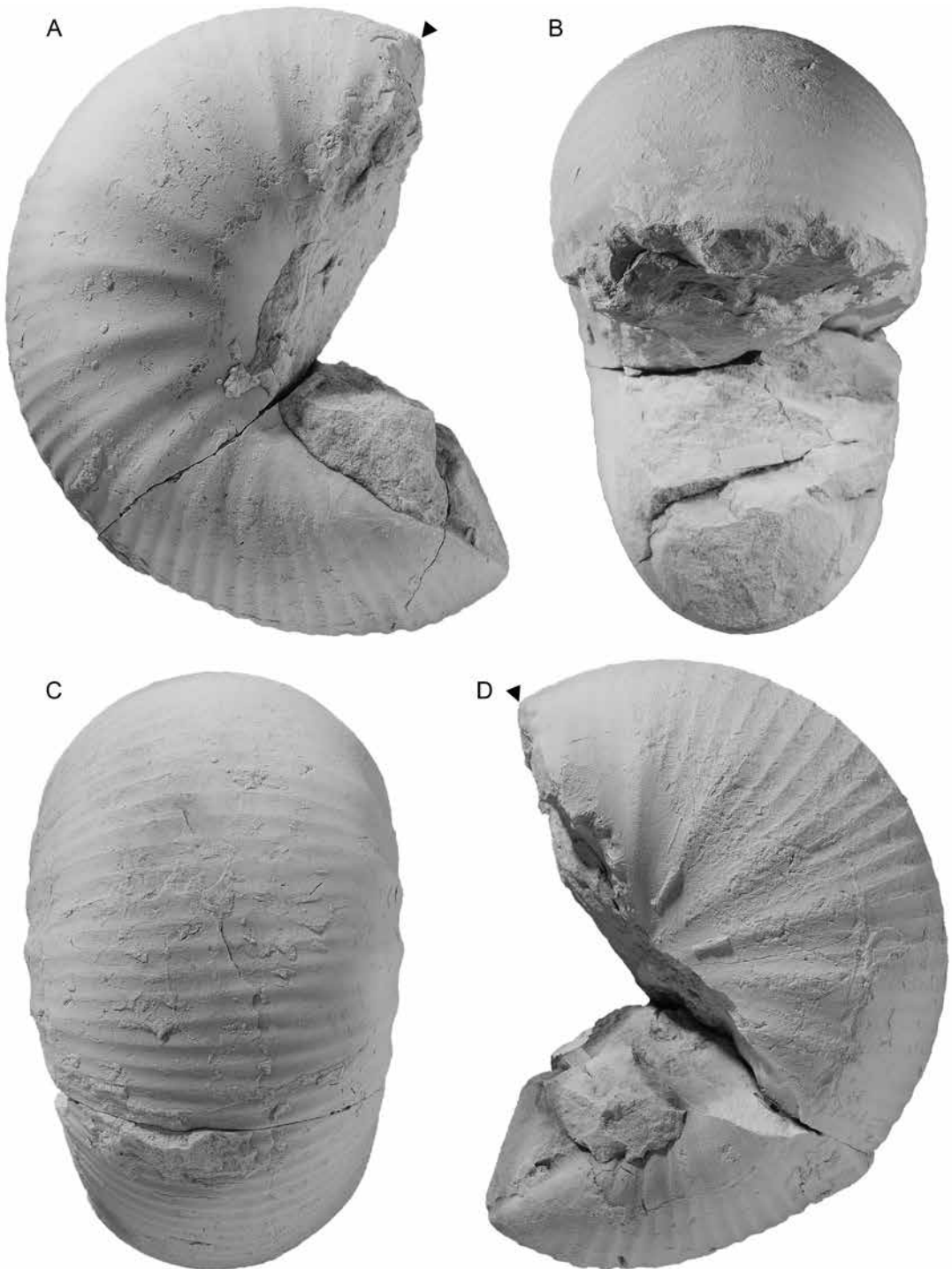


FIG. 18. *Scaphites* (*S.*) *depressus* Reeside, 1927, macroconch, TMP2016.041.0011, 132.5 m, Wapiabi Formation, Ram River, Alberta. A. Right lateral; B. apertural; C. ventral; D. left lateral.

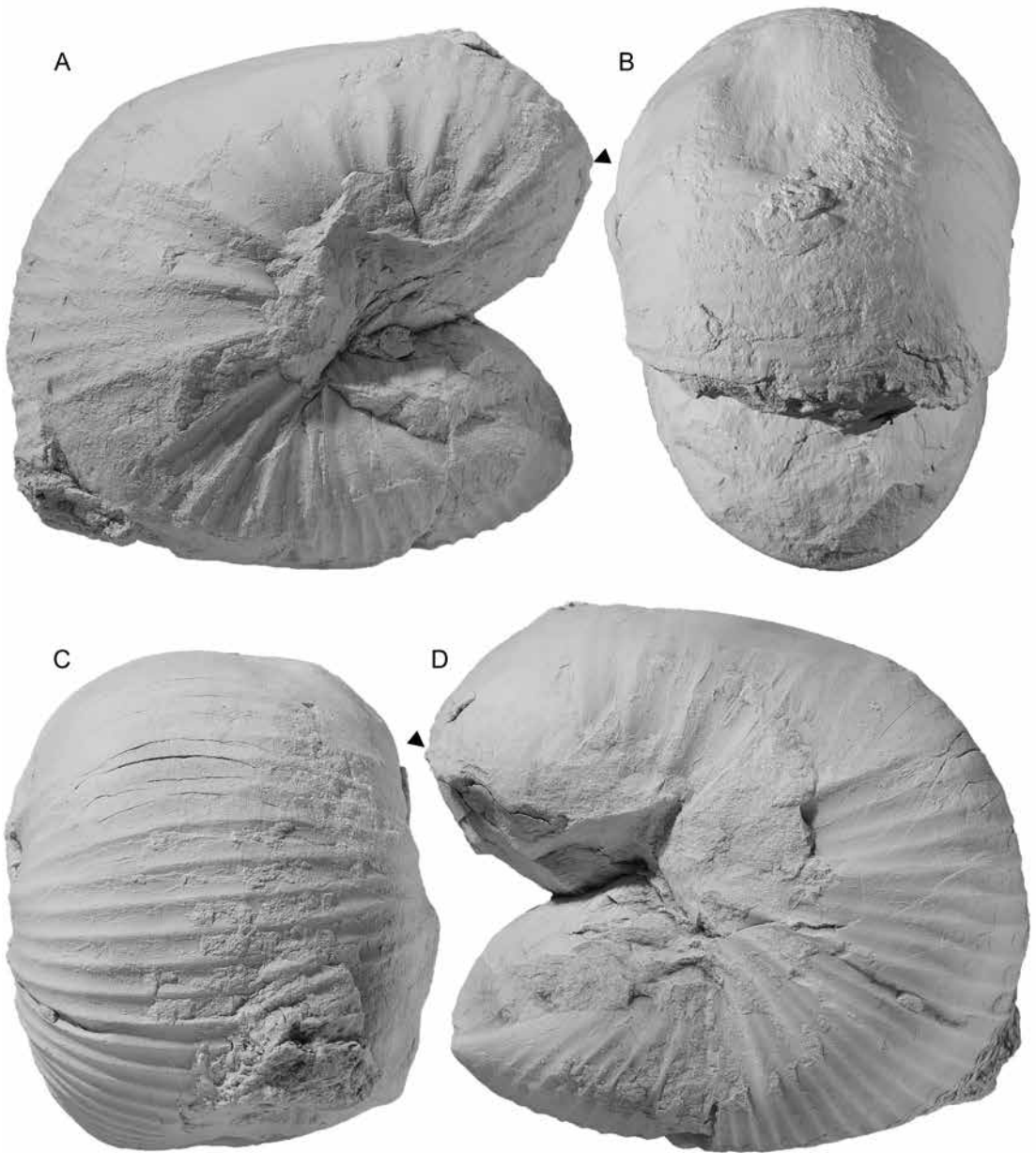


FIG. 19. *Scaphites* (*S.*) *depressus* Reeside, 1927, macroconch, TMP2016.041.0012, 132.5 m, Wapiabi Formation, Ram River, Alberta. **A.** Right lateral; **B.** apertural; **C.** ventral; **D.** left lateral.

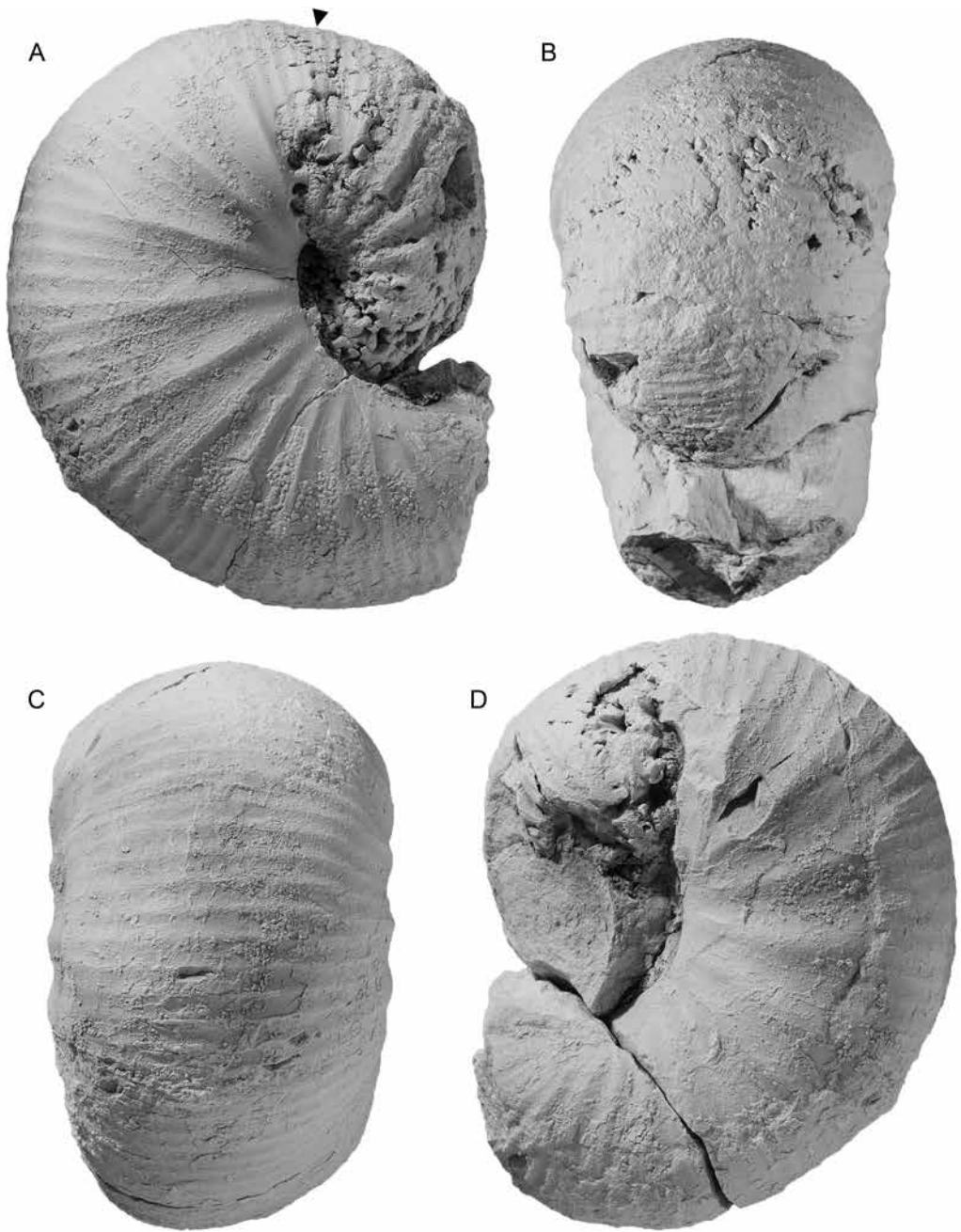


FIG. 20. *Scaphites* (*S.*) *depressus* Reeside, 1927, macroconch, TMP2016.041.0025, 127.3 m, Wapiabi Formation, Ram River, Alberta. A. Right lateral; B. apertural; C. ventral; D. left lateral.

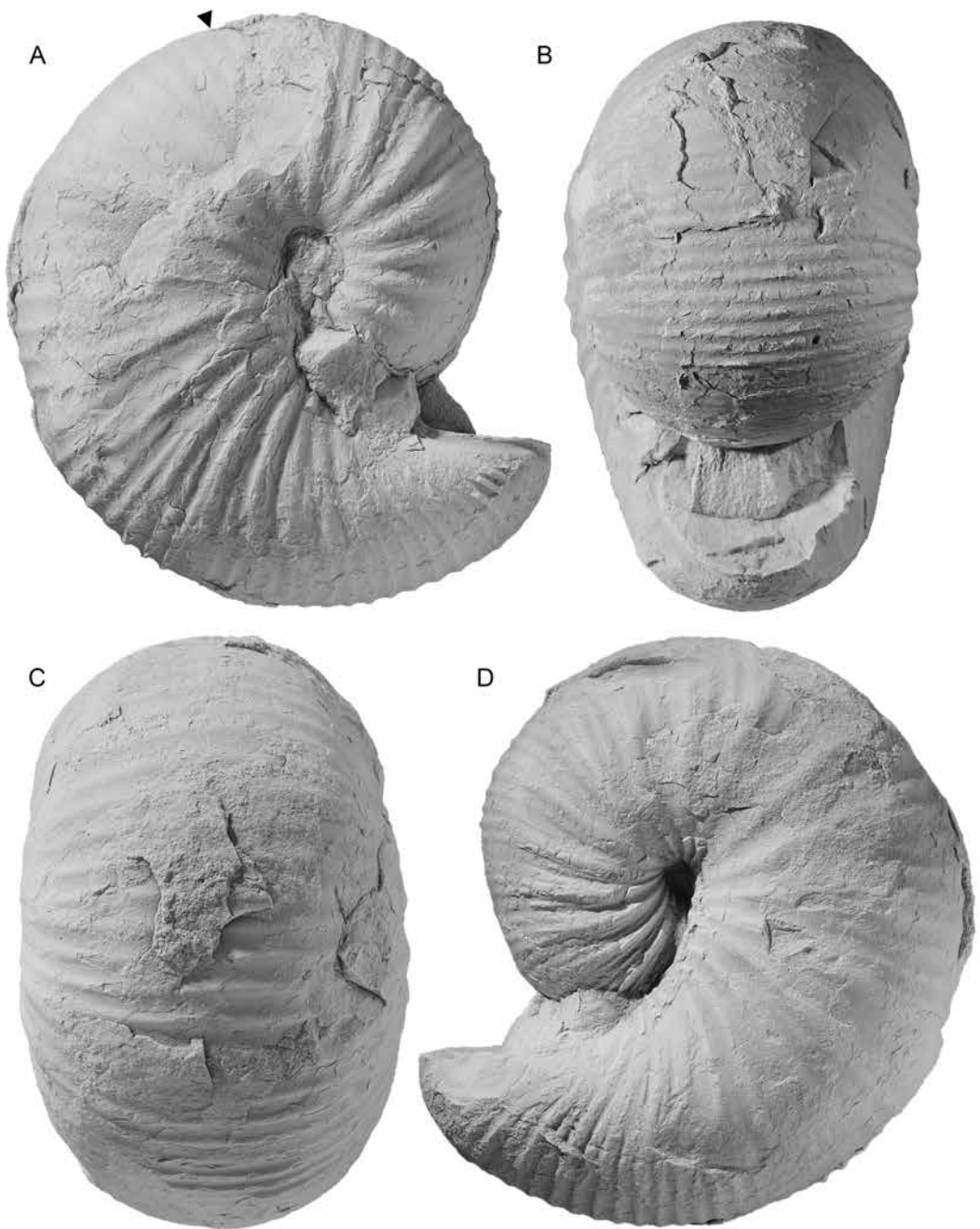


FIG. 21. *Scaphites* (*S.*) *depressus* Reeside, 1927, macroconch, TMP2016.041.0069, 83.3 m, Wapiabi Formation, E. Thistle Creek, Alberta. A. Right lateral; B. apertural; C. ventral; D. left lateral.

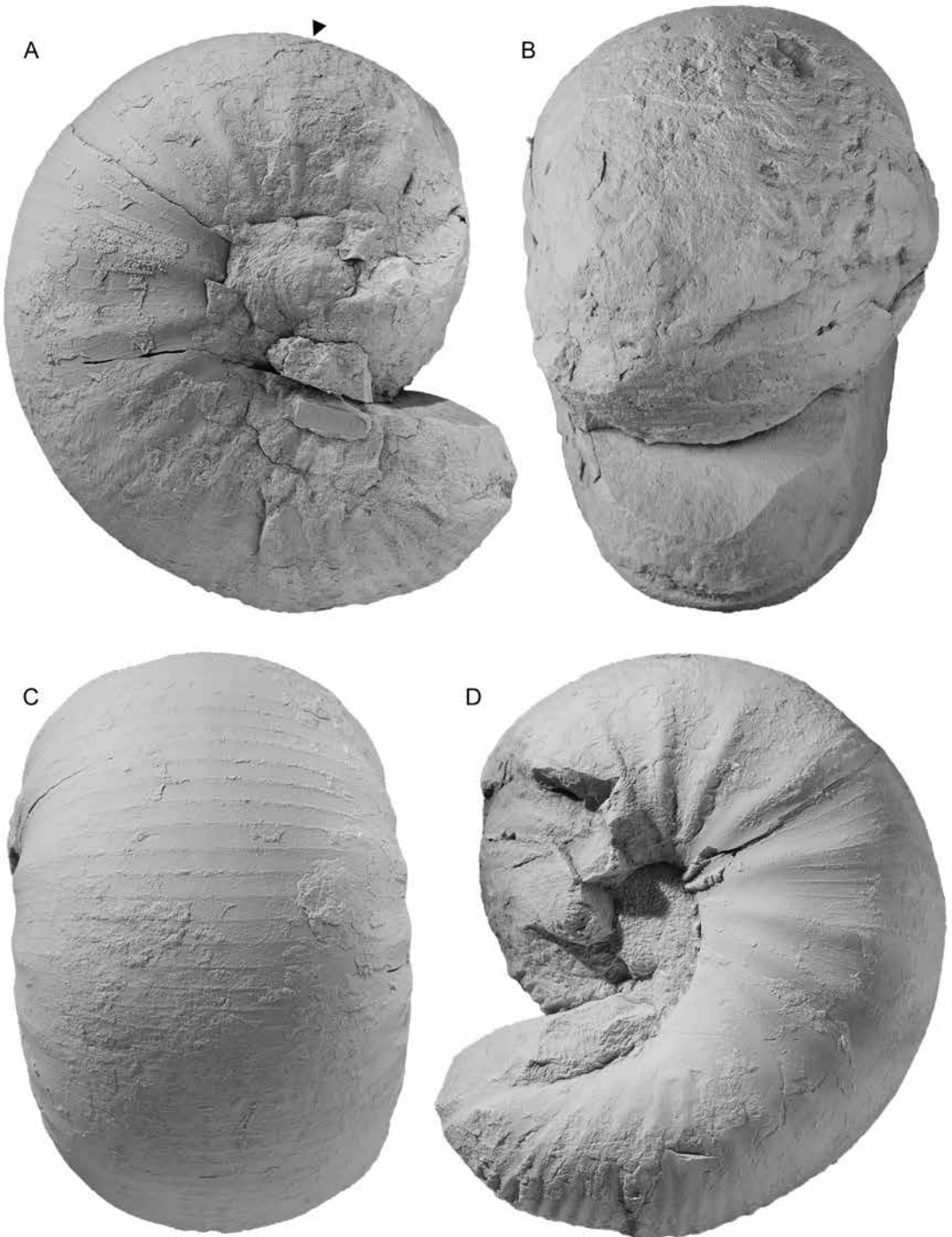


FIG. 22. *Scaphites* (*S.*) *depressus* Reeside, 1927, macroconch, TMP2016.041.0212, 102.0 m, Wapiabi Formation, W. Thistle Creek, Alberta. A. Right lateral; B. apertural; C. ventral; D. left lateral.

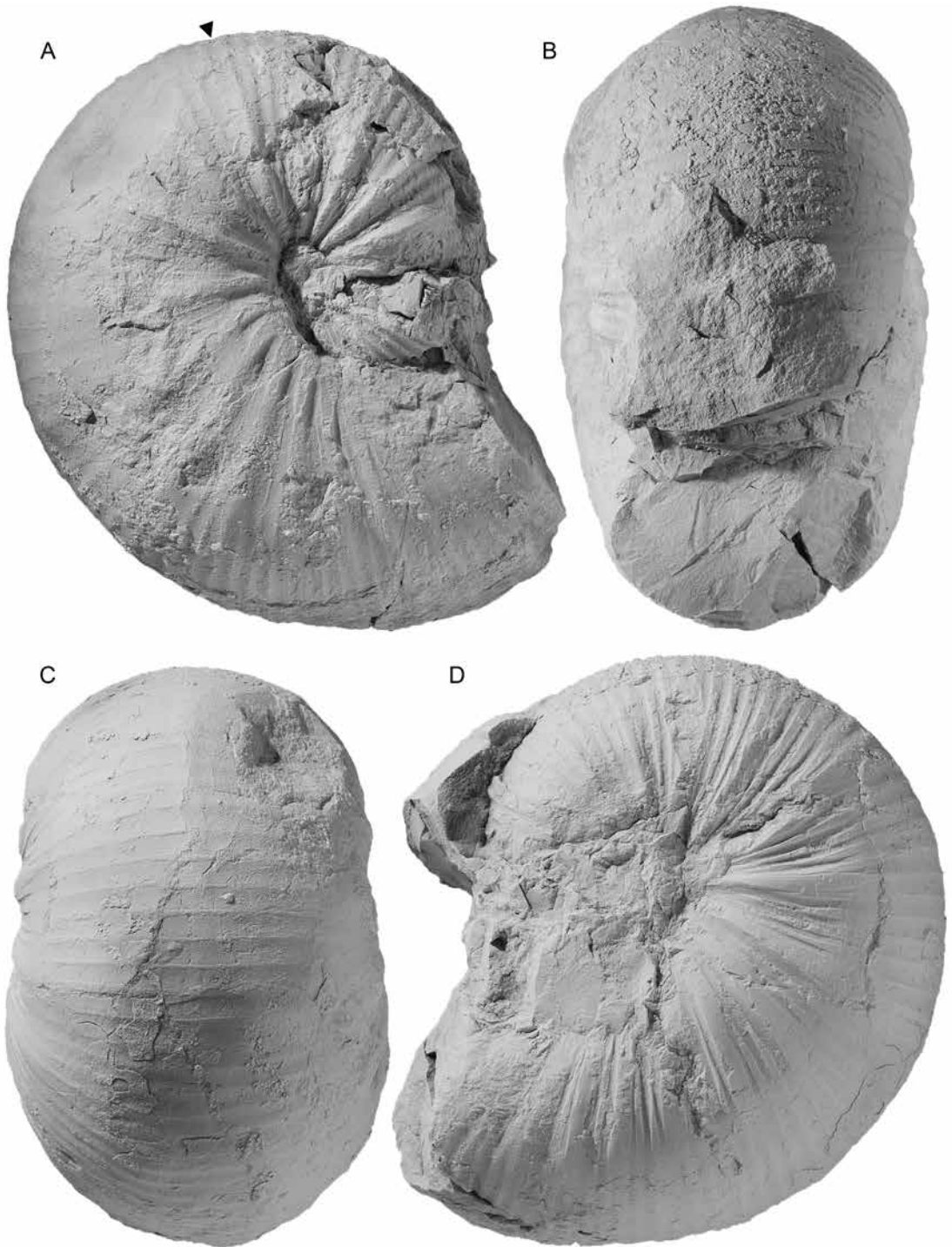


FIG. 23. *Scaphites* (*S.*) *depressus* Reeside, 1927, macroconch, TMP2016.041.0213, 106.7 m, Wapiabi Formation, W. Thistle Creek, Alberta. A. Right lateral; B. apertural; C. ventral; D. left lateral.

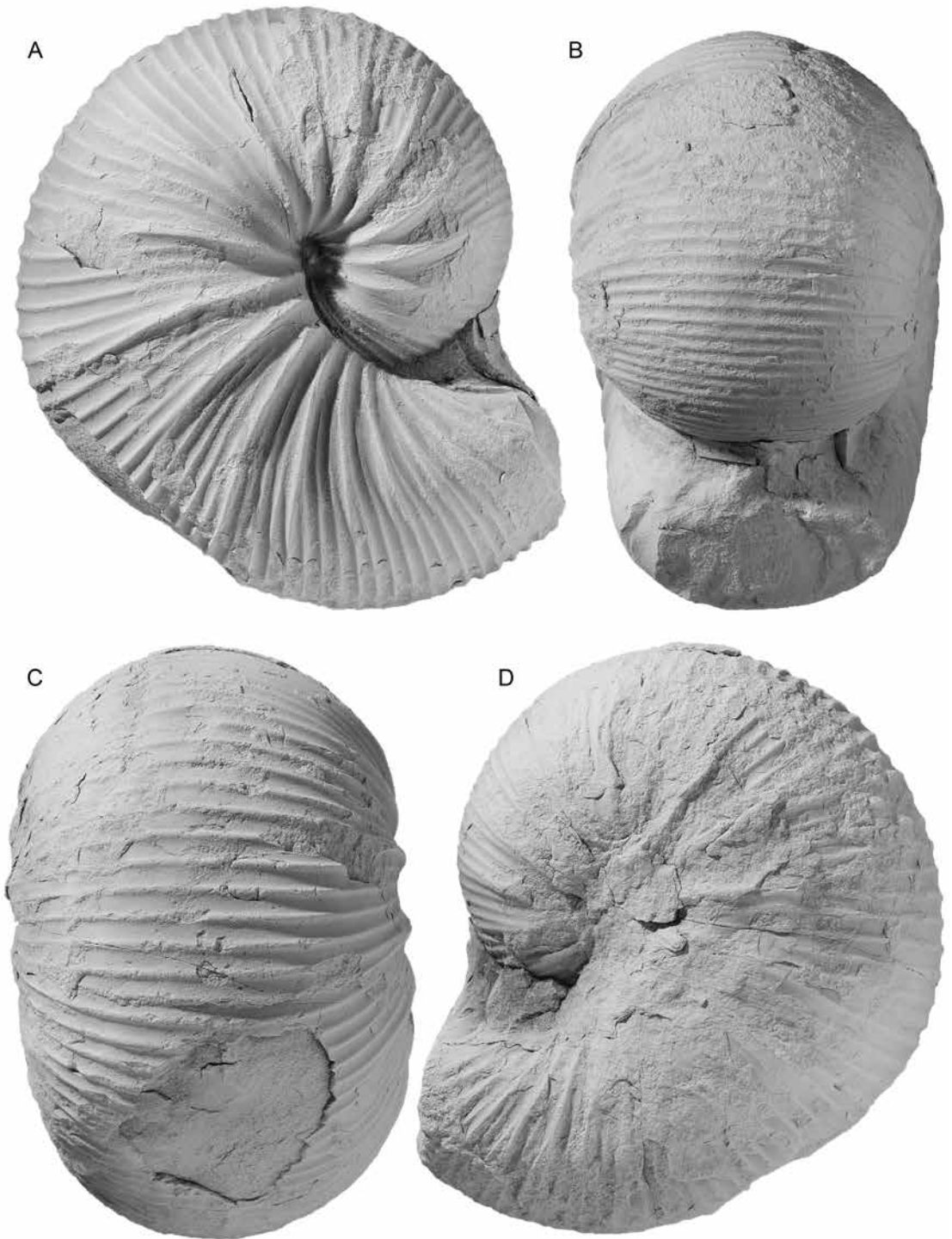


FIG. 24. *Scaphites (S.) depressus* Reeside, 1927, macroconch, TMP2016.041.0216, 107.0 m, Wapiabi Formation, W. Thistle Creek, Alberta. A. Right lateral; B. apertural; C. ventral; D. left lateral.

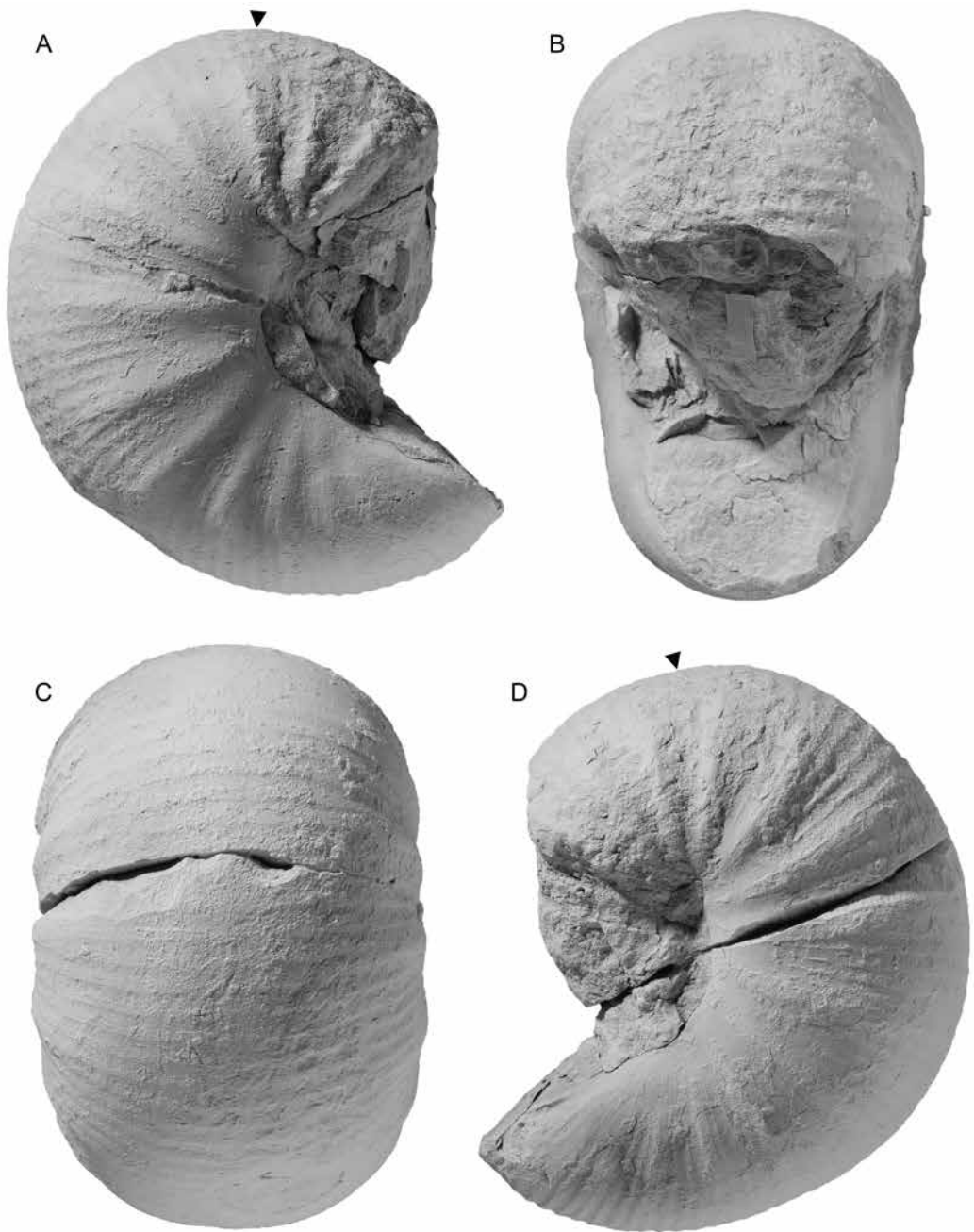
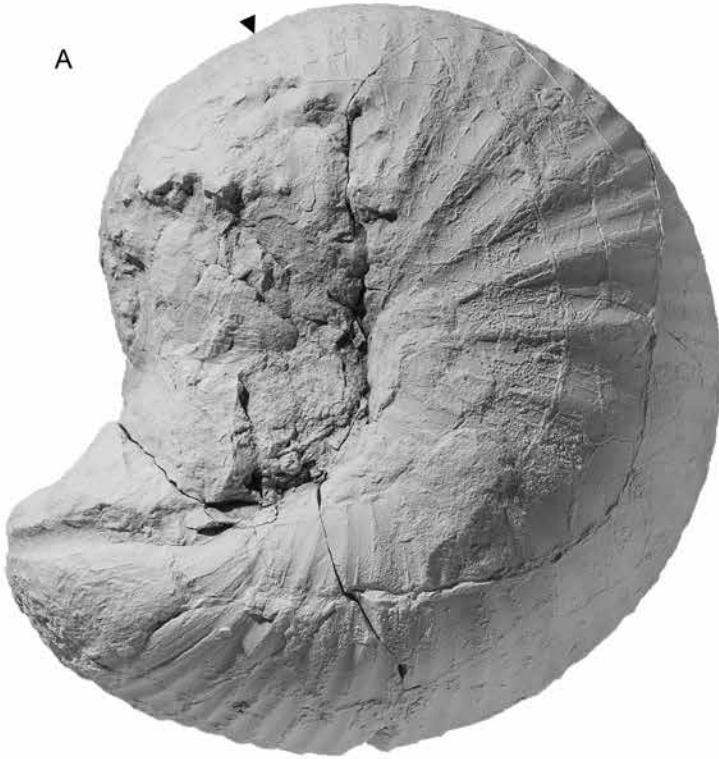


FIG. 25. *Scaphites* (*S.*) *depressus* Reeside, 1927, macroconch, TMP2016.041.0219, 114.9 m, Wapiabi Formation, W. Thistle Creek, Alberta. A. Right lateral; B. apertural; C. ventral; D. left lateral.

A



B



C



MACROCONCH DESCRIPTION: In the measured sample, LMAX averages 90.6 mm and ranges from 74.3 to 122.7 mm (table 7). The ratio of the size of the largest specimen to that of the smallest is 1.65. The size distribution is unimodal with a peak between 90 and 95 mm (fig. 17). Adults are robust with a circular outline in side view. The exposed phragmocone occupies approximately one whorl and terminates slightly below or slightly above the line of maximum length. The septal angle averages -2.5° . The umbilical diameter of the phragmocone is small and averages 5.4 mm. The body chamber consists of a short shaft and recurved hook. The umbilical shoulder of the shaft is straight in side view. LMAX/ H_S averages 2.23 and ranges from 2.01 to 2.51. The body chamber is tightly coiled leaving hardly any gap between the phragmocone and hook. LMAX/ H_P averages 2.55 and ranges from 2.34 to 2.85. TMP 2016.041.0298–.0300 from Sheep River, which occur in the lower part of the *Scaphites* (*S.*) *depressus* Zone, are slightly more loosely uncoiled than most specimens of this species, and are reminiscent of *S.* (*S.*) *ventricosus*. In all of our specimens, the aperture is reduced in size relative to that at midshaft. The apertural angle averages 70.2° and ranges from 61° to 81° .

The whorl section of the phragmocone along the line of maximum length is depressed and subquadrate with maximum whorl width at one-third whorl height. The umbilical wall is steep and subvertical; the flanks are broadly rounded and nearly parallel; the ventrolateral shoulder is sharply rounded; and the venter is broadly rounded. W_P/H_P averages 1.46 and ranges from 1.32 to 1.74. As the shell passes from the phragmocone into the body chamber, the whorl width and height increase only slightly, so that the whorl section at midshaft is nearly the same as that along the line of maximum length. It is depressed and subquadrate with maximum whorl width at one-third whorl height. The umbilical wall is steep and subvertical; the flanks are broadly rounded and nearly parallel; the ven-

tolateral shoulder is sharply rounded; and the venter is broadly rounded. W_S/H_S averages 1.39 and ranges from 1.27 to 1.58. Adoral of the midshaft, the whorl width and, especially, the whorl height abruptly decrease. As a result, the whorl section at the point of recurvature is much more depressed than that at midshaft. W_H/H_H averages 1.54 and ranges from 1.32 to 1.87. The umbilical wall is flat and slopes outward, the flanks are sharply rounded, and the venter is broadly rounded. The shell culminates in a constricted aperture with a dorsal lappet.

On the exposed phragmocone, primary ribs emerge at the umbilical seam and are straight and rectiradiate on the umbilical wall and shoulder. They develop into broad elongate swellings that gradually reach their maximum strength at one-third whorl height, but never form nodes. They each subdivide into two or three secondary ribs, with another one or two longer secondary ribs intercalating between them. Ribs are sharp and uniformly strong on the broadly rounded venter, which they cross with a slight adoral projection. They are closely spaced on the adapical end of the phragmocone with a rib density of 3.75 to 6 ribs/cm. They become more widely spaced on the adoral end of the phragmocone with a rib density of 3 to 5 ribs/cm.

The same pattern of ornamentation persists onto the body chamber. Primary ribs are rectiradiate on the umbilical wall and shoulder. They develop into elongate swellings that follow the curvature of the flanks and never culminate in nodes. They are prominent, rectiradiate, and equally spaced on the shaft, becoming weaker, prorsiradiate, and more closely spaced on the hook. At one-half whorl height coincident with the ventrolateral shoulder, each rib subdivides into two secondary ribs, with two to four longer secondary ribs intercalating between them. Ribs are uniformly strong and wirelike on the venter of the shaft, which they cross with a slight adoral projection. They are widely spaced with a rib density of 2 to 4.5 ribs/cm, becoming more closely spaced on the venter of the

FIG. 26. *Scaphites* (*S.*) *depressus* Reeside, 1927, macroconch, TMP2016.041.0303, 158.8 m, Wapiabi Formation, Sheep River, Alberta. **A.** Right lateral; **B.** apertural; **C.** ventral.

TABLE 8

Measurements of *Scaphites (Scaphites) depressus* microconchs. See figure 2 for description of measurements. All measurements are in mm. Rib density is reported to the nearest 0.25 ribs/cm on the adapical and adoral parts of the phragmocone, the midshaft, and the hook, depending upon the preservation of the specimen. Height (m) is the height in the measured stratigraphic section.* = above measured section.

Study No.	TMP No.	Locality	Height (m)	LMAX	LMAX/HP	UD	WP/HP	WS/HS	WH/HH	Rib density			
										Adap.	Adoral	Shaft	Hook
1	2016.041.0003	Ram Riv.	132.5	62.2	-	-	-	1.28	1.69	6	5.5	-	6
3	2016.041.0005	Ram Riv.	132.5	59.4	2.35	-	1.23	1.37	1.39	-	5	5	5.5
4	2016.041.0006	Ram Riv.	132.5	-	-	-	-	-	-	-	4.5	4.5	5
6	2016.041.0008	Ram Riv.	132.5	-	-	3.5	-	-	-	-	-	-	-
11	2016.041.0013	Ram Riv.	132.5	75.8	2.49	-	1.22	-	-	-	5	4.5	5
13	2016.041.0015	Ram Riv.	111.4	-	-	-	-	-	-	-	4	-	-
20	2016.041.0022	Ram Riv.	132.9	-	-	-	-	1.43	1.46	-	-	5	5
36	2016.041.0068	E. Thistle Ck.	82.0	58.0	-	-	-	-	-	6	5	4.5	6
75	2016.041.0209	W. Thistle Ck.	100.3	68.5	-	-	-	1.40	-	-	4	4.5	5
86	2016.041.0220	W. Thistle Ck.	118.7	-	-	-	-	-	-	-	-	4	5
87	2016.041.0221	W. Thistle Ck.	121.0	64.8	2.67	5.1	-	1.13	-	-	5	4	5
89	2016.041.0223	W. Thistle Ck.	121.0	56.0	2.51	-	1.37	1.38	1.50	-	4.25	4	5
100	2016.041.0274	Cardinal Riv.	96.8	70.8	2.30	3.8	1.46	1.42	-	4.5	4.5	3.75	5
102	2016.041.0276	Cardinal Riv.	121.0	60.1	-	-	-	-	-	-	-	-	-
103	2016.041.0277	Cardinal Riv.	139.0	58.0	2.47	-	1.38	1.31	1.36	-	4	4	4.75
104	201.041.0278	Cardinal Riv.	141.5-143.5	70.3	2.42	3.5	1.58	1.40	-	5	4	3.75	4.5
106	2016.041.0280	Cardinal Riv.	141.5-143.5	55.9	-	-	-	-	-	6	5	4.5	5
109	2016.041.0297	Sheep Riv.	-	-	-	-	-	-	-	-	-	-	4
113	2016.041.0301	Sheep Riv.	149.0	73.0	2.63	-	-	-	-	5	4	3.5	-
114	2016.041.302	Sheep Riv.	149.0	55.8	-	-	-	-	-	-	4.5	4.25	5
117	2016.041.0305	Sheep Riv.	158.8	76.2	2.53	-	-	1.31	1.29	-	5	3.5	5
123	2016.041.0352	Bighorn Riv.	142.2	62.9	2.50	-	-	1.48	1.57	-	4	-	6
124	2016.041.0353	Bighorn Riv.	142.2	69.1	-	-	-	1.53	1.62	-	4	4	5
125	2016.041.0354	Bighorn Riv.	Above*	70.0	-	-	-	-	-	-	5	4	5

Study No.	TMP No.	Locality	Height (m)	LMAX	LMAX/HP	UD	WP/HP	WS/HS	WH/HH	Adap.	Rib density		
											Adoral	Shaft	Hook
126	2016.041.0355	Bighorn Riv.	Above*	-	-	-	-	-	-	-	-	4.5	5
139	2016.041.0377	Bighorn Dam	107.3	-	-	-	-	-	-	-	-	5	6
143	2016.041.0381	Bighorn Dam	109.6	64.9	-	5.8	-	-	-	5	4	-	4
144	2016.041.0382	Bighorn Dam	115.8	77.5	2.76	-	1.69	1.42	1.77	-	5	4	6
145	2016.041.0383	Bighorn Dam	112.8	-	-	-	-	-	-	-	-	-	5
146	2016.041.0384	Bighorn Dam	112.8	-	-	-	-	-	-	-	-	4.5	-
147	2016.041.0385	Bighorn Dam	113.0	66.1	2.25	-	-	1.30	-	-	4	4	5
149	2016.041.0387	Bighorn Dam	116.0	61.5	2.55	-	-	1.58	1.46	-	-	5	6
Average				65.3	2.49	4.3	1.42	1.38	1.52	5.5	4.5	4.25	5.25

hook, with a rib density of 3.25 to 5.25 ribs/cm. They cross the venter of the hook with a slight to strong adoral projection.

A suture is not well enough preserved in any of the specimens in our study, but according to Cobban (1952), it is complex with asymmetrically bifid first lateral lobes (fig. 9D, E).

MICROCONCH DESCRIPTION: Many of the microconchs are simply miniatures of the macroconchs. For example, TMP2016.041.0278 is simply a scaled-down version of TMP2016.041.0069. Other microconchs such as TMP2016.041.0221 are not only smaller than the macroconchs, but are also more elongate with a more concave umbilical shoulder in lateral view. LMAX averages 65.3 mm and ranges from 55.8 to 77.5 mm (table 8). The size distribution is unimodal with a peak between 60 and 65 mm (fig. 17).

The shell proportions of microconchs are similar to those of macroconchs. The whorl section of the phragmocone along the line of maximum length is depressed and subquadrate with maximum whorl width at one-third whorl height. The umbilical wall is steep and subvertical; the flanks are broadly rounded and nearly parallel; the ven-

trolateral shoulder is sharply rounded; and the venter is broadly rounded. W_p/H_p averages 1.42 and ranges from 1.22 to 1.69. As the shell passes from the phragmocone into the body chamber, the whorl width and height increase only slightly, so that the shape of the whorl section at midshaft is nearly the same as that along the line of maximum length. It is depressed subquadrate with maximum whorl width at one-third whorl height. The umbilical wall is steep and subvertical; the flanks are broadly rounded and nearly parallel; the ventrolateral shoulder is sharply rounded; and the venter is broadly rounded. W_s/H_s averages 1.38 and ranges from 1.13 to 1.58. Adoral of the midshaft, the whorl width and height decrease slightly, resulting in a slightly more depressed whorl section at the point of recurvature. W_H/H_H averages 1.52 and ranges from 1.29 to 1.77. The umbilical wall is flat and slopes outward, the flanks are sharply rounded, and the venter is broadly rounded. The shell culminates in a constricted aperture.

The pattern of ornamentation on microconchs is the same as that on macroconchs. On the exposed phragmocone, primary ribs emerge at the

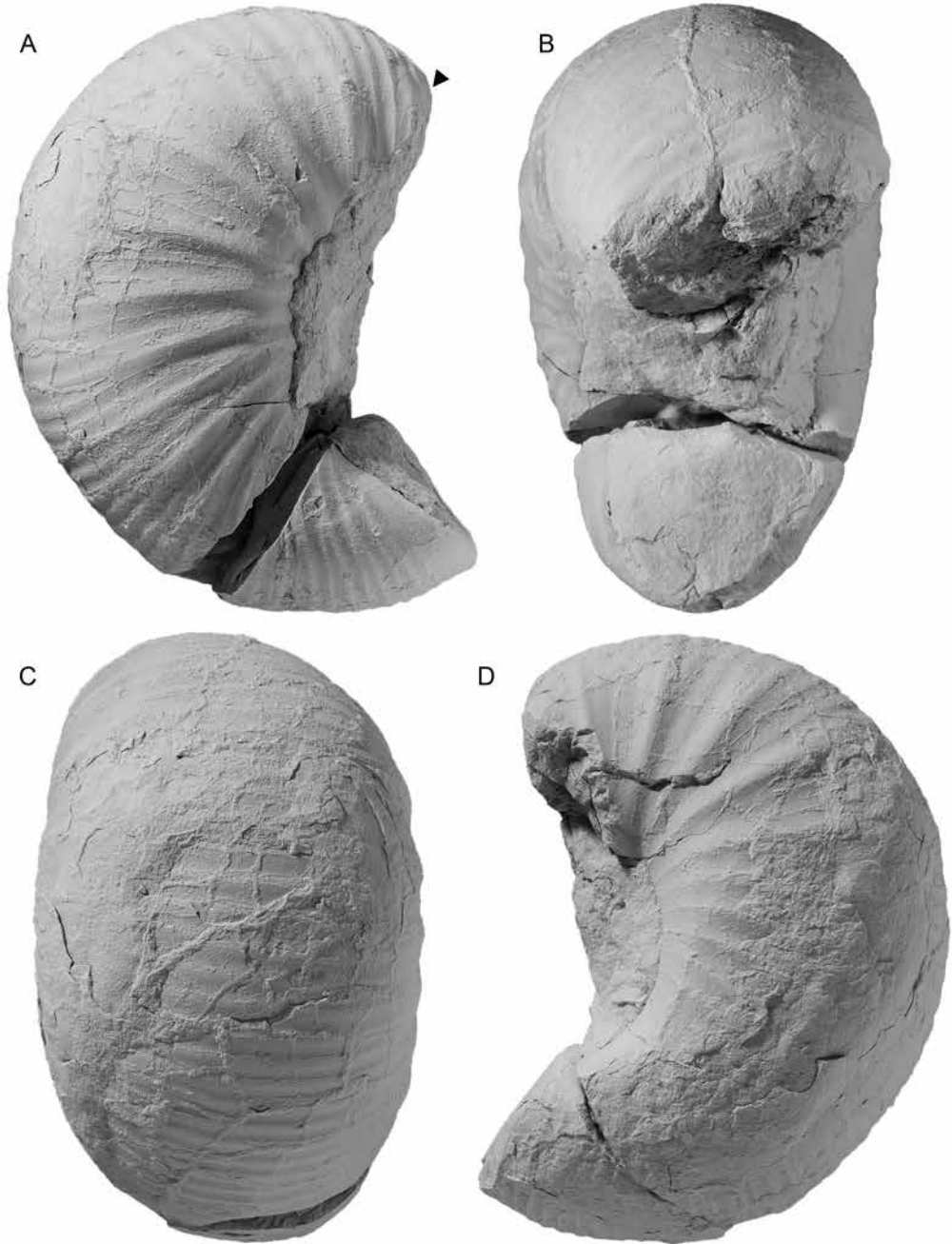


FIG. 27. *Scaphites (S.) depressus* Reeside, 1927, macroconch, TMP2016.041.0350, 109.4 m, Wapiabi Formation, Bighorn River, Alberta. A. Right lateral; B. apertural; C. ventral; D. left lateral.

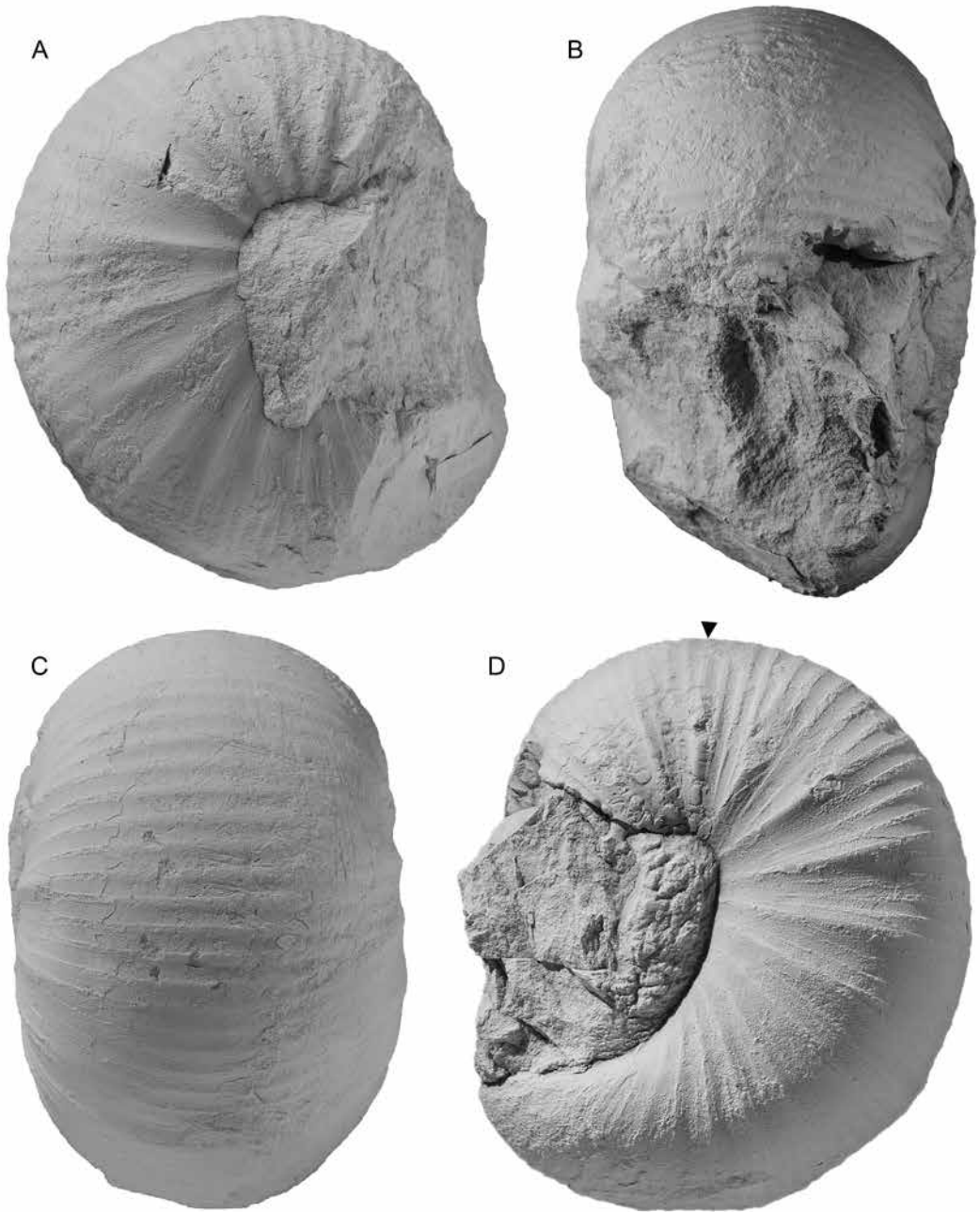


FIG. 28. *Scaphites* (*S.*) *depressus* Reeside, 1927, macroconch, TMP2016.041.0388, 133.0 m, Wapiabi Formation, Bighorn Dam, Alberta. **A.** Right lateral; **B.** apertural; **C.** ventral; **D.** left lateral.

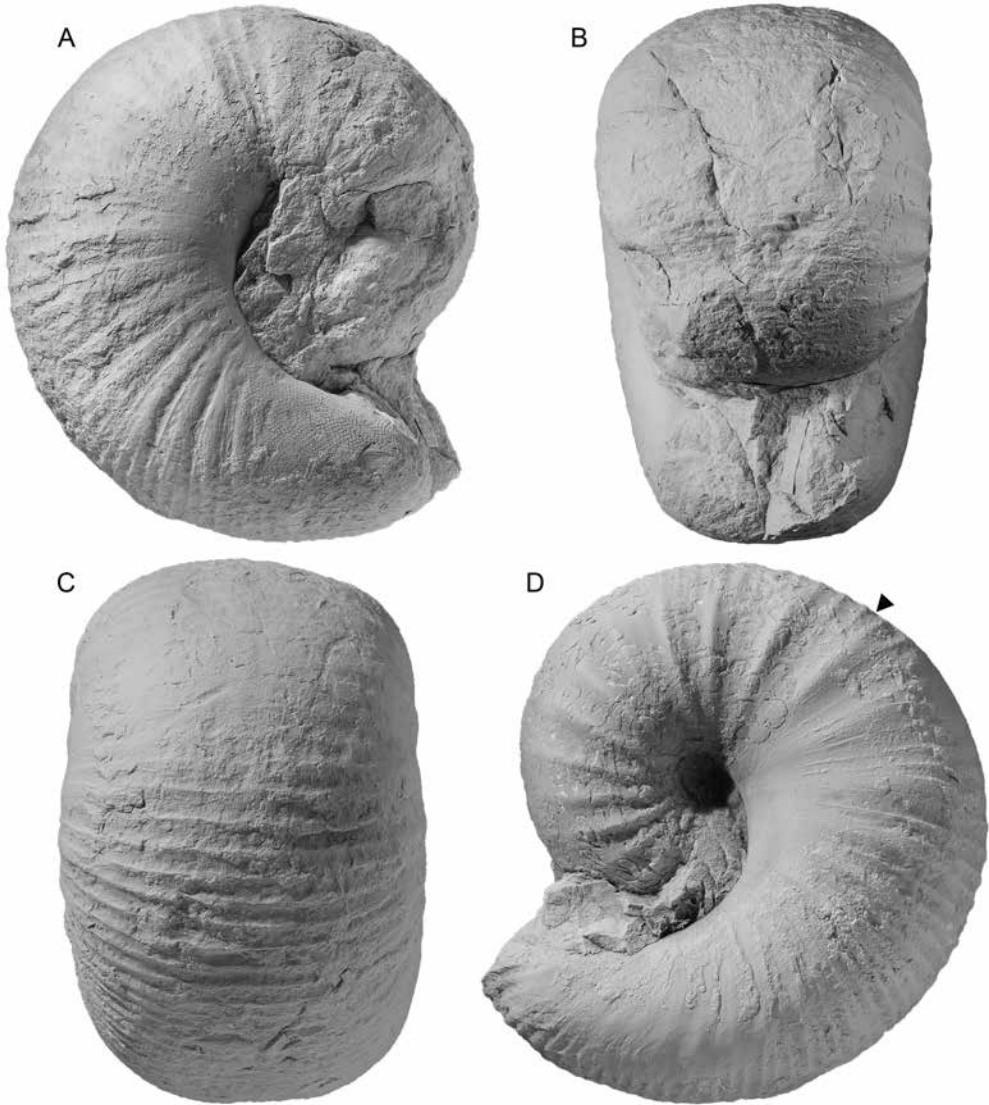


FIG. 29. *Scaphites* (*S.*) *depressus* Reeside, 1927, microconch, TMP2016.041.0382, 115.8 m, Wapiabi Formation, Bighorn Dam, Alberta. A. Right lateral; B. apertural; C. ventral; D. left lateral.

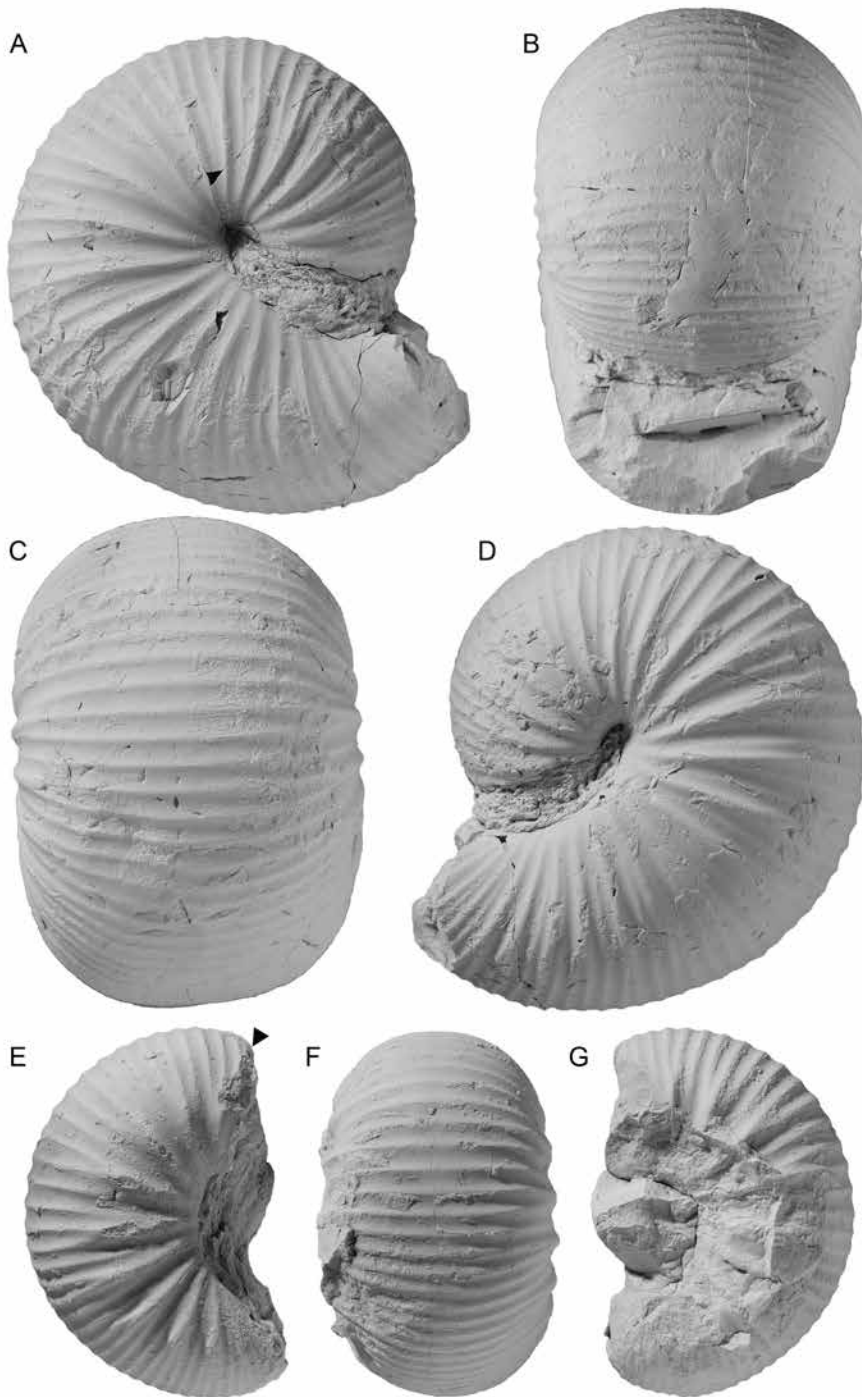


FIG. 30. *Scaphites* (*S.*) *depressus* Reeside, 1927, microconchs. A–D. TMP2016.041.0278, 141.5–143.5 m, Wapiabi Formation, Cardinal River, Alberta. A. Right lateral; B. apertural; C. ventral; D. left lateral. E–G. TMP2016.041.0223, 121.0 m, Wapiabi Formation, W. Thistle Creek, Alberta. E. Right lateral; F. ventral; G. left lateral.

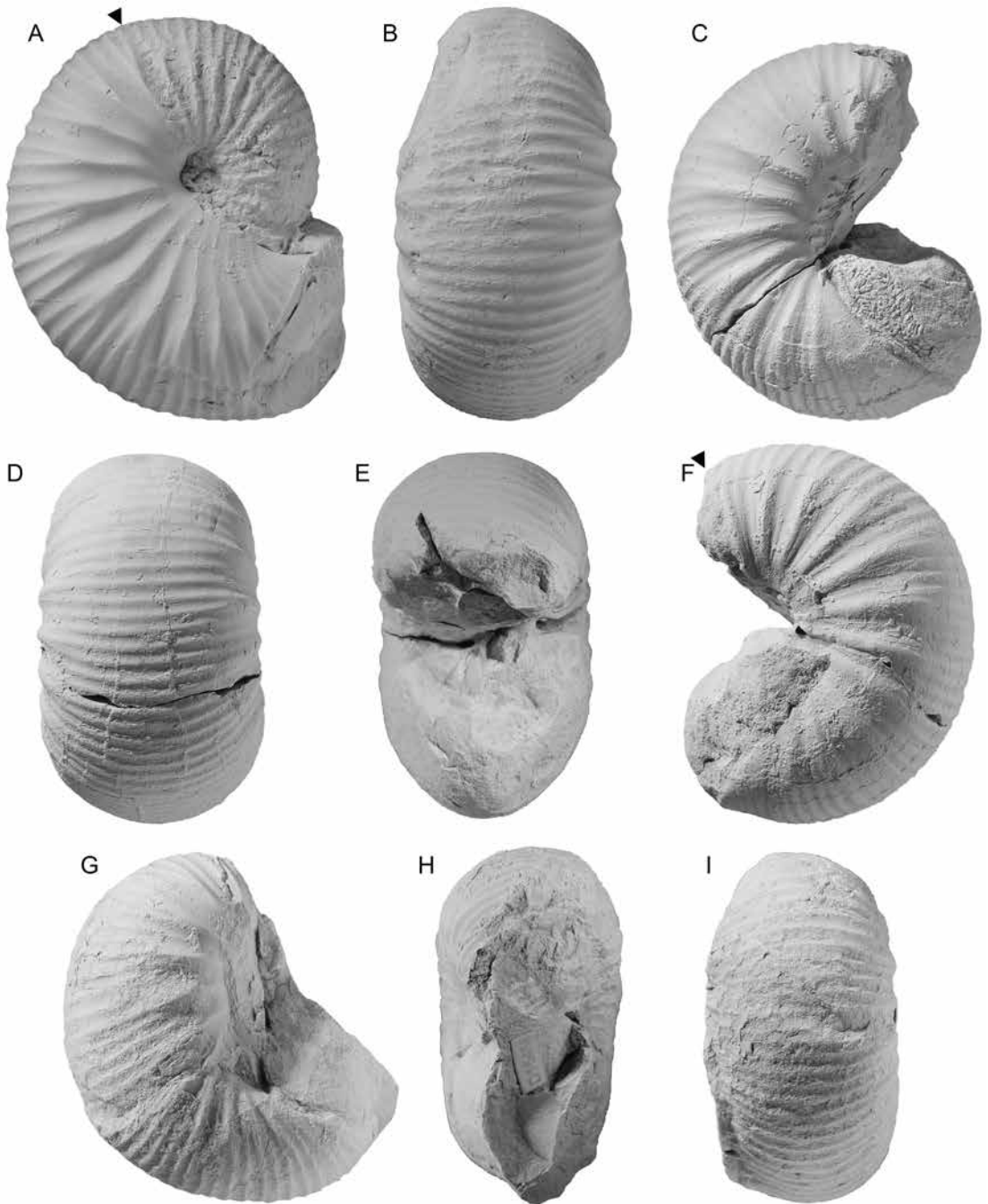


FIG. 31. *Scaphites* (*S.*) *depressus* Reeside, 1927, microconchs. **A, B.** TMP2016.041.0221, 121.0 m, Wapiabi Formation, West Thistle Creek, Alberta. **A.** Right lateral; **B.** ventral. **C-F.** TMP2016.041.0005, 132.5 m, Wapiabi Formation, Ram River, Alberta. **C.** Right lateral; **D,** ventral; **E.** apertural, **F.** left lateral. **G-I.** TMP2016.041.0302, 149.0 m, Wapiabi Formation, Sheep River, Alberta. **G.** Right lateral; **H.** apertural. **I.** ventral.

umbilical seam and are straight and rectiradiate on the umbilical wall and shoulder. They develop into broad elongate swellings that are straight or weakly concave or convex. They branch into two secondary ribs, with another longer secondary rib intercalating between them. Ribs are sharp and uniformly strong on the broadly rounded venter, which they cross with a slight adoral projection. They are closely spaced on the adapical end of the phragmocone with a rib density of 4.5 to 6 ribs/cm. They become slightly more widely spaced on the adoral end of the phragmocone with a rib density of 4 to 5.5 ribs/cm.

The same pattern of ribbing persists onto the body chamber. Primary ribs are rectiradiate on the umbilical wall and shoulder. They form elongate swellings that are widely spaced on the shaft, becoming more closely spaced on the hook. In a few, more compressed specimens, these ribs develop into bullae at the ventrolateral shoulder before branching into two or three secondary ribs, with one longer secondary rib intercalating between them. Ribs are uniformly strong and wirelike on the venter of the shaft, which they cross with a slight adoral projection. The rib density ranges from 3.5 to 5 ribs/cm. The ribs become more closely spaced on the venter of the hook, with a rib density of 4 to 6 ribs/cm. They cross the venter of the hook with a slight adoral projection.

The suture of the microconchs is the same as that of the macroconchs.

REMARKS: Dimorphism is present in *Scaphites* (*S.*) *depressus*. The microconchs have previously been referred to as the co-occurring variety *Scaphites* (*S.*) *depressus* var. *stantoni* by Reeside (1927a) but we argue that they are simply microconchs of the typical form. The size distribution of microconchs and macroconchs is each unimodal with a peak between 60 and 65 mm and 90 and 95 mm, respectively (fig. 17). The average size of microconchs is 72.1% that of macroconchs (or conversely, the average size of macroconchs is 138.7% that of microconchs).

Two macroconchs of *Scaphites* (*S.*) *depressus* are encrusted with cheilostome bryozoans belong-

ing to the genus *Conopeum* (fig. 32). The colonies are sheetlike and cover an area of approximately 2 cm². They occur on the internal molds of the ammonites near the apertural margin, indicating that they must have encrusted the inside surfaces of the body chambers after the ammonites died. This suggests that the shells must have rested on the sea floor for at least several months.

Outside the study area, *Scaphites* (*S.*) *depressus* is widely distributed in the Kevin Member of the Marias River Shale in north-central Montana and the Cody Shale in western Wyoming. It is rare in the Smoky Hill Chalk Member of the Niobrara Formation in southwestern Colorado and in the Mancos Shale in western Colorado and eastern Utah.

Scaphites (*S.*) *depressus* co-occurs with *Clioscapites saxitonianus* at several sites in Alberta and Montana. At Cardinal River, Alberta, the two species co-occur at a height of 141.5–143.5 m and at West Thistle Creek, Alberta, they co-occur at a height of 121.0 and 123.6 m. Cobban et al. (2005) also noted the co-occurrence of these two species in the Bad Heart Sandstone in central western Alberta and in the Virgelle Sandstone in southwestern Montana.

Clioscapites saxitonianus (McLearn, 1929)

Figures 9F, G, 33–36

1929. *Scaphites ventricosus* Meek and Hayden var. *saxitonianus* McLearn: 77, pl. 18, figs. 1–3; pl. 19, figs. 1, 2.
1952. *Clioscapites saxitonianus* (McLearn). Cobban: 36, pl. 13, figs. 1–10.
1952. *Clioscapites saxitonianus* (McLearn) var. *keytei* Cobban: 37, pl. 20, figs. 5–7.
1965. *Clioscapites saxitonianus* (McLearn, 1929) var. *septentrionalis* Birkelund: 132, pl. 45, figs. 2–5; pl. 46, figs. 1–3; text-figs. 115, 116.
1965. *Clioscapites* sp. aff. *saxitonianus* (McLearn, 1929). Birkelund: 135, pl. 46, figs. 4–7; pl. 47, figs. 1, 2; text-fig. 117.
1977. *Clioscapites saxitonianus* (McLearn). Kauffman: pl. 24, figs. 5, 6.

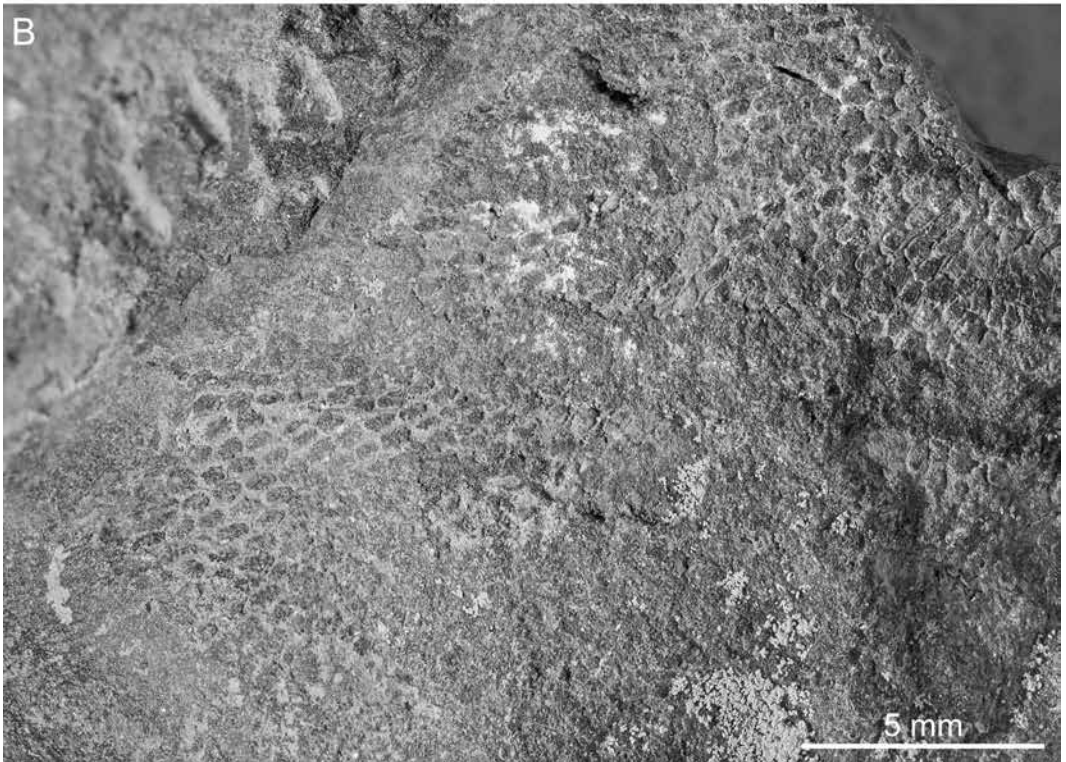
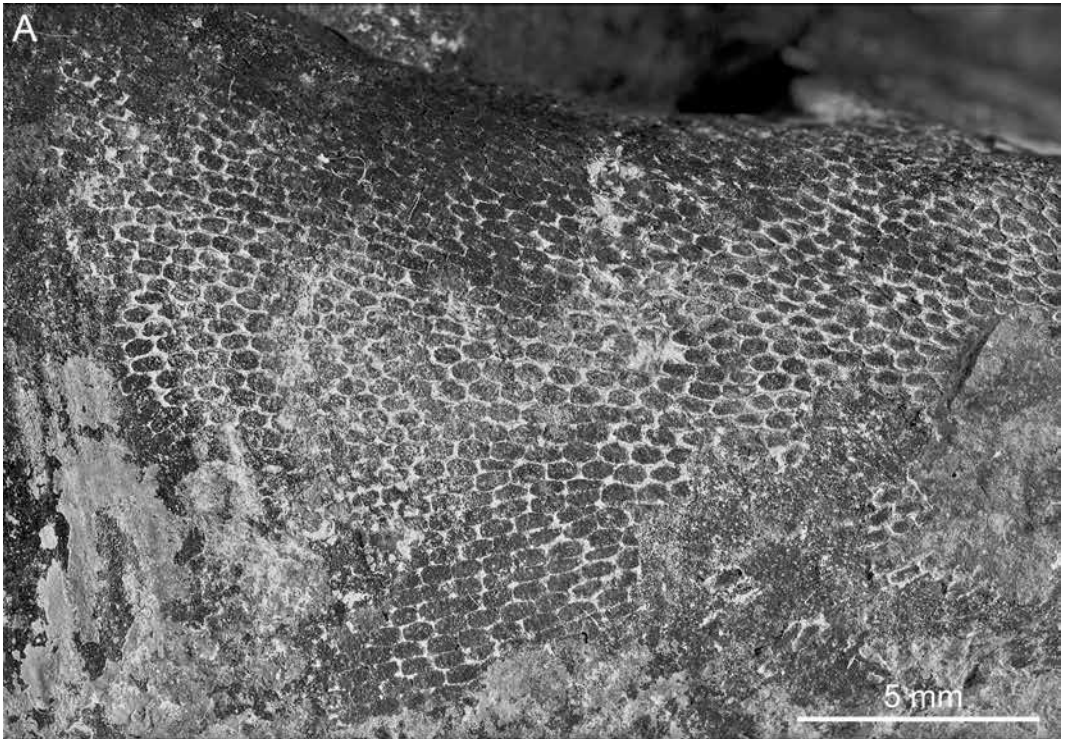


TABLE 9

Measurements of *Clioscaphtes saxitonianus*, macroconchs.

See figure 2 for description of measurements. All measurements are in mm, except for apertural angle (AA), which is in degrees. Rib density is reported to the nearest 0.25 ribs/cm on the adapical and adoral parts of the phragmocone, the midshaft, and the hook, depending upon the preservation of the specimen. Height (m) is the height in the measured stratigraphic section.* = above measured section.

Study No.	TMP No.	Locality	Height	LMAX	LMAX/HP	LMAX/HS	AA	UD	WP/HP	WS/HS	WH/HH	Rib density			
												Adap.	Adoral	Shaft	Hook
15	2016.041.0017	Ram Riv.	Above*	-	-	-	3.8	-	-	-	-	5	2.75	6	
16	2016.041.0018	Ram Riv.	Above*	-	-	-	-	-	-	-	-	-	2.75		
55	2016.041.0148	Cripple Ck	47.0	-	-	-	-	-	-	-	1.63	-	1.75	5	
59	2016.041.0157	James Riv.	105.7	-	-	-	-	-	-	-	-	-	1.75	4	
88	2016.041.0222	W. Thistle Ck.	121.0	-	-	-	-	-	-	-	-	-	3	4	
90	2016.041.0224	W. Thistle Ck.	123.5	-	-	-	-	-	-	-	-	-	1.5		
91	2016.041.0225	W. Thistle Ck.	123.6	-	-	-	-	-	-	-	-	-	4		
94	2016.041.0228	W. Thistle Ck.	125.9	80.4	-	2.37	60.0	-	-	1.43	1.75	-	3	4.5	
95	2016.041.0229	W. Thistle Ck.	125.9	79.8	2.84	2.38	84.0	4.6	-	-	-	-	3.75	2.5	4
97	2016.041.0231	W. Thistle Ck.	130.2	88.8	-	-	-	-	-	-	-	-	4	2.5	
98	2016.041.0232	W. Thistle Ck.	130.2	-	-	-	-	-	-	-	-	-	1.5		
105	2016.041.0279	Cardinal River	141.5–143.5	-	-	-	55.5	2.7	1.61	1.39	1.56	-	2.5	1.25	5
118	2016.041.0339	Lynx Creek	-	-	-	-	-	-	-	-	-	-	-	-	4.75
Average				83.0	2.84	2.38	66.5	3.7	1.61	1.41	1.65	5	3.5	2.5	4.75

←
 FIG. 32. Close-ups of cheliostome bryozoans of the genus *Conopeum* encrusting two macroconchs of *Scaphites* (*S.*) *depressus* Reeside, 1927. The bryozoans occur on the internal molds of the body chamber near the apertural margin. **A.** TMP2016.041.0382, 115.8 m, Wapiabi Formation, Bighorn Dam, Alberta. **B.** TMP2016.041.0009, 132.5 m, Wapiabi Formation, Ram River, Alberta.

1994. *Billcobbanoceras saxitonianum* (McLearn).
Cooper: 179.

DIAGNOSIS: Macroconchs large and stout with closely coiled shell, with a reduced aperture; apertural angle averages 66.5° ; whorl cross section of the shaft depressed with nearly flat flanks and broadly curved venter; ribs finely and closely spaced on the exposed phragmocone, coarser and more widely spaced on the shaft, and finer and more closely spaced again on the hook; primary ribs strong on the shaft attaining their maximum height as incipient nodes at the ventrolateral shoulder; microconchs smaller and more slender; suture moderately complex with asymmetrically bifid first lateral lobes.

TYPES: The holotype is NMC 9041a from the Alberta Shale of the Crownsnest River area of southwestern Alberta. The paratype is NMC 9041a; pleisotype is USNM 106739a, b. The holotype of the subspecies *keytei*, which is synonymized here with the typical form, is USNM 106727 from a calcareous concretion in the Apishapa Shale, 16 miles east of Trinidad, in sec. 1, T. 32 S., R. 62 W., Las Animas County, Colorado.

MATERIAL: The collection consists of 16 specimens, all of which are adult, comprising 13 macroconchs and 3 microconchs.

MACROCONCH DESCRIPTION: In the measured sample, LMAX averages 83.0 mm and ranges from 79.8 to 88.8 mm (table 9). The ratio of the size of the largest specimen to that of the smallest is 1.11. Adults are massive with a nearly circular outline in side view. The exposed phragmocone occupies approximately one whorl and terminates slightly above or below the line of maximum length. The umbilical diameter of the phragmocone is tiny; it averages 3.7 mm and ranges from 2.7 to 4.6 mm (table 9). The body chamber consists of a shaft and recurved hook. In side view, the umbilical shoulder of the shaft is straight and the venter of the shaft is broadly curved. LMAX/ H_s averages 2.38 and ranges from 2.37 to 2.38. The shell is tightly coiled. LMAX/ H_p equals 2.84 in TMP2016.041.0229. The aperture is reduced in size relative to that at midshaft. The apertural angle equals 66.5° and ranges from

55.5° in TMP2016.041.0279 to 84.0° in TMP2016.041.0229.

The whorl section of the phragmocone along the line of maximum length is depressed and subovoid with maximum whorl width at one-half whorl height. The umbilical wall is steep and subvertical; the flanks are broadly rounded and slope outward; the ventrolateral shoulder is sharply rounded; and the venter is broadly rounded. W_p/H_p equals 1.61 in TMP2016.041.0279. As the shell passes from the phragmocone into the body chamber, the whorl width remains nearly the same but the whorl height increases slightly, so that the whorl section at midshaft is slightly less depressed than that along the line of maximum length. The umbilical wall is steep and subvertical; the flanks are broadly rounded and slope outward; the ventrolateral shoulder is sharply rounded; and the venter is broadly rounded. W_s/H_s averages 1.41 and ranges from 1.39 to 1.43. Adoral of the midshaft, both the whorl width and especially whorl height abruptly decrease. As a result, the whorl section at the point of recurvature is more depressed than that at midshaft. The umbilical wall is flat and slopes outward; the flanks are broadly rounded; the ventrolateral shoulder is sharply rounded; and the venter is broadly rounded. W_H/H_H averages 1.65 and ranges from 1.56 to 1.75. The shell culminates in a constricted aperture with a dorsal lappet.

On the exposed phragmocone, primary ribs emerge at the umbilical seam and are straight and rectiradiate on the umbilical wall and shoulder. They develop into massive, elongate swellings that reach their maximum strength at the ventrolateral shoulder. On the adapical end of the phragmocone, the primary ribs split into bundles of two or three thinner ribs, with two or three ribs intercalating between them. The ribs are closely spaced on the venter, with a rib density of 5 ribs/cm in TMP2016.041.0017. They are sharp and uniformly strong on the venter, which they cross with a slight adoral projection. The primary ribs become more prominent and widely spaced on the adoral part of the phragmocone. They split into bundles of two or three thinner ribs with one rib interca-

TABLE 10

Measurements of *Clioscaphtes saxtonianus*, microconchs.

See figure 2 for description of measurements. All measurements are in mm. Rib density is reported to the nearest 0.25 ribs/cm on the adapical and adoral parts of the phragmocone, the midshaft, and the hook, depending upon the preservation of the specimen. Height (m) is the height in the measured stratigraphic section.

Study No.	TMP No.	Locality	Height	LMAX	LMAX/HP	UD	WP/HP	WS/HS	WH/HH	Rib density			
										Adap.	Ador.	Shaft	Hook
56	2016.041.0149	Cripple Ck.	48.6	-	-	-	-	-	-	-	-	3.75	-
92	2016.041.0226	W. Thistle Ck.	123.6	-	-	-	-	-	-	-	-	-	4.25
96	2016.041.0230	W. Thistle Ck.	125.9	58.2	-	-	-	-	-	-	-	4	-
Average				58.2	-	-	-	-	-	-	-	4	4.25

lating between them. They are widely spaced on the venter with a rib density of 2.5–4 ribs/cm.

The rib pattern on the adoral part of the phragmocone becomes even more pronounced on the shaft. The primary ribs emerge at the umbilical seam and swing slightly forward and then backward again before developing into straight, massive, elongate swellings that attain their maximum strength at the ventrolateral shoulder in the form of incipient nodes. The swellings are widely and equally spaced. At the ventrolateral shoulder, they split into bundles of two secondary ribs with another secondary rib intercalating between them. Ribs are widely and equally spaced on the venter, with a rib density of 1.25–4 ribs/cm. They are uniformly strong and cross the venter with at most a slight adoral projection. The primary ribs become weaker and more closely spaced on the hook. Each rib subdivides into two or three secondary ribs, with another secondary rib intercalating between them. Ribs cross the venter of the hook with a slight adoral projection. They are closely and equally spaced, with a rib density of 4–6 ribs/cm.

The sutures are not generally preserved. However, in TMP2016.041.0229, the first lateral lobe is slightly asymmetrically bifid (fig. 9G).

MICROCONCH DESCRIPTION: Microconchs are smaller and more slender than macroconchs. In addition, the umbilical shoulder of the shaft is concave in microconchs whereas it is straight in

macroconchs. LMAX equals 58.2 mm in TPM2016.041.0230 (table 10).

The whorl section of the phragmocone along the line of maximum length is partly visible in TPM2016.041.0230. It is depressed and subvoid with maximum whorl width at one-half whorl height. The flanks are broadly rounded and slope outward; the ventrolateral shoulder is sharply rounded; and the venter is broadly rounded. As the shell passes from the phragmocone into the body chamber, both the whorl width and height increase slightly, so that the whorl section at midshaft is nearly the same as that of the phragmocone along the line of maximum length. The inner flanks of the phragmocone are broadly rounded and slope outward; the outer flanks are nearly flat; the ventrolateral shoulder is sharply rounded; and the venter is broadly rounded. Adoral of the midshaft, both the whorl width and height decrease. As a result, the whorl section at the point of recurvature is more depressed than that at midshaft. The umbilical wall is flat and slopes outward; the flanks are broadly rounded; the ventrolateral shoulder is sharply rounded; and the venter is broadly rounded. The shell culminates in a constricted aperture with a dorsal lappet.

At the base of the body chamber, primary ribs emerge at the umbilical seam and are straight and rectiradiate on the umbilical wall and shoulder. They develop into massive, elongate swellings that reach their maximum strength at the

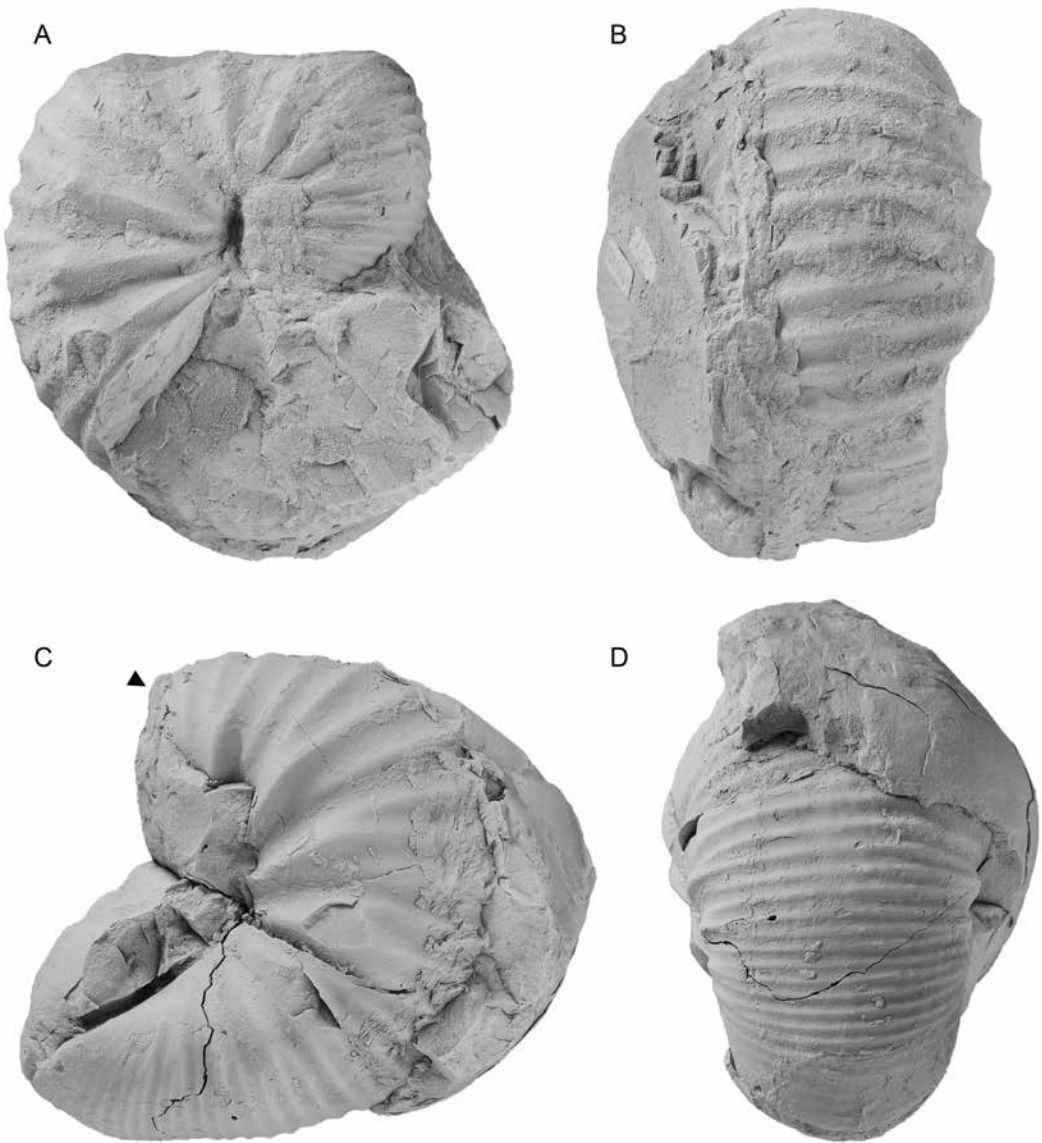


FIG. 33. *Clioscaphites saxitonianus* (McLearn, 1929), macroconchs. **A, B.** TMP2016.041.0017, above measured section, Wapiabi Formation, Ram River, Alberta. **A.** Right lateral; **B.** ventral. **C, D.** TMP2016.041.0148, 47.0 m, Wapiabi Formation, Cripple Creek, Alberta. **C.** Left lateral; **D.** ventral.

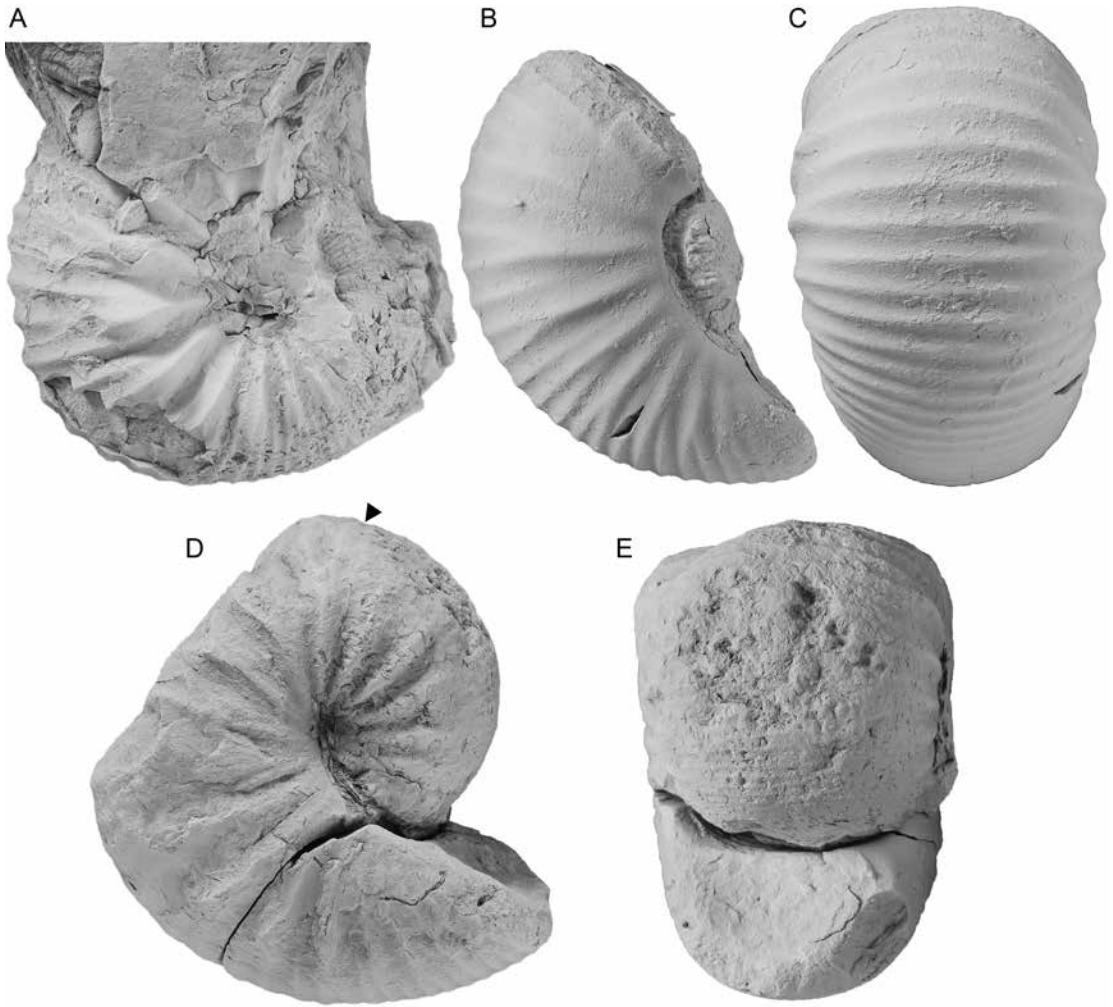


FIG. 34. *Clioscaphites saxitonianus* (McLearn, 1929), macroconchs. **A.** TMP2016.041.0018, above measured section, Wapiabi Formation, Ram River, Alberta, right lateral. **B.** **C.** TMP2016.041.0222, 121.0 m, Wapiabi Formation, W. Thistle Creek, Alberta. **B.** Right lateral; **C.** ventral. **D.** **E.** TMP2016.041.0279, 141.5–143.5 m, Wapiabi Formation, Cardinal River, Alberta. **D.** Right lateral; **E.** apertural.

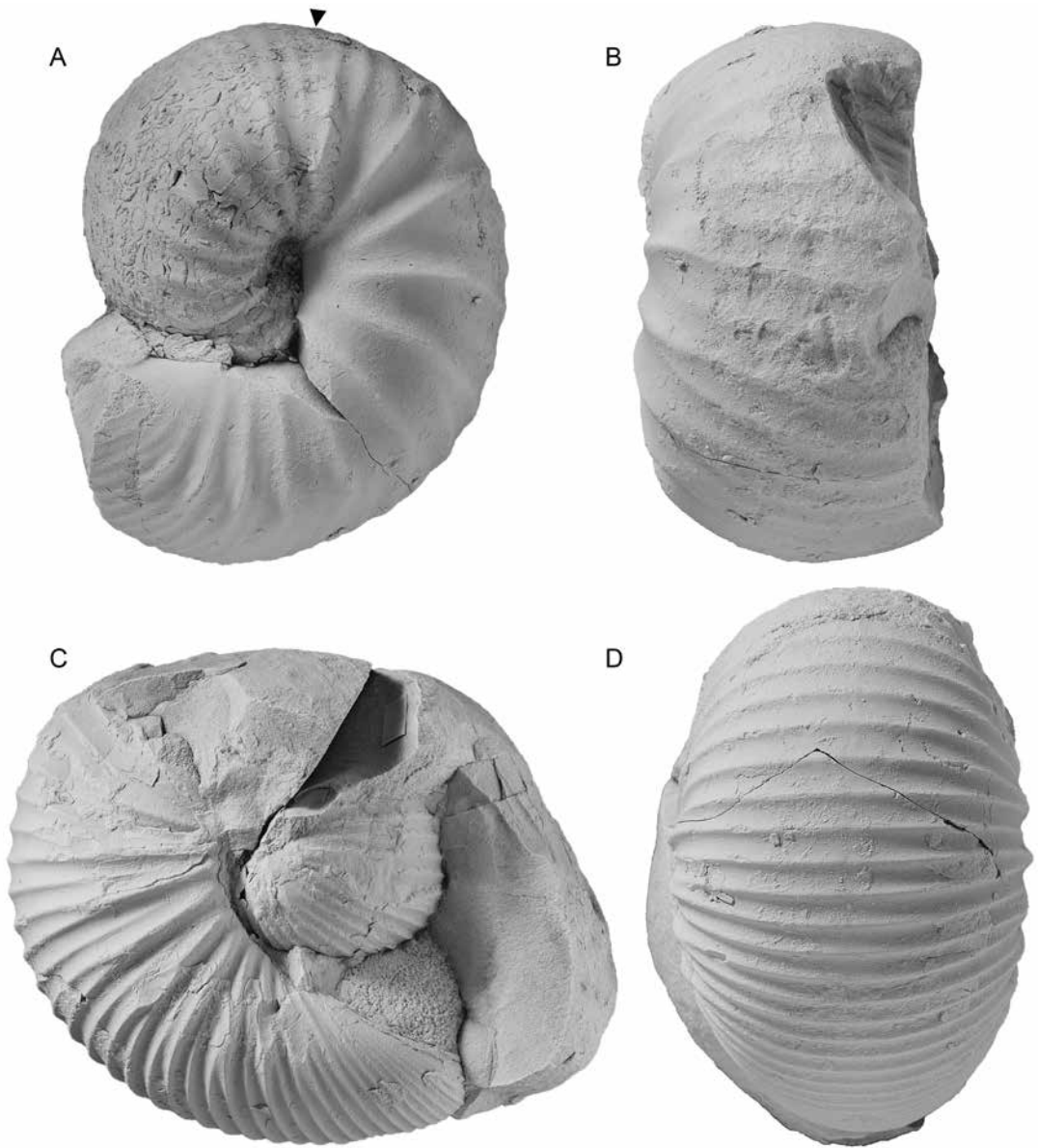


FIG. 35. *Clioscaphites saxitonianus* (McLearn, 1929), macroconchs. **A, B.** TMP2016.041.0229, 125.9 m, Wapiabi Formation, W. Thistle Creek, Alberta. **A.** Right lateral; **B.** ventral. **C, D.** TMP2016.041.0228, 125.9 m, Wapiabi Formation, W. Thistle Creek, Alberta. **C.** Right lateral; **D.** ventral.

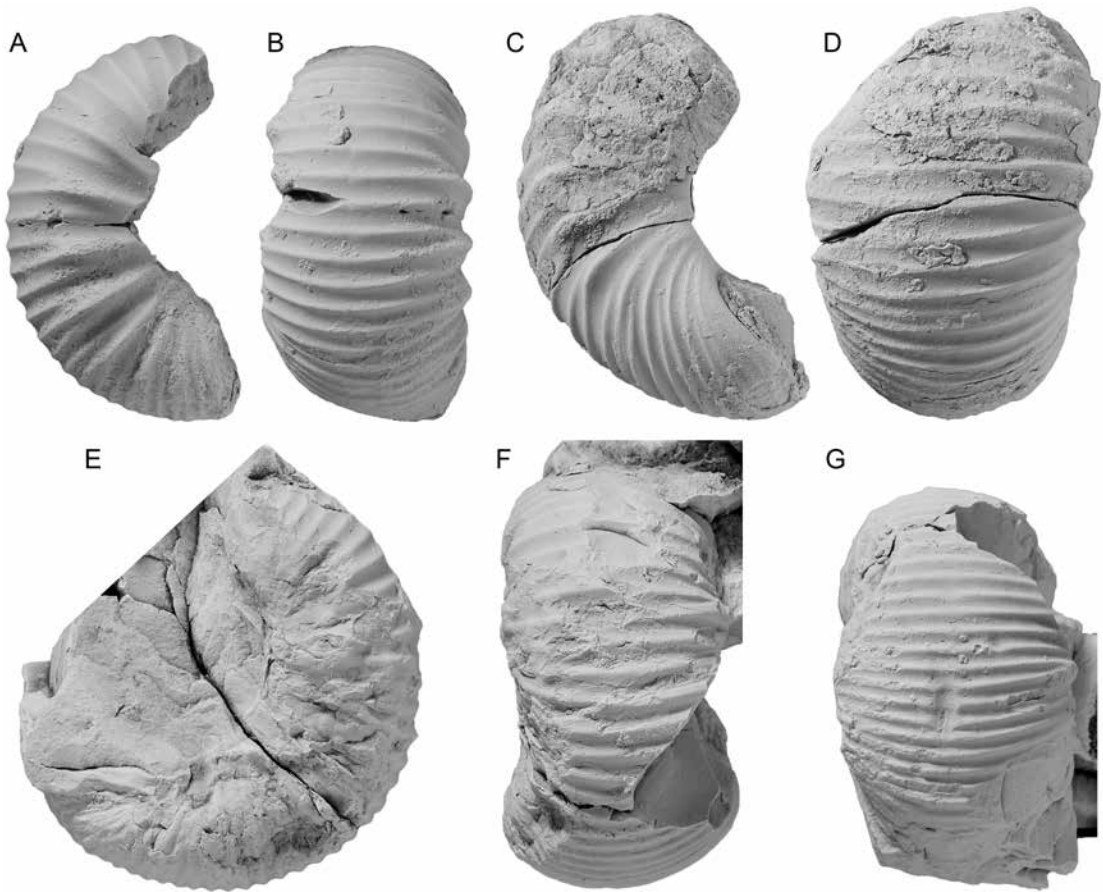


FIG. 36. *Clioscaphtes saxitonianus* (McLearn, 1929), microconchs. **A, B.** TMP2016.041.0149, 48.6 m, Wapiabi Formation, Cripple Creek, Alberta. **A.** Right lateral; **B.** ventral. **C, D.** TMP2016.041.0226, 123.6 m, Wapiabi Formation, W. Thistle Creek, Alberta. **C.** Right lateral; **D.** ventral. **E-G.** TMP2016.041.0230, 125.9 m, Wapiabi Formation, W. Thistle Creek, Alberta. **E.** Left lateral; **F.** ventral; **G.** ventral hook.

ventrolateral shoulder. The primary ribs split into bundles of two thinner ribs, with one rib intercalating between them. They are sharp and uniformly strong on the venter, which they cross with a slight adoral projection.

The ribbing pattern is similar on the shaft. The primary ribs emerge at the umbilical seam and develop into straight, massive, elongate swellings that attain their maximum strength at the ventrolateral shoulder. The swellings are widely and equally spaced. At the ventrolateral shoulder, they split into bundles of two secondary ribs with another one or two secondary ribs intercalating between them. The ribs are widely and equally spaced on the venter, with a rib density of 3.75–4 ribs/cm. They are uniformly strong and cross the venter with at most a slight adoral projection. The primary ribs become weaker and more closely spaced on the hook. Each rib subdivides into two secondary ribs, with another one or two secondary ribs intercalating between them. Ribs cross the venter of the hook with a slight adoral projection. They are closely and equally spaced, with a rib density of 4.25 ribs/cm in TMP2016.041.0226.

The suture is not preserved in any of our specimens.

REMARKS: Dimorphism is present in *Clioscaphtes saxitonianus*. The microconch was initially designated by Cobban (1952) as the variety *keytei*. Microconchs are smaller and more slender than macroconchs. In addition, the umbilical shoulder of the shaft is concave in microconchs whereas it is straight in macroconchs.

Clioscaphtes saxitonianus is distinguished from the underlying species *Scaphites* (*S.*) *depressus* by its less globose shape, flatter flanks, and coarser ornamentation on the body chamber. It is distinguished from the overlying species *Clioscaphtes vermiformis* (Meek and Hayden, 1862) by having incipient nodes rather than pointed tubercles on the body chamber and rarely having the first lateral lobe of the suture trifid.

Cooper (1994) established the genus *Billcobbanoceras* and included *Clioscaphtes saxitonianus* as one of its species. While subsequent workers have acknowledged this reassignment

(e.g., Cobban et al., 2006), none of them has ever followed it. We continue to assign this species to *Clioscaphtes* as originally described by Cobban (1952), in anticipation of a thorough taxonomic revision of these Coniacian and Santonian scaphites in the future.

OCCURRENCE: In the Upper Cretaceous of the Western Interior of North America, this species demarcates the lower Santonian *Clioscaphtes saxitonianus* Zone (Scott and Cobban, 1962). In the study area, the lowest occurrence of this species is at the base of the Santonian (surface SS0), coinciding with a major transgression and a marked change in facies to deeper-water, more offshore mudstone. This species is present in the Wapiabi Formation, Alberta, at James River (TMP2016.041.0157), West Thistle Creek (TMP2016.041.0222, .0224, and .0226–.0232), Cardinal River (TMP2016.041.0279), Cripple Creek (TMP2016.041.0148 and .0149), Lynx Creek (TMP2016.041.0339), and above the measured section at Ram River (TMP2016.041.0017 and .0018). In the U.S., this species is present in the Apishapa Shale of southeastern Colorado and in the Kevin Member of the Marias River Shale on the east flank of the Sweetgrass Arch of north-central Montana. Outside North America, it has been reported from west Greenland (Birkelund, 1965).

ACKNOWLEDGMENTS

We thank Mary Conway and Kathy Sarg (AMNH) for curation of the specimens, Stephen Thurston (AMNH) for photographing the specimens and preparing the figures, Mariah Slovacek (AMNH) for preparation of the specimens and illustrations, Mark Wilson (College of Wooster, Wooster, Ohio) for identification of the bryozoans, Neal Larson (Larson Paleontology Unlimited, Keystone, South Dakota) for preparation of the specimens, Susan Butts (Yale Peabody Museum, New Haven, Connecticut) for access to collections in her care, and Brandon Strilisky (TMP) for facilitating the accession of the specimens into the Tyrell Museum of Paleontology. We also thank Marcin Machalski (Institute of Paleobiology, War-

saw, Poland), John A. Chamberlain, Jr. (Brooklyn College, Brooklyn, New York), and Royal H. Mapes (North Carolina Museum of Natural History, Raleigh, North Carolina) for reviewing an earlier draft of this manuscript and making many helpful suggestions. This research was funded in part by NSF Grant DEB-1353510 to N.H.L. and NCN Grant UMO-2015/17/B/ST10/03228 to I.W., and through multiple cycles of Discovery Grant funding from the Natural Sciences and Engineering Research Council of Canada to A.G. Plint.

REFERENCES

- Basse, E. 1952. Ammonoïdes. In J. Piveteau (editor), *Traité de paléontologie* 2: 522–555, 581–688. Paris: Masson.
- Birkelund, T. 1965. Ammonites from the Upper Cretaceous of West Greenland. *Meddelelser om Grønland* 179 (7): 1–192.
- Braunberger, W.F. 1994. Molluscan biostratigraphy of the Cardium Formation (Upper Cretaceous, Turonian–Coniacian) and contiguous strata, Alberta Foothills and adjacent subsurface. M.Sc. thesis, University of Calgary, Calgary, Alberta.
- Braunberger, W.F., and R.L. Hall. 2001. Ammonoid faunas from the Cardium Formation (Turonian–Coniacian, Upper Cretaceous) and contiguous units, Alberta, Canada: 1. Scaphitidae. *Canadian Journal of Earth Sciences* 38 (3): 333–346.
- Casanova, R. 1970. An illustrated guide to fossil collecting. Healdsburg, CA: Naturegraph Publishers, 128 pp.
- Cobban, W.A. 1952. Scaphitoid cephalopods of the Colorado Group. U. S. Geological Survey Professional Paper 239: 1–42.
- Cobban, W.A. 1955. Some guide fossils from the Colorado Shale and Telegraph Creek Formation, northwestern Montana. Billings Geological Society Guidebook, 6th Annual Field Conference: Sweetgrass Arch–Disturbed Belt, Montana, 198–207.
- Cobban, W.A. 1968. Stratigraphy and paleontology. In H.A. Tourtelot and W.A. Cobban, Stratigraphic significance and petrology of phosphate nodules at base of Niobrara Formation, east flank of Black Hills, South Dakota. U.S. Geological Survey Professional Paper 594-L: 1–22.
- Cobban, W.A. 1969. The Late Cretaceous ammonites *Scaphites leei* Reeside and *Scaphites hippocrepis* (DeKay) in the Western Interior of the United States. U.S. Geological Survey Professional Paper 619: 1–27.
- Cobban, W.A. 1976. Ammonite record from the Mancos Shale of the Castle Valley—Woodside area, east-central Utah. Brigham Young University Geological Studies 22: 117–126.
- Cobban, W.A. 1983. Molluscan fossil record from the northeastern part of the Upper Cretaceous Seaway, Western Interior. U.S. Geological Survey Professional Paper 1253A: 1–25.
- Cobban, W.A., C.E. Erdmann, R.W. Lemke, and E.K. Maughan. 1976. Type sections and stratigraphy of the Blackleaf and Marias River formations (Cretaceous) of the Sweetgrass Arch, Montana. U. S. Geological Survey Professional Paper 974: 66 p.
- Cobban, W.A., and W.J. Kennedy. 1991. A giant scaphite from the Turonian (Upper Cretaceous) of the Western Interior of the United States. U.S. Geological Survey Bulletin 1934-A: 1–2.
- Cobban, W.A., T.S. Dyman, and K.W. Porter. 2005. Paleontology and stratigraphy of upper Coniacian–middle Santonian ammonite zones and application to erosion surfaces and marine transgressive strata in Montana and Alberta. *Cretaceous Research* 26: 429–449.
- Cobban, W.A., I. Walaszczyk, J.D. Obradovich, and K.C. McKinney. 2006. A USGS zonal table for the Upper Cretaceous middle Cenomanian–Maastrichtian of the Western Interior of the United States based on ammonites, inoceramids, and radiometric ages. U. S. Geological Survey, Open-File Report, 2006-1250: 1–46.
- Collin, R., and R. Cipriani. 2003. Dollo's law and the re-evolution of shell coiling. *Proceedings of the Royal Society of London B* 270: 2551–2555.
- Collom, C. J. 2001. Systematic paleontology, biostratigraphy, and paleoenvironmental analysis of the Upper Cretaceous Wapiabi Formation and equivalents: Alberta and British Columbia, Western Canada. Ph.D. dissertation, University of Calgary, Calgary, Alberta, Canada.
- Cooper, M.R. 1994. Towards a phylogenetic classification of the Cretaceous ammonites. III. Scaphitaceae. *Neues Jahrbuch für Geologie und Paläontologie Abhandlungen* 193 (2): 165–193.
- Crick, R.E. 1978. Morphological variations in the ammonite *Scaphites* of the Blue Hill Member, Carlile Shale, Upper Cretaceous, Kansas. University of Kansas Paleontological Contributions Paper 88: 1–28.
- Cuvier, G. 1797. *Tableau élémentaire de l'histoire naturelle des animaux*. Paris: Baudouin, xvi, 710 pp.

- Davis, R.A., N.H. Landman, J.L. Dommergues, D. Marchand, and H. Bucher. 1996. Mature modifications and dimorphism in ammonoid cephalopods. *In* N.H. Landman, K. Tanabe, and R.A. Davis (editors), *Ammonoid paleobiology*: 463–539. New York: Plenum.
- Donaldson, W.S., A.G. Plint, and F.J. Longstaffe. 1998. Basement tectonic control on the distribution of the shallow marine Bad Heart Formation: Peace River Arch area, NW Alberta. *Bulletin of Canadian Petroleum Geology* 46: 576–598.
- Donaldson, W.S., A.G. Plint, and F.J. Longstaffe. 1999. Tectonic and eustatic control on deposition and preservation of Upper Cretaceous ooidal ironstone and associated facies: Peace River Arch area, NW Alberta, Canada. *Sedimentology* 46: 576–598.
- Easton, W.H. 1960. *Invertebrate paleontology*. Harper, New York, xii + 701 pp.
- Gill, T. 1871. Arrangement of the families of mollusks. *Smithsonian Miscellaneous Collections* 227: 1–49.
- Herrick, C.L., and D.W. Johnson. 1900. The geology of the Albuquerque sheet. *Bulletin of the Hadley Laboratory of the University of New Mexico Geological Series* 2: 1–76.
- Hewitt, R.A. 1996. Architecture and strength of the ammonoid shell. *In* N.H. Landman, K. Tanabe, and R.A. Davis (editors), *Ammonoid paleobiology*: 297–339. New York: Plenum.
- Hills, L.V., W.F. Braunberger, L.K. Núñez-Betelu, and R.L. Hall. 1994. Paleogeographic significance of *Scaphites depressus* in the Kanguk Formation (Upper Cretaceous), Axel Heiberg Island, Canadian Arctic. *Canadian Journal of Earth Sciences* 31: 733–736.
- Hone, D.W.E., and M.J. Benton. 2005. The evolution of large size: how does Cope's Rule work? *Trends in Ecology and Evolution* 20 (1): 4–6.
- Jacobs, D.K., N.H. Landman, and J.A. Chamberlain, Jr. 1994. Ammonite shell shape covaries with facies and hydrodynamics: Iterative evolution as a response to changes in basinal environment. *Geology* 22: 905–908.
- Jeletzky, J.A. 1970. Cretaceous macrofaunas. *Geology and Economic Minerals of Canada*. B. Economic Minerals Report 1: 649–662.
- Kauffman, E.G. 1977. Illustrated guide to biostratigraphically important Cretaceous macrofossils. Western Interior Basin, U.S.A. *Mountain Geologist* 14: 225–274.
- Kauffman, E.G., and W.G.E. Caldwell. 1993. The Western Interior Basin in space and time. *In* W.G.E. Caldwell and E.G. Kauffman (editors), *Evolution of the Western Interior Basin*, Geological Association of Canada Special Paper 39: 1–30.
- Kennedy, W.J., and W.A. Cobban. 1976. Aspects of ammonite biology, biogeography and biostratigraphy. *Special Papers in Palaeontology* 17: 94 pp.
- Kennedy, W.J., and W.A. Cobban. 1991. Coniacian faunas from the United States Western Interior. *Special Papers in Palaeontology* 45: 96 pp.
- Kullman, J., and Wiedmann, J. 1970. Significance of sutures in phylogeny of Ammonoidea. *University of Kansas Palaeontological Contributions* 44: 1–32.
- Landman, N.H. 1987. Ontogeny of Upper Cretaceous (Turonian-Santonian) scaphitid ammonites from the Western Interior of North America: systematics, developmental patterns, and life history. *Bulletin of the American Museum of Natural History* 185 (2): 117–241.
- Landman, N. H. 1989. Iterative progenesis in Upper Cretaceous ammonites. *Paleobiology* 15 (2): 95–117.
- Landman, N.H., and W.A. Cobban. 2007. Redescription of the Late Cretaceous (late Santonian) ammonite *Desmoscaphites bassleri* Reeside, 1927, from the Western Interior of North America. *Rocky Mountain Geology* 42 (2): 67–94.
- Landman, N.H., and S.M. Klofak. 2012. Anatomy of a concretion: life, death, and burial in the Western Interior Seaway. *Palaios* 27: 671–692.
- Landman, N.H., and K.M. Waage. 1993. Scaphitid ammonites of the Upper Cretaceous (Maastrichtian) Fox Hills Formation in South Dakota and Wyoming. *Bulletin of the American Museum of Natural History* 215: 1–257.
- Landman, N.H., W.A. Cobban, and N.L. Larson. 2012. Mode of life and habitat of scaphitid ammonites. *Science Direct/Geobios* 45: 87–98.
- Landman, N.H., W.J. Kennedy, W.A. Cobban, and N.L. Larson. 2010. Scaphites of the “*nodosus*” group from the Upper Cretaceous (Campanian) of the Western Interior of North America. *American Museum of Natural History Bulletin* 342: 1–242.
- Landman, N.H., W.J. Kennedy, W.A. Cobban, N.L. Larson, and S.D. Jorgensen. 2013. A new species of *Hoploscaphites* (Ammonoidea: Ancyloceratina) from cold methane seeps in the Upper Cretaceous of the U.S. Western Interior. *American Museum Novitates* 3781: 1–39.
- Landman, N.H., et al. 2017. Nautilid nurseries: Hatchlings and juveniles of *Eutrephoceras dekayi* from the lower Maastrichtian (Upper Cretaceous) Pierre Shale of east-central Montana. *Lethaia*.

- Logan, W.N. 1898. The invertebrates of the Benton, Niobrara and Fort Pierre Groups. Geological Survey of Kansas, 4. Paleontology Pt. 8: 433–518.
- Machalski, M. 2005. Late Maastrichtian and earliest Danian scaphitid ammonites from central Europe: taxonomy, evolution, and extinction. *Acta Palaeontologica Polonica* 50 (4): 653–696.
- Makowski, H. 1962. Problem of sexual dimorphism in ammonites. *Palaeontologia Polonica* 12: 1–92.
- McLearn, F.L. 1929. Cretaceous invertebrates: Mesozoic paleontology of Blairmore region, Alberta. Canada National Museum Bulletin 58: 73–79.
- Meek, F.B. 1876. A report on the invertebrate Cretaceous and Tertiary fossils of the upper Missouri country. U.S. Geological Survey of the Territories Report 9: 629 pp.
- Meek, F.B., and F.V. Hayden. 1862. Descriptions of new Cretaceous fossils from Nebraska Territory, collected by the expedition sent out by the Government under the command of Lieut. John Mullan, U.S. Topographical Engineers, for the location and construction of a wagon road from the sources of the Missouri to the Pacific Ocean. Academy of Natural Sciences of Philadelphia Proceedings 1862: 21–28.
- McKinney, M.L., and K.J. McNamara. 1991. Heterochrony: the evolution of ontogeny. New York: Plenum, 437 pp.
- Nielsen, K.S., C.J. Schröder-Adams, D.A. Leckie, J.W. Haggart, and K. Elberdak. 2008. Turonian to Santonian paleoenvironmental changes in the Cretaceous Western Interior Sea: the Carlile and Niobrara formations in southern Alberta and southwestern Saskatchewan, Canada. *Palaeogeography, Palaeoclimatology, Palaeoecology* 270: 64–91.
- Olson, E.C., and R.L. Miller. 1958. Morphological integration. Chicago: University of Chicago Press, 317 pp.
- Owen, D.D. 1852. Report of a geological survey of Wisconsin, Iowa, and Minnesota; and incidentally of a portion of Nebraska Territory made under instructions from the United States Treasury Department. Philadelphia: Lippincott, Grambo, 2 vols., 638 pp.
- Plint, A.G., R.G. Walker, and K.M. Bergman. 1986. Cardium Formation 6. Stratigraphic framework of the Cardium in subsurface. *Bulletin of Canadian Petroleum Geology* 34: 213–225.
- Plint, A.G., B. Norris, and W.S. Donaldson. 1990. Revised definitions for the Upper Cretaceous Bad Heart Formation and associated units in the Foothills and Plains of Alberta and British Columbia. *Bulletin of Canadian Petroleum Geology* 38: 78–88.
- Reeside, J.B., 1927a. Cephalopods from the lower part of the Cody Shale of Oregon Basin, Wyoming. U.S. Geological Survey Professional Paper 150-A: 1–19.
- Reeside, J.B., 1927b. The scaphites, an Upper Cretaceous ammonite group. U.S. Geological Survey Professional Paper 150-B: 21–40.
- Rosenkrantz, A. 1942. The marine Cretaceous sediments at Ummik. *Meddelelser om Grønland* 135: 37–42.
- Scott, G.R., and W.A. Cobban. 1962. *Clioscaphtes saxitonianus* (McLearn), a discreet ammonite zone in the Niobrara Formation at Pueblo, Colorado. U.S. Geological Survey Professional Paper 450-C: C85.
- Scott, G.R., and W.A. Cobban. 1964. Stratigraphy of the Niobrara Formation at Pueblo, Colorado. U.S. Geological Professional Paper 454-L: L1–L27.
- Sageman, B.B., et al. 2014. Integrating $^{40}\text{Ar}/^{39}\text{Ar}$, U-Pb, and astronomical clocks in the Cretaceous Niobrara Formation, Western Interior Basin, USA. *Geological Society of America Bulletin* 126: 956–973.
- Schröder-Adams, C.J., J.O. Herrle, and Q. Tu. 2012. Albian to Santonian carbon isotope excursions and faunal extinctions in the Canadian Western Interior Sea: Recognition of eustatic sea-level controls on a forebulge setting. *Sedimentary Geology* 281: 50–58.
- Shank, J.A. 2012. Sedimentology and allostratigraphy of the Cardium Formation (Turonian-Coniacian) in southern Alberta and equivalent strata in northern Montana. Ph.D. thesis, University of Western Ontario, London, Ontario: 374 pp.
- Shank, J.A., and A.G. Plint. 2013. Allostratigraphy of the Upper Cretaceous Cardium Formation in subsurface and outcrop in southern Alberta, and correlation to equivalent strata in northwestern Montana. *Bulletin of Canadian Petroleum Geology* 61: 1–40.
- Stanton, T.W. 1894. The Colorado Formation and its invertebrate fauna. *Bulletin of the U.S. Geological Survey* 106: 288 pp.
- Stott, D.F. 1963. The Cretaceous Alberta Group and equivalent rocks, Rocky Mountain Foothills, Alberta. *Geological Survey of Canada Memoir* 317: 297 pp.
- Stott, D.F. 1967. The Cretaceous Smoky Group, Rocky Mountain Foothills, Alberta and British Columbia. *Geological Survey of Canada Bulletin* 132: 133 pp.
- Szász, L. 1976. Nouvelles espèces d'ammonites dans le Cénomaniens de la région de Hateg (Carpates méridionales).

- dionales). Dări de Seamă ale Sedintelor (3 Paléontologie), 62: 169–174.
- Tanabe, K. 1975. Functional morphology of *Otoscaphtes puerculus* (Jimbo), an Upper Cretaceous ammonite. Transactions of the Proceedings of the Palaeontological Society of Japan, New Series 99: 109–132.
- Trueman, A.E. 1941. The ammonite body chamber, with special reference to the buoyancy and mode of life of the living ammonite. Quarterly Journal of the Geological Society (London) 96: 339–383.
- Tsujita, C.J., and G.E.G. Westermann. 1998. Ammonoid habitats and habits in the Western Interior Seaway: a case study from the Upper Cretaceous Bearpaw Shale of southern Alberta, Canada. Palaeogeography, Palaeoclimatology, Palaeoecology 144: 135–160.
- Walaszczyk, I., and W.A. Cobban. 2000. Inoceramid faunas and biostratigraphy of the Upper Turonian – Lower Coniacian of the Western Interior of the United States. Special Papers in Palaeontology 64: 1–118.
- Walaszczyk, I., and W.A. Cobban. 2006. Palaeontology and biostratigraphy of the Middle-Upper Coniacian and Santonian of the US Western Interior. Acta Geologica Polonica 56: 241–348.
- Walaszczyk, I., J.A. Shank, A.G. Plint, and W.A. Cobban. 2014. Inter-regional correlation of disconformities in Upper Cretaceous strata, Western Interior Seaway: Biostratigraphic and sequence-stratigraphic evidence for eustatic change. Geological Society of America Bulletin 126: 307–316.
- Wani, R. 2007. How to recognize in situ fossil cephalopods: evidence from experiments with modern *Nautilus*. Lethaia 40: 305–311.
- Wani, R., T. Kase, Y. Shigeta, and R. DeOcampo. 2005. New look at ammonoid taphonomy, based on field experiments with modern chambered nautilus. Geology 33 (11): 849–852.
- Wedekind, R. 1916. Über Lobus, Suturallobus und Inzision. Zentralblatt für Mineralogie, Geologie und Palaeontologie B 1916: 185–195.
- Wiedmann, J. 1966. Stammesgeschichte und System der postriadischen Ammonoideen: ein Überblick. Neues Jahrbuch für Geologie und Paläontologie Abhandlungen 125: 49–79; 127:13–81.
- Williams, G.D., and C.R. Stelck. 1975. Speculations on the Cretaceous palaeogeography of North America. In Caldwell, W.G.E. (editor), The Cretaceous System in the Western Interior of North America. Geological Association of Canada Special Paper 13: 1–20.
- Wright, G.N., M.E. McMechan, and D.E.G. Potter. 1994. Chapter 3, Structure and architecture of the Western Canada Sedimentary Basin. In G. Mossop and I. Shetsen (compilers), Geological atlas of the Western Canada Sedimentary Basin. Calgary: Canadian Society of Petroleum Geologists and Alberta Research Council: 25–40.
- Yacobucci, M.M. 2004. Buckman's Paradox: variability and constraints on ammonoid ornament and shell shape. Lethaia 37: 57–69.
- Zittel, K.A. von. 1884. Handbuch der Paläontologie. Abteilung 1. Band 2: 329–522. Munich: R. Oldenbourg.

SCIENTIFIC PUBLICATIONS OF THE AMERICAN MUSEUM OF NATURAL HISTORY

AMERICAN MUSEUM NOVITATES

BULLETIN OF THE AMERICAN MUSEUM OF NATURAL HISTORY

ANTHROPOLOGICAL PAPERS OF THE AMERICAN MUSEUM OF NATURAL HISTORY

PUBLICATIONS COMMITTEE

ROBERT S. VOSS, CHAIR

BOARD OF EDITORS

JIN MENG, PALEONTOLOGY

LORENZO PRENDINI, INVERTEBRATE ZOOLOGY

ROBERT S. VOSS, VERTEBRATE ZOOLOGY

PETER M. WHITELEY, ANTHROPOLOGY

MANAGING EDITOR

MARY KNIGHT

Submission procedures can be found at <http://research.amnh.org/scipubs>

All issues of *Novitates* and *Bulletin* are available on the web (<http://digitalibrary.amnh.org/dspace>). Order printed copies on the web from:

<http://shop.amnh.org/a701/shop-by-category/books/scientific-publications.html>

or via standard mail from:

American Museum of Natural History—Scientific Publications
Central Park West at 79th Street
New York, NY 10024

∞ This paper meets the requirements of ANSI/NISO Z39.48-1992 (permanence of paper).

ON THE COVER: UPPER CRETACEOUS (CONIACIAN) MUDSTONES EXPOSED IN THE CANYON OF THE SHEEP RIVER, SW ALBERTA, ACCOMPANIED BY TWO OF THE MOST CHARACTERISTIC FOSSILS FROM THIS SECTION *SPHENOCERAMUS* EX. GR. *PACHTI* (TOP) AND *SCAPHITES* (*S.*) *DEPRESSUS* (BOTTOM).